

# VISUALIZATION AND TARGETED DISRUPTION OF PROTEIN INTERACTIONS IN LIVING CELLS

---

WEN DENG



MÜNCHEN 2013



# Visualization and Targeted Disruption of Protein Interactions in Living Cells

WEN DENG

Dissertation

an der Fakultät für Biologie

der Ludwig-Maximilians-Universität

München

vorgelegt von

Wen Deng

aus Hanzhong, China

München, den 25. 11. 2013





Erstgutachter: Prof. Dr. Heinrich Leonhardt

Zweitgutachter: Prof. Dr. Marc Bramkamp

Tag der mündlichen Prüfung: 17.01.2014



## CONTENTS

<b>SUMMARY .....</b>	<b>1</b>
<b>1. Introduction.....</b>	<b>3</b>
1.1 Methods to study protein interactions .....	3
1.1.1 Genetic assay - Y2H .....	3
1.1.2 Affinity purification based methods.....	4
1.1.3 Molecule proximity based biophysical/biochemical assays .....	6
1.1.4 Fluorescence based dynamic assays .....	11
1.2 The p53-Mdm2 interaction.....	15
1.2.1 The cellular role of p53 .....	15
1.2.2 Mdm2 and its relationship with p53.....	16
1.2.3 Inhibitors of the p53-Mdm2 interaction.....	18
1.3 Centromere characterization.....	20
1.3.1 Centromeric DNA.....	20
1.3.2 Specific histones at centromeres.....	21
1.3.3 Epigenetic features of the centromere.....	23
1.3.4 CENP-A deposition at centromeres.....	24
1.4 The kinetochore structure and CCAN (Constant Centromere Associated Network) ....	27
1.4.1 The kinetochore structure .....	27
1.4.2 Constant centromere associated network.....	28
1.5 Aims of this work.....	33
<b>2. Results.....</b>	<b>35</b>
2.1 Visualization and Targeted Disruption of Protein Interactions in Living Cells .....	35
2.2 CENP-C Facilitates the Recruitment of M18BP1 to Centromeric Chromatin.....	57
2.3 Step-Wise Assembly, Maturation and Dynamic Behavior of the Human CENP-P/O/R/Q/U Kinetochore Sub-Complex.....	81
2.4 Binding of the Heterogeneous Ribonucleoprotein K (hnRNP K) to the Epstein-Barr Virus Nuclear Antigen 2 (EBNA2) Enhances Viral LMP2A Expression.....	99
<b>3. Discussion.....</b>	<b>121</b>
3.1 F3H – a versatile tool for protein manipulation and interaction studies.....	121
3.1.1 F3H as a method to study protein-protein interactions.....	121
3.1.2 Application of the F3H assay for high-throughput screens.....	127

3.1.3	Developing a method for protein interaction inhibitor studies .....	130
3.1.4	Application of the GFP binding protein and nanobodies.....	132
3.2	Cell cycle coupled control of CENP-A incorporation.....	133
3.2.1	Recruitment of Mis18bp1 to the centromere .....	133
3.2.2	Mis18 complex regulates the epigenetic state of centromeric chromatin .....	134
3.2.3	Cell cycle-dependent regulation of the Mis18 complex and CENP-A incorporation .....	135
3.3	Assembly of CENP-O class protein .....	138
3.3.1	Dependency of CCAN protein assembly .....	138
3.3.2	The CENP-P/O/R/Q/U is not a pre-assembled complex .....	138
3.3.3	Self-assembly of the CENP-P/O/R/Q/U at kinetochores.....	139
<b>4.</b>	<b>Annex.....</b>	<b>141</b>
4.1	References .....	141
4.2	Abbreviations.....	157
4.3	Contributions .....	160
4.4	Declaration .....	161
4.5	Acknowledgements.....	162
	<b>Curriculum Vitae .....</b>	<b>163</b>

## Summary

Protein-protein interactions are directly or indirectly the basis of all biological processes. Due to their importance, many methods have been developed to detect them. Each method has advantages and disadvantages, and is suitable for different applications. Some methods test the protein in an artificial environment or require expensive equipments, high expertise and complicated experimental processes. Therefore, we developed a cell based protein interaction detection system – F3H assay, which can be widely used to study protein interactions in living cells. This F3H method takes the advantage of the GFP binding protein, a GFP recognizing single VHH domain antibody, to target GFP fusion protein to an artificial chromosomal locus. By analyzing the colocalization of the coexpressed RFP fusion proteins at the locus protein interactions could be identified.

Due to their fundamental role in biological activities, protein-protein interactions are also important targets for drug design. Since the F3H assay could visualize protein interaction in living cells in real-time, I further developed the assay to monitor the disruption of protein interactions after interaction inhibitor treatment. Using the p53-Mdm2 interaction as a test system, I successfully observed disruption of the interaction between p53-Mdm2 by several inhibitors, including both small molecular compounds and peptide inhibitors. To make this protein-protein interaction inhibitor study system more efficient, I expanded this assay to 96-well plates and established an automated analysis protocol, which allows screening for protein-protein inhibitors in a high throughput way. Our data demonstrated the versatility of the F3H method in protein interaction studies and its strong potential in protein inhibitor screening.

I applied this F3H assay to study mammalian kinetochore assembly *in vivo*. The kinetochore is a multi-protein complex formed by different classes of proteins. The CCAN (constitutive centromere-associated network) proteins are important components of functional kinetochores. Using the F3H assay, I systematically studied the interactions among the CCAN members and found some new interactions which may contribute to the assembly of the CCAN. A group of the CENP-P/O/R/Q/U proteins took our special interest, and based on interaction data, we proposed a stepwise self-assembly model for the kinetochore assembly of the CENP- P/O/R/Q/U proteins in mammalian cells.

Besides, the CENP-A incorporation mechanism was also studied in this work using our F3H assay. M18bp1 is one component of the Mis18 complex which is necessary for CENP-A incorporation after cell division. But how Mis18 complex is recruited to centromeres was unclear. I screened the interactions between M18bp1 and the CCAN proteins and found that CENP-C interacts with M18bp1. This interaction facilitates the recruitment of M18bp1 to centromere and is important for proper CENP-A incorporation. Furthermore, we studied the interactions between EB virus protein EBNA2 and its host cell protein hnRNP K, revealing a role of hnRNP K in up-regulation of viral gene expression. In conclusion, the F3H assay is a powerful method to study protein interactions and also to screen protein interaction inhibitors.



# 1. Introduction

## 1.1 Methods to study protein interactions

Proteins are the main functional executor of biological activity, and they usually do not function alone. It is normal that proteins cooperate or form complexes with other proteins under certain temporal and spatial conditions to carry out their biological function. Some proteins require modification or conformational change to be activated. These modifications or changes may depend on their interaction with other proteins. Some proteins exert their biological function as part of big multi-protein complexes. To make things more complicated, one protein may participate in several different biological activities together with different interacting partners. Therefore, it is a fundamental and important question to identify the protein interaction partners to understand how a protein functions or how it participates in the protein complex. Different methods identifying protein-protein interactions are developed to address the question.

### 1.1.1 Genetic assay - Y2H

The most classical method is the Yeast two-Hybrid (Y2H) assay (Fields et al., 1989). This method is based on the fact that the binding and activating domain of some eukaryotic transcription factors are distinct modules, which means they can also be functional if the two domains are separated and indirectly connected by other proteins.

In the Y2H assay, one protein of interest is fused to the DNA binding domain (DB) which can bind to the promoter sequence upstream of a reporter gene. And the other protein or a protein library is fused to the activating domain (AD). If the two proteins of interest interact, the DB and AD domain will be connected together by the protein pairs resulting in the expression of the reporter gene (Fig. 1B). This reporter gene expression could give the yeast cell a certain phenotype that can easily be detected. If the two proteins do not interact, there is no such phenotype due to lack of reporter gene expression (Fig. 1A). The reporter gene could be a gene important for cell survival on a selective medium (for example genes such as ADE2 or HIS3) (James et al., 1996, Ito et al., 2001) or a LacZ gene which can convert the X-gal in the medium into the blue insoluble pigment 5,5'-dibromo-4,4'-dichloro-indigo so that it could be easily recognized. Similar to this method, many modified techniques such as One-hybrid or Three-hybrid were also developed to identify protein-protein interactions, protein-DNA interactions and also protein RNA interactions (Licitra et al, 1996, Bush et al, 1996, Bernstein et al, 2002).

Y2H is a powerful method to test protein interaction or identify new protein interactors. It is a powerful tool in large scale interactor screening and in the establishment of protein interactomes. But Y2H also has some disadvantages. First, Y2H has high false

positive and false negative rate. Huang (Huang, et al. 2007) reported about 25% to 45% false positive rate and a false negative rate range from 75% to 90% for two hybrid assay data obtained in different organisms. Second, Y2H is based on a yeast expression system in which some mammalian proteins may not fold correctly or lack certain kinds of posttranslational modifications, which may be important for some interactions. Third, Y2H can only detect binary interactions, incapable of detecting proteins not present in the screening library or the host.

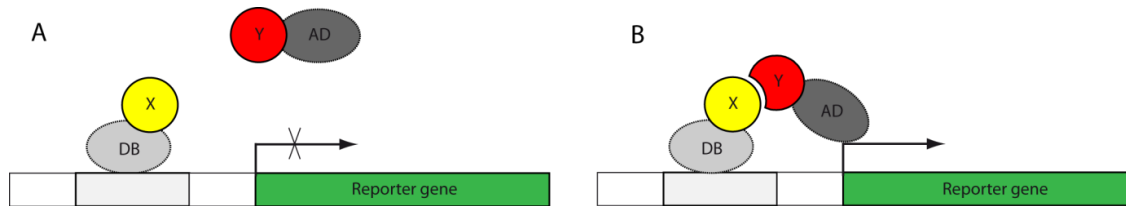


Fig. 1 Schematic representation of the Y2H protein interaction assay. Two proteins of interest, X and Y are fused to a DNA binding domain (DB) and an activating domain (AD), respectively. (A) If X and Y do not interact, the AD domain fused to Y does not bind to the promoter of the reporter gene, so there is no expression of the reporter gene. (B) X and Y interact, the AD domain fused to Y is recruited to the promoter region of the reporter gene by the DB domain fused to protein X, thus resulting in the expression of the reporter gene product. By detection of the report gene product, the interaction between X and Y can be detected.

### 1.1.2 Affinity purification based methods

Affinity based methods include co-immunoprecipitation (co-IP) and pull-down assay. These methods are based on the specific affinity of an antibody or ligand protein to the protein of interest (called 'bait'). Because of this specific affinity, the bait protein can be captured by the antibody or ligand immobilized either on beads or on a plate surface. Depending on the experimental conditions, interacting partners (called 'prey') also would be immobilized or co-purified from the mixture of proteins such as cell lysates. The co-purified proteins are then either detected by specific antibodies after gel electrophoresis or directly identified by an antibody microarray or mass spectrometry (MS) (see Fig. 2).

Co-IP is a classical biochemical technique used for protein interaction identification. Using an immobilized antibody specific against the protein of interest, the interaction partners/protein complexes are co-precipitated with the protein of interest (Fig. 2A). While the other non-binding fractions are washed away, the co-purified proteins which could be interacting partners of the bait protein, have to be identified and tested by a second method.

The Pull-down assay is quite similar to co-IP but uses affinity tags that could bind to the receptors immobilized on the solid support (Fig. 2B). For example, a protein fused to Glutathione-S-Transferase (GST) tag could bind to the GST substrate glutathione, and histidine-tagged bait proteins could be pulled out by metal affinity chromatography. The Pull-down assay does not require an antibody specific against the protein of interest, so the method is quite suitable when no specific antibodies are available.



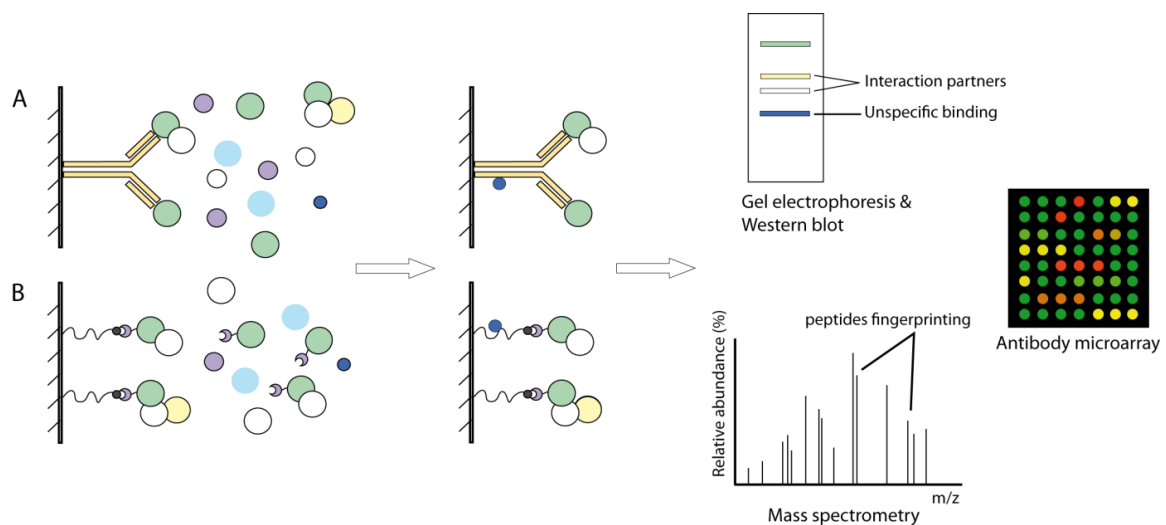


Fig. 2 Principle of affinity based protein interaction identification. Protein of interest (bait) -specific antibody (A) or the receptor of the affinity tag (B) is immobilized on the support. Cell lysates are incubated with the immobilized antibody or receptor (Left). While the interaction partners (prey) would be captured together with the protein of interest by its antibody or the affinity tag, the non-binding components would be washed away by buffer with proper salt concentration (Middle). The co-purified proteins are further analyzed by western blotting or mass spectrometry to identify them (Right).

Pull-down experiments are powerful both in known protein interaction characterization and identification of new protein interacting partners. This advantage makes it one of the most used methods in practice. Because of the high background often obtained with these methods, techniques such as tandem affinity purification (TAP) were developed (Puig et al., 2001). In TAP assays, a two-step purification is performed to reduce the unspecific bindings. The bait protein is fused with two tandem arranged tags, typically a calmodulin binding peptide (CBP) and one other affinity tag such as His-tag, separated by a tobacco etch virus protease (TEV protease) site which could be recognized and cut by TEV protease. Affinity purification is performed using the affinity to His-tag first. After the first round of purification, the purified products are digested by TEV protease to release the bait protein and its partners from the beads. The released protein complexes are further purified relying on the second tag, the CBP tag on the bait. CBP tagged bait and its partners bind to calmodulin-coated beads in the presence of calcium. After washing away the unspecific bindings, the proteins are eluted from beads by calcium chelation for further identification. By this two round purification process, the TAP method effectively reduces the unspecific bindings which bind to the purification beads or columns.

All these affinity based methods rely on cell lysates, and due to the different conditions of protein expression level, dilution and washing they may give both false positive and false negative results. Strict controls and testing by a second method should always be performed to reduce false results.

Due to the disadvantages of affinity based assays, methods independent of the antibody or ligand affinity were developed.

### 1.1.3 Molecule proximity based biophysical/biochemical assays

As an alternative approach, methods based on the spatial adjacency of interacting proteins have been developed. These methods utilize the changing physical properties or biochemical reactions which could only occur between two molecules within close proximity to indicate protein interactions. These biophysical or biochemical changes result in quite different readouts, ranging from fluorescence detection to chemical cross-linking.

#### 1.1.3.1 Bimolecular fluorescence complementation

One commonly used method is the bimolecular fluorescence complementation (BiFC) assay (Ghosh et al., 2000). In the BiFC assay, a fluorescent protein (FP) is divided into two parts and fused to two proteins of interest. Each FP fragment does not emit any fluorescence, only if the two FP fragments are brought into close proximity and re-assemble into one complete FP, the FP could be visualized, which in turn indicates that the two proteins interact with each other (Fig. 3). YFP (Hu et al., 2002), BFP, CFP (Hu et al., 2003), mRFP1 (Jach et al., 2006) and mCherry (Fan et al., 2008) have been successfully used for BiFC assay.

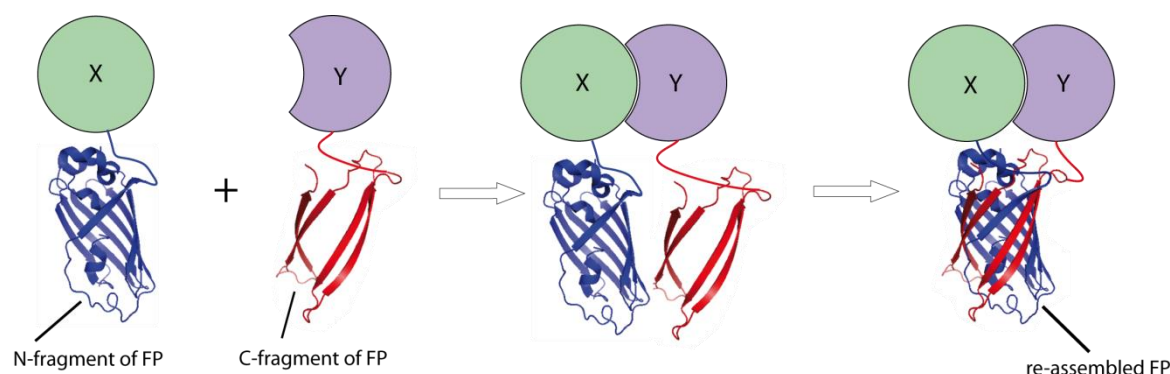


Fig. 3 Schematic representation of BiFC assay. GFP is divided into two fragments and fused to two proteins of interest (X and Y). When expressed in cells, the two fragments of GFP are brought together by the interacting protein X and Y. These two fragments then assemble into one complete GFP, detectable by fluorescence microscopy. Besides GFP, several other fluorescent proteins are successfully used in BiFC assay.

Alternatively, firefly luciferase (Paulmurugan et al., 2002, 2005) and Gaussia luciferase (Remy and Michnick, 2006) are also used in the bimolecular complementation assay instead of FPs to test protein interactions. BiFC assay can be used to study not only protein-protein interactions, but also in the field of cell metabolism or protein degradation. Proteins such as dihydrofolate reductase (Pelletier et al., 1998) and ubiquitin (Johnsson et al., 1994) have been used for complementation assay to study the corresponding biological pathways.

While BiFC could visualize protein interaction in living cells, there are also some disadvantages which limit its application. First, fluorescent protein formation by the fragments is irreversible (Kerppola, 2006), which would trap the interacting proteins in

this complex, potentially disrupting the dynamical trafficking of the proteins. Second, the intrinsic ability of the two fragments to associate with each other and forming an entire fluorescent protein independent of the interaction between the proteins fused to them may give a certain amount of background signal or even give false positive results (Walter et al., 2004; Zamyatnin et al., 2006). Third, the time requirement for fluorophore maturation after reconstitution is relatively long (which normally is more than 1 h), limiting its temporal resolution (Robida et al., 2009) which is important in living cell imaging. At last, suitable fusion constructs have to be made and artificially expressed in cells.

### 1.1.3.2 FRET and BRET

Fluorescence resonance energy transfer or Föster resonance energy transfer (FRET) is the non-radiative energy transfer between two fluorophores when they are in close spatial distance, typically occurring in the 1 - 10 nm distance.

FRET technology takes advantage of this effect and provides information about the proximity of two bio-molecules by detecting the fluorescence transfer between two fluorophores attached to test bio-molecules. To perform this assay, one protein is labeled with one fluorophore serving as a donor while the other protein is labeled with another fluorophore acting as an acceptor. The donor fluorophore is excited by an appropriate laser, and it transfers part of its energy to the acceptor fluorophore when the donor and acceptor are in close spatial distance and appropriate relative orientation. Thus the emission light of the acceptor could be detected without a direct excitation. As a requirement for FRET, the donor fluorophore must have a shorter excitation and emission wavelength than the acceptor, and there should be an overlap of emission/absorption spectra between the two fluorophores to allow the energy transfer (Fig. 4).

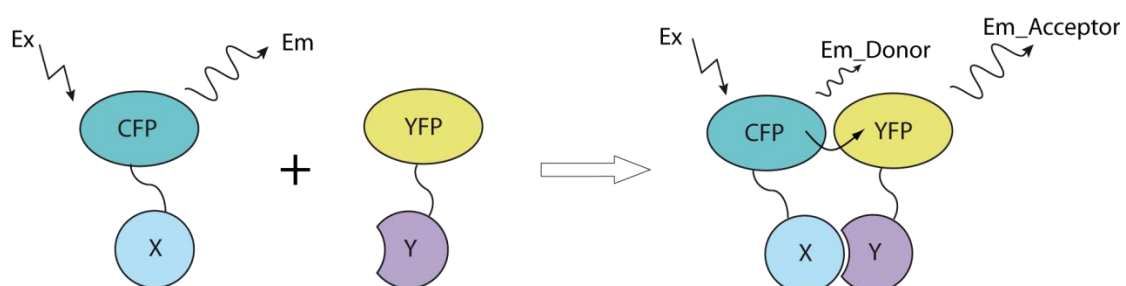


Fig. 4 Principle of the FRET assay. The proteins of interest X and Y are fused to CFP and YFP respectively. The CFP fused to X is excited by its exciting laser, and the excited CFP transfers some of its energy to the acceptor YFP when X and Y are in close proximity. In this process, the emission of CFP would reduce while the YFP can emit fluorescence because of the energy transferred from CFP. Detection the CFP and YFP emission gives information about the proximity of X and Y.

Just like FRET, bioluminescence resonance energy transfer (BRET) (Xu et al., 1999) is also based on the phenomenon of Förster resonance energy transfer. In difference with classical FRET, BRET uses luciferase to replace the donor fluorophore so that no excitation light is needed in this case. It solves problems such as cell photo response or photobleaching of the fluorophore. Additionally, for cells with high auto-fluorescence (due to high levels of NADH or flavins), BRET would also be a better choice than FRET.

FRET is also developed to BiFC-FRET to detect the interaction between 3 proteins (Shyu et al., 2008), and FLIM-FRET (Shaner et al., 2004). BiFC-FRET combines BiFC and FRET, the FP Cerulean is split into two parts and fused to two proteins of interest; the third protein of interest is fused to Venus which serves as an acceptor. Only if the first two proteins interact, the Cerulean could be re-assembled, and serve as the FRET donor. When the third protein interacts with the other two proteins, a FRET could occur and be detected. FLIM-FRET detects the lifetime change of the donor fluorescent protein, rather than detecting the fluorescence intensity change in FRET.

FRET and FRET based methods are very sensitive to changes in distance of the two proteins. Suitable fluorescent protein pair should be chosen and it requires special equipment to detect the signal such as in FLIM-FRET assay. Additionally, FRET works only when the fluorophores are in correct orientation, and it could also be sensitive to the pH of the environment. Controls should always be performed to exclude false results since FRET is affected by many factors.

#### 1.1.3.3 Proximity dependent biotinylation

Proximity dependent biotinylation is a technology developed recently, and it utilizes the bacterial BirA protein (Bifunctional protein BirA) which is a biotin protein ligase to transfer biotin to proteins with a biotin acceptor tag (BAT) or so called acceptor peptide (AP) sequence. Protein of interest X is fused to the biotin ligase BirA, and the other protein partner Y is tagged with BAT substrate sequences. If X and Y interact, the BirA will catalyze the biotinylation of BAT tagged protein Y, and this biotinylated Y could be detected by fluorophore-coupled streptavidin staining (Fernández-Suárez et al., 2008) or pull-down followed by further analysis (Kulyyassov et al. 2011) (Fig. 5A). This method was also successfully used to visualize neurexin-neuroligin *trans*-interactions at synapses in cultured living neuronal cells (Thyagarajan and Ting, 2010).

Roux and colleagues improved this method (Roux et al., 2012). They used a BirA mutant (BirA\*) which has a promiscuous target range and can biotinylate proteins in a proximity-dependent way regardless of the BAT sequences. With this mutant protein, they could biotinylate endogenous protein interacting partners in mammalian cells, and subsequently identify these proteins by MS (Fig. 5B).

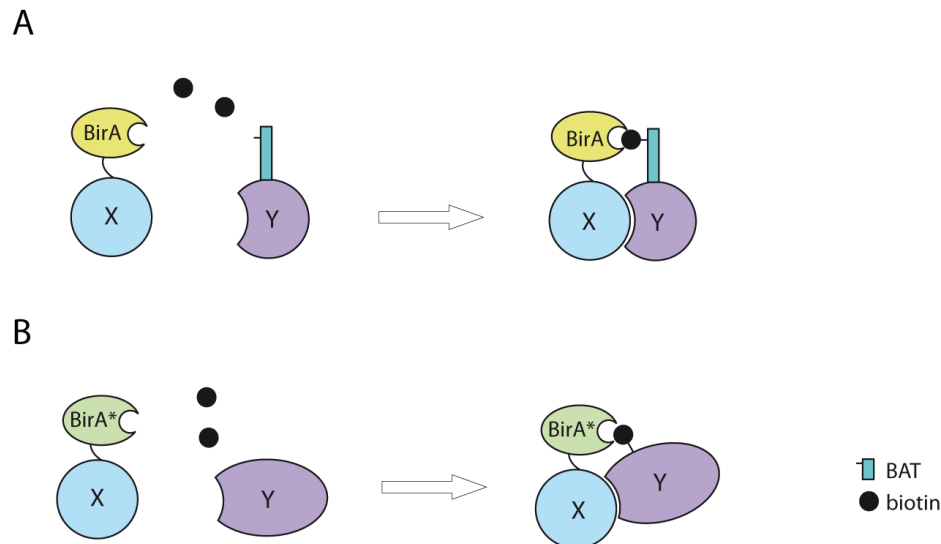


Fig. 5 Protein interaction dependent biotinylation. (A) Bacterial biotin protein ligase (BirA) is fused to protein X, and the protein Y is tagged with BirA substrate peptide BAT. If protein X and Y interact, the ligase would meet its substrate and add a biotin onto the BAT fused to protein Y. (B) a BirA mutant (BirA\*) which has a less strict substrate recognition is fused to X so that the interacting partner of protein X (protein Y) could be directly biotinylated by this mutant. These biotinylated proteins are then further analyzed by methods such as pull-down assay and mass spectrometry analysis or streptavidin mediated fluorescence imaging.

#### 1.1.3.4 Proximity dependent fluorophore labeling

Slavoff and colleagues (Slavoff et al., 2011) designed a method called Interaction-Dependent Probe Incorporation Mediated by Enzymes (ID-PRIME). This method is similar to the proximity dependent biotinylation, but instead of a biotin molecule, they transferred a fluorophore onto the target peptide to visualize protein interactions *in vivo*. They used an *Escherichia coli* LpIA (lipoic acid ligase) mutant LpIA<sup>W37V</sup>, which can covalently ligate a coumarin fluorophore onto its target peptide sequence LAP1. One protein A is fused to this ligase LpIA<sup>W37V</sup>, while its potential interacting partner B is tagged with the LAP1 substrate peptide. When the two constructs are co-transfected into mammalian cells, only if the protein pair interacts, protein B would be labeled with coumarin and fluorescence could be detected as an indication of interaction. In the absence of interaction, this labeling reaction does not occur (Fig. 6).

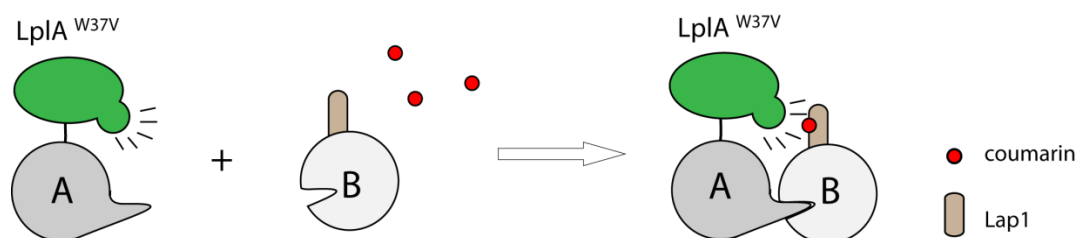


Fig. 6 Proximity dependent fluorophore labeling. Lipoic acid ligase (LpIA<sup>W37V</sup>) is fused to protein A, and the protein B is tagged with a LAP1 peptide which is the substrate of the ligase. If protein A and B interact, the ligase is brought to its substrate and adds a coumarin onto the LAP1 fused protein B. This coumarin labeled protein B can be detected with fluorescence microscopy. (Figure modified from Slavoff et al., 2011)

### 1.1.3.5 Proximity dependent chemical cross-linking

Chemical cross-linking is a technique with a long history in studying protein-protein interactions. In principle, it uses chemical reagents to cross-link the interacting proteins, and then the cross-linked protein complexes are identified by methods such as Western blotting or MS. This method is not so efficient because it requires appropriate chemical reagents to cross-link the different proteins.

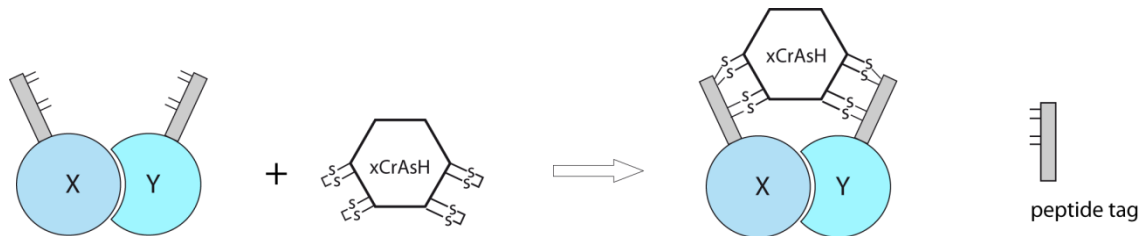


Fig. 7 Scheme of chemical cross-linking. Protein X and Y are both tagged with 12 amino acid peptide containing a tetracysteine motif. xCrAsH is added to cells, it reacts with the tetracysteine motif (shown as black lines) and cross-links X and Y covalently. This covalent complex could be visualized and further analyzed by other techniques (Figure modified from Rutkowska et al., 2011).

Rutkowska and colleagues improved this method to identify protein interaction by using a new peptide tag. They tagged both proteins of interest with a 12 amino acid peptide which contains a tetracysteine sequence motif. After expressing these two constructs in cells, they added a dimeric biarsenic derivative of carboxyfluorescein (xCrAsH) which can form a stable covalent complex with each tetracysteine motif in both proteins so that the two interaction proteins are cross-linked covalently by xCrAsH (Rutkowska et al., 2011). Besides the analysis by pull-down and MS, the cross-linked complex could be visualized by fluorescence microscopy since xCrAsH is a fluorophore (Fig. 7).

### 1.1.3.6 Proximity dependent DNA amplification

All the proximity dependent methods introduced above are using ectopically expressed proteins to study protein interactions. In addition, methods to detect endogenous protein interactions *in situ* were developed.

To visualize endogenous protein interactions *in situ*, Söderberg *et al* (Söderberg et al., 2006) used oligonucleotides which were attached to antibodies against the two proteins of interest as proximity probes. When the two antibody-attached oligonucleotides are close enough, they can guide a linear connector oligonucleotides to form circular DNA strands which can serve as templates for subsequent localized rolling-circle amplification (RCA). A RCA reaction will produce a randomly coiled, single-stranded DNA composed of up to 1,000 copies of the circular DNA template. Then the products could be detected and visualized by fluorescence *in situ* hybridization (FISH). Using this method, they visualized endogenous protein interactions both in tissue sample and in cultured cells (see Fig. 8).

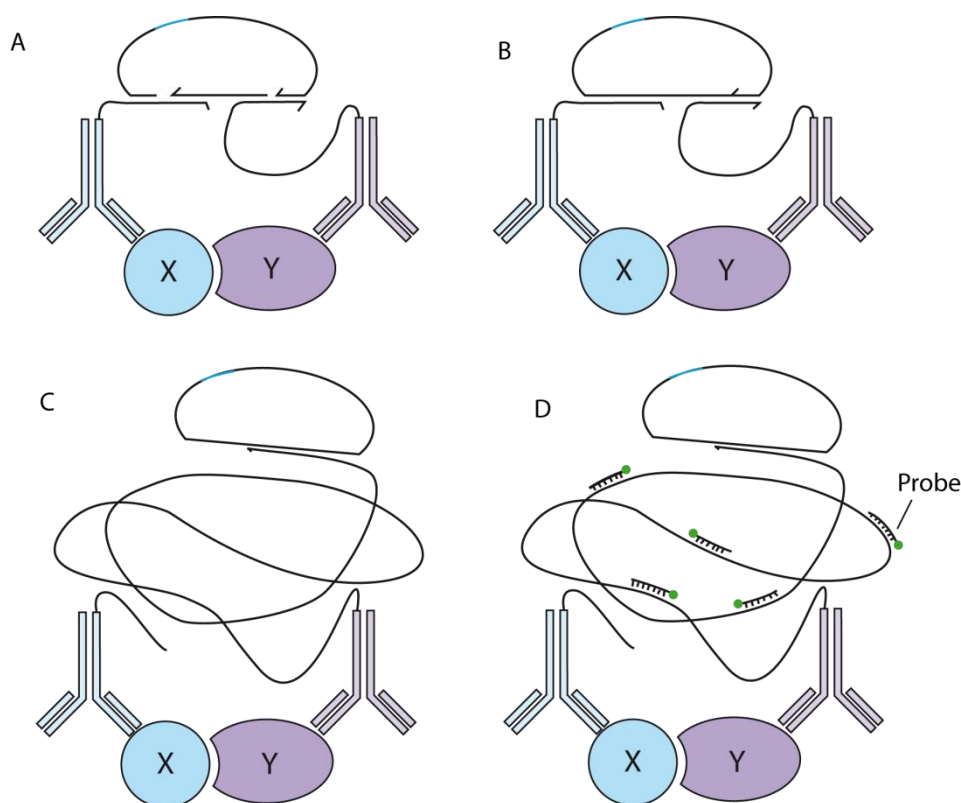


Fig. 8 Principle of proximity dependent DNA amplification. (A) Oligonucleotide probe attached antibodies against the two proteins bind to protein X and Y respectively. A circularizable linear connector oligonucleotide is added and it would form an open circular structure under the guide of the two antibody attached oligonucleotide probe. (B) The circularizable connector oligonucleotides are ligated to form a circular single DNA by enzymatic DNA ligation. (C) RCA (rolling-circle amplification) is performed using the formed DNA circle as template. (D) The amplified DNA products could be detected by Fluorescence *in situ* hybridization (FISH). (Based on Soederberg et al., 2006).

#### 1.1.4 Fluorescence based dynamic assays

To detect protein interactions in a native environment and to get more quantitative information about protein dynamics in the cells, a series of fluorescence based live cell assays were developed. Fluorescence recovery after photobleaching (FRAP) and fluorescence cross-correlation spectroscopy (FCCS) are confocal microscope based methods that can measure the mobility properties of fluorescent molecules or fluorophore labeled molecules in living cell. Both methods measure the dynamics of fluorescent molecules, but they use different strategies.

##### 1.1.4.1 FRAP

In the FRAP assay, the fluorescent protein tagged target protein is expressed, regions of interests (ROIs) in living cells are chosen and photobleached by intense laser pulses. The time-lapse fluorescence intensity recovery after photobleaching at the ROI is recorded and plotted as a recovery curve. Base on this recovery curve, a kinetic model could be simulated, and information such as dissociation rate, mean residence time, number of

mobility classes and each fraction size can be estimated (Schneider et al., 2013). The factors affecting the fluorophore dynamics can be assessed and used as an indication of protein interactions (Fig. 9).

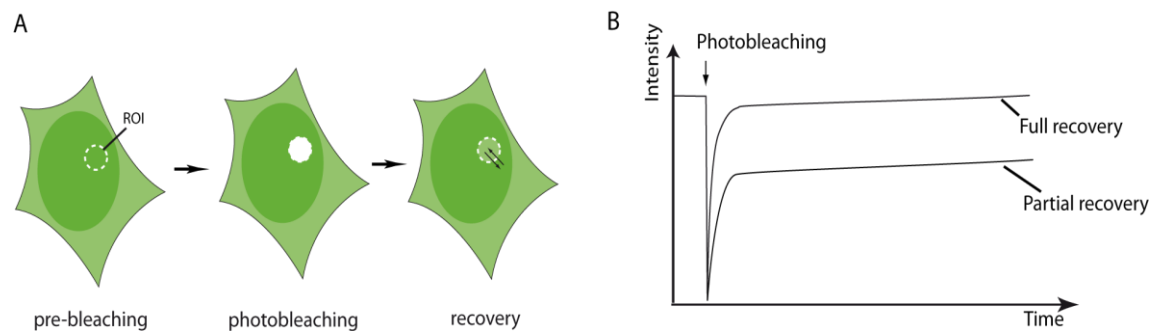


Fig. 9 Principle of FRAP assay. (A) Fluorescent protein fused protein is expressed in a cell. A ROI is chosen (white dash circle) and photobleached by intense laser irradiation. After photobleaching, the ROI area would recover its fluorescence due to the diffusion and exchange of fluorescent target protein. (B) This recovery process is recorded and plotted as a time-lapse recovery curve. Mathematical analysis can then give information about protein dynamics.

Similar to FRAP, inverse FRAP (iFRAP) or Fluorescence Loss in Photobleaching (FLIP) can be performed, which detects the loss of fluorescence from the non-photobleached region rather than monitoring the fluorescence recovery of the photobleached region measured in normal FRAP. The iFRAP offers a way to monitor the protein moving out of a certain region, such as protein movement out from Golgi in different cell-cycle phases (Zaal et al., 1999).

FRAP is a powerful tool to obtain quantitative information about protein diffusion rates and kinetics in living cell, offering deeper understanding of biological processes. But for protein interaction, it can only provide some indirect information. Based on a different principle another method, called fluorescence cross-correlation spectroscopy (FCCS), were developed.

#### 1.1.4.2 FCS/FCCS

Fluorescence correlation spectroscopy (FCS) (Elson and Magde, 1974; Magde et al., 1974) is a way to analyze fluorescent molecule dynamics by measuring the fluctuation of the fluorescence in the certain focal volume illuminated by a laser beam. The fluctuations and relative mobility of one kind of fluorescent particles in the focal volume is analyzed. With a similar principle, fluorescence cross-correlation spectroscopy (FCCS) was invented (Schwille et al., 1997), which extends the application of the FCS technique to protein-protein interaction detection (Baudendistel et al., 2005).

FCCS is a two-color FCS; it can measure two distinct fluorescent dye fluctuations in the same focal volume. The two proteins of interest are labeled with different fluorophores or fluorescent proteins, and fluorescence fluctuations in the focal volume resulting from protein movement are recorded. If the two proteins directly interact or they are in the same big protein complex, the fluorescence fluctuations of the two fluorophores are highly cross-correlated (Fig. 10, upper row). And non-interacting protein pair or proteins



not in the same complex do not result in highly cross-correlated fluorescence fluctuations between the two fluorophores (Fig. 10, lower row). Mathematical analysis of the fluctuations gives not only the cross-correlation function between the two fluorophores, but also information about concentration of the molecules and dissociation constants of their interaction. A highly positive cross-correlated fluctuation suggests that the two proteins have a similar moving pattern, indicating they may interact or are in the same complex.

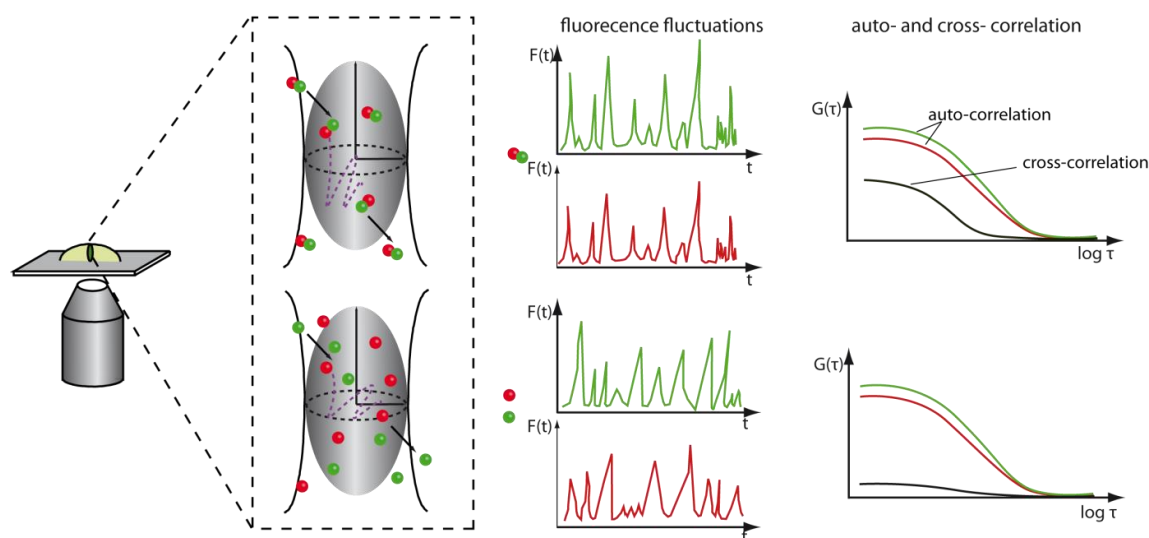


Fig. 10 FCCS analysis principle. Living cells are detected under a confocal microscope, and the focal volume is zoomed in and shown as gray ellipsoid. The movements of fluorophores (red and green spots) into and out of the focal volume are illustrated with arrows (left). The time related fluorescence fluctuations caused by fluorophore movement are recorded in both channels (middle). Fluorescence fluctuations auto-correlation and cross-correlation functions of the two colors are simulated (right), a similar movement pattern between the two fluorophores indicates an interaction (upper plot curves).

Recently, also inverse-FCS (iFCS) and inverse-FCCS (iFCCS) were developed (Wennmalm et al., 2009, 2010). In these assays, the biomolecule is not labeled, and the signal is detected from medium surrounding the analyzed molecule. The movements of biomolecules through the FCS-detection volume substitute a fraction of the surrounding medium, causing transient dropping of the detected signal. By analyzing this fluorescence fluctuation in the medium, one can get the information about the biomolecules (iFCS). If one molecule is labeled with a fluorophore, by analyzing the cross-correlation of the labeled small molecule and unlabeled particle, one can get binding information (iFCCS).

Unlike the methods such as FRET, FCCS are not restricted by close spatial proximity of the fluorophore, so it could be used to study large protein complex. In addition to protein interactions, it also provides information about protein dynamics. All the same, FCS/FCCS also has its limitations. It has an upper limit of the fluorescent particle

concentration, and it can not measure the immobile fraction which is possible in FRAP assays.

Each method has its advantages and disadvantages, and is suitable for different applications (Table 1).

Table 1 Comparison of protein-protein interaction study methods

Method	Advantages	Disadvantages	
Y2H	has simple experimental processes, is suitable for large scale screening	bait and prey lack PTMs; has high false result rate; can only detect binary protein pairs	-
IP/co-IP	suitable for identification of endogenous multi-protein complexes. Combined with isotope labeling (SILAC), could be used for quantitative proteomics	highly depends on antibody availability and specificity; results may be biased towards interaction affinity, prey abundance and kinetics of the interaction	<i>in vitro</i>
Pull-down	using affinity tags, does not require specific antibodies	usually has high background; overexpression of bait may give artificial results	<i>in vitro</i>
TAP	two-step purification, enhanced purity of the preys	overexpression of bait, may give artificial results	<i>in vitro</i>
Chemical cross-linking	detects endogenous protein complexes, has the potential to analyze transient interactions	highly depends on availability of suitable cross-linking reagent	<i>in vivo</i> or <i>in vitro</i>
BiFC	visualizes interactions in living cells	irreversible reassembly of complimentary parts, has a limited time resolution	<i>in vivo</i>
FRET	visualizes interaction in real time	artificial expression constructs are required. FRET is distance- and direction- sensitive, giving both false positive and false negative results	<i>in vivo</i>
FCCS	provides more quantitative information, high sensitivity	specialized equipment is required, results may be affected by fluorophore concentration and diffusion speed.	<i>in vivo</i> or <i>in vitro</i>
F2H	visualizes protein interactions at near native condition in living cell in real time, simple in practice	tests binary interaction only, artificial expression constructs needed.	<i>in vivo</i>

Methods in protein interaction studies are not limited to those summarized above. Some physical methods, such as NMR spectroscopy (reviewed by Takeuchi et al. 2006), isothermal titration calorimetry (ITC) and surface plasmon resonance (SPR), are also used to detect protein-protein interactions *in vitro*. All these methods make it possible to investigate how proteins cooperate together and affect each other, giving us more insights into the respective biological processes.

## 1.2 The p53-Mdm2 interaction

p53 is a transcription factor which plays multiple roles in biological processes. In particular, p53 is known as a tumor suppressor with growth suppressive and proapoptotic activity. p53 is mainly controlled by its interacting partner Mdm2 (murine double minute 2), which reduces the stability and activity of p53. Mdm2-p53 interaction inhibitor could release the p53 from the p53-Mdm2 complex thus increase the antitumor activity of p53. Because of the important role of this interaction in cell fate regulation, it is a very promising target for antitumor drug design.

### 1.2.1 The cellular role of p53

p53 was first identified as an oncoprotein, which accumulated in tumor cells (DeLeo et al., 1979; Dipplod et al., 1981), and it was also shown to interact with and to be regulated positively by SV40 large T antigen (Chang et al., 1979; Linzer and Levine., 1979). Because of these tumor related character, *p53* gene was considered as an oncogene at that time. One decade later, it was shown that the previous identified p53 was a mutant of the wild-type p53 and that p53 is a tumor suppressor gene (Baker et al., 1989; Finlay et al., 1989). In addition, it was discovered that p53 is mutated in 50% of all human cancers, suggesting that it is the most important tumor suppressor (Hollstein et al., 1991; 1996). Moreover, it was demonstrated that p53 plays critical roles in genome stability, DNA repair and cell apoptosis.

p53 is composed of an N-terminal transactivation domain, a DNA binding domain and a C-terminal oligomerization domain (Fig. 11). In addition to these domains, p53 also contains several nuclear localization signal (NLS), nuclear export signal (NES) peptide sequences and a proline-rich domain (Fabbro and Henderson, 2003). The N-terminal transactivation domain of p53 contains two parts, the transactivation domain 1, which is aspartic and glutamic acid- rich, and the transactivation domain 2, which is proline-rich. These two transactivation domains interact with numerous proteins. Some of them are important regulators of p53, such as Mdm2; and the others, like TBP, TAFII31 and p300/CBP, are components of the transcriptional machinery, activating p53 target gene expression (reviewed by Scoumanne et al., 2005). It was proposed that AD1 mediates cell cycle arrest while AD2 regulates genes involved in apoptosis (Harms and Chen, 2006). The sequence-specific DNA-binding domain locates in the middle part of the whole protein, and it is important because more than 80% of all p53 mutations in human cancer cells are found in this particular functional domain (Olivier et al., 2002). The DNA binding domain of p53 binds to specific DNA sequences in or nearby the promoter of its target genes (el-Deiry et al., 1992). It was shown that this domain was indispensable for p53's proapoptotic activity (el-Deiry et al., 1992; Pietenpol et al., 1994). Mutants, which had no DNA binding activity, block the transactivation activity. The C-terminal part of p53 (aa293-393) can be further divided into a tetramerization domain (aa326 to aa353) and a regulatory domain (aa363-393). The tetramerization domain is responsible for the

tetramer formation of p53 via dimerizing two dimers formed by p53 monomers. This tetramerization is necessary for its activity. The regulatory domain contains many lysine and arginine residues, which can be post-translationally modified to regulate the function and stability of p53.

As a transcription factor, p53 controls the expression of multiple downstream genes, many of which are involved in cell cycle control, apoptosis and cellular senescence. One of these genes is p21 (Dulic et al., 1994; el-Deiry et al., 1993). Under cellular stress, p53 transactivates and up-regulates p21 expression. p21 itself can inhibit Cdk2 and Cdk4, resulting in cell growth arrest. Another gene called p53R2 was shown to be activated by p53 and to participate in DNA damage repair and cell cycle arrest in G2/M phase. p53 also controls many genes involved in angiogenesis and DNA repair.

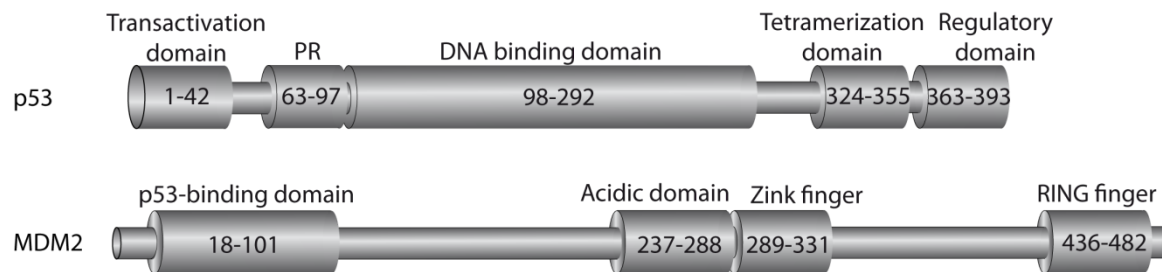


Fig. 11 Schematic representation of human P53 and MDM2 protein structure. Domains of p53 and MDM2 are shown. P53 contains an N-terminal transactivation domain which can activate its target genes. The DNA binding domain locates in the middle of P53, adjacent to the proline-rich domain (PR), binds to specific DNA sequences. At the C-terminal, the tetramerization domain is responsible for tetramer formation of P53, and the regulatory domain contains many lysine and arginine residues, which both are potential sites for posttranslational modifications. MDM2 interacts with p53 via its p53-binding domain at the N-terminus. In the middle of Mdm2, there is an acidic domain and a zinc finger. The RING type E3 ligase domain is at the C-terminus.

### 1.2.2 Mdm2 and its relationship with p53

p53 can be modified and regulated by many proteins, the most famous one is Mdm2 which controls the stability of p53 by ubiquitination. Mdm2 was first identified as an interaction partner of p53, which possessed a potential inhibitory effect on p53 mediating gene transactivation (Momand et al., 1992; Oliner et al., 1993). Crystal structure of p53 and Mdm2 complex revealed that Mdm2 binds to the transactivation domain of p53, inhibiting the transactivation activity of p53 (Kussie et al., 1996). Later, it was reported that Mdm2 promotes the proteasomal degradation of p53 (Haupt et al., 1997; Kubbuta et al., 1997). *In vitro* studies discovered that Mdm2 is an E3 ligase (Honda et al., 1997), which belongs to the family of RING type E3 ligase (Fang et al., 2000). The p53 binding domain is located at the N-terminus of Mdm2 and the RING finger domain is at the C-terminus (Fig. 11). These studies indicated that there are two different ways how Mdm2 inhibits p53: Firstly, Mdm2 inhibits p53-activity by direct binding and secondly by mediating p53-degradation. Inactive mutants of Mdm2 showed that the E3

ligase activity was sufficient for Mdm2 to inhibit p53 (Itahana et al., 2007; Clegg et al., 2008).

Interestingly, Mdm2 was also identified to be a direct transcriptional target of p53 (Barak et al., 1993; Wu et al., 1993), which means p53 can up-regulate the expression level of Mdm2. Thus, p53 increases the expression of Mdm2, but in return, the up-regulated Mdm2 promotes the degradation of p53 (Lahav et al., 2004). Therefore, p53 and Mdm2 form a negative feedback loop (Fig. 12). Under normal condition, p53 is kept at a low level by this p53-Mdm2 feedback loop, whereas under stress conditions, the amount of p53 is rapidly up-regulated.

Besides Mdm2, MdmX (also known as Mdm4) was identified as a regulator of p53 (Shvarts et al., 1996). MdmX is a homolog of Mdm2. Like Mdm2, MdmX also binds to the N-terminal transactivation domain of p53 via its own N-terminal domain. In contrast to Mdm2, the C-terminal RING domain of MdmX lacks any E3 ligase activity (Parant et al., 2001), but it can form a heterodimer with Mdm2 (Sharp et al., 1999; Tanimura et al., 1999), and stimulates the activity of Mdm2 (Linares et al., 2003). MdmX is revealed to negatively regulate p53 activity by direct binding (Fig. 12). As a substrate of Mdm2, MdmX is negatively regulated by Mdm2 (Kawai et al., 2003). Knockout of either *mdm2* or *mdmx* results in early embryonic lethality and this lethality could be rescued by *p53* knockout, which suggested that both Mdm2 and MdmX are important negative regulators of p53.

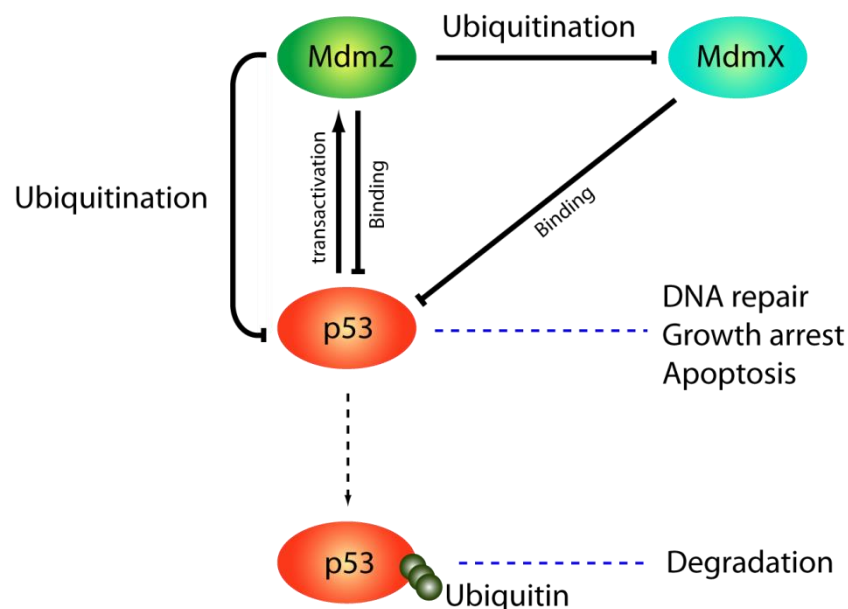


Fig. 12 Relationship of p53, Mdm2 and MdmX. Mdm2 and MdmX bind to the transactivation domain of p53, inhibiting its transcriptional activity. Moreover, Mdm2 promotes proteasomal degradation of p53 by ubiquitination. While Mdm2 inhibits the activity of p53, Mdm2, itself as a down-stream target gene of p53, is positively regulated by p53. Mdm2 also down-regulates MdmX via ubiquitination. Mdm2 and MdmX negatively control the p53 activity, and p53/Mdm2 form a negative feed-back loop.

### 1.2.3 Inhibitors of the p53-Mdm2 interaction

Since p53 plays an important role in tumor suppression, it is an attractive target of anti-tumor drug design. As the main negative regulator of p53, different methods to decrease the amount or activity of Mdm2 were used, such as the inhibition of Mdm2 expression or its E3 ligase activity. And most importantly, inhibitors specifically abolishing the p53-Mdm2 interaction are the most promising target for cancer drug development.

The first approach was the development of peptides which inhibit the p53-Mdm2 interaction. The crystal structure of the p53-Mdm2 complex revealed a p53- binding pocket located at the N-terminus of Mdm2 (Kussie et al., 1996). By peptide mapping experiments, a 6-residue peptide region (TFSDLW) of p53 was sufficient to bind to this pocket on Mdm2. Using phage display peptide libraries, an 8-residue peptide (Ac-Phe<sup>19</sup>-Met-Asp-Tyr-Trp-Glu-Gly-Leu<sup>26</sup>-NH<sub>2</sub>) was found to inhibit p53 binding to Mdm2 (IC<sub>50</sub> is 9 μM) (Böttger et al., 1996). In addition, this peptide sequence was further modified by introducing unnatural amino acids (Ac-Phe<sup>19</sup>-Met-Aib-Pmp-(6-Cl-Trp)-Glu-Ac3c-Leu<sup>26</sup>-NH<sub>2</sub>) to fold into a stable α-helical structure, resulting in better stability and higher affinity (IC<sub>50</sub> is 5 nM) for competitively binding to Mdm2 (Garcia-Echeverria et al., 2000). The structure of this Mdm2-peptide complex revealed that the 6-chlorotryptophane (6-Cl-Trp) and the phosphonomethyl phenylalanine (Pmp) enhanced the binding activity (Sakurai et al., 2006).

Due to the fact that natural peptides are easily degraded *in vivo*, proteolysis-resistant D-peptide inhibitor of the p53-Mdm2 interaction were developed. The peptides were synthesized using D-amino acids instead of the naturally occurring L-amino acids to reduce degradation. The peptides, <sup>D</sup>PMI-α (TNWYANLEKLLR), and <sup>D</sup>PMI-β (TAWYANFEKLLR) have an affinity of 219 nM and 35 nM to MDM2 respectively in SPR-based competition assays (Liu et al., 2010a). Later a D-peptide inhibitor, <sup>D</sup>PMI-γ (DW WPLAFEALLR), was developed, with an affinity of 53 nM to Mdm2 (Liu et al., 2010b).

Though inhibitory peptides can disrupt the p53-Mdm2 interaction, their application is limited due to low cellular permeability and the toxicity, arguing against a use as a drug. Therefore, instead of peptides, small compounds were developed as inhibitors of the p53-Mdm2 interaction.

Some small compounds were identified that bind to Mdm2 with different affinities and block the p53-Mdm2 interaction. Until today, there are several classes of small compound inhibitors, including analogs of spiro-oxindole, benzodiazepine (Grasberger et al., 2005; Koblisch et al., 2006), terphenyl (Yin et al., 2005; Chen et al., 2005), quinalol (Lu et al., 2006), chalone (Stoll et al., 2001) and sulfonamide (Galatin and Abraham, 2004) (reviewed by Wendt et al., 2012).

The most famous Mdm2 inhibitor is nutlin-3, which was developed by Roche about ten years ago (Vassilev et al., 2004). They screened a compounds library for potential p53-Mdm2 inhibitors, and got three nutlins. Nutlins are all *cis*-imidazoline analogs, and

nutlin-3 is the most active molecule of the three nutlins. It binds to the N-terminal part of Mdm2 with high affinity, blocking the p53-Mdm2 interaction ( $IC_{50}$  is 90 nM), which results in the accumulation and activation of p53. The downstream targets of p53 are activated which induces cell cycle arrest and apoptosis of the tumor cells. nutlin-3 has been used in preclinical cancer therapy.

Furthermore, spiro-oxindole inhibitors such as Mi-63 (Ding et al., 2006) and Mi-219 (Shangary et al., 2008) were developed. Both compounds are based on a spiro-oxindole structure and possess a high affinity to MDM2 (Shangary et al., 2008). Mi-63 is a quite strong inhibitor of p53-Mdm2 interaction, but it has a poor pharmacokinetic (PK) profile and a modest oral bioavailability, which limits its prospects as a clinical drug. To overcome these problems, Mi-219 was further developed. While Mi-219 has an almost equal affinity as Mi-63 to Mdm2, it possesses a better oral bioavailability. It can activate wild-type p53 and induce tumor cell cycle arrest and apoptosis in cultured tumor cells (Shangary et al., 2008).

In addition to these two families of Mdm2 inhibitors, the other small molecule compounds have different characteristics and abilities to block p53-Mdm2 interaction either *in vitro* or *in vivo*. Until today, all the developed compounds are still at the pre-clinical stage. To make better anti-cancer drugs, new compounds with higher affinities and better pharmacological properties need to be developed.

### 1.3 Centromere characterization

During cell division, the genome has to be precisely duplicated and equally distributed to daughter cells. The mammalian cell division cycle is divided into interphase and mitosis. The interphase is characterized by cell growth and DNA replication, preparing the cell for subsequent cell division. After the DNA replication checkpoint passage, cells enter into mitosis. During mitosis, replicated chromosomes, the so-called sister chromatids, have to be segregated to the two daughter cells evenly to maintain genetic stability after cell division. The proper chromosome segregation is ensured by a specialized chromosome structure, the centromere, which holds the sister chromatids together and later acts as an assembly site for kinetochore formation during mitosis. The kinetochore is a multi-protein complex attached to the centromere, which connects the chromosomes with microtubules of the mitotic spindle, and thus plays a key role in accurate chromosome segregation.

Although centromeres exist in a broad range of eukaryotes from yeast to human, they are quite different in size and structure in these organisms. Additionally, in comparison to non-centromeric chromatin on the genome, the DNA and histones at centromeres are unique, characterized by specific DNA repeat elements and epigenetic modifications.

#### 1.3.1 Centromeric DNA

The DNA sequence that typically forms a centromere was first identified on chromosome III in the budding yeast *Saccharomyces cerevisiae* as a region required for normal centromere function (Clarke and Carbon, 1980). The centromere found in budding yeast, the so-called point centromere as it is quite small in size, harbors only one centromeric histone and the underlying DNA sequence is specific and conserved for budding yeast. It consists of the centromere DNA element I, II and III (CDE I, CDE II and CDE III) (Clarke and Carbon, 1980; Fitzgerald-Hayes et al., 1982; Hieter et al., 1985) (Fig. 13). These three DNA elements form a ~125 bp region on the chromosome and are sufficient for mitotic stability since this DNA sequences could enable a plasmid to function as a chromosome both mitotically and meiotically when it was artificially introduced into the plasmid. A single point mutation (cytosine (C) to thymidine (T)) in the conserved region of CDE III caused centromere function deficiency and is lethal to yeast cells (McGrew et al., 1986). Reconstruction of electronic micrographs (Winey et al., 1995) and other methods (Henikoff and Henikoff, 2012) showed that only one microtubule attaches to this point centromere site.

In comparison to the centromere of budding yeast, the centromere of fission yeast *Schizosaccharomyces pombe* consists of a longer centromeric DNA, ranging from 30 to 100 kb. It has a central region, cnt, flanked by inverted DNA repeat sequences at both left and right side (imrL and imrR) (Chikashige et al., 1989; Hahnenberger et al., 1989; Murakami et al., 1991). Repetitive outer repeats (otr) localize at both sides of the central region formed by cnt and imr (Clarke and Baum 1990; Hahnenberger et al., 1991; Kuhn



et al., 1991; Polizzi and Clarke 1991) (Fig. 13). In contrast to the point centromere of budding yeast, the centromere of fission yeast is called a regional centromere, which has a relatively big size and multiple microtubule attachment sites. Most importantly, the regional centromere has no specific conserved DNA sequence to determine centromere localization.

Regional centromeres can also be found in mammalian cells. The human centromere is quite large; it contains 171-bp tandem repeats, the so-called  $\alpha$ -satellite DNA which are up to 5 Mb long.  $\alpha$ -satellite DNA contains a 17-bp sequence element called CENP-B box, which is recognized by centromeric protein B (Earnshaw and Rothfield, 1985; Valdivia and Brinkley, 1985). Interestingly, the  $\alpha$ -satellite and the CENP-B protein are both not necessary to form a functional centromere. Similar to the human centromere, the mouse centromere consists of a 120-bp tandem repeat, the minor satellite DNA (Wong and Rattner, 1988). A comparison of yeast and human centromere is shown in figure 13.

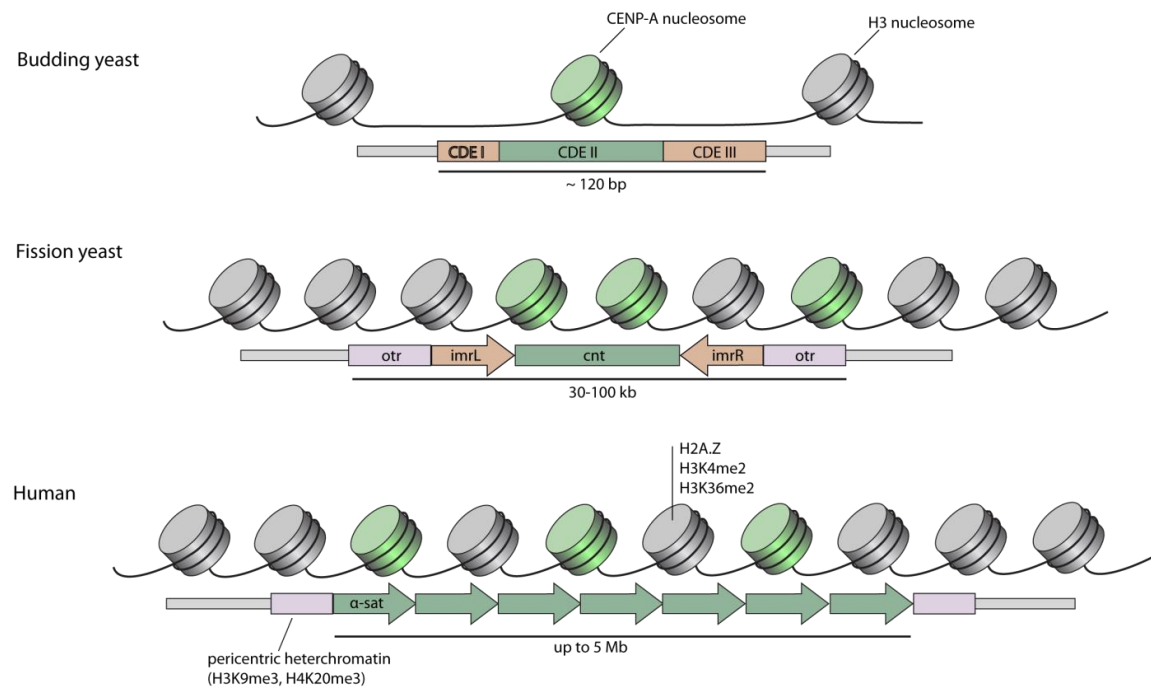


Fig. 13 Centromere features in different species. While budding yeast has a point centromere with a single CENP-A nucleosome, fission yeast and human have regional centromeres with larger size. Mammalian centromeres also contain certain histone variants and histone modification marks. (Based on Verdaasdonk and Bloom, 2011).

### 1.3.2 Specific histones at centromeres

The centromere structure and size vary between different eukaryotic species. However, all functional centromeres contain a centromere-specific histone H3 variant, CENP-A. CENP-A was first identified parallel with two other centromere proteins, CENP-B and CENP-C (Earnshaw and Rothfield, 1985). It was co-purified with core histones and also

with nucleosome particles, suggesting being a histone variant, which substitutes canonical histones at centromeres (Palmer et al., 1987). Protein and DNA sequence analyses demonstrated high sequence similarities between CENP-A and histone H3 (Palmer et al., 1991; Sullivan et al., 1994). Furthermore, it was shown that the C-terminus of CENP-A is homologous to H3, and that this C-terminal part is responsible for its tetramer formation with histone H4 (Sullivan et al., 1994; Shelby et al., 1997; Black et al., 2004). The C-terminal CENP-A centromere-targeting domain (CATD) is required for CENP-A centromere targeting and function (Black et al., 2004; Black et al., 2007; Guse et al., 2011).

The CENP-A nucleosome is also unique. In budding yeast, the centromeric DNA sequences are quite short, with only about 125 base-pair length. This short centromeric DNA together with histones forms one centromeric nucleosome which contains CENP-A (also called Cse4). This single CENP-A containing nucleosome is responsible for the kinetochore formation and microtubule binding (Furuyama and Biggins, 2007; Krassovsky et al., 2011). The composition of this CENP-A containing nucleosome is similar to the canonical nucleosome, except for the substitution of the canonical histone H3 with CENP-A (Westmann et al., 2003). In addition, recent publications demonstrated that H2A/H2B dimers at the centromere in yeast are substituted by the non-histone protein Scm3 (Camahort et al., 2007; Mizuguchi et al., 2007; Stoler et al., 2007). Scm3 dimerizes and binds to the CENP-A-H4 tetramer, forming a hexamer (Mizuguchi et al., 2007). Scm3 replaces the function of H2A/H2B at centomere, and it also is important for CENP-A incorporation and cell cycle progression (Camahort et al., 2007; Stoler et al., 2007).

The differences between the CENP-A nucleosome and the canonical H3 nucleosome were studied. *In vitro* studies of the human CENP-A nucleosome showed that it is not as stable as the canonical H3 nucleosome (Conde e Silva et al., 2007), which may facilitate the removal of mis-incorporated CENP-A from the non-centromeric chromatin. But there were also opposite opinions, the crystal structure of the human CENP-A nucleosome showed that the CENP-A nucleosome has two extra amino acid residues in the loop 1 region, which may stabilize the CENP-A nucleosome (Tachiwana et al., 2011).

Although there are lots of studies about the CENP-A nucleosome, the structure of CENP-A nucleosome is still unclear. Till now, two different structures of CENP-A nucleosome in mammalian cell have been published. The first structure shows that it contains an octameric histone core consisting of two histone tetramers (H2A, H2B, H4 and CENP-A), wrapped by DNA in a left-handed orientation (Tachiwana et al., 2011). The second structure shows that it contains only one heterotypic tetramer composed by each of the histone, and the DNA is wrapped around in a right-handed way. The CENP-A nucleosome is shown more condensed than canonical nucleosomes, and the DNA at the entry/exit sites is less constrained (Panchenko et al., 2011). This different observation on the

structures of CENP-A nucleosomes is controversial, suggesting a dynamical structure of CENP-A nucleosome and some complexity of CENP-A nucleosome organization.

### 1.3.3 Epigenetic features of the centromere

#### 1.3.3.1 DNA methylation at the centromere

DNA methylation is an epigenetic repressive mark, which plays important roles in processes like gene silencing and is essential for chromatin structure and genome stability (Lorincz et al., 2004; Thomson et al., 2010; Rizwana and Hahn, 1999). Methylation of centromeric DNA was observed in plant (Luo and Preuss, 2003), but hypomethylation of DNA at active centromeres were shown in *Arabidopsis* and maize (Zhang et al., 2008; Koo et al., 2011), with yet unknown function.

The functional role of centromeric DNA methylation is still unclear. However, it was shown that the centromere mitotic recombination in murine cells was regulated by the epigenetic state of the centromeric heterochromatin, especially by DNA methylation (Jaco et al., 2008). The importance of proper regulation is demonstrated in a human genetic disease called Immunodeficiency, Centromeric region instability, Facial anomalies (ICF) syndrome. This disease is characterized by genome instability caused by *DNMT3b* gene deficiency (Xu et al., 1999; Hansen et al., 1999). DNMT3b is one of the two active *de novo* methyltransferases. In ICF patient cells, the DNA methylation of satellite 2 DNA on chromosome 1 and on chromosome 16, satellite 3 DNA on chromosome 9, are lost due to *DNMT3b* deficiency (Jeanpierre et al., 1993; Tuck-Muller et al., 2000). These unmethylated satellites lead to de-condensation of the centromere regions resulting in instability of the genome. CENP-C was found to interact with and to recruit Dnmt3b to centromere regions to methylate centromeric DNA (Gopalakrishnan et al., 2009).

#### 1.3.3.2 Histone variants and modifications at the centromere

In addition to DNA methylation, histone modifications are important epigenetic modifications in eukaryotes. Histone tails can be targeted by several post-translational modifications such as methylation, acetylation, phosphorylation and ubiquitination at specific amino acid residues such as lysine, arginine and serine (Kuo et al., 1996; Grunstein, 1997; Mahadevan et al., 1991; reviewed by Suganuma and Workman, 2011). These histone modification marks can be recognized by specific 'reader' proteins to keep the chromatin in a condensed or open state. Until now, the only known post-translational modification of CENP-A is the phosphorylation of serine 7 catalyzed by Aurora A and B (Zeitlin et al., 2001; Kunitoku et al., 2003). This modification occurs at prophase and is required for proper localization of Aurora B at the inner kinetochore in prometaphase, and loss of this modification led to defects of kinetochore attachment to microtubules (Zeitlin et al., 2001; Kunitoku et al., 2003; Slattery et al., 2008).

In mammals, blocks of CENP-A nucleosomes and H3 nucleosomes are arranged in an alternating pattern at the centromeric region. The centromeric H3 nucleosome is also characterized by special histone modifications. H3 threonine 3 phosphorylation (H3T3ph) at the centromere catalyzed by Haspin was shown to be necessary for the accumulation of the Aurora B containing chromosomal passenger complex (CPC) (Wang et al., 2010). In addition, H2A serine 121 phosphorylation (H2AS121ph) catalyzed by Bub1 together with the H3T3ph modification target CPC to the kinetochore (Yamagishi et al., 2010). In contrast to pericentric heterochromatin, featuring high levels of histone H3 lysine 9 trimethylation (H3K9me3), centromeric chromatin lacks this modification, but contains dimethylation of H3 at lysine 4 (H3K4me2) and di-methylation of H3 at lysine 36 (H3K36me2), which both are usually associated with open chromatin (Sullivan et al., 2004; Bergmann et al., 2011).

Another H2A histone variant, H2A.Z is reported to exist in the centromeric nucleosome (Greaves et al., 2007). H2A.Z-containing nucleosomes harbor an acidic region, which is important for interacting with non-histone proteins and can be recognized by chromatin remodelers (Suto et al., 2000). Since H2A.Z also serves as a boundary between heterochromatin and euchromatin to prevent heterochromatin spreading, H2A.Z was proposed to contribute to the higher order organization of centromeric chromatin (Park et al., 2004; Greaves et al., 2007).

As discussed above, the centromeric chromatin is characterized by these special histone modifications and histone variants, in difference from both typical heterochromatin and euchromatin. These unique modifications may differentiate centromeric chromatin from the pericentric heterochromatin to facilitate the integration of CENP-A. This idea is supported by some quite recent studies. Bergmann *et al* found that artificial over-acetylation at centromeric H3K9 resulted in an over-expression of the centromeric transcripts, and blocked the incorporation of CENP-A (Bergmann et al., 2012). Another study found that histone acetylation and methylation positively and negatively control the CENP-A incorporation at ectopic chromatin site respectively, and the balance between the acetylation and methylation of H3K9 at centromeric chromatin is important for the proper CENP-A deposition (Ohzeki et al., 2012). In addition, it was shown that in budding yeast, the arginine 37 of CENP-A can be methylated. This methylation regulates kinetochore integrity and chromosome segregation (Samel et al., 2012). All these studies suggest that the epigenetic state of centromeric chromatin contributes to the proper function of centromeres.

#### 1.3.4 CENP-A deposition at centromeres

CENP-A specifically localizes at the active centromere and is the main determinant of centromere localization. For its important role in centromere maintenance, CENP-A must be incorporated into centromeric chromatin after DNA replication to keep its

abundance at centromeres. So how newly synthesized CENP-A incorporates into centromeric DNA is a vital question to understand centromere maintenance.

#### 1.3.4.1 Timing of CENP-A incorporation

The first question about CENP-A incorporation is when it does happen during the cell cycle. To maintain the genetic stability, CENP-A must be incorporated into newly synthesized centromeric DNA after DNA replication. In budding yeast, newly synthesized CENP-A incorporates into the chromatin during S phase, while DNA is replicated (Pearson et al., 2004). In contrast, in fission yeast, the incorporation occurs during S phase at which time the CENP-A expression level is at its peak, and further incorporates during the G2 phase of the cell cycle (Dunleavy et al., 2007; Takayama et al., 2008). In human cells, CENP-A incorporation is uncoupled from DNA replication since the CENP-A expression level is quite low at this time, and the expression level increases and peaks in G2 phase (Shelby et al., 2000). However, new CENP-A incorporation happens during telophase and G1 phase rather than in G2 phase (Hemmerich et al., 2008; Jansen et al., 2007). So the time point of CENP-A incorporation varies in different species. Interestingly, in human cells, the incorporation of CENP-A is gapped by mitosis, indicating that the level of CENP-A nucleosomes in mitosis is not at its peak, the function of this gap has to be further studied.

#### 1.3.4.2 The role of histone chaperons in CENP-A incorporation

It is known that the other two H3 variants, H3.1 and H3.3, are deposited by the histone chaperones, CAF1 (chromatin assembly factor 1) and HIRA (HIR histone cell cycle regulation defective homolog A) respectively. These two chaperones may also play a role in CENP-A deposition in yeast but not in human (Walfridsson et al., 2005; Foltz et al., 2006; Dunleavy et al., 2009; Foltz et al., 2009). Affinity purifications followed by mass spectrometry experiments identified the Holliday junction recognition protein (HJURP) as an interaction partner of soluble CENP-A (Dunleavy et al., 2009; Foltz et al., 2009). HJURP localizes at the centromere in G1 phase during CENP-A loading, suggesting a role in the CENP-A deposition. Additionally, knockdown of HJURP using siRNA led to a reduced protein level of CENP-A at the centromere (Foltz et al., 2009). A later study showed that HJURP directly interacts with the CATD domain of CENP-A via its N-terminal TLTY box (Shuaib et al., 2010). Additionally, Xiao *et al* found that HJURP efficiently promotes *in vitro* reconstitution of CENP-A nucleosomes (Xiao et al., 2011). These studies identified HJURP as the chaperone of CENP-A and showed that it plays an important role in CENP-A deposition.

#### 1.3.4.3 Three-step model for CENP-A chromatin establishment

CENP-A incorporation is divided into several steps including priming, uploading and maintenance. During the priming step, CENP-A is licensed to incorporate into centromeric nucleosomes. The uploading step occurs at early G1 phase, when newly

synthesized CENP-A is further incorporated into centromeric chromatin mediated by HJURP. Chromatin remodelers such as FACT (P140/P80) are also involved in this process (Foltz et al., 2006; Izuta et al., 2006, Perpelescu et al., 2009). After CENP-A is deposited into chromatin, CENP-A nucleosomes are stabilized and retained only at centromeres, avoiding loss or overspreading by the maintenance factors. ATP-dependent nucleosome remodeling, the spacing factor complex (RSF) and MgcRacGAP were shown to participate in the maintenance step (Perpelescu et al., 2009; Lagana et al., 2010).

The most important protein complex during the priming step is the Mis18 complex. The Mis18 complex is composed of Mis18 $\alpha$ , Mis18 $\beta$  and M18bp1 (mammalian homolog of *C. elegans* KNL2). This complex is shown to localize at the kinetochore in telophase and G1 phase, and knock down of the complex abolishes the recruitment of newly synthesized CENP-A to the centromere. However, no direct protein interaction between CENP-A and the Mis18 complex was detected so far (Carroll et al., 2009). Although the Mis18 complex is suggested to be involved in the histone acetylation regulation, the mechanism how the complex mediates CENP-A priming is still not clear.

## 1.4 The kinetochore structure and CCAN (Constant Centromere Associated Network)

### 1.4.1 The kinetochore structure

The kinetochore is a multi-protein complex, which assembles at centromeres in mitosis. It connects the chromosome and the mitotic spindle to ensure accurate chromosome segregation. In vertebrates, only one functional kinetochore on each single chromosome is found in normal condition. Abnormal kinetochore assembly (e.g. on non-centromeric or di-centromeric chromosomes) results in genome instability, leading to cell death or cancer formation. So it is quite important to elucidate the kinetochore structure and also the mechanism of kinetochore assembly. The regulation of the kinetochore formation is essential to maintain genomic stability of the cells.

Early studies by electron microscopy showed that the kinetochore has a three-layer structure, with an electron-dense inner plate and an outer plate separated by an electron-light layer. Based on these electron microscopy studies, a model of kinetochore is shown in Fig. 14.

In the last two decades many proteins forming this three-layer structure were identified using different biochemical approaches. CENP-A, CENP-B and CENP-C were first characterized using sera from autoimmune disease CREST patient in 1980s (Earnshaw and Rothfield, 1985). Next, CENP-H and CENP-I were found to be localized at the centromere constitutively in all cell cycle phases (Sugata et al., 1999; Nishihashi et al., 2002). Later, using pull-down assay, the interphase centromere (ICEN) complex, which contains about 40 proteins, was identified to associate with CENP-A nucleosomes in HeLa cells (Obuse et al., 2004). In 2006, more proteins which associate with centromere were identified by three independent research groups in human and chicken cells, and these proteins were named from CENP-K to CENP-U (Foltz et al., 2006; Izuta et al., 2006; Okada et al., 2006). Two years later, CENP-W (Hori et al., 2008b) and CENP-X were characterized as interaction partner of CENP-T and CENP-S, respectively (Amano et al., 2009).

These proteomics studies identified many new proteins locating at the kinetochore, some of which are not centromere proteins, such as SMARC5 (components of chromatin remodeling complex), BMI1 (member of polycomb complex), DDB1 and Cul4A (E3-ligase complex member) (Obuse et al., 2004). These non-centromeric proteins are present at the centromere only for a short time during the cell cycle.

Among all the proteins associating with the centromere, some 'core' proteins localize at the centromere during the whole cell cycle and were identified by different groups using different methods. This group of proteins together was termed constitutive centromere associated network, CCAN (Cheeseman and Desai, 2008; Hori et al., 2008a, b). Another group of proteins, composed of KNL1, Mis12 complex, Ndc80 complex, were termed

KMN network, which connects the CCAN with the mitotic spindle (Cheeseman et al., 2006) (Fig 14).

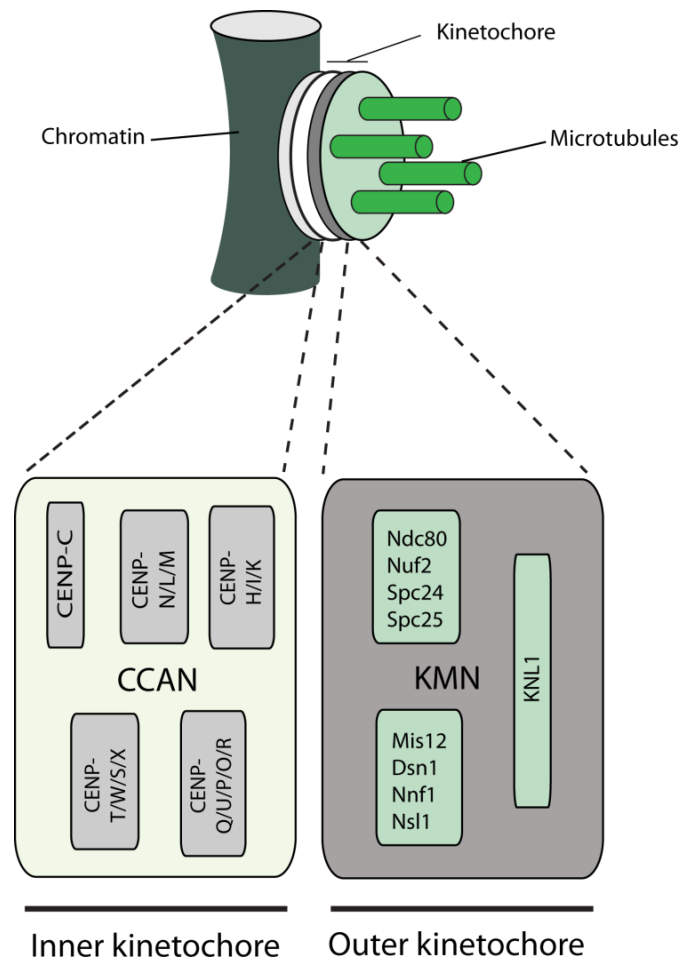


Fig. 14 Model of the kinetochore structure. Upper model shows the tri-layer structure of the kinetochore based on EM studies. The kinetochore connects the chromosome (blue) with microtubules (dark green). The inner kinetochore is composed of CCAN proteins, including five groups of CENPs. The outer kinetochore includes three groups of proteins, the so-called KMN network. (Modified from Perpelescu and Fukugawa, 2011).

## 1.4.2 Constant centromere associated network

Besides CENP-A, 15 other CENPs were identified as CCAN components. Until today, little is known about the function and organization of these CCANs. Based on differences identified by biochemical and genetic analyses, these proteins are divided into several subgroups.

### 1.4.2.1 CENP-A/B/C

CENP-A, B, C were identified using chromatin IP (ChIP), and they were proposed to form a pre-kinetochore in human cells (Ando et al., 2002). CENP-B contains a domain which is similar to the transposase of pogo transposable element. As a transposon-derived protein, the function of CENP-B in kinetochore formation is not clear. Human CENP-B binds to  $\alpha$ -satellite DNA which contains a 17 bp CENP-B box sequences. However, *cenp-b*



knockout mice are viable and do not show mitotic or meiotic defects or any other severe phenotype (Hudson et al., 1998; Perez-Castro et al., 1998; Fowler et al., 2000). In yeast, there are three homologs of the *cenp-b* gene, which are involved in promoting retrotransposon DNA replication (Zaratiegui et al., 2011) and in the regulation of DNA recombination (Matsuda et al., 2011).

CENP-C shows DNA binding activity and it binds to centromeric chromatin. It co-immunoprecipitates with histone H3 nucleosomes but does not directly bind to CENP-A containing nucleosomes (Ando et al., 2002; Hori et al., 2008a). The  $\alpha$ -satellite transcript may also play a role in CENP-C kinetochore binding (Chan et al., 2012). Its N terminal part is shown to be important for targeting proteins such as CENP-K, CENP-E, Mad2 and Mis12 complex (Kwon et al., 2007; Liu et al., 2006; Milks et al., 2009). And its C-terminus contains a motif responsible for its dimerization. Being considered as the platform of kinetochore assembly, CENP-C interacts with Nnf1 and Nsl1. These two proteins are components of Mis12 complex which is a part of the outer kinetochore. Besides Mis12 complex components, CENP-C also forms a complex with kinetochore protein KNL-1 and Ndc80 (Screpanti et al., 2011; Przewloka et al., 2011). Inhibition of its function results in defects in centromere and kinetochore assembly (Saitoh et al., 1992; Brown et al., 1993; Tomkiel et al., 1994; Fukagawa and Brow, 1997; Fukagawa et al., 1999; Kown et al., 2007).

#### 1.4.2.2 CENP-H/I/K

CENP-H was identified as centromeric protein because it colocalizes with CENP-B and CENP-C throughout the cell cycle (Sugata et al., 1999; 2000). CENP-H is required for kinetochore localization of most CCAN proteins but not for CENP-A (Fukugawa et al., 2001; Okada et al., 2006; Kwon et al., 2007). Moreover, its centromeric localization depends on CENP-A, CENP-I, CENP-K, CENP-M, CENP-N and CENP-T (Okada et al., 2006; Cheeseman et al., 2008; Foltz et al., 2006; Hori et al., 2008b).

CENP-I is a binding partner of CENP-H, and its conditional loss-of-function mutant results in prolonged prometaphase and misregulated cytokinesis in chicken DT-40 cells (Nishihashi et al., 2002). Additionally, CENP-I is required for the recruitment of CENP-F, Mad1 and Mad2 to the kinetochore, and its depletion lead to cell cycle arrest in G2 phase in HeLa cells (Liu et al., 2003). CENP-I and CENP-H are important for CENP-A deposition at centromere since CENP-A deposition is reduced in CENP-H, -I or -K deficient cells (Okada et al., 2006). CENP-K is required for CENP-Q, CENP-H and KNL-1 kinetochore localization, and also acts together with KNL-1 to recruit Ndc80 to the kinetochore (Cheeseman et al., 2008).

#### 1.4.2.3 CENP-L/M/N

CENP-L/M/N was co-purified with CENP-H/I/K, and their kinetochore localization is inter-

dependent. In addition, the knockdown of any of these three proteins results in strong mitotic defects (Okada et al., 2006).

siRNA- mediated knockdown of CENP-L induced monopolar spindles in mitotic cells (McClelland et al., 2007). CENP-L interacts with CENP-N *in vitro* (Carroll et al., 2009), but its function has to be studied further.

CENP-M was first identified as ICEN39 (Foltz et al., 2006), and also was identified as a NAC (CENP-A nucleosome associated complex) protein (Izuta et al., 2006). CENP-M is required for the localization of several CENPs at the kinetochore, including CENP-H class and CENP-O class proteins. Knockout of CENP-M lead to mitotic error and aneuploidy (Foltz et al., 2006; Izuta et al., 2006; Okada et al., 2006). *In vitro* experiments showed that CENP-N interacts directly with CENP-A nucleosome via its N-terminal part, while the C-terminus is responsible for its interaction with other CENPs such as CENP-H, CENP-K and CENP-L (Carroll et al., 2009).

#### 1.4.2.4 CENP-O/P/Q/U/R

CENP-O class proteins form a complex and knockouts of this class of genes are viable but are characterized by slow proliferation and mitotic defects. The kinetochore localization of CENP-O, -P, -Q, -U is interdependent, but CENP-R is not required for the centromeric localization of the other members. And when expressed in *E. coli*, the CENP-O class proteins were purified as a complex, suggesting CENP-O, -P, -Q, and -U form a tight complex (Hori et al., 2008b).

CENP-U is the most studied protein in this group. CENP-U knockout cells are viable, but it is required for spindle function (Foltz et al., 2006; Hori et al., 2008b). It was shown that CENP-U is a microtubule binding protein and plays an important role in kinetochore-microtubule attachment (Hua et al., 2011).

#### 1.4.2.5 CENP-S/X/T/W

CENP-T and CENP-W interact with each other to form a tight complex. In parallel with CENP-C group proteins, the localization of CENP-T/W group proteins at the kinetochore is independent of other CENP group proteins. CENP-T has a C-terminal histone fold domain (HFD), which was suggested to have DNA binding activity (Hori et al., 2008; Suzuki et al., 2011). CENP-W is a small protein with only 88 amino acids residues folding into a HFD structure. CENP-T interacts with CENP-W via its HFD domain. The long N-terminal tail of CENP-T binds to the outer kinetochore component Ndc80 and induces kinetochore- like structures (Gascoigne et al., 2011), suggesting a model that the C-terminus of CENP-T together with CENP-W forms a complex which could bind DNA. The N-terminus of CENP-T binds to outer kinetochore Ndc80 connecting the centromeric chromatin and outer kinetochore. CENP-T/W proteins are further proposed to have a role in kinetochore determination (Prendergast et al., 2011).

CENP-W was also reported to be an RNA-associated nuclear matrix protein, which interacts with and stabilize B23 (Chun et al., 2011). CENP-S was identified as interaction partner of CENP-M and CENP-U (Foltz et al., 2006). CENP-X was identified by CENP-S pull-down followed by mass spectrometric analysis (Amano et al., 2009). Both CENP-S and CENP-X deficient cells are viable, but show defects in mitotic progression. CENP-S and CENP-X are necessary targeting proteins such as KNL1 and Ndc80 to the outer kinetochore. Interestingly, like CENP-T and CENP-W, CENP-S and CENP-X also have potential histone-fold domains. And there is evidence that CENP-S interacts with CENP-T (Amano et al., 2009), indicating a connection between the two groups of proteins.



## 1.5 Aims of this work

Protein-protein interactions are important targets for drug design. A variety of methods for protein-protein interaction inhibitor screening were developed. But these methods all have their own limits such as incapability to assess the membrane permeability of the drugs or low sensitivity. To establish a new *in vivo* drug screening method, I aimed to develop the F3H assay into a protein-protein inhibitor screening assay, which could visualize the release of interacting proteins from the interaction complex, giving a reliable assessment of the inhibitory effect of the drug in living cells. To improve the efficiency of this assay, I also aimed to develop this assay into a 96-well format (Chapter 2.1), hoping to develop a new way for protein-protein interaction inhibitor screening.

During the last two decades, good progress has been made towards a better understanding of the kinetochore structure and the mechanism of centromere maintenance. Although many proteins involved in kinetochore assembly were identified, how these proteins cooperate and assemble into kinetochores remains elusive. Therefore, in this thesis, I aimed to elucidate the assembly of CCAN proteins into the kinetochore and the potential role of CCAN proteins in CENP-A incorporation by using our F3H Assay, this new *in vivo* protein interaction study method.

First, I aimed to elucidate how M18bp1 is recruited to the centromere. As a member of the Mis18 complex, M18bp1 is a key protein involving in control of CENP-A incorporation. Although it is revealed that the centromeric localization of M18bp1 occurs just before CENP-A incorporation, nothing is known about how it is recruited to the centromere. To elucidate the potential role of CCAN proteins in the centromeric recruitment of M18bp1, I planned to immobilize M18bp1 at an artificial chromosomal focus, to screen the potential interacting centromere proteins by F3H assay. siRNA-mediated knock-down experiments could be performed to further reveal the roles of the interaction in CENP-A incorporation (Chapter 2.2).

CCANs are a serial of proteins that form the inner kinetochore. Although these CCANs are divided into different groups according to their similarities and dependencies in kinetochore assembly, it is largely unknown how these CCAN proteins assemble into the kinetochore. I aimed to systematically study the interactions between the 16 CCAN proteins (unpublished data) to reveal the organization of CCAN in the kinetochore. I specially focused on one sub-group of the CCAN, CENP-P/O/R/Q/U. The existing model suggested that the CENP-P/O/R/Q/U group proteins pre-assemble into one unit, and then this pre-assembled sub-complex is packaged into the kinetochore as a whole unit. I aimed to test this hypothesis by analyzing the interactions of the five members in this sub-group with the F3H assay (Chapter 2.3).

Moreover, since the F3H assay is a versatile tool to study protein interactions *in vivo*, I also tried to apply this technology to study the interactions between human proteins and virus proteins, to better understand the function of huRNP K in EBV infection (Chapter 2.4).



## 2. Results

### 2.1 Visualization and Targeted Disruption of Protein Interactions in Living Cells

---





ARTICLE

Received 22 May 2013 | Accepted 23 Sep 2013 | Published 24 Oct 2013

DOI: 10.1038/ncomms3660

OPEN

# Visualization and targeted disruption of protein interactions in living cells

Henry D. Herce<sup>1,\*</sup>, Wen Deng<sup>2,\*</sup>, Jonas Helma<sup>2</sup>, Heinrich Leonhardt<sup>2</sup> & M. Cristina Cardoso<sup>1</sup>

Protein-protein interactions are the basis of all processes in living cells, but most studies of these interactions rely on biochemical *in vitro* assays. Here we present a simple and versatile fluorescent-three-hybrid (F3H) strategy to visualize and target protein-protein interactions. A high-affinity nanobody anchors a GFP-fusion protein of interest at a defined cellular structure and the enrichment of red-labelled interacting proteins is measured at these sites. With this approach, we visualize the p53-HDM2 interaction in living cells and directly monitor the disruption of this interaction by Nutlin 3, a drug developed to boost p53 activity in cancer therapy. We further use this approach to develop a cell-permeable vector that releases a highly specific peptide disrupting the p53 and HDM2 interaction. The availability of multiple anchor sites and the simple optical readout of this nanobody-based capture assay enable systematic and versatile analyses of protein-protein interactions in practically any cell type and species.

<sup>1</sup>Department of Biology, Technische Universität Darmstadt, 64287 Darmstadt, Germany. <sup>2</sup>Department of Biology II, Center for Integrated Protein Science Munich, Ludwig Maximilians University Munich, 82152 Planegg-Martinsried, Germany. \* These authors contributed equally to this work. Correspondence and requests for materials should be addressed to M.C.C. (email: cardoso@bio.tu-darmstadt.de) or to H.L. (email: h.leonhardt@lmu.de)

Great effort has been invested in the development of methods to identify protein interactions and screen for drugs that target specific protein–protein interactions. Although several useful *in vitro* methods have been developed, most of these assays disregard the innate complexity of living cells. In a live cell, protein–protein interactions are subjected to many influences such as subcellular localization, competitive interaction with other cellular factors and post-translational modifications. Drugs are usually screened *in vitro* in a very controlled and artificial environment. However, to work *in vivo*, the drugs must cross the cell plasma membrane and then reach their target protein in the respective subcellular compartments. Furthermore, the drug should also have enough specificity to compete and interact exclusively with its target minimizing its potential interaction with thousands of other intracellular compounds.

The most used method to study protein–protein interactions in cells is the yeast two-hybrid system (Y2H) (ref. 1). This method has a clear advantage over classical *in vitro* biochemical approaches such as co-(immuno)precipitation and co-purification analyses, as it embodies an *in vivo* technique using the yeast host cell as a live test tube. The Y2H is based on the activation of the expression of a downstream reporter gene mediated by the binding between two proteins of interest. Ultimately, this gene expression drives a change in yeast cell's phenotype that can be indirectly linked back to the interaction between the proteins under study. This method has been widely used because of its high-throughput screening capability and powerful ability to identify unknown protein-binding partners. A natural obstacle is that the two-hybrid system makes use of the yeast *Sacharomyces cerevisiae* as a host and uses a specific reporter gene. This imposes limitations upon interactions specific to mammalian pathways that do not occur in yeast and/or do not take place in the (yeast) cell nucleus. Furthermore, it relies on activation of gene expression and, as a consequence, cannot be used with proteins that are self-activating by themselves. Several fluorescent techniques such as FRET/FLIM have been developed during the last years as alternatives to study protein–protein interactions<sup>2,3</sup>. These methods require specialized equipment, special fluorophore combinations, specific acquisition software tools and/or complex post acquisition data analysis.

Here we propose a simple and general method that can be applied and adapted to study protein interactions in any species, cell type and intracellular compartment. A major advantage is that this technology does not depend on the activation of any specific reporter gene and the interaction between proteins can be studied in real time at any location within a live cell. This strategy is based on a high-affinity anti-GFP nanobody. This anti-GFP nanobody was screened and optimized to reach an affinity to GFP in the subnanoMolar range<sup>4</sup>. The basic rationale of the method is shown in Fig. 1a. A protein with high affinity to GFP (GFP-binding nanobody), which we call GFP binder protein (GBP), is covalently linked to a protein that accumulates at a specific location within the cell. We call these fusions between GBP and a localization protein (LP) GBP–LP. In this way, a GFP-labelled protein is artificially recruited to a specific location. Using a different fluorescent label for the second protein of interest then allows easy detection and measurement of the interaction between the two proteins (hence fluorescence three-hybrid assay—F3H). A convenient aspect of this method is that, after the GBP–LP plasmid is constructed, the same intracellular location determined by the LP can be used to study the interaction between any numbers of proteins where one of them is labelled with GFP.

To establish and validate the basis of this strategy, we focused on the binding and disruption of p53 and HDM2 (human double minute 2) as this is one of the most important protein interactions in cancer research. The tumour suppressor p53, also named the ‘guardian of the genome’, is the main mediator of apoptosis, cell cycle arrest and senescence in response to a broad range of DNA damages and other cellular stresses (Fig. 1b). Depending on the stress signal, p53 gets modified and activated by upstream mediators that lead p53 to activate diverse genes and response pathways. The induction of high levels of p53 prevents inappropriate propagation of mutant cells. The intracellular p53 level is the single most important determinant of its function and HDM2 is the principal cellular antagonist of p53, blocking its tumour suppressor function by binding to its transcription activation domain. The two proteins bind to each other as part of a negative autoregulatory loop aimed to keep low p53 levels in the absence of stress. HDM2 blocks p53 by binding to its

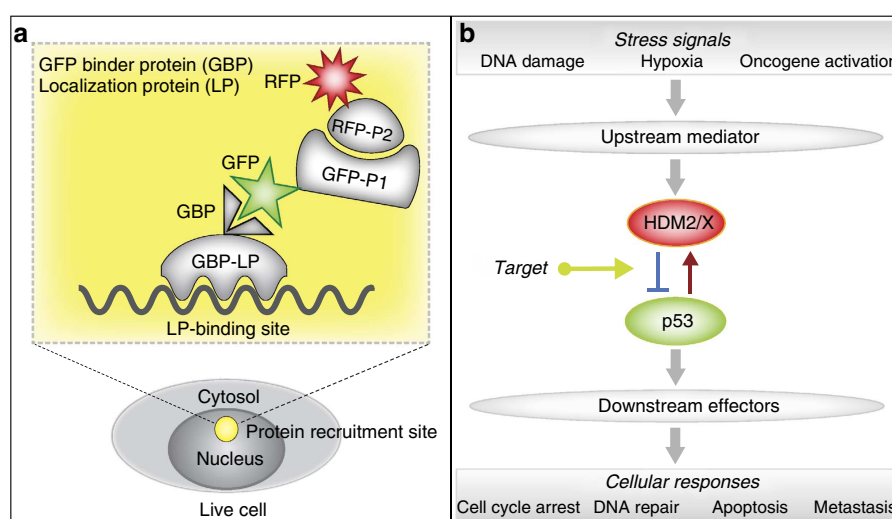


**Figure 1 | Strategy for visualizing protein interactions in living cells and outline of a fundamental biological application. (a)** Schematic representation of the fluorescence three-hybrid (F3H) to study protein–protein interactions. A GFP binder protein (GBP) is attached to a protein (LP) that accumulates at a well-defined location within the cell. This complex recruits to that particular location GFP-tagged proteins (GFP-P1). If the protein P1 interacts with a second protein P2, labelled with a different fluorescent marker, the interaction can be immediately visualized using fluorescent microscopy. **(b)** Schematic representation of the interaction between p53 and HDM2/X and its central role in cellular regulation and genome preservation.

transcription domain and reduces its levels acting as an E3 ubiquitin ligase polyubiquitinating p53 and targeting it for degradation<sup>5,6</sup>. In all cancers, the functions of p53 are limited allowing these cells to evade apoptosis and cell growth arrest<sup>7</sup>. About half of all cancers retain wild-type fully functional p53 (ref. 8) and in these the normal regulation of p53 is in many cases disrupted through direct overexpression of HDM2<sup>9</sup>. Overexpression of HDM2 provides a growth advantage to cells, promotes tumorigenesis and correlates with very poor response to cancer therapy and consequently bad prognosis<sup>9–12</sup>. Simultaneous mutation of p53 and amplification of HDM2 does not generally occur within the same tumour, suggesting that HDM2 amplification is an effective way to block p53 function<sup>9,13,14</sup>.

We present a simple visualization method for immediate recognition of protein–protein interactions, which represents a first step in capturing the kinetics of protein–protein interaction and for high-throughput methods. These types of studies are central to expand our mechanistic understanding of drug function *in vivo*.

## Results

**Visualizing and quantifying interactions in live cells.** The F3H assay offers the opportunity to determine whether the proteins are interacting from a single-fluorescence snapshot as shown in Fig. 2. To visualize the interaction between p53 and HDM2, we coupled the GBP to the Lac repressor (LacI). In cell lines where an array composed of *Lac* operator DNA sequence repeats has been stably integrated in the genome, such as in baby hamster kidney (BHK) cells<sup>15</sup>, the GBP–LacI binds to the *Lac* operator array (*LacO*). This recruits GFP-labelled proteins to the *LacO* region within the nucleus. If a second protein labelled with a different fluorescent molecule interacts with the GFP-labelled protein, then it will also display an accumulation at the *LacO* region. As shown in Fig. 2 without tethering to a particular location the difference in correlation between images (a) and (b) is very weak and the interaction or lack thereof would be difficult to score. Using the GBP–LacI sharply enhances the correlation contrast between interacting and non-interacting proteins. This can be used to determine in single snapshots the interaction between proteins of

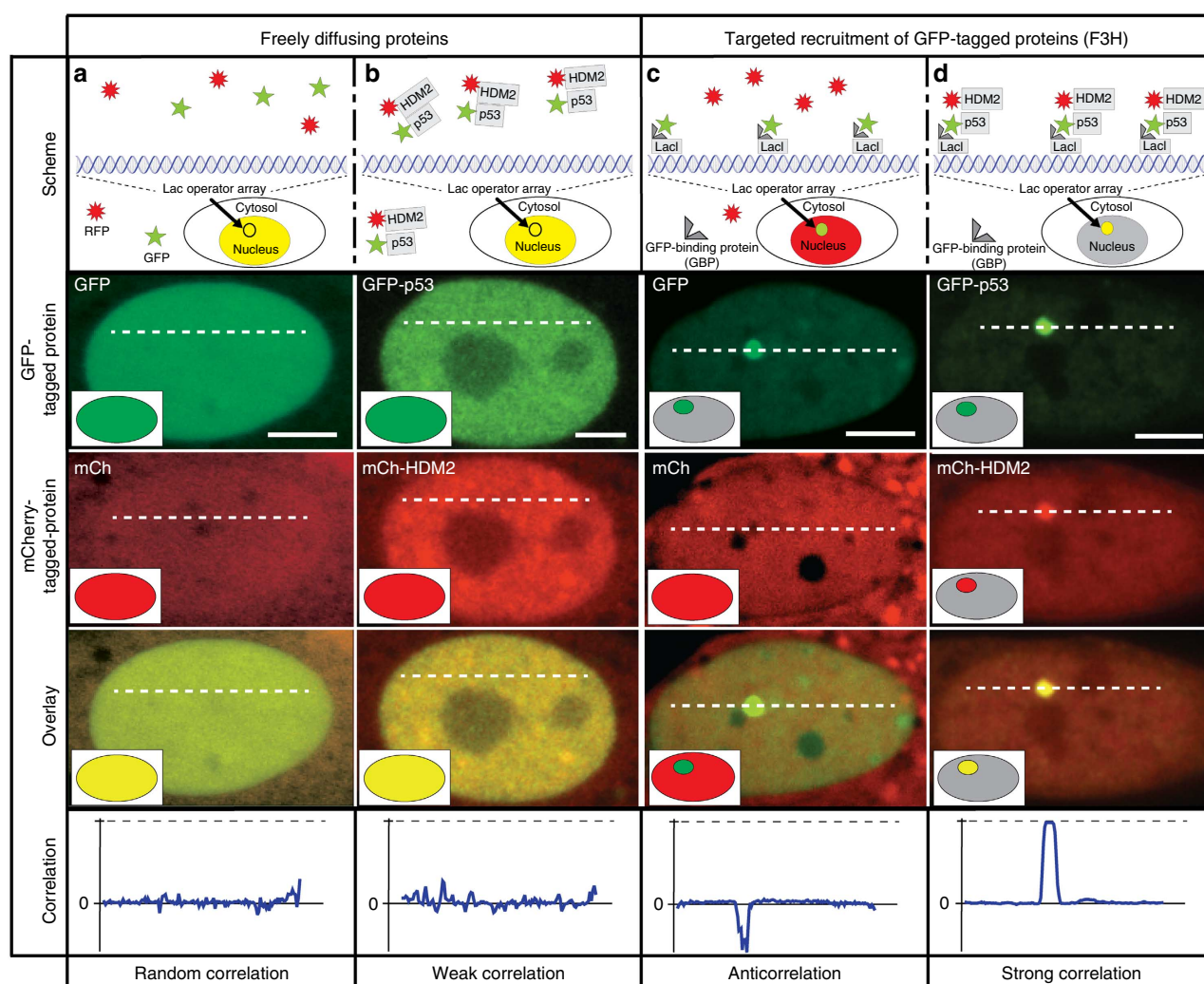


**Figure 2 | Targeted recruitment of GFP-tagged proteins allows visualization and quantification of protein–protein interactions in live cells.**

Re-localization of GFP-tagged proteins (tethered; immobilized; recruited) to the *Lac* operator using the GBP–LacI. Confocal microscopy images of non-interacting GFP and mCherry are shown and interacting GFP–p53 (pNeG–p53(NTD)) and mCh–HDM2 (pCAG–Ch–HDM2(NTD)) proteins in live cells co-transfected with and without the GBP–LacI. In the first row, a schematic representation of the transfected constructs and the respective protein distribution is shown, in the second row, a confocal image of the GFP-tagged protein, in the third row, an image of the mCherry-tagged protein, in the fourth row, the overlay of the two previous channels and in the last row, the derivative of the Pearson's correlation coefficient between the GFP image and the mCherry image along the dotted line drawn in the confocal images. In columns (a–d) representative images of cells transiently transfected with the constructs indicated in the respective schemes above are shown. Scale bar, 5  $\mu$ m.



interest. This fast and efficient visualization strategy allows following in real time the dynamics of intracellular processes and the effects of inhibitors.

**Inhibition kinetics of p53–HDM2 binding induced by Nutlin 3.** The realization that HDM2 is the master regulator of p53 has triggered the idea of developing an inhibitor for this interaction. From a broader perspective, this is one of the first examples in which it has been clearly shown that protein–protein interactions can be efficiently disrupted by small molecule inhibitors. It was long believed that protein–protein interactions could not be effectively inhibited with small molecules because of the large and poor definition of protein interfaces<sup>16</sup>. This view has recently changed and targeting the interaction between HDM2 and p53 using small molecular compounds in tumour cells has become a primary therapeutic strategy. Consequently, a large number of small chemical compounds are currently being screened and engineered. Among them, the Nutlins<sup>17</sup> are the most studied. The Nutlins are the first examples of potent and specific inhibitors of the HDM2–p53 interaction and one of them, Nutlin 3, has been extensively evaluated for its therapeutic potential and mechanism of action in human cancer.

A key advantage of the method proposed here is that it allows in live cells an immediate determination of the interaction between any pair of proteins in which one of them is labelled with GFP. This means that with a single-fluorescence snapshot at a given time point it makes it possible to determine the interaction relative to a previous time point. This allows resolving fast kinetics in live cells such as the inhibition of these interactions after treatment with a given drug.

To test this approach, we measured in live cells the disruption kinetics of the p53 and HDM2 interaction upon treatment with Nutlin 3 (Fig. 3, Supplementary Fig. S1). BHK cells (containing a stably integrated *LacO* DNA array) were transiently transfected with constructs coding for GBP–LacI, GFP–p53 and mCh–HDM2. GFP–p53 gets bound to the *LacO* array by its interaction with GBP–LacI. Before the treatment with Nutlin 3, HDM2 labelled with mCherry is also recruited to the *LacO* by its interaction with p53. No unspecific binding of p53, HDM2, GFP or mCherry to the *LacO* was detected (Supplementary Fig. S2). Figure 3a shows a cartoon representation of the interactions and signals before and after the treatment with Nutlin 3. Figure 3b shows the fluorescent images of the cells for each protein at different concentrations of Nutlin 3 and different time points. In Fig. 3c, the intensity ratio of mCh–HDM2 at the *LacO* after the treatment with Nutlin 3 is plotted relative to its intensity before the drug treatment. We observed that the time scale of the disruption is within seconds after treatment with Nutlin 3. This disruption can be partial at concentrations below 10  $\mu\text{M}$  and is almost complete at 10  $\mu\text{M}$ . As mentioned previously, it was already surprising a few years ago that small molecules can disrupt the binding of proteins. We can now in addition directly measure the fast disruption kinetics of these interactions in live mammalian cells. Furthermore, with this assay we obtained accurate and reproducible results over a broad range of expression ratios as shown in the automated analysis in Supplementary Fig. S3.

**High-throughput analysis of interaction disruption by drugs.** A clear visualization technology for these interactions can be used to develop efficient methods for high-throughput screening. Therefore, in Supplementary Fig. S4 we outline this idea comparing Nutlin 3 with other well-studied chemical compounds. In particular, we compared the effect of three drugs, RITA, Nutlin 3 and Mi 63. Using Nutlin 3 as reference and DMSO as a control, we observed that Mi 63 displays a stronger inhibition than Nutlin

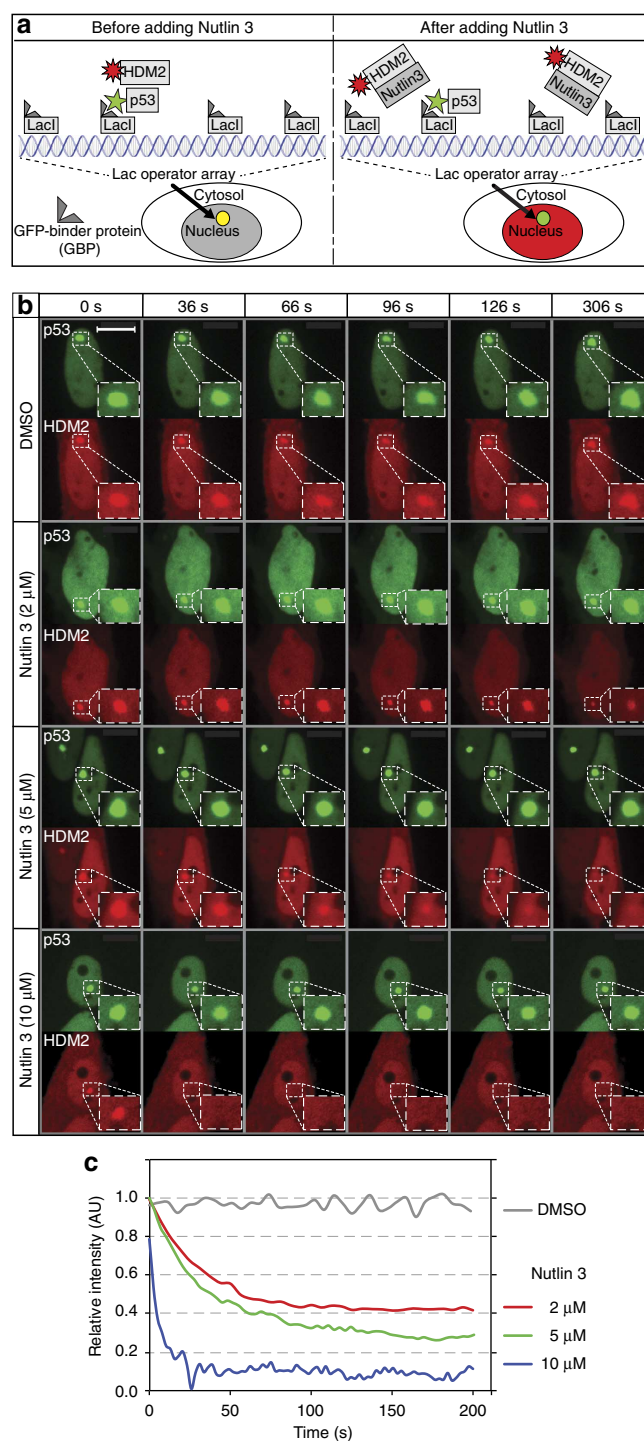


**Figure 3 | Visualization of targeted disruption of protein interactions in live cells.** BHK cells containing a stably integrated *LacO* array were transiently transfected with pNeG-p53(NTD), pCAG-Ch-HDM2(NTD) and GBP-LacI. In (a) is shown a schematic representation of the re-localization of the GFP-p53 to the *LacO* array, its interaction with mCh-HDM2 and the disruption of this interaction mediated by Nutlin 3. (b) Live cell confocal microscopy images showing the disruption kinetics of the interaction between HDM2 and p53 mediated by Nutlin 3 at 0 (DMSO, control), 2, 5 and 10  $\mu\text{M}$ . (c) Time lapse quantification of the relative binding of p53 to HDM2. Higher concentrations of Nutlin 3 resulted in faster disruption of the interaction between the proteins. In Supplementary Fig. S1 are shown the kinetic traces, the mean and the s.e. of the interaction disruption mediated by Nutlin 3 at 5  $\mu\text{M}$  obtained from five repetitions showing the reproducibility of the individual traces. Scale bar, 5  $\mu\text{m}$ .

3, while RITA does not disrupt the p53–HDM2 interaction. It has been shown that RITA has antitumor effects and it was originally proposed that it does so by disrupting the p53–HDM2 (ref. 18). *In vitro* NMR studies<sup>19</sup> have contested this suggesting that RITA does not disrupt p53–HDM2 interaction. Our results, now in live mammalian cells, agree and extend the *in vitro* NMR analysis.

**Design of a cell-permeable peptide inhibitor.** Several very strong peptide inhibitors have been reported<sup>20</sup> besides small chemical compounds like the Nutlins. Some of these peptides have been optimized to display a double high affinity not only for HDM2 but also for HDMX<sup>20</sup>. Using phage display peptide libraries a potent dual peptide inhibitor for HDM2 and HDMX, here named N8A, has been reported<sup>21</sup> (Fig. 4a). *In vitro*, this peptide has several fold higher binding affinity for HDM2 than the corresponding p53-binding region<sup>21</sup>.

Small chemical compounds such as the Nutlins do not show inhibition of the p53–HDMX interaction<sup>22</sup>. Therefore, these peptides offer a clear advantage. However, they lack cell permeability, which is essential for targeting these intracellular proteins *in vivo*. To solve this issue, as shown schematically in Fig. 4b, we coupled this peptide inhibitor to cell-penetrating peptides (CPPs)<sup>23–27</sup>. CPPs are short basic peptides, ~10 amino acids, capable of crossing the cell plasma membrane transporting other covalently attached molecules such as peptides avoiding endosomal trapping and degradation<sup>26</sup>. Using CPPs to deliver these small inhibitors has the potential disadvantage that the CPP itself can interfere with the binding of the inhibitor to the target. To overcome this potential issue, as shown in Fig. 4c, we coupled the peptide inhibitor to the CPP, in this case the TAT peptide, using a disulphide bridge so that once in the cytosol, the disulphide bridge is reduced and the inhibitor peptide is released becoming free to target HDM2.

**Visualization at different subcellular locations.** An important aspect of the F3H strategy is that it can be used with any cell type. In Fig. 5a and Supplementary Movie 1 we made use of the re-localization of GFP-tagged proteins to the *LacO* DNA array, for which it is required to have first the DNA array permanently incorporated into the cell's genome. However, with the F3H we can now use other existing structures within the cells. In the next step, we expanded the system to any mouse cell taking advantage of the naturally occurring major satellite DNA repeats rich in methylated cytosines at pericentric regions of each and every mouse chromosome. To this purpose, we made use of a fusion of the GBP with the methyl cytosine-binding domain (MBD) of MeCP2, which is known to accumulate at these chromosomal domains, also called chromocenters in interphase cells<sup>28,29</sup>. The outcome is shown in Fig. 5b where both p53 and HDM2 initially could be seen colocalizing at chromocenters and upon peptide addition total disruption of the interaction can be scored by the re-localization of the p53 away from these structures. To make the system extendable to any cell containing lamina, and not only any mouse cells, we fused the GBP to lamin B1. In this way, we could target the GFP-fusion protein to the nuclear periphery, using, for example, human HeLa cells and assay for the release of the interacting protein from the lamina. The outcome in human cells is shown in Fig. 5c and upon disruption by the addition of the peptide, the red-labelled p53 protein is seen only in the nucleoplasm displaced from the nuclear periphery. In Supplementary Fig. S5 is shown the automated detection and analysis of protein–protein interactions at the nuclear lamina using a high-throughput wide-field microscopy system. Finally, to test whether the assay would work also in the cytosol we fused the GBP to centrin and, hence targeted the GFP-fusion to the

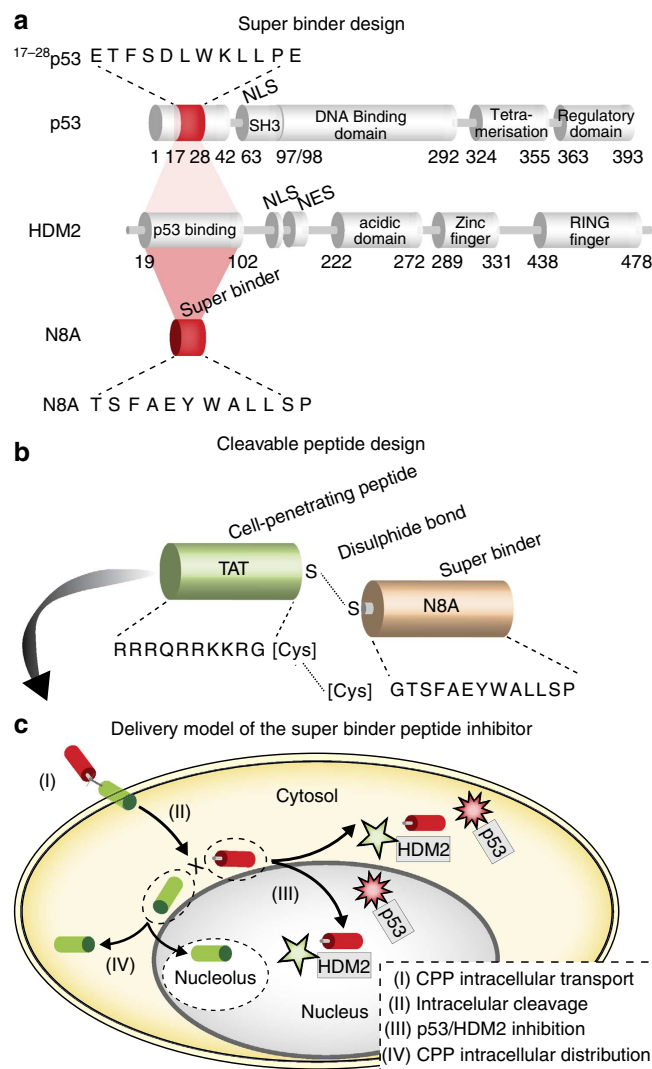


**Figure 4 | Rationally designed *in vivo* cleavable cell-permeable peptide to inhibit and disrupt the binding between p53 and HDM2.** (a) Short sequence from p53 responsible for the binding between p53 and HDM2. Below this sequence the main domains of p53 and HDM2 are depicted along with a short peptide (N8A) that has been shown *in vitro* to have higher affinity for HDM2 than p53. (b) The N8A peptide is not able to reach the interior of living cells. Therefore, it was coupled by a disulphide bond to a cell-penetrating peptide (TAT) that is capable of transporting it into living cells. (c) The design is based on a delivery model in which (I) the TAT peptide transports the N8A peptide into the cell, (II) in the cytosol the disulphide bridge is cleaved releasing the N8A peptide from the TAT peptide, (III) the peptide inhibitor is free to diffuse throughout the nucleus and the cytosol inhibiting the binding between p53 and HDM2, (IV) while the TAT peptide accumulates preferentially at the cytosol and the nucleolus.

centrioles. As shown in Fig. 5d, the colocalization and, upon peptide addition, disruption of the p53 and HDM2 interaction could also be easily measured in the cytosol. In Supplementary Fig. S6 is shown the automated detection and analysis of protein–protein interactions at the centrioles using a high-throughput system. Thus, our approach is totally flexible and is applicable to various subcellular compartments, cell types and species.

## Discussion

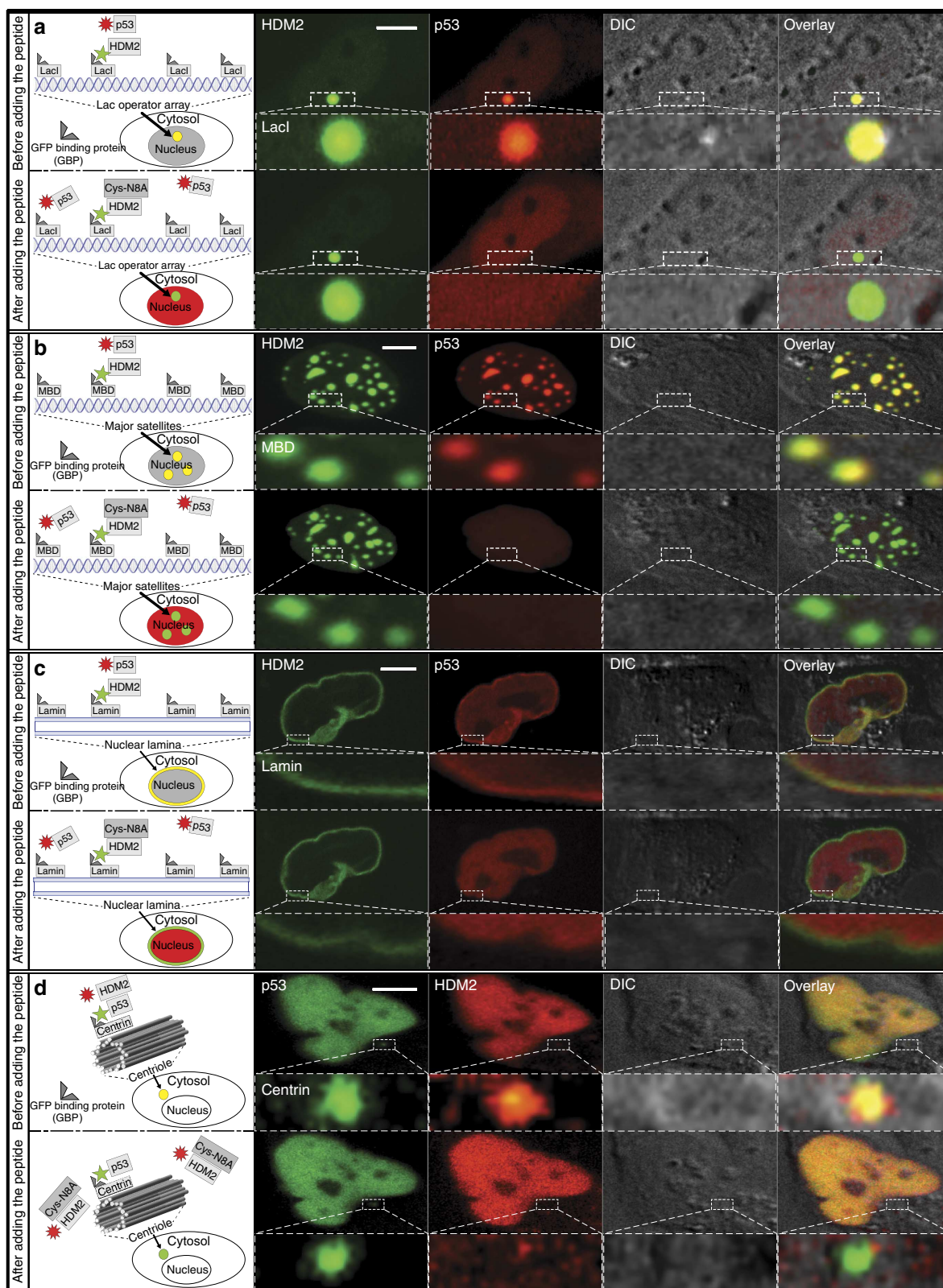
In summary, the cell-based method presented here can be used to study protein–protein interactions and their inhibition *in vivo* in



any cell type. In particular, it provides real-time kinetics of these interactions in live cells and can be applied to characterize and/or screen for specific inhibitors. We applied and validated the F3H approach by visualizing the binding and targeted disruption of p53 and HDM2 in real time in live cells using different drugs including Nutlin 3 and a novel cell-permeable and *in vivo* cleavable peptide inhibitor.

## Methods

**Peptide synthesis and analyses.** The individual peptides were synthesized by BIOSYNTAN GmbH using simultaneous peptide synthesis on the following instruments: SYRO, MultiSynTec GmbH, Germany, using the Fmoc/But strategy developed Sheppard. Couplings were performed using 3–6 equiv Fmoc-amino acid/HOBt/TBTU and 6–12 equiv *N*-methylmorpholine in the following resin: Tentagel HL RAM resin; RAPP Polymere GmbH, Tuebingen, Germany, loading 0.36 mmol g<sup>-1</sup> resin. The peptide fragment RRRQRKRGC was synthesized with



dipyridyl-disulphide during the deprotection reaction. The unsymmetrical dimerization between the TAT peptide fragment RRRQRKRKGC and the N8A peptide CGTSFAEYWALLSP-amide (Supplementary Fig. S7) was performed in solution (pH 6.0). The protecting groups used are: Cys(Trt), Arg(Pbf), Ser(But), Thr(But), Tyr(But), Asp(OBut), Glu(OBut), Asn(Trt), Gln(Trt), Lys(Boc), His(Trt) and Trp(Boc). Peptides were deprotected and cleaved from the resin by trifluoroacetic acid (TFA)/water (95:2.5) 2 h, room temperature; adding 3% triisopropylsilane<sup>30</sup>.

For preparative HPLC, the HPLC instrument Shimadzu LC-8A with UV-vis detector SPD-6A was used with an Ultrasep ES (RP-18), 10  $\mu$ m, (250  $\times$  20 mm) column. Solvent was as described below with a corresponding gradient in 30 min. Flow: 15.0 ml min<sup>-1</sup>. Detection: 220 nm.

For analytical HPLC, the HPLC Shimadzu LC-9A with photodiode array detector SPD-M6A was used with an Ultrasep ES (RP-18), 7  $\mu$ m, (250  $\times$  3.0 mm) column. Solvent A = 0.05% TFA in water; solvent B = 0.05% TFA in 80% ACN/water. Flow: 0.6 ml min<sup>-1</sup>. Linear gradient: 2.5% B per min. Detection: 220 nm (Supplementary Fig. S8).

Peptides were further analysed by MALDI-TOF using a MALDI2 DE instrument, Shimadzu, Japan, in linear mode. Calculated molecular weight as average mass: 3,040.6; molecular weight detected: 3,041.4 (Supplementary Fig. S9).

**Plasmids.** The mammalian expression constructs coding for HDM2 and p53 deletions as well as p53 full-length protein fused with eGFP or mCherry are schematically shown in Supplementary Fig. S10 together with the GFP binder nanobody<sup>31,32</sup> (GBP)-localization constructs used to recruit the GFP-tagged proteins to different regions within the cell.

The DNA sequence coding for the N-terminal domain of p53 (aa 1–81) and HDM2 (aa 1–128) were amplified from human cDNA by PCR using fusion high-fidelity DNA Polymerase (New England BioLabs) and cloned in frame into NLS-eGFP, or eGFP, or mCherry plasmids with *Asi*I and *Not*I restriction endonucleases (New England BioLabs). The human full-length p53 fused to GFP was obtained from Addgene (catalogue no. 12091)<sup>33</sup>.

pGBP-LacI was constructed by deleting the mRFP-coding sequence from pGFPbinderImR plasmid using *Bam*HI and *Bsr*GI restriction endonucleases<sup>34</sup>. GBP-LaminB1 was described previously<sup>31</sup>.

To construct the pMBD-GBP plasmid, pEGFP-C2 vector (CLONTECH Laboratories, Inc.) was digested by *Nhe*I and *Hind*III (New England BioLabs), and the MBD domain of rat MeCP2 and GBP were both ligated into the backbone. pGBP-Centrin was constructed by replacing the LacI of pGBP-LacI with the Centrins2 ORF using *Bam*HI and *Hind*III restriction endonucleases (New England BioLabs).

**Cell culture and transfection.** The following cell lines were used in this study: BHK cells containing multiple lac operator<sup>15</sup> repeats, C2C12 mouse myoblast cells<sup>35</sup>, U2OS human osteosarcoma cells<sup>36</sup>, HeLa human cervical carcinoma cells<sup>37</sup>. All cell lines were grown in a humidified atmosphere at 37 °C and 5% CO<sub>2</sub>, in Dulbecco's modified Eagle's medium (DMEM) supplemented with 1  $\mu$ M gentamycin and 10% (BHK, U2OS and HeLa) or 20% (C2C12) fetal calf serum.

All cell lines were transiently transfected using PEI (poly-ethyleneimine; 1 mg ml<sup>-1</sup> in ddH<sub>2</sub>O, neutralized with HCl). For the transfection, 200  $\mu$ l DMEM serum-free with 12  $\mu$ l of PEI was vortexed for 2 min and added to 200  $\mu$ l serum-free DMEM with 4  $\mu$ g DNA. After incubating the DNA-PEI mixture for 15 min at room temperature, the solution was added to the cells drop wise and incubated overnight at 37 °C and 5% CO<sub>2</sub>.

**Drug treatment.** Nutlin 3 (Sigma) was dissolved in DMSO as a 10 mM stock solution. Mi 63 and RITA were a kind gift from Dr. Holak (MPI Biochemistry, Martinsried, Germany).

For high-throughput assays BHK cells plated onto 96-well plates (Greiner Bio-One) were triple-transfected with the plasmids indicated in the corresponding figures. Sixteen hours later, the medium was changed to phenol red free medium

supplemented with the Nutlin 3 or the other compounds at various concentrations for 30 min, then fixed with 3.7% formaldehyde and DNA counterstained with DAPI. For each concentration, triplicate wells were treated.

For live cell microscopy cells were plated on poly-L-Lysine coated eight-well  $\mu$ -Slide (ibidi GmbH) and transfected as described. Cells were imaged live on a spinning disk confocal system before and immediately after addition of Nutlin 3 or peptide inhibitors.

**High-throughput microscopy and image analysis.** After cell fixation, images were acquired automatically with an Operetta high-content imaging system at the wide-field mode using a  $\times$  40 air objective (PerkinElmer). DAPI, eGFP and Cherry fluorescent fusion proteins were excited and the emissions were recorded using standard filter sets. Exposure time was controlled to avoid saturated pixels, typically from 50–200 ms, 30 different fields were imaged in each well. The imaging time can be calculated as 150 ms per channel  $\times$  3 channels  $\times$  30 fields per well  $\times$  96 wells = 1,296 s = 21.6 min, adding to this the time for objective movement, re-focusing, filter swapping, the total time for 96-well plate takes about 90 min. The images were then analysed with the Harmony analysis software (PerkinElmer) with a flow diagram shown in Supplementary Fig. S11. Briefly, the images were first segmented by intensity and area size according to the DAPI fluorescence using the top-hat method to define the cell nucleus area (cells, blue in Supplementary Fig. S11), and nucleus masks were produced and recorded. Then the *LacO* foci were recognized by intensity in the eGFP channel within the nucleus areas, which were defined in the former step, and cells with one *LacO* spot were kept for subsequent analysis (cells with spot, green in Supplementary Fig. S11). The cell with one green spot in the nucleus and a red signal was considered as triple-transfected cell with a spot (brown in Supplementary Fig. S11). In these cells, the mean intensities of mCherry channel at the *LacO* were recorded according to *LacO* foci masks gotten from the GFP channel, and the ratio of mCherry mean intensity at the *LacO* spot (spot<sub>mCherry</sub>) to the mean intensity of whole nucleus (nucleus<sub>mCherry</sub>) were calculated, and then used to subgroup the cells into 'interacting cells' (yellow in Supplementary Fig. S11) or 'non-interacting cells'. The percentages of 'interacting cells' in each well were plotted and used as an indication of the drug inhibitory effect. Depending on the application, it might be helpful to also consider the relative enrichment of mCherry fusion proteins at the *LacO*.

**Live cell confocal microscopy and image analysis.** Transfected cells plated on  $\mu$ -Slide 8-well were selected and imaged in peptide inhibitor-free medium. Immediately after addition of the peptide inhibitor at 8  $\mu$ M final concentration, 3D stacks were acquired at 1 min time intervals for up to 1 h. Time lapse imaging was carried out on a UltraVIEW VoX spinning disc confocal system (PerkinElmer, UK) in a closed live cell microscopy chamber (ACU control, Olympus, Japan) heated to 37 °C, with 5% CO<sub>2</sub> and 60% air humidity, mounted on a Nikon Ti microscope (Nikon, Japan). Image acquisition was performed using a  $\times$  60/1.45 NA Planapochromat oil immersion objective lens. Images were obtained with a cooled 14-bit EMCCD camera (C9100-50, CamLink). To visualize the GFP signal, a 488 nm excitation laser and a 521-nm emission filter were used, the mCherry protein was excited using a 561-nm laser and the emission was filtered through a 587 nm filter.

For the analysis of correlation between fluorescent signals in Fig. 2, the derivative of the Pearson's coefficient along the plotted line was computed. This shows the change in correlation along the selected line.

The intensity plot in Supplementary Movie 1 was computed by extracting first the LacI spot, at each z-stack confocal plane, by computing the mean GFP intensity over the nucleus and extracting the pixels with intensity values 1.5 times higher than the mean. We visually verified that these criteria were correctly extracting only the LacI spot. After extracting the LacI spot for each confocal plane of the z-stack, this was used as a mask to extract the pixels corresponding the LacI spot in the mCherry channel. The GFP and mCherry signals at the LacI spot were normalized by dividing the intensity in each pixel by the average intensity of each signal in the nucleus. The plot shows the result after the integration of these normalized signals at the LacI spot before and after adding the peptide inhibitor. To perform this

**Figure 5 | A rationally designed *in vivo* cleavable cell-permeable peptide that inhibits and disrupts the binding between p53 and HDM2.** The peptide was tested in several mammalian cell lines (a–d). Starting from hamster cell lines containing stably integrated Lac operator (*LacO*) DNA arrays, the system is expanded onto application on any mouse cell exploiting the natural occurrence of large regions around centromeres naturally containing arrays of major satellite DNA sequences rich in methylated cytosines and, hence, accumulating methyl cytosine-binding domain (MBD) proteins. On a next step, the system is expanded to any cell containing a nuclear lamina composed of lamin intermediate filament proteins. Finally, the system is transferred to the cytosol making use of targeting it to the centriole via the centrin protein. In the first column, a cartoon representation of the protein interactions and inhibition at each recruitment site within the cell is shown. In the second column, a confocal image of a representative live cell of the GFP channel is shown followed by the mCherry channel in the third column, a transmission light image in the fourth column and in the last column the overlay of all the channels. In each row are shown the images before and after adding the N8A peptide to a final concentration of 8  $\mu$ M. An amplified image of the recruitment site is shown below each microscopic image. (a) Recruitment of GFP-HDM2 to the *LacO* array in hamster BHK cells. Cells transiently transfected with pNeG-HDM2(NTD), pCAG-Ch-p53(NTD) and GBP-LacI. (b) Recruitment of GFP-HDM2 to major satellite pericentric repeats rich in MBD proteins in mouse C2C12 cells. Cells transiently transfected with pNeG-HDM2(NTD), pCAG-Ch-p53(NTD) and GBP-MBD. (c) Recruitment of GFP-HDM2 to the nuclear lamina in human HeLa cells. Cells transiently transfected with pNeG-HDM2(NTD), pCAG-Ch-p53(NTD) and GBP-Lamin B1. (d) Recruitment of p53-GFP to the centriole in HeLa cells. Cells transiently transfected with p53-GFP, pCAG-Ch-HDM2(NTD) and GBP-Centrin2. Scale bar, 5  $\mu$ m.

analysis, we wrote a program that performed automatically this analysis at each time point, and produced as an output the plot and the movie.

## References

- Fields, S. & Song, O. A novel genetic system to detect protein-protein interactions. *Nature* **340**, 245–246 (1989).
- Cremazy, F. G. *et al.* Imaging *in situ* protein-DNA interactions in the cell nucleus using FRET-FLIM. *Exp. Cell. Res.* **309**, 390–396 (2005).
- Tsuganezawa, K. *et al.* A fluorescent-based high-throughput screening assay for small molecules that inhibit the interaction of MdmX with p53. *J. Biomol. Screen.* **18**, 191–198 (2013).
- Kirchhofer, A. *et al.* Modulation of protein properties in living cells using nanobodies. *Nat. Struct. Mol. Biol.* **17**, 133–138 (2010).
- Montes de Oca Luna, R., Wagner, D. S. & Lozano, G. Rescue of early embryonic lethality in mdm2-deficient mice by deletion of p53. *Nature* **378**, 203–206 (1995).
- Jones, S. N., Roe, A. E., Donehower, L. A. & Bradley, A. Rescue of embryonic lethality in Mdm2-deficient mice by absence of p53. *Nature* **378**, 206–208 (1995).
- Lane, D. How cells choose to die. *Nature* **414**, 27 (2001).
- Vousden, K. H. Activation of the p53 tumor suppressor protein. *Biochim. Biophys. Acta.* **1602** 47–59, 2002.
- Momand, J., Jung, D., Wilczynski, S. & Niland, J. The MDM2 gene amplification database. *Nucleic Acids Res.* **26**, 3453–3459 (1998).
- Bond, G. L. *et al.* A single nucleotide polymorphism in the MDM2 promoter attenuates the p53 tumor suppressor pathway and accelerates tumor formation in humans. *Cell* **119**, 591–602 (2004).
- Oliner, J. D., Kinzler, K. W., Meltzer, P. S., George, D. L. & Vogelstein, B. Amplification of a gene encoding a p53-associated protein in human sarcomas. *Nature* **358**, 80–83 (1992).
- Zhou, M. *et al.* Incidence and prognostic significance of MDM2 oncoprotein overexpression in relapsed childhood acute lymphoblastic leukemia. *Leukemia* **14**, 61–67 (2000).
- Shimada, H. *et al.* Phase I/II adenoviral p53 gene therapy for chemoradiation resistant advanced esophageal squamous cell carcinoma. *Cancer Sci.* **97**, 554–561 (2006).
- Cheok, C. F., Verma, C. S., Baselga, J. & Lane, D. P. Translating p53 into the clinic. *Nat. Rev. Clin. Oncol.* **8**, 25–37 (2011).
- Tsukamoto, T. *et al.* Visualization of gene activity in living cells. *Nat. Cell. Biol.* **2**, 871–878 (2000).
- Arkin, M. R. & Wells, J. A. Small-molecule inhibitors of protein-protein interactions: progressing towards the dream. *Nat. Rev. Drug. Discov.* **3**, 301–317 (2004).
- Vassilev, L. T. *et al.* *In vivo* activation of the p53 pathway by small-molecule antagonists of MDM2. *Science* **303**, 844–848 (2004).
- Issaeva, N. *et al.* Small molecule RITA binds to p53, blocks p53-HDM-2 interaction and activates p53 function in tumors. *Nat. Med.* **10**, 1321–1328 (2004).
- Krajewski, M., Ozdow, P., D'Silva, L., Rothweiler, U. & Holak, T. A. NMR indicates that the small molecule RITA does not block p53-MDM2 binding *in vitro*. *Nat. Med.* **11**, 1135–1136 (2005).
- Botter, V. *et al.* Comparative study of the p53-mdm2 and p53-MDMX interfaces. *Oncogene* **18**, 189–199 (1999).
- Li, C. *et al.* Systematic mutational analysis of peptide inhibition of the p53-MDM2/MDMX interactions. *J. Mol. Biol.* **398**, 200–213 (2010).
- Hu, B., Gilkes, D. M., Farooqi, B., Sebt, S. M. & Chen, J. MDMX overexpression prevents p53 activation by the MDM2 inhibitor Nutlin. *J. Biol. Chem.* **281**, 33030–33035 (2006).
- Tunemann, G. *et al.* Cargo-dependent mode of uptake and bioavailability of TAT-containing proteins and peptides in living cells. *FASEB J.* **20**, 1775–178 (2006).
- Herce, H. D. & Garcia, A. E. Molecular dynamics simulations suggest a mechanism for translocation of the HIV-1 TAT peptide across lipid membranes. *Proc. Natl Acad. Sci. USA* **104**, 20805–20810 (2007).
- Herce, H. D. *et al.* Arginine-rich peptides destabilize the plasma membrane, consistent with a pore formation translocation mechanism of cell-penetrating peptides. *Biophys. J.* **97**, 1917–1925 (2009).
- Ter-Avetisyan, G. *et al.* Cell entry of arginine-rich peptides is independent of endocytosis. *J. Biol. Chem.* **284**, 3370–3378 (2009).
- Lattig-Tunemann, G. *et al.* Backbone rigidity and static presentation of guanidinium groups increases cellular uptake of arginine-rich cell-penetrating peptides. *Nat. Commun.* **2**, 453 (2011).
- Nan, X., Campoy, F. J. & Bird, A. MeCP2 is a transcriptional repressor with abundant binding sites in genomic chromatin. *Cell* **88**, 471–481 (1997).
- Brero, A. *et al.* Methyl CpG-binding proteins induce large-scale chromatin reorganization during terminal differentiation. *J. Cell. Biol.* **169**, 733–743 (2005).
- Karas, M. & Hillenkamp, F. Laser desorption/ionization of proteins with molecular masses exceeding 10,000 daltons. *Anal. Chem.* **60**, 2299–2301 (1988).
- Rothbauer, U. *et al.* A versatile nanotrapp for biochemical and functional studies with fluorescent fusion proteins. *Mol. Cell. Proteomics* **7**, 282–289 (2008).
- Rothbauer, U. *et al.* Targeting and tracing antigens in live cells with fluorescent nanobodies. *Nat. Methods* **3**, 887–889 (2006).
- Boyd, S. D., Tsai, K. Y. & Jacks, T. An intact HDM2 RING-finger domain is required for nuclear exclusion of p53. *Nat. Cell. Biol.* **2**, 563–568 (2000).
- Zolghadr, K. *et al.* A fluorescent two-hybrid assay for direct visualization of protein interactions in living cells. *Mol. Cell. Proteom.* **7**, 2279–2287 (2008).
- Yaffe, D. & Saxel, O. Serial passaging and differentiation of myogenic cells isolated from dystrophic mouse muscle. *Nature* **270**, 725–727 (1977).
- Ponten, J. & Saksela, E. Two established *in vitro* cell lines from human mesenchymal tumours. *Int. J. Cancer* **2**, 434–447 (1967).
- Scherer, W. F., Syverton, J. T. & Gey, G. O. Studies on the propagation *in vitro* of poliomyelitis viruses. IV. Viral multiplication in a stable strain of human malignant epithelial cells (strain HeLa) derived from an epidermoid carcinoma of the cervix. *J. Exp. Med.* **97**, 695–710 (1953).

## Acknowledgements

We thank Anne Lehmkuhl for excellent technical support. W.D. received a fellowship of the Chinese Scholarship Council. H.D.H. received support from N.I.H. grant R01-GM086801. This work was funded by grants of the Deutsche Forschungsgemeinschaft (DFG SPP 1623) to M.C.C. and H.L.

## Authors' contributions

Experiments were designed by H.H., H.L., M.C.C. and W.D. Experiments were performed by H.H., J.H. and W.D. The data analysis was performed by H.H., J.H. and W.D. H.H., H.L., M.C.C. and W.D. wrote the manuscript. H.L. and M.C.C. are equally contributing senior authors.

## Additional information

**Supplementary Information** accompanies this paper at <http://www.nature.com/naturecommunications>

**Competing financial interests:** The authors declare no competing financial interests.

**Reprints and permission** information is available online at <http://npg.nature.com/reprintsandpermissions/>

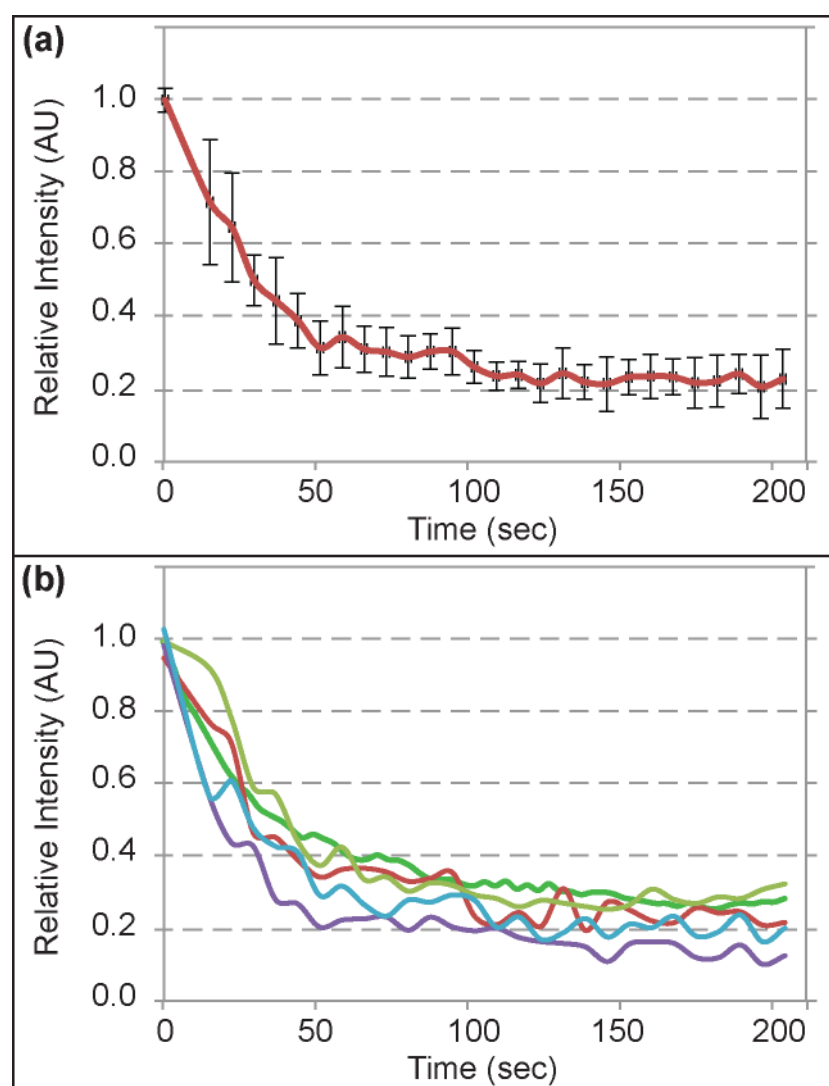
**How to cite this article:** Herce, H. D. *et al.* Visualization and targeted disruption of protein interactions in living cells. *Nat. Commun.* 4:2660 doi: 10.1038/ncomms3660 (2013).



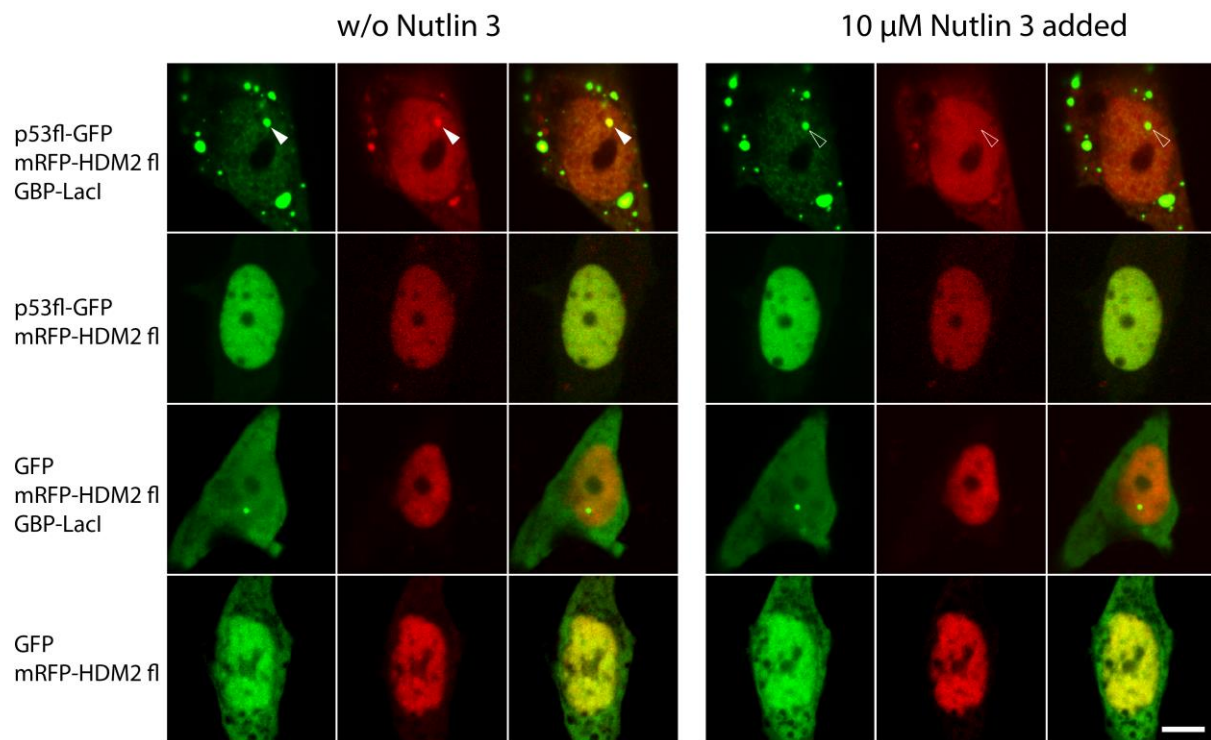
This work is licensed under a Creative Commons Attribution-NonCommercial-NoDerivs 3.0 Unported License. To view a copy of this license, visit <http://creativecommons.org/licenses/by-nc-nd/3.0/>



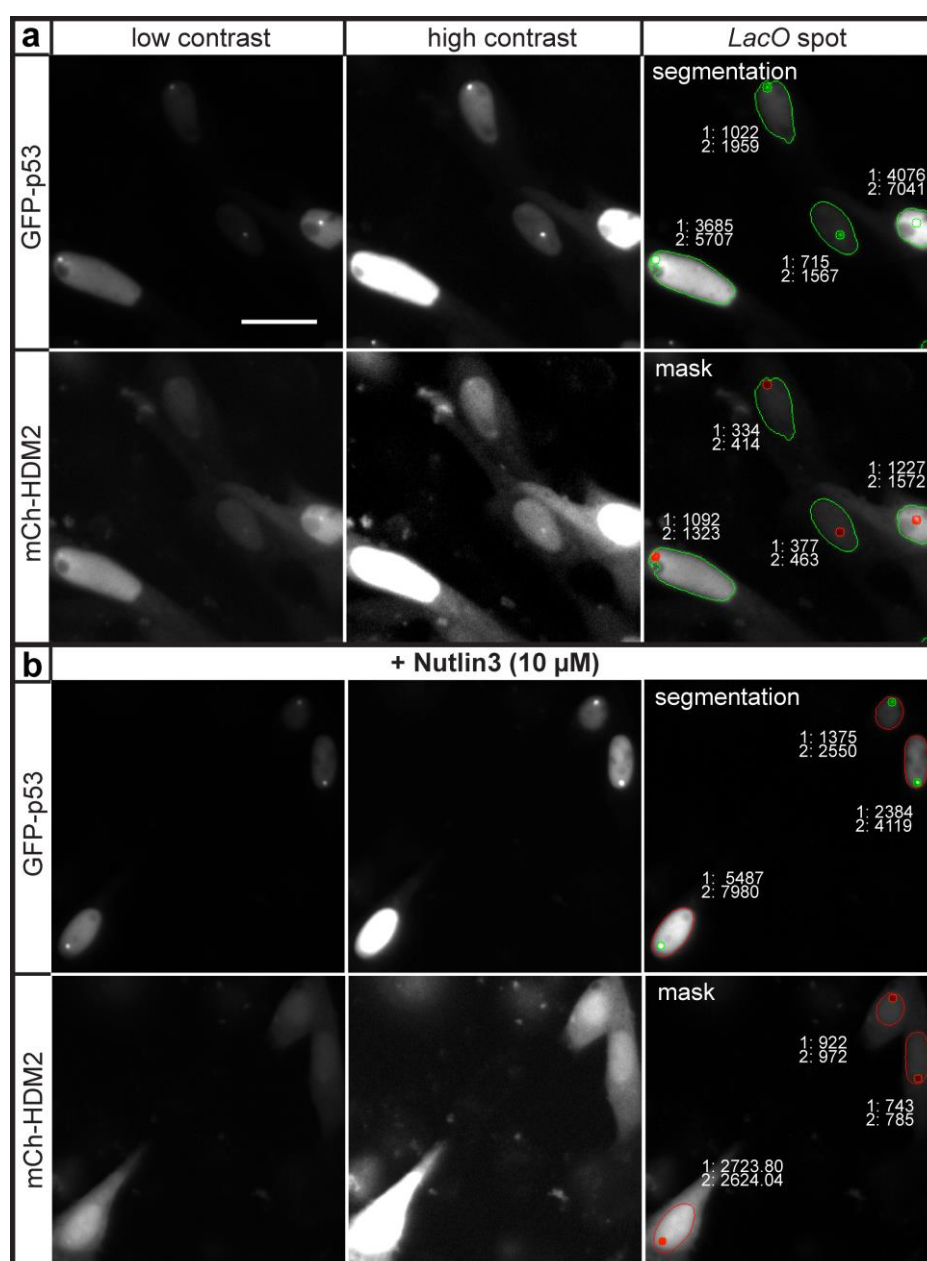
## Supplementary Figures



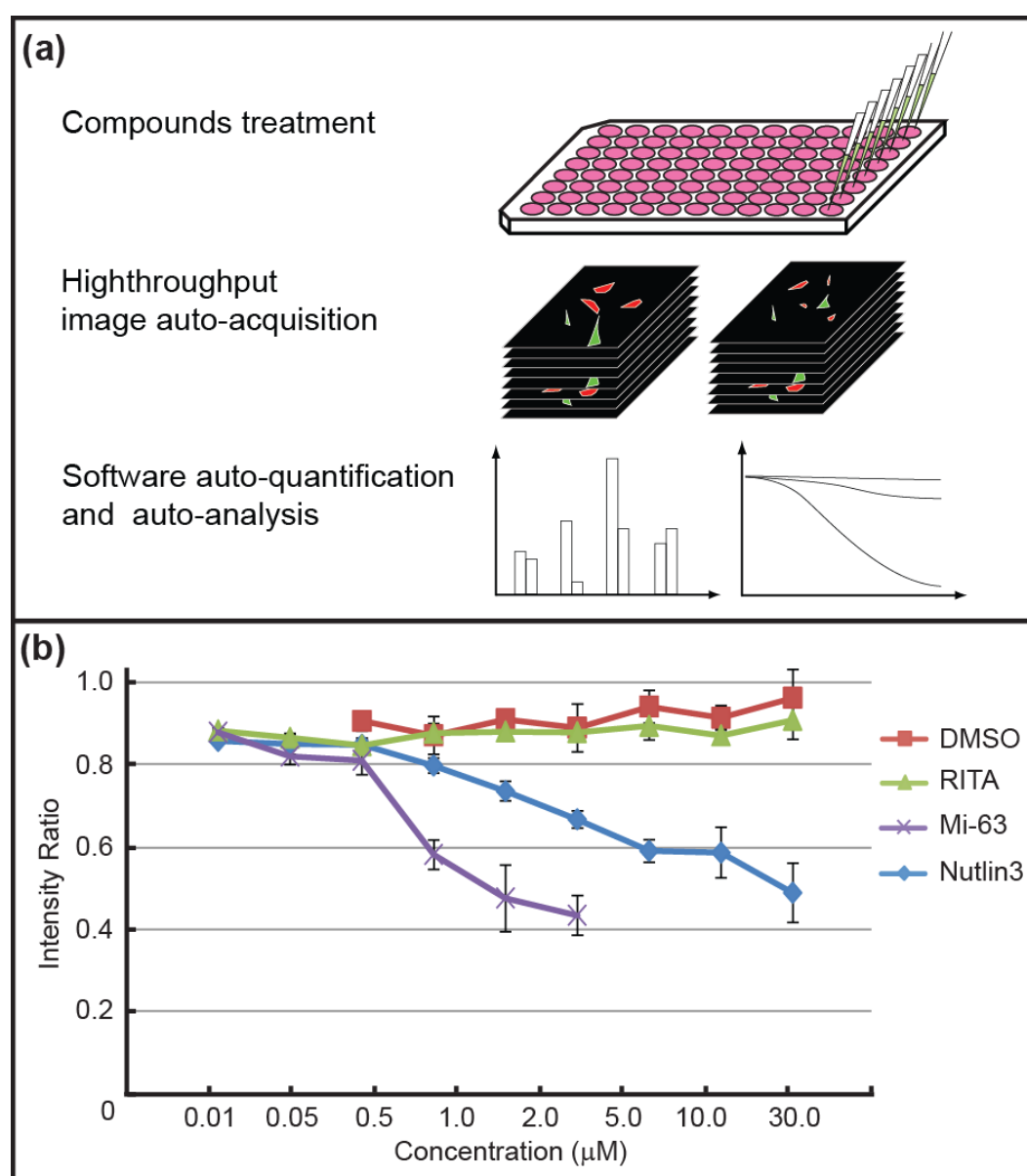
**Supplementary Figure S1.** Inhibition kinetics of p53/HDM2 binding induced by Nutlin 3 on live cells. Reproducibility of the p53/HDM2 binding disruption kinetics induced by Nutlin 3 measured using the F3H binding assay at the *LacO* array. BHK cells containing a stably integrated *LacO* array were transiently transfected with pNeG-p53(NTD), pCAG-mCh-HDM2(NTD) and GBP-LacI. In (a) is shown the mean and standard error of the time lapse quantification of the relative binding of HDM2 to p53 after drug treatment. The assay was performed in quintuplicates. In (b) are shown the individual time lapse traces of each single experiment of the five repeats.



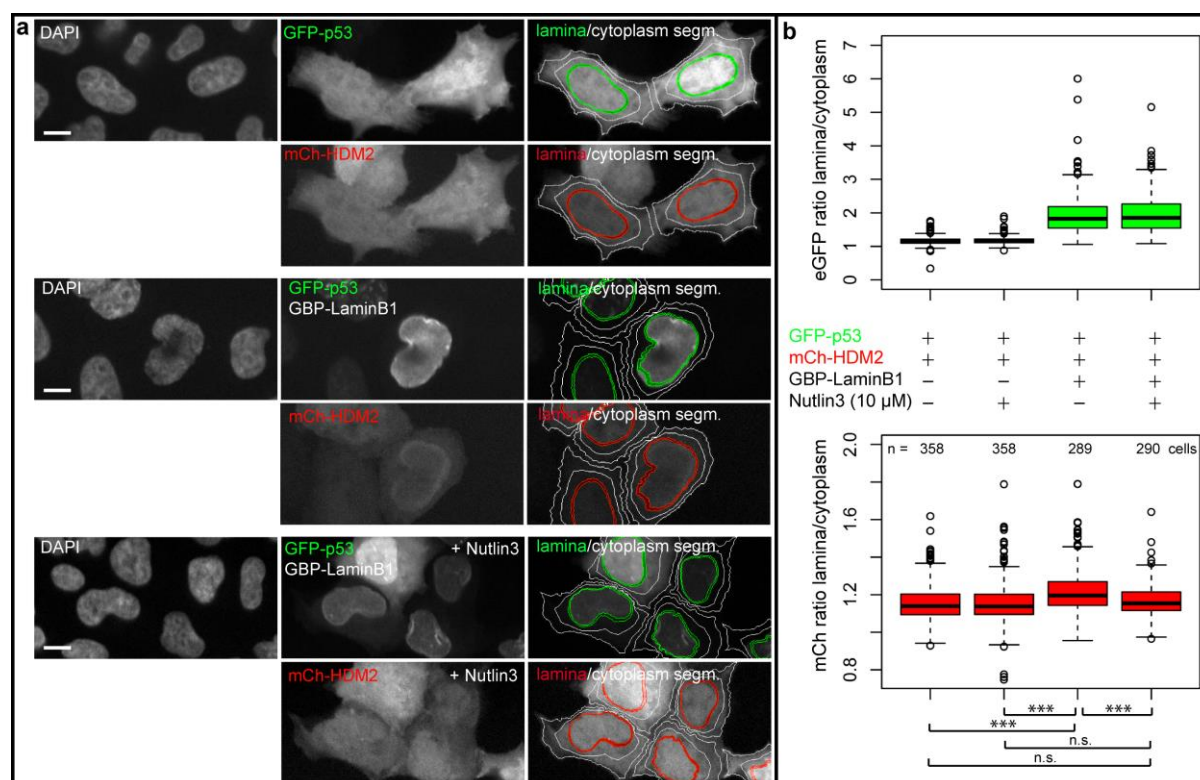
**Supplementary Figure S2.** Full length p53, HDM2, GFP and mCherry proteins do not show unspecific binding to the *LacO* array. Images of live BHK cells co-transfected with full-length p53-GFP, full-length Ch-HDM2 and GBP-LacI are shown (the first row). Ch-HDM2 colocalized with p53-GFP at the *LacO* spot (filled arrowhead). After treatment with 10  $\mu$ M Nutlin 3, the Ch-HDM2 was released from the *LacO* spot (open arrowhead). GFP control and control without GBP-LacI were performed to exclude unspecific binding. Scale bar, 5  $\mu$ m.



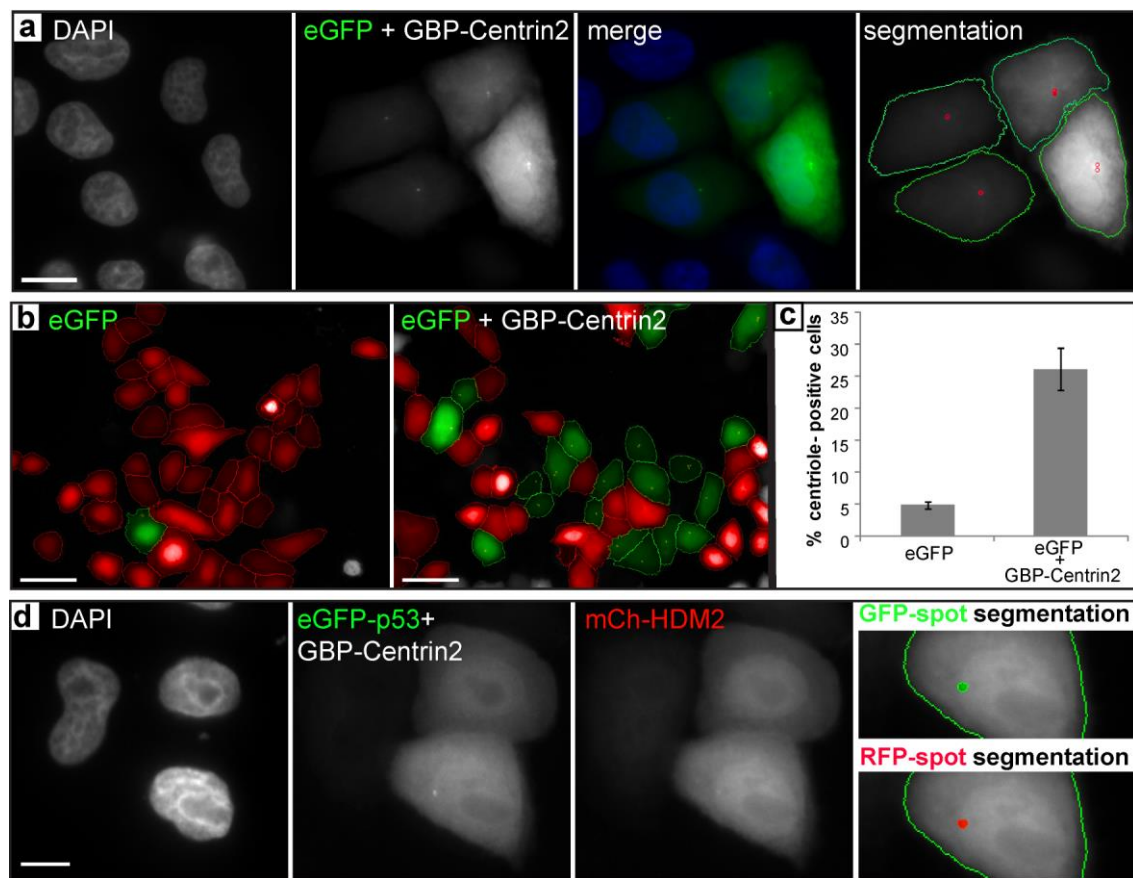
**Supplementary Figure S3.** Automated wide field image detection and analysis of protein-protein interactions at the *LacO* array can be made over a wide range of protein expression levels. Shown are BHK cells co-expressing GBP-LacI, GFP-p53 (pNeG-p53 (NTD), upper panel, a, b) and mCh-HDM2 (pCAG-mCh-HDM2 (NTD), lower panel, a, b). Low and high contrast images (left and middle, respectively) are presented to highlight heterogeneous protein levels. On the right is shown the automated intensity threshold segmentation of nucleus and *LacO* spot regions. Green (a) and red (b) nucleus borders indicate classification as interaction-positive and interaction-negative cells, respectively. Mean fluorescence intensities of nucleus (1) and spot (2) regions (16 bit grayscale) are indicated. Scale bar, 10 μm.



**Supplementary Figure S4.** Comparative analysis of drug efficacy on disrupting protein interactions. High throughput screening. (a) Cells were seeded onto a 96-well plate and treated with Nutlin 3, Mi-63 and RITA at the concentrations indicated. Cells were fixed and images acquired automatically using a Perkin Elmer Operetta imaging platform. The intensity ratio of mCh/GFP at the *LacO* spot in each cell was measured. (b) mCh/GFP intensity ratio of p53 and HDM2 at the *LacO* spot when treated with different concentrations of DMSO (control), RITA, Mi-63 and Nutlin 3. Mi-63 has a stronger inhibiting effect than Nutlin 3, while RITA does not hinder the interaction between p53 and HDM2. Technical triplicates were performed, and the normalized mean percentage with standard error of the mean are shown. The total number of positively triple transfected cells analyzed per data point was 1,200. The present test required 37,200 positively triple transfected cells obtained out of a total of 316,000 imaged cells.

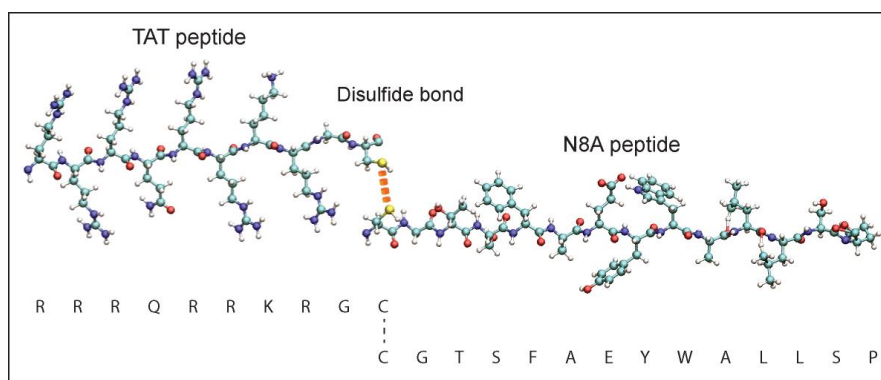


**Supplementary Figure S5.** Automated wide field image acquisition and analysis of protein-protein interactions at the nuclear lamina using the GBP-LaminB1. Images were acquired using the confocal mode of an automated Perkin Elmer Operetta imaging platform. The assay was performed in HeLa cells using an NLS-free version of GFP-p53 (pCAG-eGFP-p53) and mCh-HDM2 (pCAG-mCh-HDM2). (a) The proteins display a diffuse distribution throughout the cells upon co-expression (upper panel). Triple-transfection with GBP-LaminB1 causes GFP-p53 recruitment at the nuclear lamina and co-recruitment of mCh-HDM2 (middle panel). Nutlin3 treatment causes diffuse redistribution of mCh-HDM2 (lower panel). For quantitative analysis, a laminar ROI (red or green) and a cytoplasmic ROI (white) were automatically segmented (right side). Scale bars, 10  $\mu$ m. (b) Box plot representations of eGFP (top) and mCherry (bottom) intensity ratios between the lamina and the cytoplasm ROIs in absence and presence of GBP-LaminB1 and in absence and presence of Nutlin3. Medians are shown as solid black lines and the top and bottom box ends represent upper and lower quartiles, respectively. Whiskers represent the minimal and maximal data points within the 1.5x interquartile range. Data sets were tested for significance with an unpaired t-test ( $p < 0.001$ ). The number of cells analyzed is indicated above the boxplot diagram.

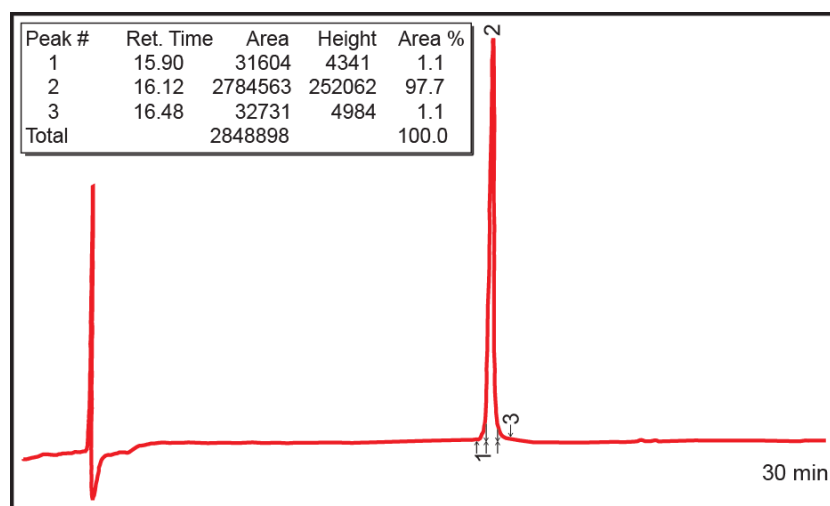


**Supplementary Figure S6.** Automated wide field image detection and analysis of protein-protein interactions at the centriole (cytoplasm) using the GBP-Centrin2 construct. (a) HeLa cells co-expressing GBP-Centrin2 and eGFP at different expression levels allowing automated intensity threshold segmentation of centriolar eGFP localization in the cytoplasm. Images were acquired using an automated Perkin Elmer Operetta imaging platform. Scale bar, 10  $\mu$ m. (b, c) Quantitative, automated image analysis. Green segmentation masks indicate classification of centriole-positive cells, red indicates classification of centriole-negative cells. Scale bar, 50  $\mu$ m. The error bars represent the standard deviation from technical triplicates. The shown data are a representative depiction from three independent transfection experiments. (d) Centriolar recruitment of eGFP-p53 (pCAG-eGFP-p53) and mCh-HDM2 (pCAG-mCh-HDM2) and intensity threshold based spot segmentation in both the eGFP and mCherry channel. Scale bar, 10  $\mu$ m.



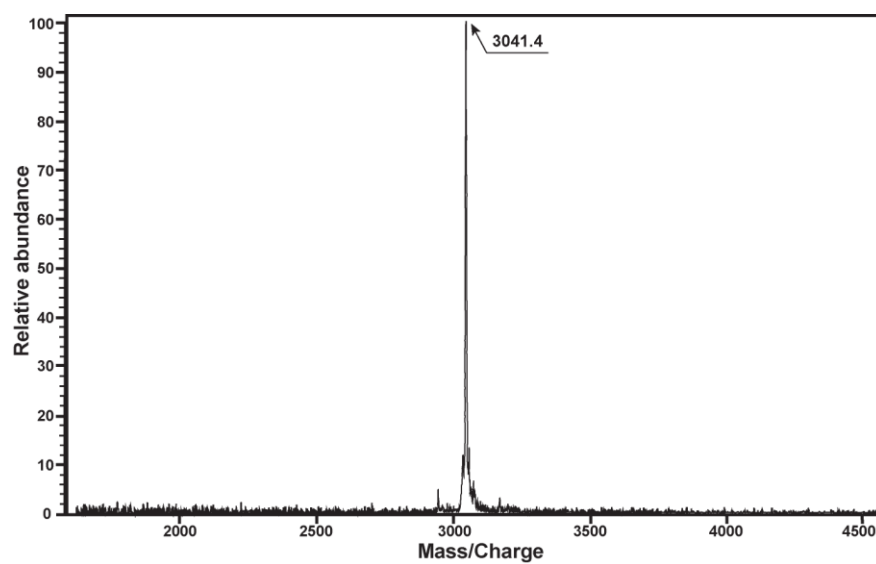


**Supplementary Figure S7.** Sequence and stretched structure of the TAT peptide coupled by a disulfide bridge to the N8A peptide inhibitor.

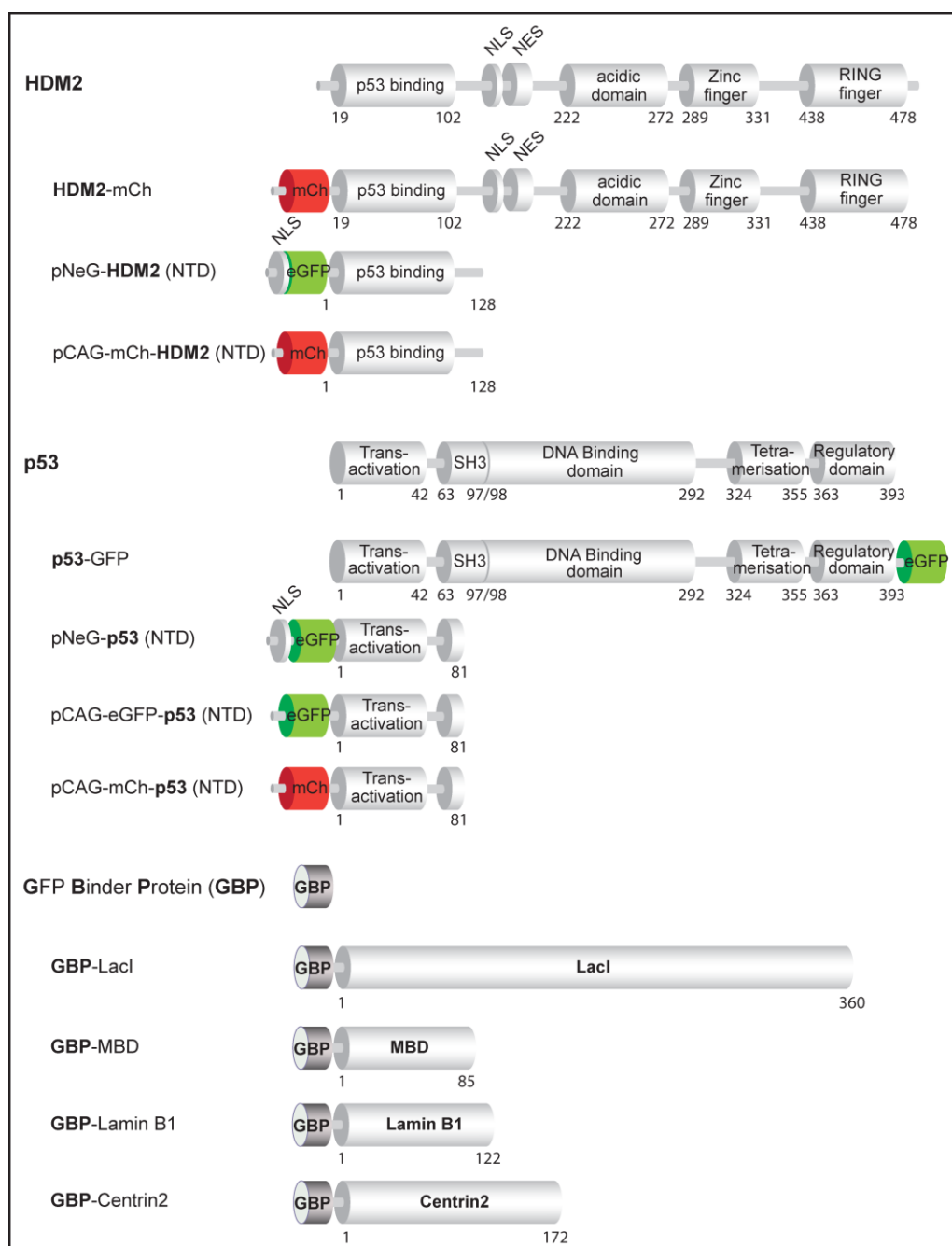


**Supplementary Figure S8.** Analytical HPLC chromatogram of the N8A peptide coupled through a disulfide bridge to the TAT peptide.

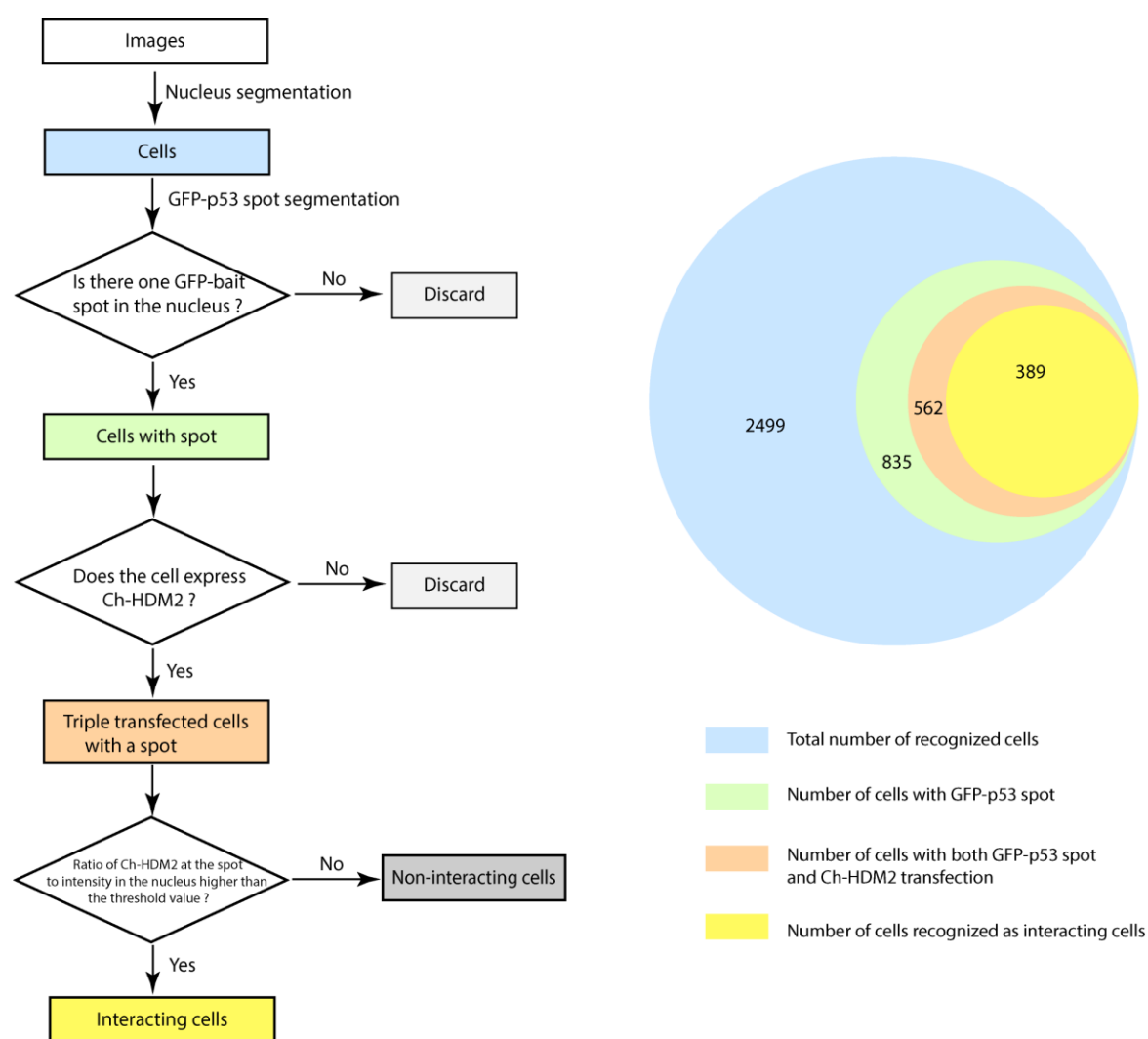




**Supplementary Figure S9.** Mass spectrum of the N8A peptide coupled through a disulfide bridge to the TAT peptide.



**Supplementary Figure S10.** Summary of chimeric fusion proteins. Schematic representation of the human HDM2, human p53 and llama derived **GFP Binder Protein (GBP)** together with the corresponding chimeric fusion protein constructs.



**Supplementary Figure S11.** Analysis flow diagram and cell populations of the high throughput assay using the GBP-LacI system. On the left, flow diagram of the high throughput analysis protocol. Cells are heuristically analyzed and divided into different groups. Cells in all the groups are evaluated, and the information, such as numbers and fluorescence intensities are measured. On the right, classification and number of cells in each group analyzed in one well. In this well, 30 fields were imaged and analyzed. From these 30 images, a total of 2,499 cells are recognized, about 33% (835 cells) of which are with one GFP-p53 spot in the nucleus. In the cells with a GFP-p53 spot, approximate 67% (562 cells) express mCh-HDM2. In these 562 cells, 389 about 70% are automatically recognized as interacting cells. In this context it should be mentioned that the prior establishment of stable cell lines changes these statistics as practically all cells become informative.



## 2.2 CENP-C Facilitates the Recruitment of M18BP1 to Centromeric Chromatin

---



# CENP-C facilitates the recruitment of M18BP1 to centromeric chromatin

Silvia Dambacher,<sup>1,2,†</sup> Wen Deng,<sup>1,3,†</sup> Matthias Hahn,<sup>1,2,†</sup> Dennis Sadic,<sup>1,2</sup> Jonathan J. Fröhlich,<sup>1,2</sup> Alexander Nuber,<sup>1,2</sup> Christian Hoischen,<sup>4</sup> Stephan Diekmann,<sup>4</sup> Heinrich Leonhardt<sup>1,3</sup> and Gunnar Schotta<sup>1,2,\*</sup>

<sup>1</sup>Ludwig Maximilians University and Munich Center for Integrated Protein Science (CiPS<sup>M</sup>); Munich, Germany; <sup>2</sup>Adolf-Butenandt-Institute; Munich, Germany;

<sup>3</sup>Department of Biology II; Ludwig Maximilians University; Munich, Germany; <sup>4</sup>Leibniz Institute for Age Research; Fritz Lipmann Institute; Jena, Germany

<sup>†</sup>These authors contributed equally to this paper.

Centromeres are important structural constituents of chromosomes that ensure proper chromosome segregation during mitosis by providing defined sites for kinetochore attachment. In higher eukaryotes, centromeres have no specific DNA sequence and thus, they are rather determined through epigenetic mechanisms. A fundamental process in centromere establishment is the incorporation of the histone variant CENP-A into centromeric chromatin, which provides a binding platform for the other centromeric proteins. The Mis18 complex, and, in particular, its member M18BP1 was shown to be essential for both incorporation and maintenance of CENP-A.

Here we show that M18BP1 displays a cell cycle-regulated association with centromeric chromatin in mouse embryonic stem cells. M18BP1 is highly enriched at centromeric regions from late anaphase through to G1 phase. An interaction screen against 16 core centromeric proteins revealed a novel interaction of M18BP1 with CENP-C. We mapped the interaction domain in M18BP1 to a central region containing a conserved SANT domain and in CENP-C to the C-terminus. Knock-down of CENP-C leads to reduced M18BP1 association and lower CENP-A levels at centromeres, suggesting that CENP-C works as an important factor for centromeric M18BP1 recruitment and thus for maintaining centromeric CENP-A.

## Introduction

Centromeres are sites for kinetochore attachment during mitosis. In order to prevent chromosome segregation defects, cells have to ensure that each chromosome has one functional centromere. Centromeres have no fixed DNA sequence that can be recognized by specific binding proteins, therefore it is assumed that epigenetic mechanisms ensure maintenance of the centromeric structure. The histone H3 variant CENP-A is a central component of centromeric chromatin. CENP-A aids in recruiting numerous proteins that build the constitutive centromere-associated network (CCAN),<sup>1–3</sup> an essential step in establishing a proper kinetochore structure.<sup>4</sup> Two proteins directly bind CENP-A and have the potential to bridge centromeric chromatin with kinetochore components. The first protein, CENP-C, recognizes the C-terminal region of CENP-A through an internal region.<sup>5</sup> The C-terminus of CENP-C mediates its dimerization,<sup>6,7</sup> the extreme N-terminus interacts with the Mis12 complex, which, in turn, bridges to outer kinetochore components.<sup>8</sup> The second protein directly recognizing CENP-A is CENP-N,<sup>9</sup> which also interacts with other centromeric components. Notably, disruption of either CENP-C or CENP-N leads to reduced levels of CENP-A at centromeres, suggesting that both proteins have additional functions in establishment or maintenance of centromere identity.<sup>5,9</sup>

The incorporation of CENP-A into the centromere is a strictly cell cycle-regulated process. During replication of centromeres, CENP-A is equally distributed onto the daughter strands, diluting the amount per centromere to 50%. To preserve centromere function, CENP-A needs to be subsequently replenished. Expression levels of CENP-A peak in G<sub>2</sub> phase, though incorporation into the centromere only occurs in late mitosis and early G<sub>1</sub> phase.<sup>10–13</sup> The histone chaperone that mediates incorporation of CENP-A is the Holliday junction-recognizing protein (HJURP).<sup>14,15</sup> HJURP can incorporate CENP-A only in domains that show a signature of actively transcribed chromatin.<sup>16</sup> Therefore, centromeric chromatin needs to be prepared (licensed), by currently unknown mechanisms. Mis18 $\alpha$ , Mis18 $\beta$  and M18BP1 which form the Mis18 complex in humans have been suggested to play an important role in this licensing mechanism.<sup>17–19</sup> Disruption of Mis18 complex components leads to failure in CENP-A incorporation,<sup>17,19</sup> which could be explained by lack of HJURP recruitment to centromeres.<sup>20,21</sup> Neither of the Mis18 complex proteins directly interact with CENP-A,<sup>9</sup> therefore, an important question within the understanding of CENP-A establishment is how this complex is specifically targeted to centromeric chromatin.

Here we show that M18BP1 is a cell cycle-regulated component of centromeric chromatin. By screening 16 CCAN proteins we

\*Correspondence to: Gunnar Schotta; Email: gunnar.schotta@med.uni-muenchen.de  
Submitted: 10/29/11; Revised: 12/04/11; Accepted: 12/06/11  
<http://dx.doi.org/10.4161/nucl.3.1.18955>

identify CENP-C as a novel interaction partner of M18BP1. We mapped the interaction domain to a central region of M18BP1 encompassing the conserved SANT domain. CENP-C facilitates the recruitment of M18BP1 to centromeric chromatin during specific stages of the cell cycle, as RNAi depletion of CENP-C leads to reduced levels of centromeric M18BP1. In summary, our work identifies CENP-C as an important centromere component that recruits M18BP1 to centromeric chromatin.

## Results

**M18BP1 is a centromere-associated protein in mouse ES (mES) cells.** In HeLa cells, prominent centromeric association of Mis 18 complex members was observed from late mitosis (ana/telophase) until the end of G<sub>1</sub> phase.<sup>17</sup> In order to determine the localization of M18BP1 in mouse cells we generated M18BP1 knock-in mES cells (K1B2) by introducing an EGFP tag into the endogenous M18BP1 locus (Fig. S1A). The K1B2 cells express M18BP1 at near endogenous levels (Fig. S1B), suggesting that the transcriptional

regulation of M18BP1 is not impaired by the alterations to this locus. We determined the localization of M18BP1-EGFP in these cells by comparing the EGFP signal with CENP-A staining to ask whether M18BP1 localizes to the centromeres. Three classes of staining patterns could be observed (Fig. 1A): (1) diffuse nuclear; (2) weak centromeric; and (3) strong centromeric foci. We then asked which cell cycle stage would correspond to the strong centromeric association of M18BP1. K1B2 cells show the typical cell cycle profile of mES cells, that is, the majority of cells are in S phase with an additional high percentage of cells in G<sub>2</sub>/M phase. In contrast to other frequently analyzed cell types, such as HeLa cells and mouse fibroblasts, the population of G<sub>1</sub> cells is comparably low in mES cells. We visualized the different cell cycle stages in K1B2 cells using specific markers. First we expressed RFP-tagged PCNA in K1B2 cells, which is an indicator of different S phase stages.<sup>22</sup> All K1B2 cells which showed defined PCNA dots, indicative of ongoing replication showed weak or diffuse M18BP1-EGFP signals (Fig. 1B). A significant number of cells outside S phase showed comparatively stronger signals, suggesting that centromeric

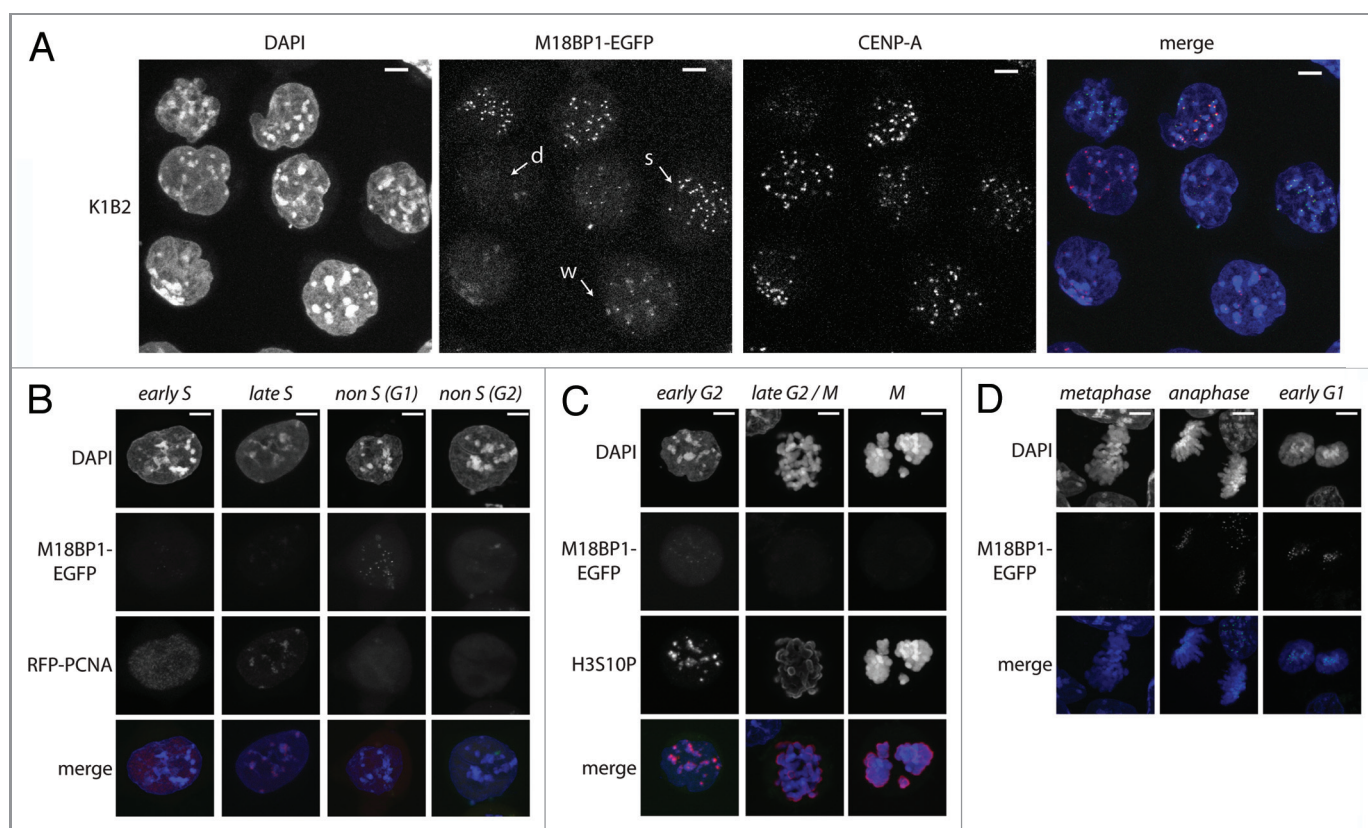


**Figure 1.** M18BP1 associates with centromeres in a cell-cycle dependent manner. (A) Localization of endogenously tagged M18BP1-EGFP in the K1B2 mES cell line. K1B2 cells were stained for CENP-A and confocal stacks were recorded. Maximum intensity projections are shown. M18BP1-EGFP showed different patterns: strong enrichment at centromeres (s), weak enrichment (w), no enrichment/diffuse nuclear (d). Scale bars are 20 μm. (B) M18BP1 distribution during S phase. K1B2 cells were transfected with a RFP-PCNA expression construct to detect cells in different S phase stages. M18BP1-EGFP showed intermediate to low centromeric enrichment throughout S phase. Cells which are not in S phase fall into two different staining patterns: M18BP1 is highly enriched at centromeres (presumably G1) and cells with low/no centromeric M18BP1 signals (presumably G2). (C) M18BP1 distribution in G2/M phase. K1B2 cells were stained with H3S10P antibodies to visualize different stages of G2 and M phase. Starting from early G2 phase (weak H3S10P signal) to M phase (strong H3S10P signal) M18BP1 appeared to be largely absent from centromeres. (D) M18BP1 localization in different mitotic stages. In metaphase cells, M18BP1 is absent from centromeres, however, starting from late anaphase, M18BP1 showed strong signals at centromeric regions. Scale bars in (B–D) are 5 μm.



M18BP1 association is low throughout S phase (Fig. 1B) and is only enriched in G<sub>1</sub> or G<sub>2</sub>/M phase. We therefore tested whether M18BP1 begins to be enriched after S phase, in G<sub>2</sub>/M. In order to visualize G<sub>2</sub>/M cells, we performed immunofluorescence staining for H3S10 phosphorylation.<sup>23</sup> All K1B2 cells that were positive for H3S10P showed only weak centromeric M18BP1 signals (Fig. 1C, early G<sub>2</sub>), leading to the conclusion that the highly enriched M18BP1 signals appear in G<sub>1</sub> phase cells. Interestingly, in G<sub>2</sub> phase cells, M18BP1 does not seem to associate with all centromeres as we detect numerous CENP-A spots without M18BP1 enrichment (Fig. S2). Late G<sub>2</sub> and prometaphase cells did not show significant centromeric signals for M18BP1 (Fig. 1C, late G<sub>2</sub>/M). Finally, we tested at which step after mitosis M18BP1 starts being localized to centromeric regions by examining distinct mitotic stages in K1B2 cells. Notably, we find that metaphase cells still display very low M18BP1 signals, though as soon as cells enter anaphase/telophase, M18BP1 is highly enriched at centromeres (Fig. 1D). In those cells centromeric CENP-A signals are still relatively low as deposition of new CENP-A only occurs at later stages in the cell cycle.<sup>12</sup> In summary, our localization analysis demonstrates that in mES cells, M18BP1 is not constitutively enriched at centromeric chromatin but rather associates with centromeres from anaphase continuing to G<sub>1</sub> phase. This is the time when CENP-A incorporation takes place.

**Centromere interaction screen for M18BP1.** M18BP1 is known to be important for preparing centromeric chromatin for CENP-A incorporation. However, still very little is known about how M18BP1 actually recognizes centromeric chromatin. We

pursued the idea that M18BP1 might be recruited through interaction with components of the CCAN network. To test this hypothesis we performed an F3H interaction screen of M18BP1 with proteins of the CCAN network. The F3H interaction assay utilizes a BHK cell line with a lac operator repeat array stably integrated into its genome (Fig. 2A). This cell line was transfected with an expression vector encoding the lac repressor (lacI) which directly binds to the lac operator sequence fused with a GFP binding protein (GBP). These cells further expressed the EGFP tagged bait protein (M18BP1-EGFP) and individual RFP/ mCherry tagged prey proteins (CCAN proteins). M18BP1-EGFP is bound by the lacI-GBP fusion protein at the lac operator arrays and can be detected at the well-discernible nuclear lacO focus. Prey protein interaction with M18BP1 is identified by localization to this nuclear focus (Fig. 2A). The red/green signal intensity ratio provides a measure for the strength of the tested interaction.

We tested M18BP1 for interaction with 16 proteins of the CCAN network using the F3H assay. In agreement with previous analyses we did not detect a direct interaction with CENP-A (Fig. 2B). Interestingly, we found a strong interaction with another protein of the inner centromere, CENP-C. None of the other CCAN proteins that we tested showed significant interaction with M18BP1 (Fig. 2C).

M18BP1 harbors two evolutionarily conserved domains, the SANT domain in the C-terminal part of the protein and the SANTA domain which is toward the N-terminus. To test which region of M18BP1 participates in the interaction with CENP-C

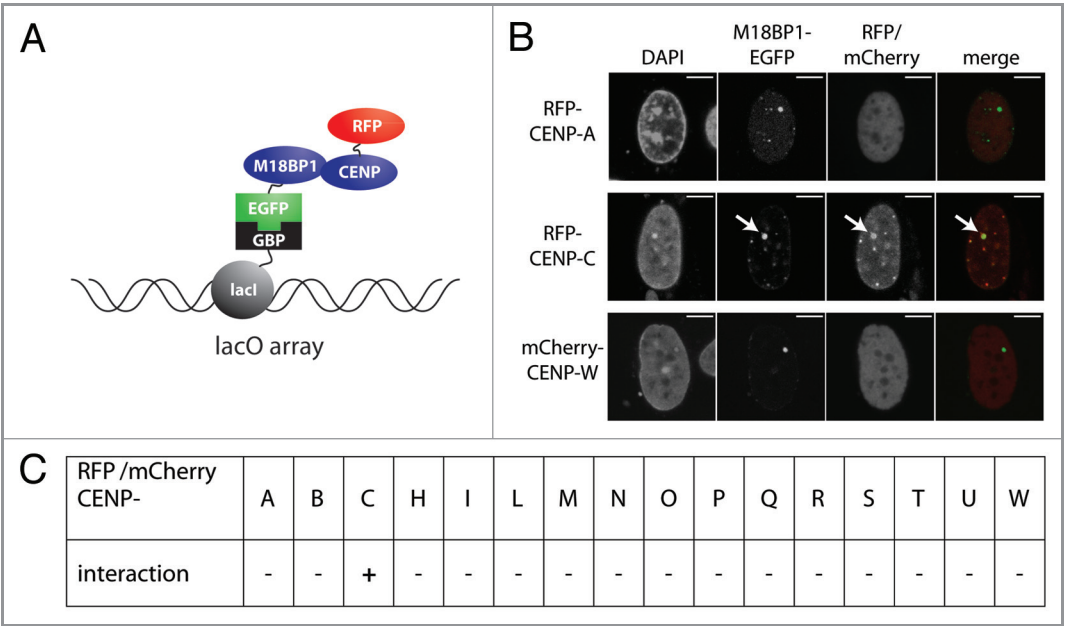


**Figure 2.** F3H interaction screen for M18BP1 interaction partners. (A) Scheme depicting the F3H screening strategy. Cells containing a lac operator array were transfected with plasmids expressing a lac repressor-GBP fusion protein, M18BP1-EGFP and mCherry/RFP-CCAN proteins. The lac repressor binds to the lac operator array and through the GBP recruits M18BP1-EGFP. CCAN proteins interacting with M18BP1 are consequently enriched at the lac operator array. (B) Representative examples for M18BP1 interacting (CENP-C) and non-interacting (CENP-A and CENP-W) proteins are shown. Scale bar is 5µm. (C) Summary of interaction tests between M18BP1 and CCAN proteins. Interactions were tested with the F3H assay using M18BP1-EGFP and 16 RFP or mCherry fusions with CCAN proteins. From all 16 tested CCAN proteins, only CENP-C showed a clear interaction with M18BP1.

we tested a panel of M18BP1 truncated proteins (Fig. 3A). The N-terminus of M18BP1 (M1, aa1–440) showed no interaction with CENP-C, but the C-terminus (M2, aa441–998) clearly interacted (Fig. 3B). The central region (M3, aa325–800) and a truncated protein lacking the SANTA domain (M4, aa441–800) displayed clear interactions with CENP-C. In order to then test whether the SANT domain is sufficient for the CENP-C interaction, we assessed a truncated protein harboring only the SANT domain (M5, aa735–800). This failed to interact with CENP-C, suggesting that additional parts of M18BP1 participate in this interaction. We scrutinized these observations by quantifying the interactions in several hundred cells per construct through measurement of the ratio between red and green intensity values at the M18BP1-EGFP foci. Although, by confocal imaging we can detect red/green colocalization of M18BP1-M4 and CENP-C in 73% of the cells (Fig. 3B), the average red/green signal ratio is relatively low (Fig. 3C). This, however, can be explained by relatively low expression levels of RFP-CENP-C in the combination with M18BP1-M4. In summary, our F3H data show that CENP-C interacts with a central region of M18BP1 comprising the SANT domain.

**M18BP1 directly interacts with CENP-C.** We then aimed to further define the M18BP1-CENP-C interaction. First, we wanted to analyze whether M18BP1 co-localizes with CENP-C. To do this, we transfected K1B2 cells with a plasmid expressing RFP-tagged CENP-C and performed confocal imaging. We found many cells showing a clear overlap between M18BP1-EGFP and RFP-CENP-C signals. However, there was also a large percentage of cells with prominent CENP-C signals, with no M18BP1 co-localization (Fig. 4A). These data suggest that the interaction between these two proteins is highly regulated in vivo.

In order to test whether CENP-C and M18BP1 can interact in vivo, we performed co-immunoprecipitation experiments. We transfected HEK293 cells with expression plasmids for CENP-C-EGFP and myc-M18BP1, prepared nuclear extract and purified CENP-C-EGFP using GFP trap affinity beads. In the bound material we could clearly detect co-purification of the EGFP-tagged CENP-C and the myc-tagged M18BP1 (Fig. 4B). We then wanted to further map the interaction domains between M18BP1 and CENP-C using in vitro binding assays. CENP-C has several conserved domains which have already been implicated in different biochemical interactions and in vivo functions, such as

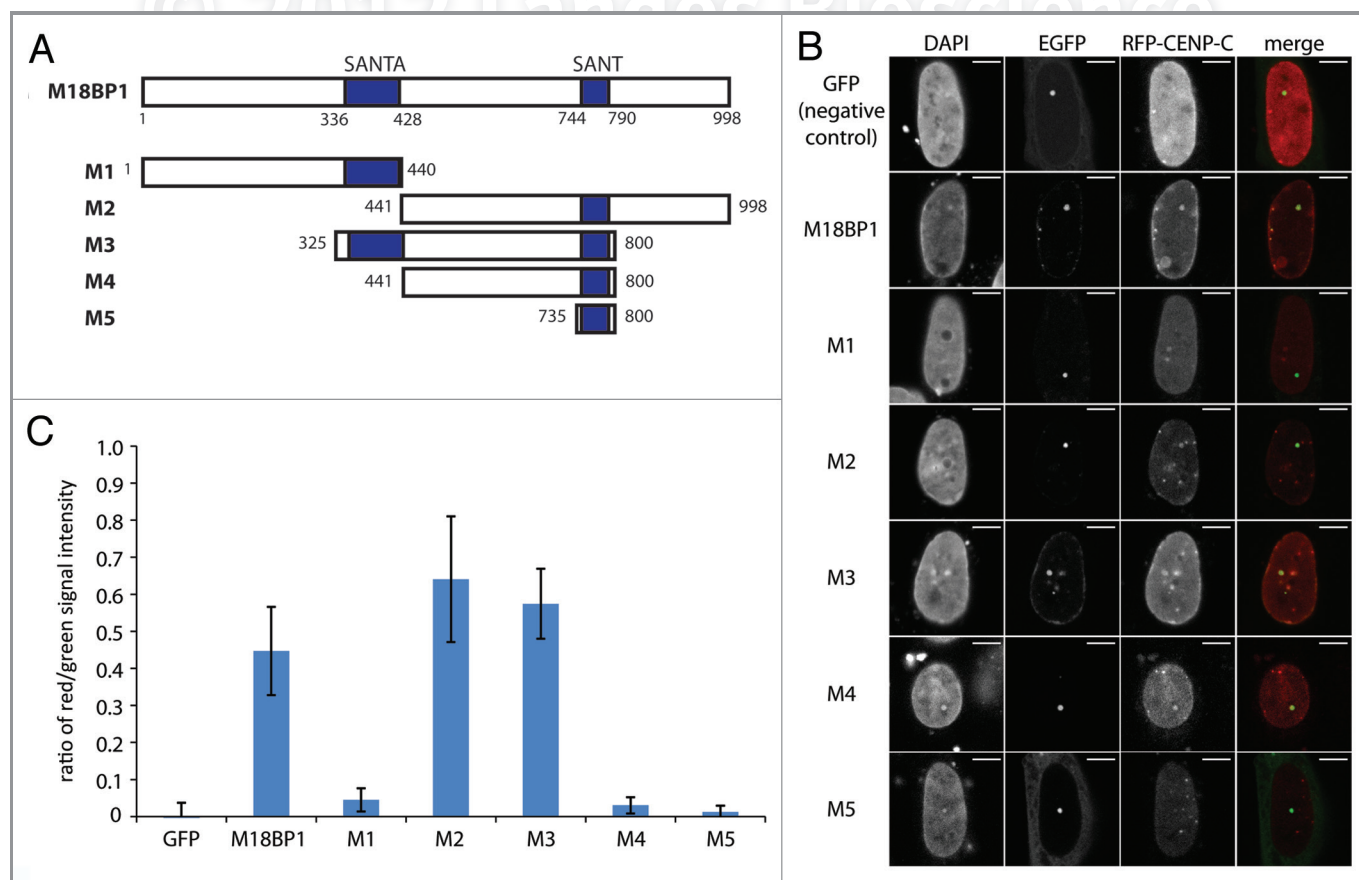


**Figure 3.** Mapping of the M18BP1-CENP-C interaction domains by F3H. (A) Scheme of M18BP1 truncations used in the interaction tests. (B) Representative F3H images of the negative control (GFP only) and EGFP tagged M18BP1 truncations tested with RFP-CENP-C. Overlap of red and green signals at the nuclear *lacO* focus indicates interaction. (C) Quantification of the F3H M18BP1-CENP-C interaction data. Intensities of red and green signals at the nuclear *lacO* focus were measured in several hundred cells each. The ratio between red and green signals was determined to measure the strength of the tested interactions.

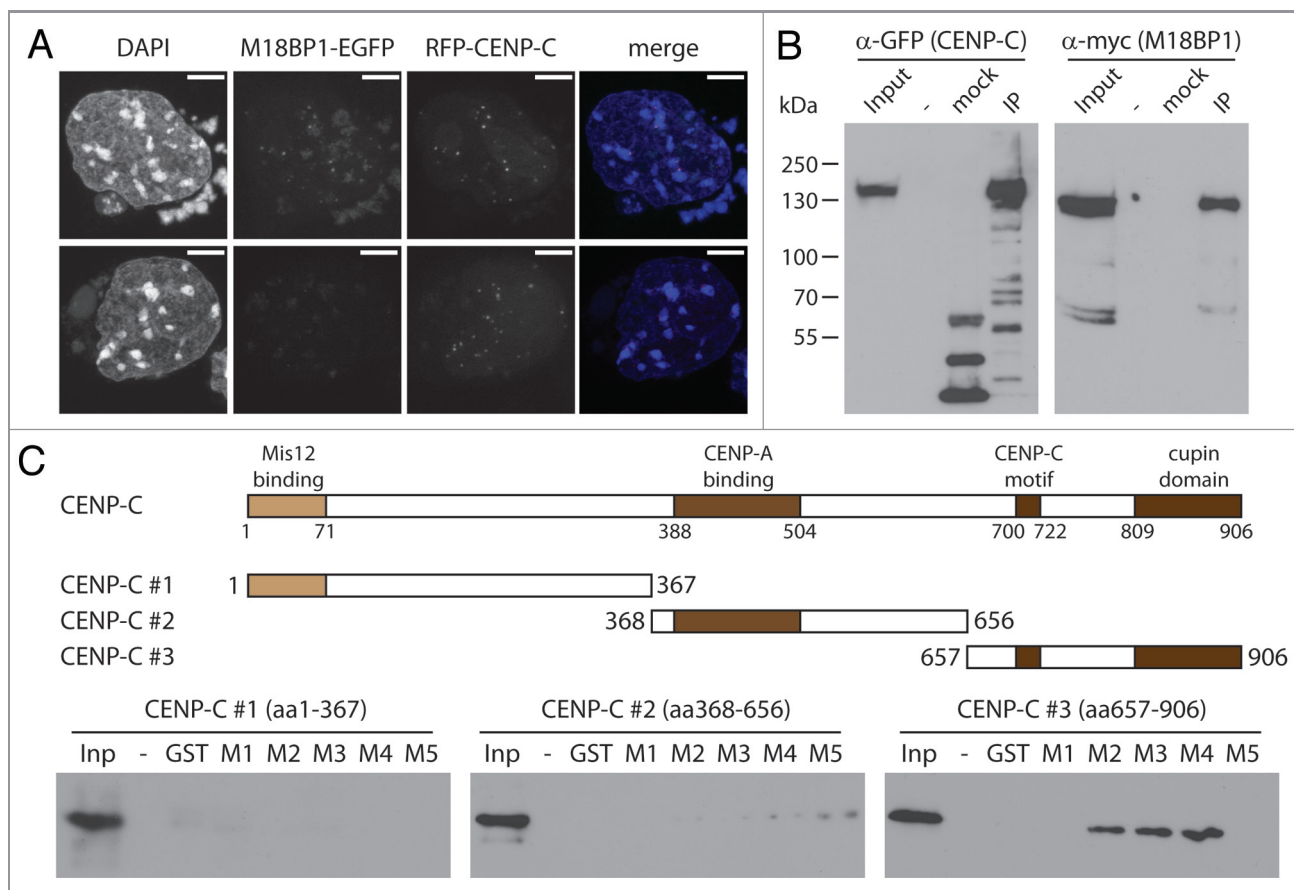


**Figure 4.** M18BP1 and CENP-C interact in vitro. (A) Co-localization of RFP-CENP-C and M18BP1-EGFP. K1B2 cells were transfected with a RFP-CENP-C expression construct. Maximum intensity projections of two representative staining patterns are shown. Scale bar is 5  $\mu$ m. (B) Co-immunoprecipitation of CENP-C and M18BP1. HEK293FT cells were transfected with expression plasmids for EGFP-CENP-C and myc-M18BP1. Nuclear extracts from these cells were incubated with agarose beads (control) and GFP-Trap affinity beads to enrich for EGFP-CENP-C and interacting bound proteins. Protein gel blot analysis shows the nuclear extract (Inp), proteins bound to agarose beads (mock) and proteins that were enriched with GFP-Trap agarose beads (IP). An empty lane is indicated by “-”. EGFP-CENP-C and myc-M18BP1 were detected using antibodies against GFP and myc, respectively. (C) Interaction tests between M18BP1 and CENP-C truncations. The scheme shows the domain structure of mouse CENP-C and the truncation constructs that were used in this assay. Recombinant GST-tagged M18BP1 truncations (M1-M5) were incubated with in vitro translated myc-CENP-C truncation proteins and bound to GST beads. The bound CENP-C protein truncations were detected using myc antibody. Only the C-terminal CENP-C fragment showed clear interaction with M18BP1. The M18BP1 fragments M1-M5 are depicted in **Figure 3A**.

connection to the outer kinetochore proteins, CENP-A binding and CENP-C dimerization (**Fig. 4C**, schematic). We generated in vitro translated proteins of three CENP-C truncations and tested their interaction with recombinant GST tagged M18BP1 truncations (M1-M5). In these assays we could only detect significant interaction of M18BP1 with CENP-C #3, containing the CENP-C motif and the cupin domain (**Fig. 4C**). These data provide an extension of the F3H analysis; confirming that the large central region of M18BP1 is required for CENP-C binding.

**CENP-C is required for the recruitment of M18BP1 to centromeres.** Our data show that M18BP1 interacts with CENP-C in vitro and in vivo. CENP-C itself binds to centromeres through direct interaction with CENP-A. We therefore hypothesized that CENP-C facilitates the recruitment of M18BP1 to centromeric chromatin. In order to test this hypothesis we performed CENP-C knock-down experiments in K1B2 cells in which we could easily assess the localization of endogenously

expressed M18BP1-EGFP. We prepared pLKO-based lentiviral vectors with three independent shRNA oligos against CENP-C and one control oligo containing an unrelated sequence (**Table S1**). CENP-C knock-down cells were analyzed by qPCR five days post infection to determine the knock-down efficiency of the individual oligos. Importantly, all three knock-down oligos resulted in effective downregulation of CENP-C mRNA (**Fig. 5A**) and protein (**Fig. S3**), with shCENP-C #3 showing the strongest knock-down. Crucially, the expression level of M18BP1 was unchanged. CENP-C knock-down did not lead to significant changes in the cell cycle profile of K1B2 cells, however, we did notice an increase in the number of cells with sub-G1 DNA content (**Fig. S4**) as well as reduced cell numbers at day five after knock-down (**Fig. S5**), indicating elevated cell death upon CENP-C knock-down.

To test whether CENP-C affects the localization of M18BP1 we investigated M18BP1-EGFP and CENP-A patterns in the CENP-C knock-down cells. In control knock-down cells, M18BP1-EGFP



shows the typical distribution of different centromere enrichment levels: strong, weak and diffuse nuclear (Fig. 5B, arrows). We observed that the number of cells with centromeric association of M18BP1 was reduced in all three knock-down cell lines (Fig. 5B). In order to quantify this phenotype we determined the distribution of M18BP1 staining patterns in control and CENP-C knock-down cells. Importantly, in all knock-down cell lines the percentage of cells with “weak” M18BP1-EGFP enrichment at centromeres was reduced, whereas M18BP1-EGFP “diffuse” cells were increased (Fig. 5C). In knock-down shCENP-C #3 we even detected reduced numbers of M18BP1 ‘strong’ cells, suggesting that more efficient CENP-C knock-down more severely impairs centromeric M18BP1 recruitment. We then asked whether the reduced centromeric M18BP1 recruitment corresponds to specific cell cycle stages by co-staining of control and CENP-C knock-down cells with specific cell cycle markers (Fig. S6). In shControl cells we could reproduce the results of our initial cell cycle analysis in K1B2 cells: G<sub>1</sub> cells showed strong centromeric signals, G<sub>2</sub> cells showed weak signals. Importantly, upon CENP-C knock-down we detected G<sub>1</sub> and G<sub>2</sub> phase cells which had clearly lost centromeric M18BP1 (Fig. S6),

indicating that the role of CENP-C in ensuring centromeric M18BP1 localization is not restricted to a particular cell cycle stage.

M18BP1 was proposed to ‘prime’ centromeres for deposition of CENP-A.<sup>17,19</sup> In order to investigate whether reduced centromeric M18BP1 recruitment would also lead to less efficient CENP-A incorporation, we divided CENP-A staining patterns into low, medium and high and determined the percentage of cells showing these patterns in control and CENP-C knock-down cells. In particular knock-down shCENP-C #3 which had the strongest effect on centromeric M18BP1 recruitment lead to significantly reduced CENP-A levels (Fig. 5C).

In summary our data demonstrate that the interaction between CENP-C and M18BP1 is an important recruitment mechanism for M18BP1 to centromeric chromatin, which appears necessary for the correct deposition of CENP-A.

## Discussion

The deposition of CENP-A into centromeric chromatin is essential to ensure proper segregation of chromosomes. The

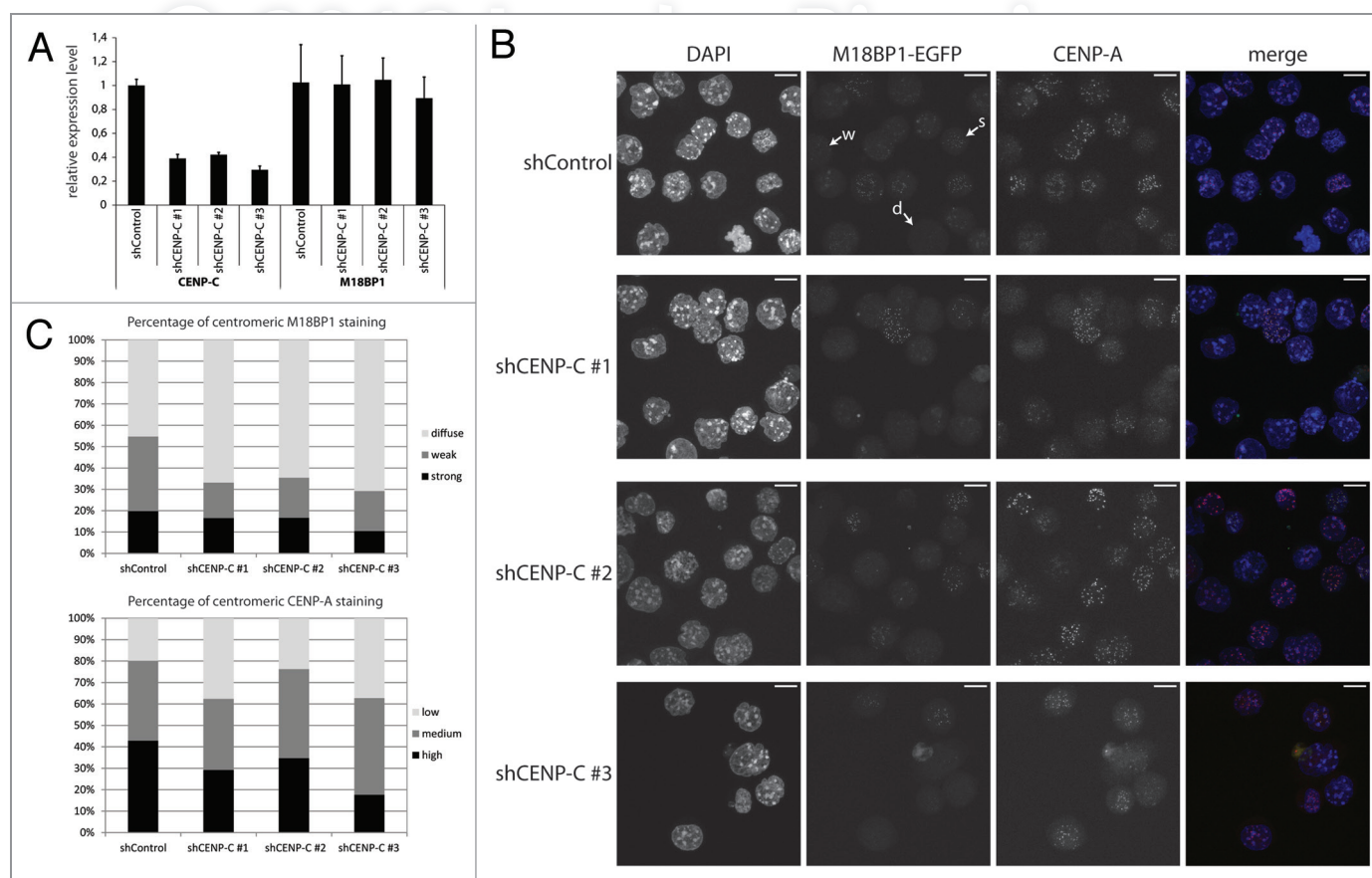


**Figure 5.** CENP-C knock-down leads to impaired centromeric recruitment of M18BP1. (A) RT-qPCR for CENP-C and M18BP1 five days after knock-down. Expression levels in the control knock-down cell line (shControl) and the three CENP-C knock-down cell lines (shCENP-C #1-#3) were normalized to the geometric mean of GAPDH and Actin. (B) Representative maximum intensity projections of confocal stacks of control and CENP-C knock-down cells that were stained for CENP-A. Arrows point to example cells for the three classes of M18BP1 signals: strong (s), weak (w) and no enrichment/diffuse nuclear (d). Scale bars are 10µm. (C) Quantification of the M18BP1 signals in control vs. CENP-C knock-down cell lines. M18BP1 and CENP-A staining patterns were classified in several hundred cells. The bar graph depicts the percentages of each class.

Mis18 complex member M18BP1 was shown as an essential factor to prepare centromeric chromatin for CENP-A deposition and to ensure its maintenance.<sup>17,19,24</sup> Our data constitute the first analysis of endogenously expressed M18BP1 in mES cells. We report that M18BP1 associates with centromeric chromatin during distinct cell cycle stages. M18BP1 shows highest abundance at centromeres from anaphase through to late G<sub>1</sub> phase. These data are in agreement with observations in human cells, where M18BP1 also associates with centromeres starting from late telophase through to G<sub>1</sub> phase<sup>17</sup> and suggest that M18BP1-mediated processes might be evolutionarily conserved in higher mammals.

We have furthered the understanding of how M18BP1 is recruited to centromeres through identification of a novel interaction between the C-terminus of CENP-C with a central region in M18BP1, which contains a SANT domain. The SANT domain is highly conserved and found in many chromatin-associated proteins, but very little is known about its potential functions. It has been implicated in the mediation of protein-protein interactions and binding to histone modifications.<sup>25</sup> We do not detect a direct interaction between the isolated M18BP1 SANT domain and CENP-C, however, it is possible that this domain is only functional in a larger protein context. More detailed experiments are necessary to further understand the functional roles of this domain in M18BP1. Our interaction data are consistent with a very recent study which appeared during the preparation of this manuscript.<sup>26</sup> Moree et al. found that *X. laevis* xM18BP1 isoforms interact with xCENP-C, and they could also show that human M18BP1 interacts with human CENP-C. In their study the interaction domain with xM18BP1 was mapped to the C-terminus of xCENP-C containing the CENP-C motif and the cupin domain. Mouse CENP-C (906aa) is much smaller than xCENP-C (1400aa), however, the major domains, such as CENP-A binding domain, CENP-C motif and cupin domain are conserved. We could show that in the mouse the interaction with M18BP1 is also mediated through a C-terminal fragment of CENP-C containing the CENP-C motif and the cupin domain, and thus the M18BP1 interaction site in CENP-C seems to be evolutionarily conserved.

Our data moreover demonstrate an important function for CENP-C in mediating the centromeric recruitment of M18BP1. When CENP-C protein levels are reduced to around 40–50% (shCENP-C #1 and #2) we found reduced numbers of “weak” centromeric M18BP1 cells. The numbers of “strong” centromeric M18BP1 cells, a staining pattern which we found characteristic for G<sub>1</sub> phase cells, seemed to be unaltered. More severely reduced CENP-C levels (shCENP-C #3) resulted in lower numbers of cells with “weak” and “strong” centromeric M18BP1. Our cell cycle marker analysis revealed that the role of CENP-C in mediating centromeric M18BP1 recruitment is not restricted to selective cell cycle stages. However, we cannot exclude the possibility that CENP-C has additional functions that indirectly regulate the centromeric association of M18BP1 during distinct cell cycle phases. In this context it is interesting to note that when we transiently express CENP-C in K1B2 cells, we find a high percentage of cells in which CENP-C is abundantly

associated with centromeres, but M18BP1 does not co-localize. It is therefore plausible to assume that further regulatory mechanisms exist, e.g., post-translational modifications, which influence the in vivo interaction between these two proteins. Both M18BP1 and CENP-C can be phosphorylated and sumoylated at multiple sites.<sup>27–30</sup> It will be challenging to understand how these modifications are regulated and how they influence interactions between the different centromeric proteins in a cell cycle-dependent manner.

The centromeric recruitment of M18BP1 appears important for correct deposition of CENP-A. In particular strong depletion of CENP-C with knock-down oligo shCENP-C #3 leads to reduced levels of centromeric CENP-A. These data are consistent with Moree et al., which demonstrate in the *Xenopus* system that upon xCENP-C depletion, centromeric deposition of new CENP-A is impaired.<sup>26</sup> The failure to correctly establish CENP-A might be due to loss of centromeric M18BP1 at critical cell cycle stages. In human cells, CENP-A deposition is mediated by HJURP during G<sub>1</sub> phase. Loss of M18BP1 leads to reduced HJURP association with centromeres and consequently to reduced deposition of newly synthesized CENP-A.<sup>14,15</sup> In our mES cell system strong CENP-C knock-down results in cells which lose M18BP1 during G<sub>1</sub> phase when CENP-A deposition normally occurs. We therefore postulate that those cells will also have problems in correctly establishing centromeric CENP-A patterns. We do not detect a large number of cells which have lost CENP-A upon CENP-C knock-down. We think that this could be explained by the high cell lethality of the CENP-C knock-down. Therefore, at the current stage of analysis, we cannot distinguish whether critically low CENP-A levels would induce apoptosis in ES cells, or whether CENP-C has additional functions that could be critical for survival of ES cells. Also, the functions of M18BP1 need to be investigated in more detail to understand how the centromeric recruitment of this molecule drives the subsequent deposition of CENP-A during G<sub>1</sub> phase and whether M18BP1 features additional roles during other cell cycle stages when its centromeric recruitment is much lower but still detectable.

## Materials and Methods

**M18BP1 knock-in cell line.** The M18BP1-EGFP targeting constructs were obtained using the recombineering cloning technique described previously.<sup>31</sup> To generate retrieval and mini-targeting vectors, PCR fragments were amplified from the BAC clone RP23–396P24 (Children's Hospital Oakland Research Institute). For the retrieval plasmid, PCR fragments were cloned into the pL253 plasmid using NotI, HindIII and SpeI. A genomic region of 7 kb, spanning the last exons of M18BP1, was retrieved from the BAC clone using recombineering in EL350 bacteria. The mini-targeting plasmid was constructed by generating PCR fragments flanking the M18BP1 stop codon. These PCR fragments were cloned together with the floxed Neomycin selection cassette from pL452 (EcoRI-BamHI fragment) into pBluescript IISK+ using NotI, EcoRI, BamHI and SalI. In a subsequent cloning step, the EGFP tag was inserted with

EcoRI. For the final targeting vector, the 7 kb region was mini-targeted by recombining with the NotI-Sall fragment containing the EGFP and floxed Neomycin selection cassette from the mini-targeting plasmid.

To generate M18BP1 knock-in cells, the NotI-linearized targeting vector was electroporated into feeder-independent wild type mES cells. Cells were selected in 180 µg/ml G418 (PAA) and 2 µM Ganciclovir (Invivogen). Single colonies were picked and screened by nested PCR to obtain the final mES cell clone (K1B2). Primers used for cloning and PCR screening are listed in Table S1.

**Cell culture and transfections.** BHK cells containing a *lac* operator repeat array<sup>32</sup> were cultured in DMEM medium with 10% FCS and seeded on coverslips in 6-well plates for microscopy. After attachment cells were co-transfected with expression vectors for the indicated fluorescent fusion proteins and a LacI-GBP fusion<sup>33,34</sup> using polyethylenimine (Sigma). After about 16 h cells were fixed with 3.7% formaldehyde in PBS for 10 min, washed with PBST (PBS with 0.02% Tween), stained with DAPI and mounted in Vectashield medium (Vector Laboratories).

Mouse ES cells were cultivated on gelatinized plates in High Glucose DMEM with L-Glutamine and sodium pyruvate, complemented with 15% FCS, β-mercaptoethanol, non essential amino acids (PAA), penicillin/streptomycin (PAA) and LIF in a 37°C incubator at 5% CO<sub>2</sub>. For transfection with Lipofectamine 2000 (Invitrogen), mES cells were seeded on matrigel (BD Biosciences) coated coverslips.

HEK 293FT cells (Invitrogen) were cultivated on gelatinized plates in High Glucose DMEM with L-Glutamine and sodium pyruvate (PAA) complemented with 10% FCS, β-mercaptoethanol, non essential amino acids (PAA) and penicillin/streptomycin (PAA) in a 37°C incubator at 5% CO<sub>2</sub>. The cells were transiently transfected one day after seeding using standard calcium phosphate transfection.

**Microscopy.** F3H samples were analyzed with a confocal fluorescence microscope (TCS SP5, Leica) equipped with a 63 × / 1.4 numerical aperture Plan-Apochromat oil immersion objective as described.<sup>34</sup> DAPI, EGFP and mCherry/RFP were excited by 405 nm diode laser, 488 nm argon laser and 561 nm diode-pumped solid-state laser, respectively. Images were recorded with a frame size of 512 × 512 pixels.

K1B2 cells were imaged using a Leica TCS SP5 confocal laser scanning microscope with a HCX PL APO CS 63x/1.3 NA glycerol immersion objective. Sequential excitation at 405 nm, 488 nm, 543 nm and 633 nm was provided by diode, argon and helium-neon gas lasers, respectively. Emission detection ranges of the photomultipliers were adjusted to avoid crosstalk between the channels. Maximum intensity projections of the confocal sections were generated using ImageJ software.

**Intensity ratio measurement.** Images were acquired with an IN Cell Analyzer 2000 (GE Healthcare) using a 40 × air objective and analyzed with the IN Cell Analyzer 1000 Workstation 3.7 (GE Healthcare). Green and red fluorescence intensities at the *lac* spots were quantified. After background subtraction, intensity ratios of red (prey) to green (bait) were calculated and plotted using Excel software (Microsoft).

**Lentiviral knockdown and infection of K1B2 cells.** Lentiviral shRNA sequences (Table S2) were selected from the TRC library<sup>35</sup> or designed using the TRC shRNA designer (<http://www.broadinstitute.org/rnai/public/>).

For lentiviral knock-downs one non-targeting shRNA and three shRNAs targeting mouse CENP-C mRNA (NCBI RefSeq NM\_007683.3) were cloned into the lentiviral knock-down vector pLKOmod1<sup>36</sup> with MluI/XmaI.

For restricting lentiviral transduction to mouse cells, we replaced the commonly used VSVg protein during viral packaging with the ecotropic envelope protein of Moloney Murine Leukemia Virus. The new packaging vector pLP-ecoenv was generated by removing the VSVg sequence of pLP-VSVg (Invitrogen) by EcoRI digest, followed by T4 polymerase filling of the remaining vector and ligation of a EcoRI/NotI cut and T4 polymerase filled PCR product of the M-MLV ecotropic envelope sequence

(Primers: eco env fw 5'-CGAATTGCGCCGCCACCATGG CGCGTTCAACGCTCTCAAAA-3'; eco env rw 5'-TACGC GGCCGCTATGGCTCGTACTCTAT-3').

Lentiviral production was performed by seeding 4 million HEK293FT cells (Invitrogen) one day before transfection in gelatinized 10 cm dishes. On the following day, cells were transiently cotransfected with 8 µg psPAX2, 8 µg pLP-ecoenv and 8 µg of the respective pLKOmod1 vector using standard calcium phosphate transfection. Conditioned medium containing recombinant lentiviruses was harvested 48 h post transfection, aliquoted, snap frozen and stored at -80°C until further use.

K1B2 cells were transduced by seeding 3 × 10<sup>6</sup> cells onto gelatinized 15 cm dishes containing mES cell medium supplemented with 4 µg/ml Polybrene (Sigma) and up to 20% conditioned virus medium. After 24 h the medium was replaced. 48 h post transduction, cells with stable integration of the pLKOmod1 vector were selected in mES cell medium containing 1.4–2 µg/ml puromycin (PAA) and then maintained in this selection medium until analysis.

Knock-down efficiency was determined at day five post infection by qRT-PCR and protein gel blotting. The following antibodies were used: CENP-C (Abcam ab50974), Suv4-20h2 (Hahn et al., in preparation).

**RT-qPCR for monitoring M18BP1 and CENP-C expression levels.** RNA of control and CENP-C knock-down cells was harvested at day 5 after transduction using RNeasy (Qiagen). 1.25 µg RNA was used for cDNA synthesis using Superscript III Kit (Invitrogen) and random hexameric primers (NEB). QPCR reactions were performed in technical triplicates using a Roche Light Cycler 480 with FAST SYBR<sup>®</sup> Master Mix (Applied Biosystems), and gene-specific primers (Table S3). Ct-values were normalized to the geometric mean of Actin and GAPDH for each individual cDNA and fold changes were calculated by the 2<sup>-ΔΔCt</sup>-method.<sup>37</sup>

**Immunofluorescence.** Immunofluorescence analyses were performed as described<sup>38</sup> using the following antibodies: CENP-A (C51A7, Cell Signaling Technology), H3S10P (06-570, Upstate) and Alexa 647 (A31573, Molecular Probes).

**Plasmids.** Encoding sequences of CENPs were amplified by PCR (Expand high fidelity<sup>PLUS</sup> PCR System, Roche, Penzberg,



Germany). As forward primers we used 5'-GGGGACAAGT-TTGTACAAAAAGCAGGCTTCGAAAACCTGATTTTCAG-GGCGCCACC-3' as flanking regions followed by 20–26 bases of coding regions starting with 5'-ATGG-3' and as reverse primers we used 5'-GGGGACCACTTTTGTACAAGAAAGCTGGGT-3' as flanking regions followed by 20–26 bases of coding sequences without stop codon. CENP encoding PCR fragments were transferred into vector pDONR221 by BP recombination reaction (Invitrogen, Carlsbad, CA, USA). After verification by DNA sequencing (MWG Biotech, Ebersberg, München, Germany), genes were transferred by LR recombination reactions to various modified pEGFP-C and pmCh-C (BD Biosciences, Clontech, Palo Alto, CA, USA) based destination vectors. The resulting expression vectors encode CENPs fused to the C-termini of EGFP and mCherry with SGTSLYKKAGFENLYFQGAT as linker sequence and TQLSCTKW added to the C-terminal ends of the FP-CENP fusions. Complete sequences are provided upon request. Correct full length expression of fusion constructs was confirmed by protein gel blots.

Full-length open reading frames of mouse M18BP1, the M18BP1 truncations and the mouse CENP-C truncations were PCR amplified from mouse cDNA derived from mES cells and cloned into the pDONR/Zeo GATEWAY entry vector (Invitrogen) using Gateway BP Clonase II enzyme mix (Invitrogen). PCR primers are listed in Table S4. Entry clones were recombined into target vectors pEGFP-N1-GW, pCMVmyc-GW and pGEX6P1-GW<sup>39</sup> using LR Clonase II enzyme mix (Invitrogen).

**In vitro binding assays.** Recombinant M18BP1 protein truncations (C1 aa1–440, C2 aa441–998, C3 aa325–800, C4 aa441–800, C5 aa735–800) were expressed as GST tagged versions in *E. coli* and purified on Glutathione-S-Sepharose (GE Healthcare). In vitro translation of CENP-C protein truncations (aa1–367, aa368–656, aa657–906) was performed using TnT<sup>®</sup> Quick Coupled Transcription/Translation System (Promega). 10 µl of the in vitro translated myc-tagged CENP-C and 5 µg M18BP1 GST-fusion protein coupled to Glutathione-S-Sepharose were incubated in IP buffer (50 mM Tris pH7.5, 150 mM NaCl, 1 mM EDTA, 0.1% NP40, 20% glycerol and proteinase inhibitor cocktail (Roche)) overnight at 4°C on a rotating wheel. The beads were washed four times with IP buffer containing 1 M NaCl and resuspended in 50 µl SDS loading

buffer (Roth). Bound proteins were separated on SDS polyacrylamidgels and detected by immunoblotting using  $\alpha$ -myc antibody (9E10).

**Co-immunoprecipitation in HEK293FT cells.** HEK293FT cells (Invitrogen) were co-transfected with plasmids expressing EGFP-CENP-C and myc-M18BP1. Isolated nuclei were resuspended in high salt IP buffer (50 mM Tris pH 7.5, 500 mM NaCl, 1 mM EDTA, 0.1% NP40, 20% glycerol) with 4 strokes through a 19.5G syringe needle. After incubation on ice for 30 min the solution was sonicated 3x10<sup>3</sup> at an amplitude of 30 in a Branson sonifier. The nuclear extract was diluted to a final concentration of 150 mM NaCl with no salt IP buffer and precipitates were removed by centrifugation. The extract was incubated overnight at 4°C on a rotating wheel with GFP-Trap beads (ChromoTek) and agarose beads. The beads were washed five times with IP buffer containing 300 mM NaCl and afterwards resuspended in SDS loading buffer (Roth). Proteins were separated on SDS-polyacrylamidgels and analyzed by protein gel blotting using  $\alpha$ -myc (9E10) and  $\alpha$ -GFP (Roche # 11814460001) antibodies.

#### Disclosure of Potential Conflicts of Interest

No potential conflicts of interest were disclosed.

#### Acknowledgments

We would like to thank S. F. Lichtenthaler and P.-H. Kuhn for generously providing the pLKMod1 vector. We thank N.G. Copeland for providing us with reagents for the bacterial recombineering system. We further thank A. Schmid and F. Büddefeld for help with cloning and C. Foster for critical reading of the manuscript.

G.S. and H.L. were supported by grants from DFG (TR-SFB) and BMBF (Episys). G.S. received additional support from Weigand'sche Stiftung. H.L. was further supported by the BioImaging Network and the Nanosystems Initiative Munich (NIM). SD wants to thank the DFG (SPP1128, SPP1395) and the TAB (2007 FE 9011) for support.

#### Supplemental Material

Supplemental material may be downloaded here:  
<http://www.landesbioscience.com/journals/nucleus/article/18955/>

#### References

1. Foltz DR, Jansen LE, Black BE, Bailey AO, Yates JR, 3rd, Cleveland DW. The human CENP-A centromeric nucleosome-associated complex. *Nat Cell Biol* 2006; 8:458–69; PMID:16622419; <http://dx.doi.org/10.1038/ncb1397>
2. Obuse C, Yang H, Nozaki N, Goto S, Okazaki T, Yoda K. Proteomics analysis of the centromere complex from HeLa interphase cells: UV-damaged DNA binding protein 1 (DDB-1) is a component of the CEN-complex, while BMI-1 is transiently co-localized with the centromeric region in interphase. *Genes Cells* 2004; 9:105–20; PMID:15009096; <http://dx.doi.org/10.1111/j.1365-2443.2004.00705.x>
3. Okada M, Okawa K, Isobe T, Fukagawa T. CENP-H-containing complex facilitates centromere deposition of CENP-A in cooperation with FACT and CHD1. *Mol Biol Cell* 2009; 20:3986–95; PMID:19625449; <http://dx.doi.org/10.1091/mbc.E09-01-0065>
4. Guse A, Carroll CW, Moree B, Fuller CJ, Straight AF. In vitro centromere and kinetochore assembly on defined chromatin templates. *Nature* 2011; 477:354–8; PMID:21874020; <http://dx.doi.org/10.1038/nature10379>
5. Carroll CW, Milks KJ, Straight AF. Dual recognition of CENP-A nucleosomes is required for centromere assembly. *J Cell Biol* 2010; 189:1143–55; PMID:20566683; <http://dx.doi.org/10.1083/jcb.201001013>
6. Cohen RL, Espelin CW, De Wulf P, Sorger PK, Harrison SC, Simons KT. Structural and functional dissection of Mif2p, a conserved DNA-binding kinetochore protein. *Mol Biol Cell* 2008; 19:4480–91; PMID:18701705; <http://dx.doi.org/10.1091/mbc.E08-03-0297>
7. Sugimoto K, Kuriyama K, Shibata A, Himeno M. Characterization of internal DNA-binding and C-terminal dimerization domains of human centromere/kinetochore autoantigen CENP-C in vitro: role of DNA-binding and self-associating activities in kinetochore organization. *Chromosome Res* 1997; 5:132–41; PMID:9146917; <http://dx.doi.org/10.1023/A:1018422325569>

8. Screpanti E, De Antoni A, Alushin GM, Petrovic A, Melis T, Nogales E, et al. Direct binding of Cenp-C to the Mis12 complex joins the inner and outer kinetochore. *Curr Biol* 2011; 21:391-8; PMID:21353556; <http://dx.doi.org/10.1016/j.cub.2010.12.039>
9. Carroll CW, Silva MC, Godek KM, Jansen LE, Straight AF. Centromere assembly requires the direct recognition of CENP-A nucleosomes by CENP-N. *Nat Cell Biol* 2009; 11:896-902; PMID:19543270; <http://dx.doi.org/10.1038/ncb1899>
10. Bernad R, Sanchez P, Rivera T, Rodriguez-Corsino M, Boyarchuk E, Vassias I, et al. Xenopus HJURP and condensin II are required for CENP-A assembly. *J Cell Biol* 2011; 192:569-82; PMID:21321101; <http://dx.doi.org/10.1083/jcb.201005136>
11. Hemmerich P, Weidtkamp-Peters S, Hoischen C, Schmiedeborg L, Erliandri I, Diekmann S. Dynamics of inner kinetochore assembly and maintenance in living cells. *J Cell Biol* 2008; 180:1101-14; PMID:18347072; <http://dx.doi.org/10.1083/jcb.200710052>
12. Jansen LE, Black BE, Foltz DR, Cleveland DW. Propagation of centromeric chromatin requires exit from mitosis. *J Cell Biol* 2007; 176:795-805; PMID:17339380; <http://dx.doi.org/10.1083/jcb.200701066>
13. Schuh M, Lehner CF, Heidmann S. Incorporation of *Drosophila* CID/CENP-A and CENP-C into centromeres during early embryonic anaphase. *Curr Biol* 2007; 17:237-43; PMID:17222555; <http://dx.doi.org/10.1016/j.cub.2006.11.051>
14. Dunleavy EM, Roche D, Tagami H, Lacoste N, Ray-Galler D, Nakamura Y, et al. HJURP is a cell-cycle-dependent maintenance and deposition factor of CENP-A at centromeres. *Cell* 2009; 137:485-97; PMID:19410545; <http://dx.doi.org/10.1016/j.cell.2009.02.040>
15. Foltz DR, Jansen LE, Bailey AO, Yates JR, 3rd, Bassett EA, Wood S, et al. Centromere-specific assembly of CENP-a nucleosomes is mediated by HJURP. *Cell* 2009; 137:472-84; PMID:19410544; <http://dx.doi.org/10.1016/j.cell.2009.02.039>
16. Bergmann JH, Rodriguez MG, Martins NM, Kimura H, Kelly DA, Masumoto H, et al. Epigenetic engineering shows H3K4me2 is required for HJURP targeting and CENP-A assembly on a synthetic human kinetochore. *EMBO J* 2011; 30:328-40; PMID:21157429; <http://dx.doi.org/10.1038/emboj.2010.329>
17. Fujita Y, Hayashi T, Kiyomitsu T, Toyoda Y, Kokubu A, Obuse C, et al. Priming of centromere for CENP-A recruitment by human hMis18alpha, hMis18beta, and M18BP1. *Dev Cell* 2007; 12:17-30; PMID:17199038; <http://dx.doi.org/10.1016/j.devcel.2006.11.002>
18. Hayashi T, Fujita Y, Iwasaki O, Adachi Y, Takahashi K, Yanagida M. Mis16 and Mis18 are required for CENP-A loading and histone deacetylation at centromeres. *Cell* 2004; 118:715-29; PMID:15369671; <http://dx.doi.org/10.1016/j.cell.2004.09.002>
19. Maddox PS, Hyndman F, Monen J, Oegema K, Desai A. Functional genomics identifies a Myb domain-containing protein family required for assembly of CENP-A chromatin. *J Cell Biol* 2007; 176:757-63; PMID:17339379; <http://dx.doi.org/10.1083/jcb.200701065>
20. Pidoux AL, Choi ES, Abbott JK, Liu X, Kagansky A, Castillo AG, et al. Fission yeast Scm3: A CENP-A receptor required for integrity of subkinetochore chromatin. *Mol Cell* 2009; 33:299-311; PMID:19217404; <http://dx.doi.org/10.1016/j.molcel.2009.01.019>
21. Williams JS, Hayashi T, Yanagida M, Russell P. Fission yeast Scm3 mediates stable assembly of Cnp1/CENP-A into centromeric chromatin. *Mol Cell* 2009; 33:287-98; PMID:19217403; <http://dx.doi.org/10.1016/j.molcel.2009.01.017>
22. Leonhardt H, Rahn HP, Weinzierl P, Sporbert A, Cremer T, Zink D, et al. Dynamics of DNA replication factories in living cells. *J Cell Biol* 2000; 149:271-80; PMID:10769021; <http://dx.doi.org/10.1083/jcb.149.2.271>
23. Hsu JY, Sun ZW, Li X, Reuben M, Tatchell K, Bishop DK, et al. Mitotic phosphorylation of histone H3 is governed by Ipl1/aurora kinase and Glc7/PP1 phosphatase in budding yeast and nematodes. *Cell* 2000; 102:279-91; PMID:10975519; [http://dx.doi.org/10.1016/S0092-8674\(00\)00034-9](http://dx.doi.org/10.1016/S0092-8674(00)00034-9)
24. Lagana A, Dorn JF, De Rop V, Ladouceur AM, Maddox AS, Maddox PS. A small GTPase molecular switch regulates epigenetic centromere maintenance by stabilizing newly incorporated CENP-A. *Nat Cell Biol* 2010; 12:1186-93; PMID:21102442; <http://dx.doi.org/10.1038/ncb2129>
25. Boyer LA, Latek RR, Peterson CL. The SANT domain: a unique histone-tail-binding module? *Nat Rev Mol Cell Biol* 2004; 5:158-63; PMID:15040448; <http://dx.doi.org/10.1038/nrm1314>
26. Moree B, Meyer CB, Fuller CJ, Straight AF. CENP-C recruits M18BP1 to centromeres to promote CENP-A chromatin assembly. *J Cell Biol* 2011; 194:855-71; PMID:21911481; <http://dx.doi.org/10.1083/jcb.201106079>
27. Chung TL, Hsiao HH, Yeh YY, Shia HL, Chen YL, Liang PH, et al. In vitro modification of human centromere protein CENP-C fragments by small ubiquitin-like modifier (SUMO) protein: definitive identification of the modification sites by tandem mass spectrometry analysis of the isopeptides. *J Biol Chem* 2004; 279:39653-62; PMID:15272016; <http://dx.doi.org/10.1074/jbc.M405637200>
28. Mayya V, Lundgren DH, Hwang SI, Rezaul K, Wu L, Eng JK, et al. Quantitative phosphoproteomic analysis of T cell receptor signaling reveals system-wide modulation of protein-protein interactions. *Sci Signal* 2009; 2:ra46; PMID:19690332; <http://dx.doi.org/10.1126/scisignal.2000007>
29. Nousiainen M, Sillje HH, Sauer G, Nigg EA, Korner R. Phosphoproteome analysis of the human mitotic spindle. *Proc Natl Acad Sci USA* 2006; 103:5391-6; PMID:16565220; <http://dx.doi.org/10.1073/pnas.0507066103>
30. Olsen JV, Blagoev B, Gnani F, Macek B, Kumar C, Mortensen P, et al. Global, in vivo, and site-specific phosphorylation dynamics in signaling networks. *Cell* 2006; 127:635-48; PMID:17081983; <http://dx.doi.org/10.1016/j.cell.2006.09.026>
31. Liu P, Jenkins NA, Copeland NG. A highly efficient recombineering-based method for generating conditional knockout mutations. *Genome Res* 2003; 13:476-84; PMID:12618378; <http://dx.doi.org/10.1101/gr.749203>
32. Tsukamoto T, Hashiguchi N, Janicki SM, Tumber T, Belmont AS, Spector DL. Visualization of gene activity in living cells. *Nat Cell Biol* 2000; 2:871-8; PMID:11146650; <http://dx.doi.org/10.1038/35046510>
33. Rothbauer U, Zolghadr K, Tillib S, Nowak D, Schermelleh L, Gahl A, et al. Targeting and tracing antigens in live cells with fluorescent nanobodies. *Nat Methods* 2006; 3:887-9; PMID:17060912; <http://dx.doi.org/10.1038/nmeth953>
34. Zolghadr K, Mortusewicz O, Rothbauer U, Kleinhaus R, Goehler H, Wanker EE, et al. A fluorescent two-hybrid assay for direct visualization of protein interactions in living cells. *Mol Cell Proteomics* 2008; 7:2279-87; PMID:18622019; <http://dx.doi.org/10.1074/mcp.M700548-MCP200>
35. Moffat J, Grueneberg DA, Yang X, Kim SY, Kloepper AM, Hinkle G, et al. A lentiviral RNAi library for human and mouse genes applied to an arrayed viral high-content screen. *Cell* 2006; 124:1283-98; PMID:16564017; <http://dx.doi.org/10.1016/j.cell.2006.01.040>
36. Kuhn PH, Wang H, Dislich B, Colombo A, Zeitschel U, Ellwart JW, et al. ADAM10 is the physiologically relevant, constitutive alpha-secretase of the amyloid precursor protein in primary neurons. *EMBO J* 2010; 29:3020-32; PMID:20676056; <http://dx.doi.org/10.1038/emboj.2010.167>
37. Vandesompele J, De Preter K, Pattyn F, Poppe B, Van Roy N, De Paepe A, et al. 2002Accurate normalization of real-time quantitative RT-PCR data by geometric averaging of multiple internal control genes. *Genome Biol* 2002; 3: H0034; PMID:12184808; <http://dx.doi.org/10.1186/gb-2002-3-7-research0034>
38. Lehnertz B, Ueda Y, Derijck AA, Braunschweig U, Perez-Burgos L, Kubicek S, et al. Suv39h-mediated histone H3 lysine 9 methylation directs DNA methylation to major satellite repeats at pericentric heterochromatin. *Curr Biol* 2003; 13:1192-200; PMID:12867029; [http://dx.doi.org/10.1016/S0960-9822\(03\)00432-9](http://dx.doi.org/10.1016/S0960-9822(03)00432-9)
39. Schotta G, Sengupta R, Kubicek S, Malin S, Kauer M, Callen E, et al. A chromatin-wide transition to H4K20 monomethylation impairs genome integrity and programmed DNA rearrangements in the mouse. *Genes Dev* 2008; 22:2048-61; PMID:18676810; <http://dx.doi.org/10.1101/gad.476008>



Supplementary Material to:

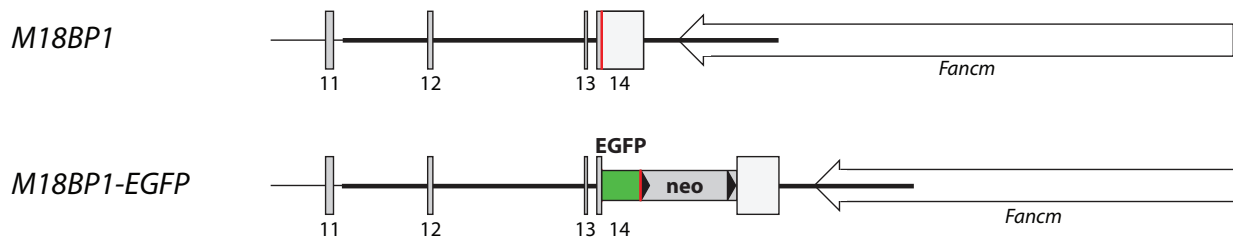
**CENP-C facilitates the recruitment of M18BP1 to centromeric chromatin**

Silvia Dambacher, Wen Deng, Matthias Hahn, Dennis Sadic, Jonathan Fröhlich, Alexander Nuber, Christian Hoischen, Stephan Diekmann, Heinrich Leonhardt and Gunnar Schotta  
Nucleus 2012; 3(1): In Press. DOI: 10.4161/nucl.3.1.18955

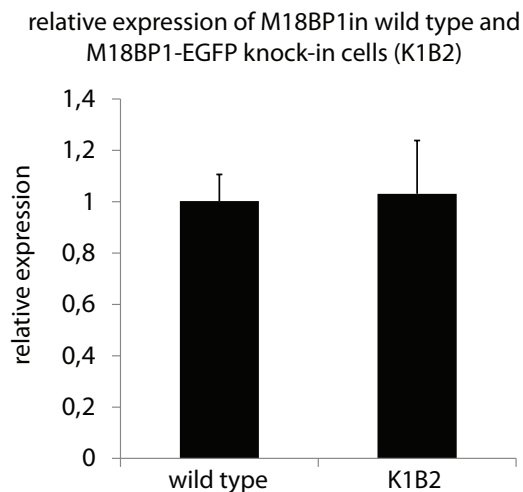
### Supplementary Figure S1. Generation of M18BP1-EGFP knock-in cells.

(A) Targeting strategy for the M18BP1-EGFP knock-in allele. Part of the M18BP1 locus containing the last exons (11-14) is depicted in the scheme. The last exon contains the regular STOP codon (red line), followed by the 3' UTR. The targeting construct comprises the region shown by the thick black line. The knock-in allele contains the EGFP tag just before the regular STOP codon, followed by the loxP flanked Neomycin selection cassette. (B) RT-qPCR quantification of M18BP1 expression levels in the parental wild type mES cell line and the K1B2 cell line which carries the M18BP1-EGFP knock-in allele. Average expression levels from triplicate experiments, normalized to Actin and GAPDH are shown.

**A**

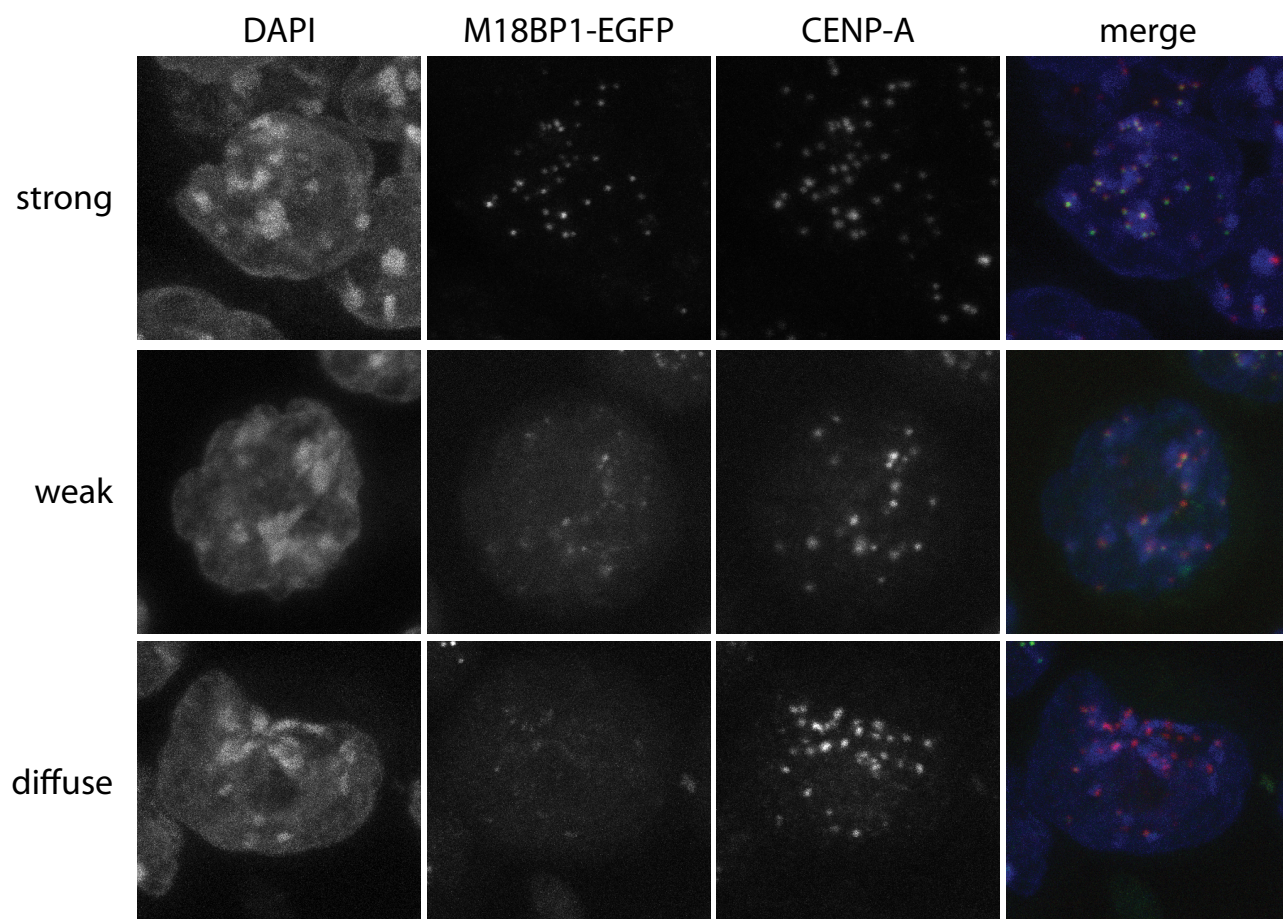


**B**



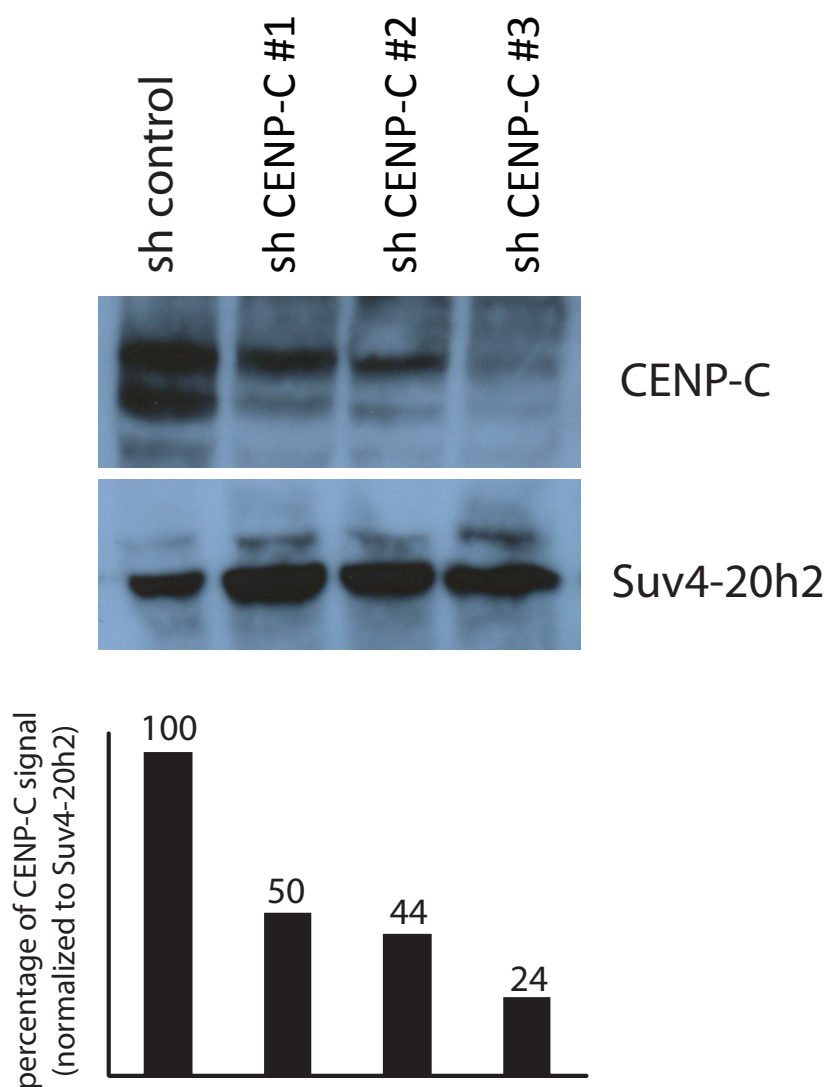
### Supplementary Figure S2. Centromeric localization of M18BP1.

Localization of endogenously tagged M18BP1-EGFP in the K1B2 mES cell line. K1B2 cells were stained for CENP-A and confocal stacks were recorded. Maximum intensity projections of individual cells representing the different M18BP1 staining patterns: strong enrichment at centromeres (s), weak enrichment (w), no enrichment/diffuse nuclear (d) are shown.



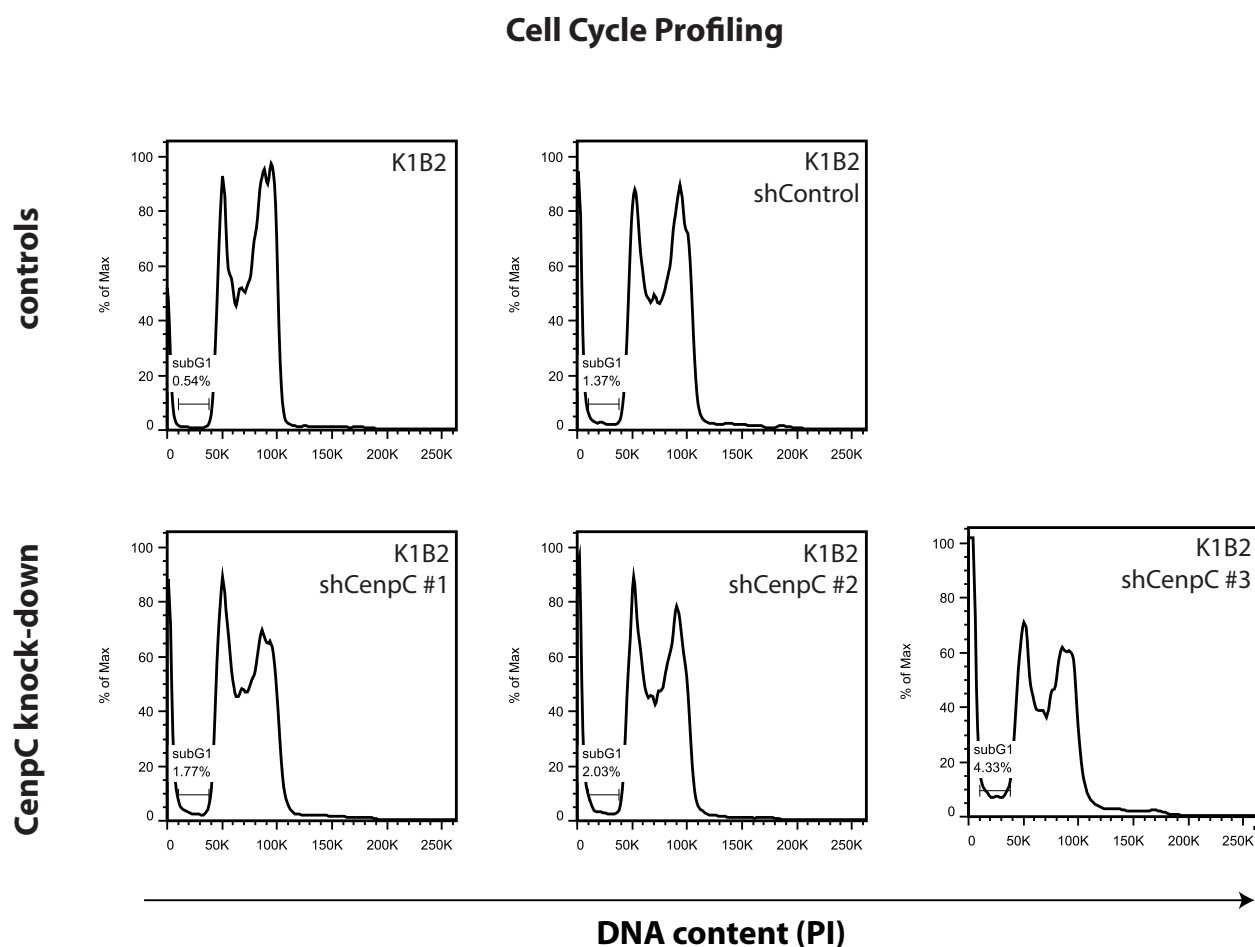
### Supplementary Figure S3. CENP-C protein levels in control vs. CENP-C knock-down cells.

Five days after infection with the lentiviral knock-down vectors, control and CENP-C knock-down cells were harvested and nuclear extracts from these cells were probed for CENP-C, and Suv4-20h2 which served as loading control, by western blotting. Compared to shControl cells, all three knock-down oligos lead to reduced CENP-C protein levels, with shCENP-C #3 showing the strongest effect.



### Supplementary Figure S4. Cell cycle profiles of K1B2 and CENP-C knock-down cells.

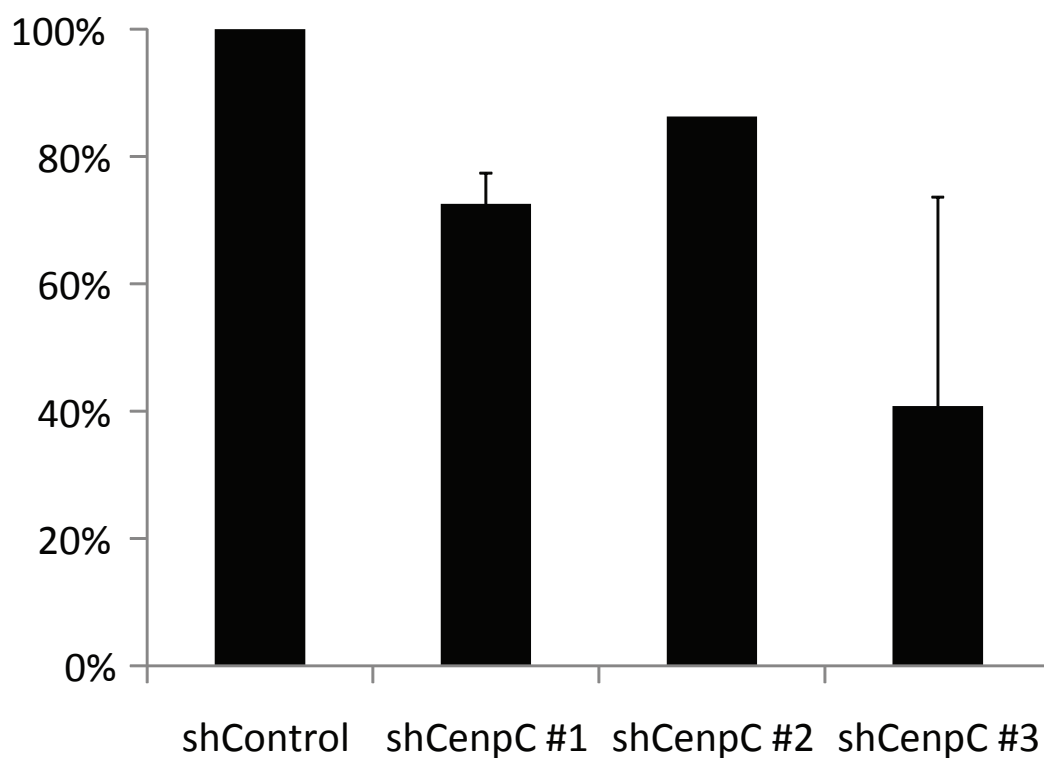
Five days after infection with the lentiviral knock-down vectors, control and CENP-C knock-down cells were harvested, fixed and stained for DNA content with propidium iodide (PI). FACS analysis revealed a normal cell cycle profile, however, the CENP-C knock-down cells tend to show higher levels of sub-G1 cells, indicative of cell death. This effect is most apparent with knock-down shCENP-C #3, which shows the strongest reduction of CENP-C mRNA levels.



**Supplementary Figure S5. Relative cell numbers of shControl and shCENP-C knock-down populations.**

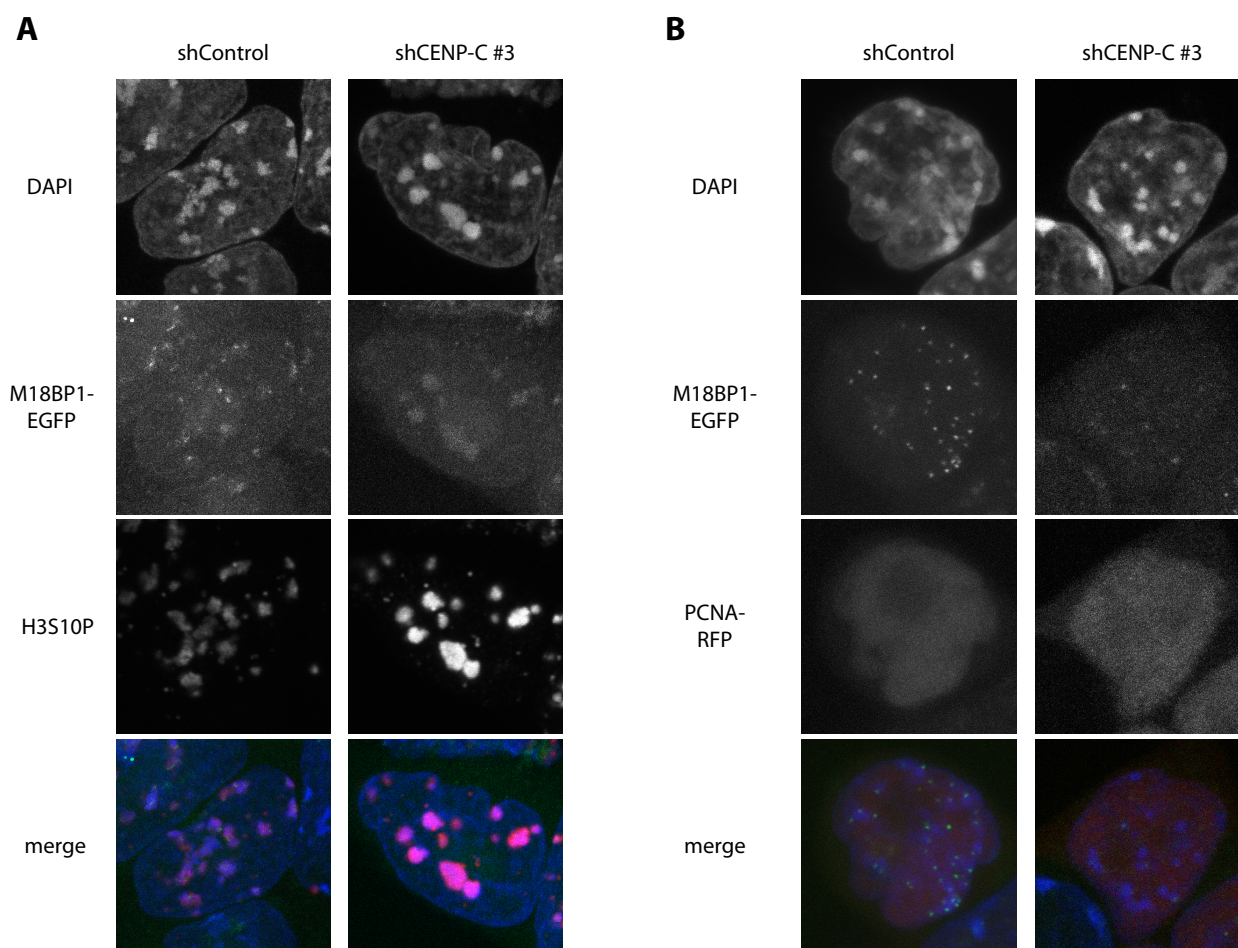
Five days after infection with the lentiviral knock-down vectors, control and CENP-C knock-down cells were harvested and counted. The cell number of the control population was set to 100%. The bar graph shows relative cell numbers for the individual shCENP-C knock-down populations.

**Relative number of surviving cells  
5 days after transduction of CenpC  
targeting shRNAs**



### Supplementary Figure S6. Cell cycle analysis in CENP-C knock-down cells.

(A) Five days after infection with the lentiviral knock-down vectors, control and CENP-C knock-down cells were stained with H3S10P antibodies to detect cells in G2 phase. Maximum intensity projections of representative examples for G2 phase cells are shown. Control cells display a ‘weak’ centromeric staining pattern, in the CENP-C knock-down sample we observe cells which have lost the centromeric M18BP1 signals. (B) Four days after infection with the lentiviral knock-down vectors, control and CENP-C knock-down cells were transfected with PCNA-RFP expression plasmids. G1 cells which are characterized by small nuclei and diffuse PCNA signals were examined for M18BP1-EGFP localization. Control cells show ‘strong’ centromeric M18BP1-EGFP signals. In the CENP-C knock-down population we can detect G1 phase cells which have lost or strongly reduced centromeric enrichment of M18BP1.



**Supplementary Table 1. Primers used for cloning the M18BP1-EGFP targeting construct.**

<b>primer</b>	<b>orientation</b>	<b>primer sequence 5'-3'</b>
cloning fragment AB	f	ATAGCGGCCGCCTAACTCAAATGCAAAACC
cloning fragment AB	r	CGCAAGCTTTGATTAATAGTTTTTCACTAT
cloning fragment YZ	f	TCCAAGCTTCCATGACTTGCTCACCTTG
cloning fragment YZ	r	TGCACTAGTTATGAAAGAACTCTCATAATG
cloning fragment CD	f	ATAGCGGCCGCTCTCCACCACCAACACGGA
cloning fragment CD	r	TCGGAATTCGTCAGAATTGGAAAAGTAAT
cloning fragment EF	f	CGAGGATCCTGATAGACGACTTGCAGGAAT
cloning fragment EF	r	TCTGTGCGACAGTCCACAATCTTAACTCTG
nested PCR outer	f	ACCGCTTCCTCGTGCTTTAC
nested PCR outer	r	AAAGCCAAGCTCACTGTTTC
nested PCR inner	f	GATTGGGAAGACAATAGCAGGCATG
nested PCR inner	r	GCGCAAGTAAATCATCAAAAGGCTG



**Supplementary Table 2. ShRNA oligonucleotide sequences.**

name	species	direction	sequence – in 5' to 3' direction (targeted sequence in bold)	TRC code	targeted mRNA
non targeting shRNA	none	fw	CGCGTCCGGCAACAAGATGAAGAGCACCAACTCGAGT TGGTGCTCTTCATCTTGTGTTTTGGAAA	SHC202V	none
		rw	CCGGTTTCCAAAAACAACAAGATGAAGAGCACCAACT CGAGTTGGTGCTCTTCATCTTGTGTCGCGGA		
shCENP-C1 #1	Mm	fw	CGCGTCCGGGCATGTTGGCCAAGATATATTCTCGAGA ATATATCTTGGCCAACATGCTTTTTGGAAA	from TRC designer	NM_0076 83.3
		rw	CCGGTTTCCAAAAAGCATGTTGGCCAAGATATATTCTC GAGAAATATATCTTGGCCAACATGCCCGGA		
shCENP-C #2	Mm	fw	CGCGTCCGGGTTTCGTCGATCTAATAGAATACTCGAGTA TTCTATTAGATCGACGAACTTTTGGAAA	from TRC designer	NM_0076 83.3
		rw	CCGGTTTCCAAAAAGTTCGTCGATCTAATAGAATACTC GAGTATTCTATTAGATCGACGAACCCGGA		
shCENP-C #3	Mm	fw	CGCGTCCGGGACATCACCGAATGTTTCATTTCTCGAGAA ATGAACATTCCGGTGATGTCTTTTTGGAAA	from TRC designer	NM_0076 83.3
		rw	CCGGTTTCCAAAAAGACATCACCGAATGTTTCATTTCTC GAGAAATGAACATTCCGGTGATGTCCCGGA		

**Supplementary Table 3. Primers used for quantitative PCR.**

<b>gene</b>	<b>mRNA</b>	<b>direction</b>	<b>sequence in 5' to 3' direction</b>
CENP-C	NM_007683.3	fw	aagccgacccatctcaatag
		rw	taagatccatggggacaagc
beta Actin	NM_007393.3	fw	ggcatcactattggcaacg
		rw	tccataccaagaaggaagg
M18BP1	NM_172578.2	fw	ctccaaaaggccagcatcacg
		rw	ttgccggaggtaggctgtcc
GAPDH	NM_008084.2	fw	tcaagaaggtggtgaagcag
		rw	gttgaagtcgcaggagacaa

**Supplementary Table 4. Primers used for cloning of M18BP1 and CENP-C truncation constructs.**

<b>gene</b>	<b>mRNA</b>	<b>direction</b>	<b>sequence in 5' to 3' direction</b>
M18BP1	NM_172578.2	fw	ggggacaagtttgtacaaaaagcaggcttaactatgattgtaacaccttga
		rw	ggggaccactttgtacaagaaagctgggtcgtcagaattggaaaagtaa
M18BP1 (aa1-440)	NM_172578.2	fw	ggggacaagtttgtacaaaaagcaggcttaactatgattgtaacaccttga
		rw	ggggaccactttgtacaagaaagctgggtctcttctgtttctctgtg
M18BP1 (aa441-998)	NM_172578.2	fw	ggggacaagtttgtacaaaaagcaggcttaactatgcaggaaacagcaagag
		rw	ggggaccactttgtacaagaaagctgggtcgtcagaattggaaaagtaa
M18BP1 (aa325-800)	NM_172578.2	fw	ggggacaagtttgtacaaaaagcaggcttaactatgactgttgtaaagaag
		rw	ggggaccactttgtacaagaaagctgggtcatgtttcgggacacctgg
M18BP1 (aa441-800)	NM_172578.2	fw	ggggacaagtttgtacaaaaagcaggcttaactatgcaggaaacagcaagag
		rw	ggggaccactttgtacaagaaagctgggtcatgtttcgggacacctgg
M18BP1 (aa735-800)	NM_172578.2	fw	ggggacaagtttgtacaaaaagcaggcttaactatggaccatctacctggtt
		rw	ggggaccactttgtacaagaaagctgggtcatgtttcgggacacctgg
CENP-C (aa1-367)	NM_007683.3	fw	ggggacaagtttgtacaaaaagcaggcttaactatggcctCgttcacatctggatc
		rw	ggggaccactttgtacaagaaagctgggtctttattttcaggagatcgacaa
CENP-C (aa368-656)	NM_007683.3	fw	ggggacaagtttgtacaaaaagcaggcttaactatgcaatctgagactgccaaaac
		rw	ggggaccactttgtacaagaaagctgggtcttcataattcttgaacctggaag
CENP-C (aa657-906)	NM_007683.3	fw	ggggacaagtttgtacaaaaagcaggcttaactatgccaggagcagtaattctg
		rw	ggggaccactttgtacaagaaagctgggtccctttttatttgagtaaaaagaag



### 2.3 Step-Wise Assembly, Maturation and Dynamic Behavior of the Human CENP-P/O/R/Q/U Kinetochore Sub-Complex

---



# Step-Wise Assembly, Maturation and Dynamic Behavior of the Human CENP-P/O/R/Q/U Kinetochore Sub-Complex

Anja Eskat<sup>1,2a</sup>, Wen Deng<sup>2,3</sup>, Antje Hofmeister<sup>1</sup>, Sven Rudolphi<sup>1</sup>, Stephan Emmerth<sup>3ab</sup>, Daniela Hellwig<sup>1ac</sup>, Tobias Ulbricht<sup>1</sup>, Volker Döring<sup>1</sup>, James M. Bancroft<sup>5</sup>, Andrew D. McAinsh<sup>5</sup>, M. Cristina Cardoso<sup>4</sup>, Patrick Meraldi<sup>3</sup>, Christian Hoischen<sup>1</sup>, Heinrich Leonhardt<sup>2</sup>, Stephan Diekmann<sup>1\*</sup>

**1** Molecular Biology, FLI, Jena, Germany, **2** Department of Biology II, Center for Integrated Protein Science, Ludwig Maximilians University Munich, Planegg-Martinsried, Munich, Germany, **3** Institute of Biochemistry, ETH Zurich, Zurich, Switzerland, **4** Department of Biology, Technische Universität Darmstadt, Darmstadt, Germany, **5** Centre for Mechanochemical Cell Biology, Warwick Medical School, University of Warwick, Coventry, United Kingdom

## Abstract

Kinetochore are multi-protein megadalton assemblies that are required for attachment of microtubules to centromeres and, in turn, the segregation of chromosomes in mitosis. Kinetochore assembly is a cell cycle regulated multi-step process. The initial step occurs during interphase and involves loading of the 15-subunit constitutive centromere associated complex (CCAN), which contains a 5-subunit (CENP-P/O/R/Q/U) sub-complex. Here we show using a fluorescent three-hybrid (F3H) assay and fluorescence resonance energy transfer (FRET) in living mammalian cells that CENP-P/O/R/Q/U subunits exist in a tightly packed arrangement that involves multifold protein-protein interactions. This sub-complex is, however, not pre-assembled in the cytoplasm, but rather assembled on kinetochores through the step-wise recruitment of CENP-O/P heterodimers and the CENP-P, -O, -R, -Q and -U single protein units. SNAP-tag experiments and immuno-staining indicate that these loading events occur during S-phase in a manner similar to the nucleosome binding components of the CCAN, CENP-T/W/N. Furthermore, CENP-P/O/R/Q/U binding to the CCAN is largely mediated through interactions with the CENP-N binding protein CENP-L as well as CENP-K. Once assembled, CENP-P/O/R/Q/U exchanges slowly with the free nucleoplasmic pool indicating a low off-rate for individual CENP-P/O/R/Q/U subunits. Surprisingly, we then find that during late S-phase, following the kinetochore-binding step, both CENP-Q and -U but not -R undergo oligomerization. We propose that CENP-P/O/R/Q/U self-assembles on kinetochores with varying stoichiometry and undergoes a pre-mitotic maturation step that could be important for kinetochores switching into the correct conformation necessary for microtubule-attachment.

**Citation:** Eskat A, Deng W, Hofmeister A, Rudolphi S, Emmerth S, et al. (2012) Step-Wise Assembly, Maturation and Dynamic Behavior of the Human CENP-P/O/R/Q/U Kinetochore Sub-Complex. PLoS ONE 7(9): e44717. doi:10.1371/journal.pone.0044717

**Editor:** Barbara Mellone, University of Connecticut, Storrs, United States of America

**Received:** April 23, 2012; **Accepted:** August 6, 2012; **Published:** September 18, 2012

**Copyright:** © 2012 Eskat et al. This is an open-access article distributed under the terms of the Creative Commons Attribution License, which permits unrestricted use, distribution, and reproduction in any medium, provided the original author and source are credited.

**Funding:** This work was supported by Deutsche Forschungsgemeinschaft (DFG DI 258/17-1, SPP1128, SPP1395), and Thüringer Aufbaubank (2007 FE 9011). The funders had no role in study design, data collection and analysis, decision to publish, or preparation of the manuscript.

**Competing Interests:** The authors have declared that no competing interests exist.

\* E-mail: diekmann@fli-leibniz.de

These authors contributed equally to this work.

<sup>a</sup> Current address: Institute of Biochemistry, ETH Zurich, Zurich, Switzerland

<sup>b</sup> Current address: Friedrich Miescher Institute for Biomedical Research, Basel, Switzerland

<sup>c</sup> Current address: HKI, Jena, Germany

## Introduction

During mitosis, accurate chromosome segregation is essential for the correct transmission of the genetic material to the daughter cells. A multi-protein complex, the kinetochore, assembles at the centromere of each chromatid in order to mediate this function. Kinetochore contains an inner core that is present throughout the cell cycle [1,2], and a set of outer kinetochore proteins that stably associate with the inner core during mitosis [3,4]. The kinetochore is built from two major conserved protein networks, (1) the CCAN (constitutive centromere associated network) complex [5–13] which is associated to centromeric nucleosomes [5,14–16] that consist of repetitive  $\alpha$ -satellite DNA containing the histone H3 variant CENP-A [17,18], and (2) the KMN network [7,19–27] which directly connects the kinetochore to microtubules [3,28,29].

Functionally, the CCAN is required for the efficient recruitment of CENP-A into centromeric nucleosomes at the end of mitosis [6,14,30,31] and the maintenance of centromeric chromatin, but is also involved in chromosome alignment, kinetochore fiber stability and bipolar spindle assembly [1,2,5,6,8,32–34]. The CCAN was suggested to establish, in interphase, an inner kinetochore structure which functions as an assembly platform for KMN network proteins in mitosis, and only the KMN proteins then connect the inner kinetochore to microtubules [3]. However, ectopical CENP-T and -C alone are able to establish a functional outer kinetochore [16,35] indicating that instead of being only a structural platform, the CCAN seems to be a regulator of the mitotic kinetochore-microtubule attachment [36].

The CCAN proteins CENP-U, -O, -P, -Q and -R were identified as a CCAN subclass (named CENP-O class proteins)

[3,5,6,10,37]. CENP-PORQU proteins are non-essential showing, when depleted, common mitotic defects and slower proliferation rates [6,10,33,38]. Kinetochore localization of CENP-PORQU is interdependent [5,10,36]. In chicken DT40 cells, and when these genes are expressed in *E. coli*, CENP-O, -P, -U and -Q form a stable complex to which CENP-R can associate [10]. These data describe the CENP-PORQU complex as a stable unit which might function as a structural element in the CCAN. However, CENP-PORQU proteins have different protein specific functions: CENP-U [39] as well as CENP-Q [36] are able to bind to microtubules, only depletion of CENP-O seems to destabilise microtubule bundles at kinetochores influencing bipolar spindle assembly [34,39], and CENP-U interacts with Hec1, an interaction negatively regulated by Aurora-B kinase [39]. In the complex, CENP-P is closely associated with CENP-O, and CENP-U binds to CENP-Q [10,40–42]. In order to resolve these different views, we analysed protein binding, complex architecture and dynamics of the human kinetochore CENP-PORQU sub-complex by various *in vivo* techniques.

## Materials and Methods

### Plasmids

Plasmids pIC133, pIC190, pIC141, pIC140, and pIC235 encoding LAP-CENP-K, -Q, -P, -O, respectively -R fusion proteins were a kind gift of Dan Foltz and Iain Cheeseman. The full length cDNA clone of CENP-L, IRAUp969 EO882D, was from RZPD, Berlin, Germany). They were used for amplification of full length CENP-K, -L, -Q, -P, -O, and -R by PCR (Expand high fidelity<sup>PLUS</sup> PCR System, Roche, Penzberg, Germany) applying forward primer 5'-GGGGACAAGTTTGTACAAAAAAGCAGGCTTCGAAAACCTGTATTTTCAGGGCGCCACCA-TGGGCATGAATCAGGAGGATTTAGATCC -3' and reverse primer 5'-GGGGACCACTTTGTACAAAGAAAGCTGGGTC-TGATGGAAAGCTTCTAATCTTATT -3' for CENP-K, forward primer 5'-GGGGACAAGTTTGTACAAAAAAGCAGGCTTCGAAAACCTGTATTTTCAGGGCGCCACCATGGATTCTTACAGTGCACCAAG -3' and reverse primer 5'-GGGGACCACTTTGTACAAAGAAAGCTGGGTCCTCAATTTGAAAAAT-TGCCAGTTCTG for CENP-L, forward primer 5'-GGGGA-CAAGTTTGTACAAAAAAGCAGGCTTCGAAAACCTGTAT-TTTCAGGGCGCCACCATGGGCATGCTCTGGTAAAGCAAA-TGCTTC -3' and reverse primer 5'-GGGGACCACTTTGTACAAAGAAAGCTGGGTAGATGCATCCAGTTTCTTATAGG -3' for CENP-Q, forward primer 5'-GGGGACAAGTTTGTACAAAAAAGCAGGCTTCGAAAACCTGTATTTTCAGGGCGCCACCATGGAGCAG-GCGAACCCTTT -3' and reverse primer 5'-GGGGACCACTTTGTACAAAGAAAGCTGGGTGGAGACCAGACTCATAT-CCAAC -3' for CENP-O, and forward primer 5'-GGGGACCAAGTTTGTACAAAAAAGCAGGCTTCGAAAACCTGTATTTTCAGGGCGCCACCATGGGCATGCTTAAAGATCA-CTGAA -3' and reverse primer 5'-GGGGACCACTTTGTACAAAGAAAGCTGGGTGTTTAAATGGCTTTAAGGAATT-CA -3' for CENP-R. The CENP-Q, -P, -O, and -R harbouring linear PCR fragments were transferred into vector pDONR221 by BP recombination reaction (Invitrogen, Carlsbad, CA, USA). After verification by sequencing (MWG Biotech, Ebersberg, Munich, Germany), the genes were cloned by LR recombination reactions into various modified pFP-C and pFP-N (BD Biosciences, Clontech,

Palo Alto, CA, USA) based Destination vectors. As the result we obtained expression vectors carrying the genes coding for CENP-Q, -P, -O, and -R fused to the C-termini as well as to the N-termini of EGFP and mCherry. In the constructed fluorescent proteins (FP)-CENP-Q, -P, -O, and -R, the amino acid (aa) linker between the fused proteins is SGTSLYKKAGFENLYFQGAT. Due to the cloning protocol, the aa sequence TQLSCTKW is added to the C-terminal ends of FP-CENP-Q, -P, -O, and -R. In the constructs where CENP-Q, -P, -O, and -R are fused to the N-termini of EGFP respectively mCherry, the (aa) linker is TQLSCTKWLDPPVAT. The cloning of CENP-U and -C [43] and CENP-N [44] have been described previously. Vector pIRES2 used for the simultaneous expression of EGFP and mRFP, was a friendly gift of J. Langowski (Heidelberg). For expression of a mRFP-EGFP fusion protein, we digested vector pmRFP-C1 with SnaBI and XmaI and ligated the resulting 1012 bps DNA fragment containing mRFP into a 7106 bp DNA obtained from a SnaBI-XmaI digest of vector pH-G-C. In the resulting Gateway expression vector pH-mR-G-C, the amino acid linker between mRFP and EGFP is SGLRSRAQASNSAVDGTAGPVAT. Full length protein expression of the fusion constructs was confirmed by Western Blots.

### Live cell FRET measurements

FRET was measured by applying the acceptor photo-bleaching method using the FRET pair EGFP-mCherry. Co-transfected HEp-2 cells grown on coverslips were analyzed using a confocal laser scanning microscope (LSM 510 Meta) and a C-Apochromat 63×/1.2NA oil immersion objective (Carl Zeiss, Jena, Germany). EGFP fluorescence was excited with the Argon 488 nm laser line and analyzed using the Meta detector (ChS1+ChS2: 505–550 nm). mCherry fluorescence was excited with the 561 nm laser line (DPSS 561-10) and detected in one of the confocal channels using a 575–615 nm band-pass filter. To minimize cross talk between the channels, each image was collected separately in the multi-track-mode, i.e. both fluorophores were excited and recorded specifically and separately. Cells moderately expressing both fusion proteins with comparable expression levels were selected for analysis. Acceptor photo-bleaching was achieved by scanning a region of interest (ROI) including up to five centromeres of a nucleus 50 times (scans at 1.6 μsec pixel time) using the 561 nm laser line at 100% intensity. Bleaching times per pixel were identical for each experiment, however, total bleaching times varied depending on the size of the bleached ROIs. 4 donor and acceptor fluorescence images were taken before and up to 4 images after the acceptor photo-bleaching procedure to assess changes in donor and acceptor fluorescence. To minimize the effect of photo-bleaching of the donor during the imaging process, the image acquisition was performed at low laser intensities. To compare the time course of different experiments, donor intensities in the ROI were averaged and normalized to the intensity measured at the first time point after photo-bleaching, and acceptor intensities in the ROI were averaged and normalized to the mean intensity measured at time points 2–4 before photo-bleaching. The FRET efficiency was calculated by comparing the fluorescence intensity ( $I_{DA}$ ) before bleaching (in presence of the acceptor) with the intensity ( $I_D$ ) measured after bleaching (in the absence of the acceptor) according to  $E = 1 - I_{DA}/I_D$ . The FRET efficiencies of numerous bleached and unbleached locations were compared by a paired t-test ( $\alpha = 0.05$ ). The difference between the means is a measure for the FRET-value, which was interpreted to have occurred when the paired t-test revealed a statistically significant difference between the two input groups with a p-value below 0.001. A p-value >0.001 was interpreted as an indication for insignificant FRET.



In two cases, the acceptor-bleaching FRET data were confirmed by additional fluorescence lifetime FLIM experiments. In FLIM experiments, the donor fluorescence lifetime was determined by time-correlated single photon counting (TCSPC) in living human HEP-2 cells. For donor fluorescence excitation, a pulsed picosecond diode laser (LDH Series, PicoQuant, Berlin, Germany) with a frequency of 20 MHz along with a dedicated driver (PDL Series, PicoQuant) was used. Via a fiber coupling unit, the excitation light was guided into a confocal laser scanning microscope (LSM 510 Meta). Laser power was adjusted to give average photon counting rates of  $10^4$ – $10^5$  photons/sec (0.0001–0.001 photon counts per excitation event) or less to avoid pulse pile-up. Images of  $256 \times 256$  pixels were acquired with a  $63 \times$  C-Apochromat water immersion objective (NA 1.20, Carl Zeiss). Photons emitted by the sample were collected by the water immersion objective and detected by a single photon avalanche diode (PDM series, PicoQuant). The data were acquired by the PicoHarp 300 TCSPC module (PicoQuant) working in the TTTR mode (time-tagged time-resolved). To calculate the fluorescence lifetime, the SymPhoTime software package (v4.7, PicoQuant) was used. Selected areas of the images corresponding to single centromeres (resulting in the fluorescence lifetime histograms) or the sum of all centromeric regions were fitted by maximum likelihood estimation (MLE). Depending on the quality of a fit indicated by the value of  $\chi^2$ , a mono- or bi-exponential fitting model including background was applied. A model was rejected when  $\chi^2$  exceeded a value of 1.5. In this way, the presence of scattered light in few measurements could be identified and separated. However, due to low photon numbers and too close time constants, the simultaneous presence of two different donor fluorescence lifetimes for complexes with donor-only and donor plus acceptor in one centromere could not be separated by a bi-exponential fit. A donor fluorescence lifetime obtained from a centromere in a cell co-expressing donor and acceptor molecules was considered to be significantly different from the control measurement, when the lifetime differed from the mean of the control values by  $>3$  standard deviations. The FRET efficiency was calculated by comparing the donor fluorescence lifetime ( $\tau_{DA}$ ) in the presence of the acceptor with the respective fluorescence lifetimes ( $\tau_D$ ) of control measurements obtained in absence of an acceptor following  $E = 1 - \tau_{DA}/\tau_D$ .

### F3H

BHK cells containing a *lac* operator repeat array [45] were cultured in DMEM medium with 10% FCS and seeded on coverslips in 6-well plates for microscopy. After attachment, cells were co-transfected with expression vectors for the indicated fluorescent fusion proteins and a LacI-GBP fusion [46,47] using polyethylenimine (Sigma, St. Louis, USA). After about 16 hrs cells were fixed with 3.7% formaldehyde in PBS for 10 minutes, washed with PBST (PBS with 0.02% Tween), stained with DAPI and mounted in Vectashield medium (Vector Laboratories, Servison, Switzerland).

Samples were analyzed with a confocal fluorescence microscope (TCS SP5, Leica, Wetzlar, Germany) equipped with a  $63 \times / 1.4$  numerical aperture Plan-Apochromat oil immersion objective as described [47]. DAPI, EGFP and mCherry were excited by 405 nm diode laser, 488 nm argon laser and 561 nm diode-pumped solid-state laser, respectively. Images were recorded with a frame size of  $512 \times 512$  pixels.

### Cell culture, transfection and Western Blots

HeLa, HEP-2 and U2OS cells (ATCC, Manassas, USA) were cultured and Western blots were carried out as described [44,48].

In order to determine cell cycle dependent CENP-O/Q/P levels, HEP-2 or HeLa cells were synchronised by double-thymidine block. Aliquots of equal cell numbers were taken after 2, 4, 6, 8 and 10 hrs after release and lysed. In the Western blot, CENP-O [33], CENP-P [36] and CENP-Q (Rockland, Gilbertsville, USA) are identified by specific primary antibodies which are then detected by fluorescently labelled secondary antibody (Molecular Probes, Eugene, USA). CENP-O/P/Q amounts are quantified by the ODYSSEY Infrared Imaging System (LiCor, Lincoln, USA) following the protocol of the manufacturer.

### Fluorescence Cross-Correlation Spectroscopy (FCCS)

FCCS analyses [49,50] were performed at 37°C on an LSM 710 Confocor3 microscope (Carl Zeiss, Jena, Germany) using a C-Apochromat infinity-corrected  $40 \times / 1.2$  NA water objective. U2OS cells were double transfected with vectors for the simultaneous expression of EGFP and mCherry fusion proteins and analysed. On cells expressing both fusion proteins at relatively low and comparable levels, we selected spots for the FCCS measurements in areas of the nucleoplasm which were free of kinetochores. For illumination of the EGFP-fusion proteins, we used the 488 nm laser line of a 25 mW Argon/2-laser (Carl Zeiss) and for simultaneous illumination of the mCherry fusion proteins a DPSS 561-10-laser (Carl Zeiss), both at moderate intensities between 0.2 and 0.5%. The detection pinhole was set to a relatively small diameter of 40  $\mu$ m (corresponding to about 0.8 airy units). After passing a dichroic beam splitter for APDs (avalanche photodiode detector; NTF 565), the emission of mCherry was recorded in channel 1 through a BP-IR 615–680 nm bandpass filter by an APD (Carl Zeiss), whereas the emission of EGFP was simultaneously recorded in channel 2 through a BP-IR 505–540 nm bandpass filter by a second APD. Before each measurement, we analysed possible crosstalk between the channels and used only cells without or with very little crosstalk. In addition, measurements with autocorrelation values below 1.06 for both, the mRFP channel as well as the EGFP channel, were not further analysed. For the measurements,  $10 \times 10$  time series of 10 sec each were simultaneously recorded for mCherry and for EGFP. After averaging, the data were superimposed for fitting with the Fit-3Dfree-1C-1Tnw model of the ZEN-software (Carl Zeiss), a diffusion model in three dimensions with triplet function. Applying this procedure, we obtained autocorrelations of channels 1 and 2 as well as the cross-correlation of channels 1 versus channel 2. Before starting a set of experiments, the pinhole was adjusted. As negative control, U2OS cells were transfected with vector pIRES2, separately expressing EGFP and mRFP as single molecules with fluorescence intensities comparable to those in the FCCS analysis with CENP fusion proteins. As a positive control, U2OS cells were transfected with pH-mR-G-C expressing a mRFP-EGFP fusion protein, again with fluorescence intensities comparable to those in the FCCS analysis with CENP fusion proteins.

### Cellular imaging

*In vivo* and *in situ* cellular imaging including immuno-fluorescence, SNAP-tag analysis, FRAP, RICS and cell cycle synchronisation were conducted as described in Orthaus et al. [48,51], Hellwig et al. [43,44] and McClelland et al [8]. For immuno-fluorescence, primary antibodies were used at 1:250 (PCNA), 1:300 (anti-CENP-Q), 1:250 (CREST) with DAPI at 1:2000.

## Results

### CENP-O class proteins form a tightly packed complex

In chicken DT40 cells, the CENP-O class proteins form a tight kinetochore sub-complex [10]. Here we analysed the CENP-O class protein packaging at kinetochores in living human cells by measuring which proteins are in close proximity. We tagged all five CENP-O class proteins with fluorescent proteins, either EGFP or mCherry, at either termini, and confirmed by live cell imaging in human U2OS cells that all tagged CENP-O class proteins localise to kinetochores during interphase and mitosis, consistent with published results [5,6,10,33,36,39]. This kinetochore localisation was independent of which terminus of the CENP proteins was tagged.

Then, by FRET we measured the proximity between chromophores tagged to CENP-O class proteins. FRET between the donor fluorophore (here: EGFP) and the acceptor fluorophore (here: mCherry) can only generate a positive result when the distance between donor and acceptor is less than  $\sim 10$  nm. When FRET occurs, both the intensity and lifetime of the donor fluorescence decrease while the intensity of the acceptor emission increases. We measured the FRET donor fluorescence intensity with or without photo-inactivation of the acceptor (acceptor-photo-bleaching FRET, AB-FRET) and, in order to confirm our AB-FRET results, in two cases also the donor fluorescence lifetime (FLIM). In AB-FRET, the acceptor chromophore is destroyed by photo-bleaching, thereby preventing FRET from the donor to the acceptor. Thus, when the donor is in close proximity to the acceptor (sufficient for FRET,  $< 10$  nm), photo-bleaching of the acceptor results in an observable increase in donor fluorescence. In our experiments, two separate kinetochore locations were identified in each image (marked “1” and “2”; Fig. 1A and 1D). In spot “2” the acceptor (CENP-R-mCherry (Fig. 1A), CENP-P-mCherry (Fig. 1D)) was photo-bleached, while spot “1” was not photo-bleached, serving as an internal control for any non-FRET effects. During bleaching of the acceptor (CENP-R-mCherry) in spot 2, the donor (EGFP-CENP-U) fluorescence intensity significantly increased indicating that FRET occurred between EGFP-CENP-U and CENP-R-mCherry (Fig. 1B). Careful quantification indicated that such FRET transfer occurred in 60% of the cases, yielding a FRET efficiency  $E_{\text{FRET}}$  between 6 and 18% (40 bleached spots in 18 cells, black bars in Fig. 1C). The unbleached control spots show a narrow fluorescence variation  $E_{\text{var}}$  around zero (39 bleached spots in 18 cells, grey bars in Fig. 1C). The  $E_{\text{FRET}}$  distribution is significantly different from the  $E_{\text{var}}$  control distribution ( $p < 0.001$ ). Such experiments demonstrated that the majority of pairs gave a positive FRET signal suggesting that the CENP-PORQU subunits are closely associated (see Table 1). Importantly, a number of pairs did not show FRET: We detected no FRET between EGFP-CENP-Q/CENP-P-mCherry (Fig. 1D–F). Here, after acceptor-bleaching, the donor fluorescence did not increase (Fig. 1E) and the distribution of the  $E_{\text{FRET}}$  values (black bars, Fig. 1F) superimposes with the distribution of the  $E_{\text{var}}$  control values (grey bars). Furthermore, we did not observe FRET between EGFP-CENP-P/CENP-O-mCherry and between EGFP-CENP-U/CENP-O-mCherry (see Table 1). For CENP-Q-EGFP and mCherry-CENP-P and for CENP-P-EGFP and mCherry-CENP-O, we confirmed these results by measuring FRET at kinetochores in the lifetime domain (FLIM) by time-correlated single photon counting (TCSPC) using the same fluorescent protein FRET pair EGFP-mCherry. This approach is less error prone compared to acceptor-bleaching FRET in the intensity domain, however, it is considerably more elaborate and time-consuming. We determined the CENP-Q-EGFP donor lifetime in

the absence of an acceptor as  $\tau = 2.45 \pm 0.10$  nsec. When the acceptor is close, the donor life time decreases due to energy transfer to the acceptor: for CENP-Q-EGFP/mCherry-CENP-P we measured  $\tau = 2.08 \pm 0.04$  nsec and for CENP-P-EGFP/mCherry-CENP-O we measured  $\tau = 2.16 \pm 0.05$  nsec. The FLIM results (marked by “F” in Table 1) indicate the proximity between CENP-Q and -P as well as between CENP-P and -O and confirm our acceptor-bleaching FRET data. We conclude that in human cells at kinetochores, CENP-O class proteins are in close proximity to one another. In earlier studies we had detected FRET between the CENP-U N-terminal region and the N-termini of CENP-B and CENP-I, but not to the N-termini of CENP-A and CENP-C [43].

If the orientation of the fluorophore dipole moment of the acceptor relative to that of the donor were known, or at least one of them would rotate freely faster than nanoseconds, a more detailed distance between donor and acceptor could be deduced from the measured  $E_{\text{FRET}}$  values. In our live cell experiments however, this information is not available to us. We therefore do not deduce defined distance values but interpret the appearance of FRET as an indication that donor and acceptor chromophores are close to one another within 10 nm. Our FRET data depend on which protein terminus is tagged: if the two protein termini are clearly separated in space, a fluorophore fused to one terminus might show FRET to another protein while the fluorophore fused to the other terminus might not. In a number of cases, we could not detect FRET between two fusion proteins. Measuring no FRET signal might either be due to donor and acceptor fluorophores being distal ( $> 10$  nm) or, alternatively, that donor and acceptor dipole moments are oriented relative to one another in an unfavorable way so that FRET cannot occur although donor and acceptor are close. Therefore, observing no FRET signal cannot be used for structural information.

### PORQU undergoes a post-loading oligomerisation step

Recombinant CENP-Q that is expressed and purified from *E. coli* lysates, exists as a soluble homo-octameric complex [36]. We therefore asked if CENP-Q oligomerises at kinetochores in living human cells. Indeed, we observed FRET at kinetochores between the N-termini of CENP-Q and between its C-termini in interphase cells, suggesting that CENP-Q oligomerises when kinetochore-bound. In order to find out when in the cell cycle CENP-Q oligomerizes, we carried out cell cycle dependent FRET measurements between C- and N-termini of CENP-Q (see Table 1, Fig. 2). U2OS cells were synchronised by double thymidine block and released into S-phase. Subsequent cell cycle phases were identified by CENP-F and PCNA staining. We found no FRET in G1, early and mid S-phase, however, we detected a significant FRET signal in late S-phase for both, the CENP-Q N- and C-termini, and in G2 for the CENP-Q N-termini (Fig. 2). Consistent with this, quantitative immuno-fluorescence demonstrates that CENP-Q protein levels increase at kinetochores during S-phase and become maximal in late S-phase (see below). We also detected a FRET proximity between two CENP-U N-termini at kinetochores in late but not in early or middle S-phase (data not shown).

### PORQU proteins show multiple pair-wise interactions

Then we asked which of the CENP-O class proteins is able to interact with other protein members of this class. In the mammalian three-hybrid (F3H) assay applied here [46,47], EGFP tagged CENP-O class proteins (bait) were recruited to the *lac* operator repeat array by the GFP-binding protein fused to the Lac repressor (GBP-LacI) forming a green spot in the nucleus (Fig. 3).

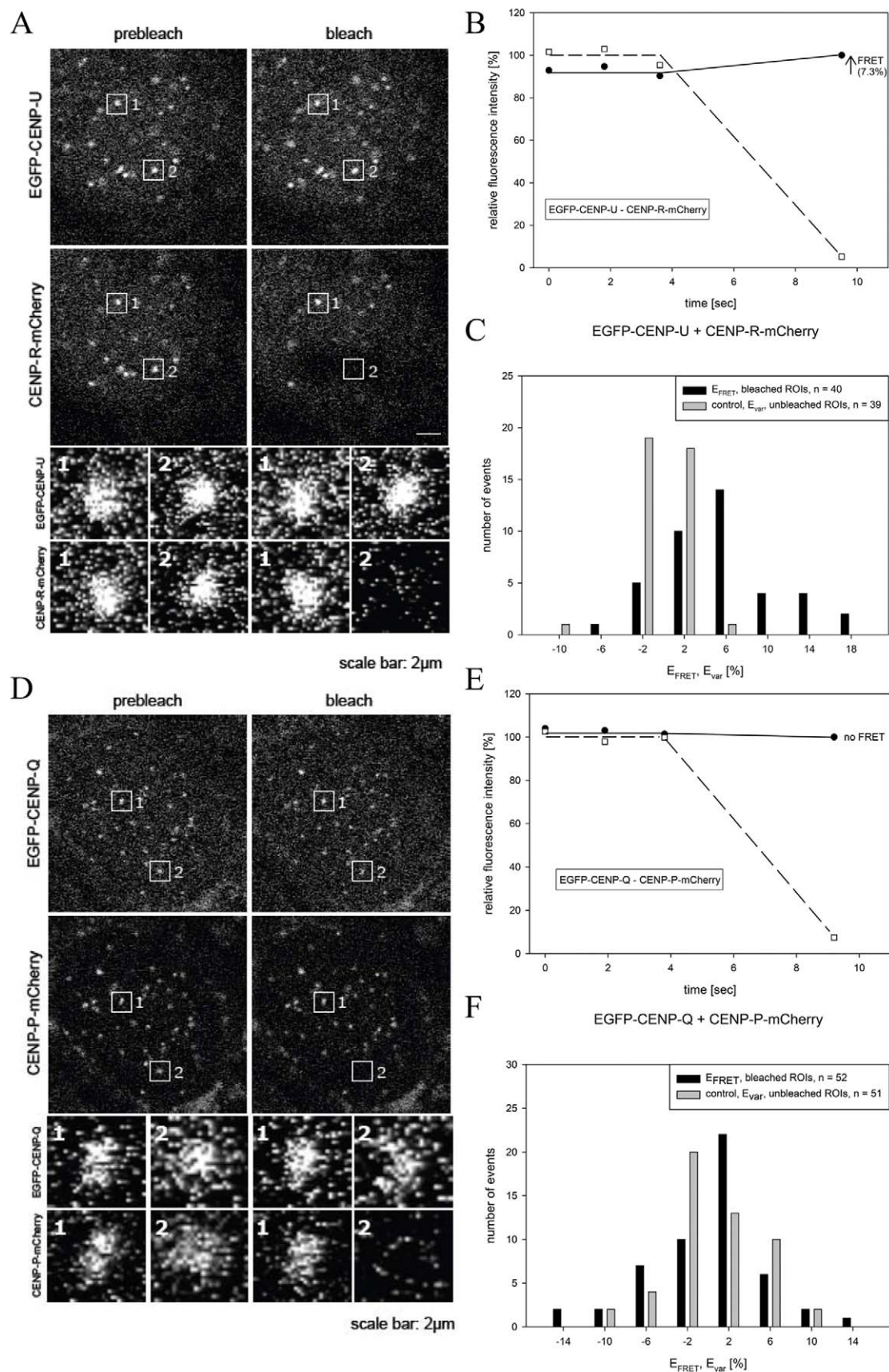


**Figure 1. Acceptor-bleaching FRET of the protein pairs EGFP-CENP-U/CENP-R-mCherry (FRET signal) and EGFP-CENP-Q/CENP-P-mCherry (no FRET signal).** Typical HEP-2 cell nuclei are displayed in (A) and (D) showing centromere location of all four CEN proteins. Two of these locations, spot 1 and spot 2 in each of the two graphs, were selected for fluorescence intensity analysis before and after acceptor bleaching (see enlargements below). Spot 1 served as control and showed no detectable intensity change. At spot 2, the acceptor fluorophore mCherry was bleached (compare pre-bleach and post-bleach in (A) and (D)). In (B) and (E), the time course of the fluorescence intensity of the donor and the acceptor of both FRET pairs are shown. The acceptor intensities in the ROI ("region of interest"; open squares) were averaged and normalized to the mean intensity measured at the three time points before bleaching. The donor intensities in the ROI were averaged and normalized to the intensity measured at the time point after bleaching. Bleaching of the acceptor resulted in a fluorescence intensity increase of the donor (black dots) for EGFP-CENP-U (B) indicating the presence of FRET (see arrow), but no fluorescence intensity increase for EGFP-CENP-Q (E) indicating the absence of FRET. (C) and (F): Donor fluorescence intensity variation observed during acceptor bleaching normalized to the intensity measured at the first time point after bleaching. Control: spot 1 (acceptor not bleached) yielding  $E_{var}$  (grey bars), FRET measurement: spot 2 (acceptor bleached) yielding  $E_{FRET}$  (black bars). For protein pairs indicated, number of observed single cases (grouped into  $E_{var}$  or  $E_{FRET}$  value ranges of 4%) displayed versus values of  $E_{var}$  or  $E_{FRET}$ . (C) EGFP-CENP-U (donor) and CENP-R-mCherry (acceptor): distribution of  $E_{FRET}$  (40 bleached kinetochores) is clearly distinct from the distribution of  $E_{var}$  (39 non-bleached kinetochores) indicating FRET. (F): EGFP-CENP-Q (donor) and CENP-P-mCherry (acceptor): distribution of  $E_{FRET}$  (52 bleached kinetochores) superimposes the distribution of  $E_{var}$  (51 non-bleached kinetochores) indicating no FRET.

Co-expressed mCherry-tagged CENP-O class proteins (prey) may either interact with the EGFP-tagged protein at the *lac* operator array (visible as red spot and yellow in the overlay) or may not interact resulting in a disperse distribution. For each mCherry fusion, EGFP was used to control for unspecific interactions. In the upper two rows of Fig. 3A, the clear interaction between EGFP-CENP-O and mCherry-CENP-P as well as EGFP-CENP-P and

mCherry-CENP-O are shown. The lower two rows show the corresponding results for CENP-O and CENP-Q. While EGFP-CENP-Q did not interact with and recruit mCherry-CENP-O to the *lac* spot, we found a very weak interaction in the reverse combination. Such differences for reverse combinations might be explained by sterical hindrance at the interaction site due to the attachment to GBP-LacI for one but not the other tagged terminal region. All results of this F3H interaction assay are listed in Table 2. The results of this CENP-O class protein interaction analysis indicate strong interactions between particular members of this class (Fig. 3B). CENP-O, -P and -Q each are able to strongly recruit and thus specifically bind two, while CENP-U and -R are able to recruit three of the remaining four proteins. In addition, CENP-U and CENP-R are able to bind to themselves. We detected homo-interaction of CENP-R also by a Yeast-two-Hybrid (Y2H) assay. CENP-U binding to itself is supported by our FRET data indicating close proximity between CENP-U N-termini in late S-phase (see above). Our data that CENP-P is closely associated with CENP-O, and CENP-U with CENP-Q, agree well with published results [10,41,42]; here we detected an additional weaker interaction between CENP-Q and CENP-R. However, none of the CENP-O class proteins is able to recruit all four other proteins of this class which would be expected when the

**Table 1. FRET interactions between CENP-O class proteins.**

EGFP fusion	mCherry fusion	p	FRET
EGFP-CENP-P	mCherry-CENP-O	<0.001	++
EGFP-CENP-P	CENP-O-mCherry	0.093	–
CENP-P-EGFP	mCherry-CENP-O	<0.001	++F
CENP-P-EGFP	CENP-O-mCherry	<0.001	++
EGFP-CENP-Q	mCherry-CENP-O	<0.001	++
EGFP-CENP-Q	CENP-O-mCherry	<0.001	++
EGFP-CENP-Q	mCherry-CENP-P	<0.001	++
EGFP-CENP-Q	CENP-P-mCherry	0.724	–
EGFP-CENP-Q	mCherry-CENP-Q	<0.001	++
CENP-Q-EGFP	CENP-Q-mCherry	<0.001	++
CENP-Q-EGFP	mCherry-CENP-P	<0.001	++F
EGFP-CENP-U	mCherry-CENP-O	<0.001	++
EGFP-CENP-U	CENP-O-mCherry	0.655	–
EGFP-CENP-U	mCherry-CENP-P	0.003	+
EGFP-CENP-U	CENP-P-mCherry	<0.001	++
EGFP-CENP-U	mCherry-CENP-Q	<0.001	++
EGFP-CENP-U	mCherry-CENP-R	<0.001	++
EGFP-CENP-U	CENP-R-mCherry	<0.001	++
CENP-U-EGFP	mCherry-CENP-P	<0.001	++
EGFP-CENP-B	CENP-Q-mCherry	<0.001	++
EGFP-CENP-O	mCherry-CENP-K	<0.001	++
CENP-O-EGFP	mCherry-CENP-K	0.004	+
EGFP-CENP-R	mCherry-CENP-K	<0.001	++
CENP-R-EGFP	mCherry-CENP-K	<0.001	++
EGFP-CENP-U	mCherry-CENP-K	<0.001	++
CENP-U-EGFP	mCherry-CENP-U	0.167	–
EGFP-CENP-U	mCherry-CENP-U	<0.001	++
CENP-N-EGFP	mCherry-CENP-K	<0.001	++

The FRET pair EGFP-mCherry is used. "F" indicates that for these fusions FRET was detected also by FLIM. ++: strong FRET, +: weak FRET, –: no FRET.

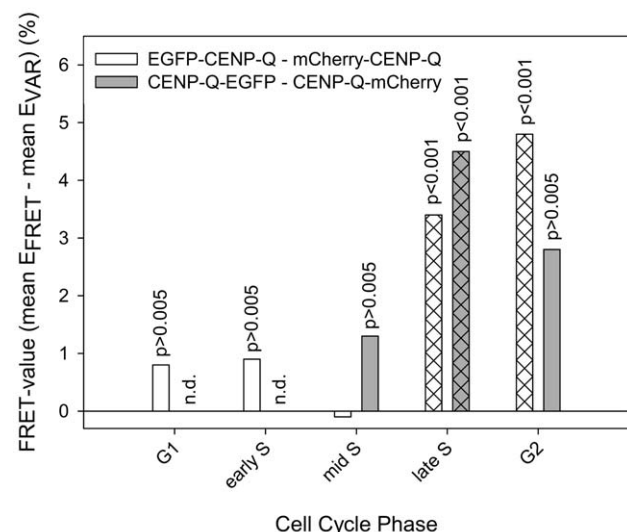


**Figure 2. Cell cycle-dependent FRET between CENP-Q C- (grey bars) and N-termini (white bars).** In late S-phase and G2, significant FRET is observed ( $p < 0.001$ ). In G1, early and mid S-phase, no FRET is observed ( $p > 0.005$ ).

complex pre-forms in the nucleoplasm. Furthermore, ectopic recruitment to the *lac* operator repeat array obviously is not strong enough to enable indirect binding: e.g. CENP-L recruits CENP-R, and CENP-R recruits CENP-Q, but CENP-L is not able to attract CENP-Q to this site. Thus, this F3H assay is, to a large extent, specific for direct interactions.

### CENP-PORQU subcomplex contacts other CCAN proteins

Kinetochore localization is determined by CENP-A which is recognized by CENP-N and CENP-C [14–16]. CENP-L binds to the C-terminal region of CENP-N *in vitro* [14] and CENP-K kinetochore localisation depends on the presence of CENP-N and -C [5,8,14,52]. We therefore asked, if these kinetochore proteins, being directly or closely linked to CENP-A, are able to recruit single CENP-PORQU proteins or the whole complex to an ectopic chromatin site in human cell nuclei *in vivo*. We studied the interaction of CENP-C, -L, -K and -N with CENP-PORQU proteins by F3H; the results are listed in Table 2 and displayed in Fig. 3B. CENP-N shows binding to CENP-R and some weak binding to CENP-U, however, only for mCherry-tagged CENP-N (prey) while EGFP-tagged CENP-N (bait) does not show any interaction with CENP-PORQU proteins. CENP-L shows strong binding to CENP-R and moderate binding to CENP-U (strong in one, weak in the other version; see Table 2) and very weak binding to CENP-C (only in one orientation). Furthermore, RFP-tagged CENP-L also shows weak interactions with CENP-Q and CENP-K. Next to CENP-L, also CENP-K shows strong interactions with CENP-PORQU proteins: CENP-K strongly interacts with CENP-O and -U, moderately with CENP-R (strong in one, weak in the other version; see Table 2), and in one version weakly with CENP-Q. CENP-K also weakly binds to itself. By Y2H we detected an interaction between CENP-K and CENP-O, consistent with results of McClelland et al. [8], and an interaction between CENP-K and CENP-H, supporting data of Qui et al. [53], however no interaction had been detected by Y2H between CENP-O and either CENP-H or CENP-N [8]. We thus conclude that to some extent CENP-N, but more efficiently CENP-L and even more so CENP-K mainly recruit CENP-O, -U and -R to kinetochores but much less so CENP-Q, and not CENP-P. This finding agrees with results of Okada et al. [6] who observed in human and DT40 cells that the localization of CENP-O, -P, -Q and -H was disrupted in CENP-K and CENP-L depleted cells. Our results extend their observations by identifying the pairwise interactions responsible for the observed data: Potentially CENP-P and CENP-Q are disrupted from CENP-K and -L depleted cells due to being members of the CENP-PORQU complex and not due to specific protein-protein interactions. Similarly, the dependence of CENP-U kinetochore localization on the presence of CENP-H and -I [38] might be explained by CENP-H and -I being required for CENP-K binding which then recruits the CENP-PORQU complex. F3H yields more direct data on protein-protein interactions than depletion experiments which by their very nature also influence the presence of proteins down-stream of the depleted protein.

We observed no recruitment to the ectopic chromatin site of any CENP-PORQU protein by CENP-C. Furthermore, CENP-L and -N do not recruit all five CENP-PORQU proteins, again indicating that the CENP-PORQU complex does not pre-form in the nucleoplasm.

We confirmed these F3H results by FRET studies. We measured the close neighbourhood of CENP-K to several CENP-PORQU proteins and to CENP-N, and found proximities between the N-terminus of CENP-K with both termini of CENP-R, the N-termini of CENP-O and -U and to the C-terminus of

CENP-N (see Table 1). These results place CENP-K inbetween CENP-N and the CENP-PORQU proteins.

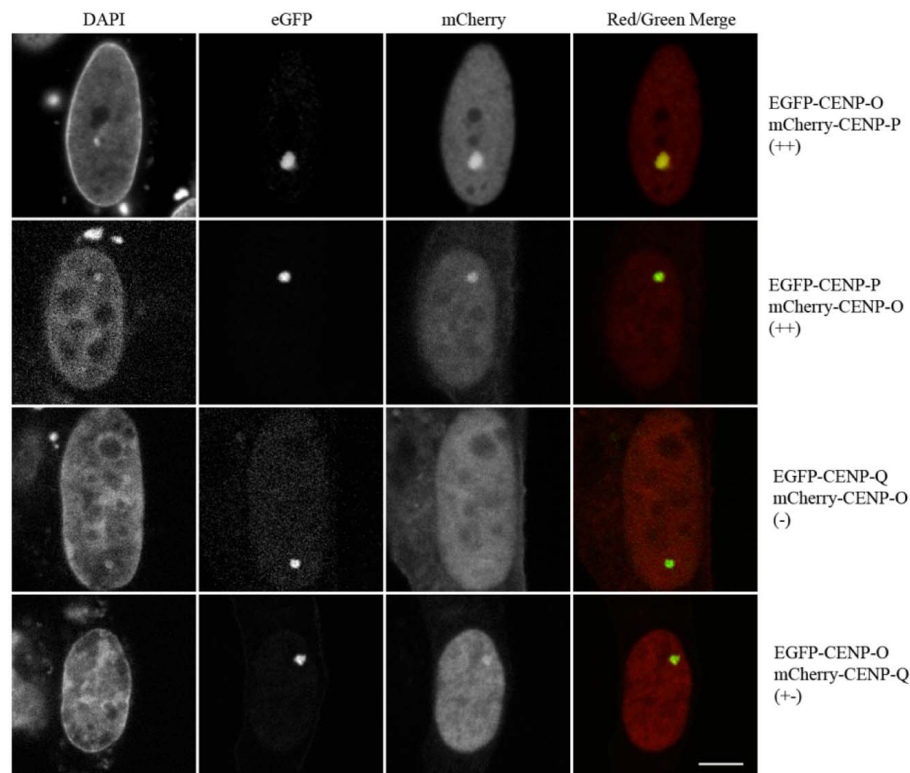
### PORQU does not preassemble in the cytoplasm

In order to analyse CENP-PORQU complex pre-assembly, in interphase we measured the mobility of the five CENP-O class proteins in the nucleoplasm of human U2OS cells by Raster Image Correlation Spectroscopy (RICS) [54] and found fast mobility between 4.7 and 5.9 ( $\pm 15\%$ )  $\mu\text{m}^2/\text{sec}$ . The proteins are thus more mobile than other inner kinetochore proteins [44,55]. The experimental variation of the measured mobilities, however, does not allow for a conclusion on multimerisation. We therefore performed Fluorescence Cross-Correlation Spectrometry (FCCS) studies to determine if CENP-O class proteins form hetero-dimers in the nucleoplasm. In double-transfected U2OS cells we analysed various protein pairs: EGFP-CENP-O/mCherry-CENP-P, EGFP-CENP-P/mCherry-CENP-Q, EGFP-CENP-R/mCherry-CENP-Q, EGFP-CENP-Q/mCherry-CENP-Q, CENP-O-EGFP/mCherry-CENP-Q, EGFP-CENP-U/mCherry-CENP-Q, EGFP-CENP-R/mCherry-CENP-R, EGFP-CENP-R/CENP-R-mCherry, CENP-U-EGFP/CENP-U-mCherry, CENP-U-EGFP/mCherry-CENP-U and EGFP-CENP-U/mCherry-CENP-O. For these protein pairs we found unequivocal cross-correlation only between CENP-O and CENP-P. From 12 cells, all 12 showed cross-correlation indicating that CENP-O and CENP-P move together, i.e. they are part of one and the same complex in the nucleoplasm outside kinetochores. The cross-correlation analysis (Fig. 4A) resulted in a correlation of 1.020 (Fig. 4A, insert b) indicating that 29% of the molecules are co-migrating in the nucleoplasm. As negative control, U2OS cells were analysed separately expressing EGFP and mRFP as single molecules. The cross-correlation curve (Fig. 4B) resulted in a value of 1.001 (Fig. 4B, insert b) indicating the absence of any complexation between EGFP and mRFP. As a positive control, U2OS cells were transfected with pH-mR-G-C expressing a mRFP-EGFP fusion protein. Cross-correlating the two channels against each other, we obtained a value of 1.029 indicating that about 50% of the molecules are detected as a complex (Fig. 4C). We obtained similar cross-correlation values for the fusion EGFP-mCherry, in agreement with results of Kohl et al. [56]. For such fusion proteins, 100% cross correlation should be observed. The lower value of 50% could be explained by a much slower maturation and lower stability of mRFP compared to EGFP: EGFP molecules bound to an immature mRFP are interpreted by FCCS as free molecules. Thus, cross-correlation values seem to underestimate the percentage of co-migrating molecules. Consequently, hetero-dimerisation of EGFP-CENP-O and mCherry-CENP-P probably is higher than the calculated 20–30%, we estimate 40–60%.

In 2 out of 12 analyzed cells, a weak cross-correlation ( $\sim 10\%$ ) was observed for CENP-Q and CENP-R indicating that in a few cases CENP-Q and CENP-R co-migrate in the nucleoplasm outside kinetochores. The other analyzed protein pairs showed no cross-correlation demonstrating that the CENP-PORQU complex does not pre-form in the nucleoplasm outside kinetochores. CENP-R and CENP-U are able to bind to themselves at an ectopic chromatin site (see above). However, by FCCS we did not detect any cross correlation, clearly indicating that these proteins do not stably aggregate in the nucleoplasm. Recombinant CENP-Q can oligomerise to octamers [36] and, when kinetochore-bound, oligomerises in late S-phase, as detected by FRET (see above). In the nucleoplasm, however, CENP-Q does not form di- or multimers, as shown here by FCCS. This FCCS result is confirmed by the absence of a FRET signal between two tagged



A



B

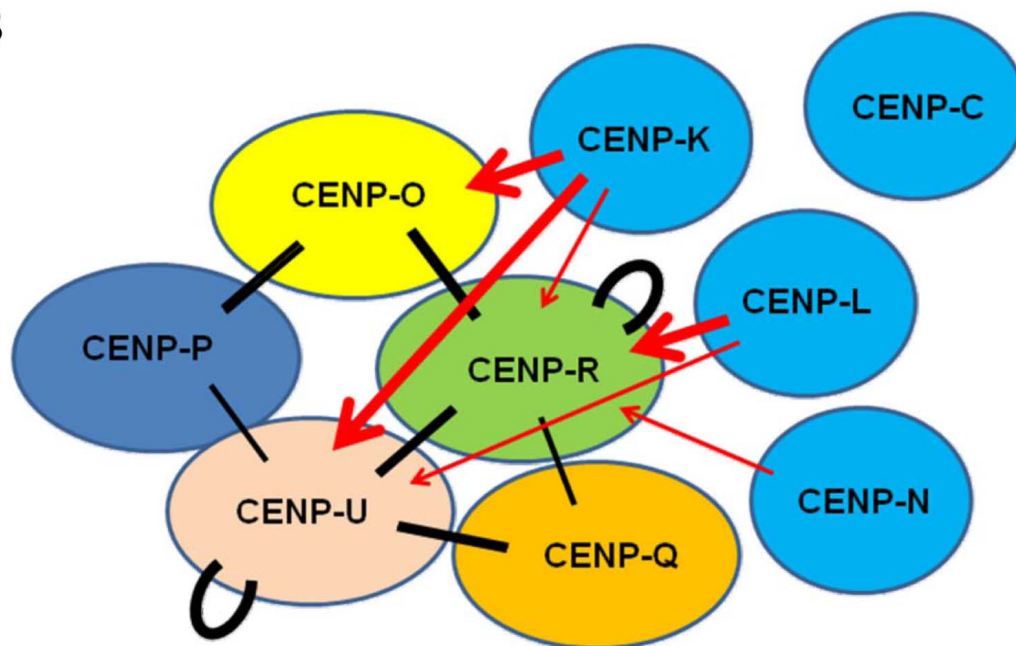


**Figure 3. Centromere protein interactions analyzed by F3H assay.** (A) EGFP tagged centromere proteins (bait, green) were recruited to the *lac* operator repeat array by the GFP-binding protein fused to the Lac repressor (LacI-GBP). Co-expressed mCherry tagged centromere proteins (prey, red) may either interact with the GFP-tagged protein (yellow in the overlay) or may not interact resulting in a disperse distribution. Upper two rows: interaction between EGFP-CENP-O and mCherry-CENP-P, EGFP-CENP-P and mCherry-CENP-O. Lower two rows: EGFP-CENP-Q did not interact with and recruit mCherry-CENP-O to the *lac* spot, but shows a weak interaction in the reverse combination. For all results see Table 1. Bar: 5  $\mu$ m. (B): Strong F3H interactions are displayed (++: thick lines, +: thin lines). Black bars: interactions between CENP-PORQU proteins, red arrows: recruitment of CENP-PORQU proteins by CENP-K, -L, and -N. CENP-C is not able to recruit any of the CENP-PORQU proteins (data see Table 2).  
doi:10.1371/journal.pone.0044717.g003

**Table 2.** F3H analysis of CENP-O class protein interactions.

mCherry\EGFP	CENP-O	CENP-P	CENP-Q	CENP-R	CENP-U	CENP-K	CENP-L	CENP-N	CENP-C
CENP-O	—	++	—	++	—	+	—	—	—
CENP-P	+	—	+—	+—	+	—	—	—	—
CENP-Q	+—	—	—	+	+	—	—	—	—
CENP-R	++	+—	+	++	++	+—	++	—	—
CENP-U	—	+	++	++	++	++	+—	—	—
CENP-K	++	—	+—	+	++	+—	—	—	—
CENP-L	—	—	+—	+	+	+—	—	—	+—
CENP-N	—	—	—	+	+—	—	—	—	—
CENP-C	—	—	—	—	—	—	—	—	—

GFP-tagged CENP-O class proteins, CENP-K, -L, -N and -C (rows) were bound to ectopic chromosomes sites. When RFP-tagged CENP-O class proteins, CENP-K, -L, -N and -C (lines) were recruited to these proteins, this was visible by a yellow dot. Signal intensity at the nuclear spot was used as an indicator for interaction strength. ++, +: strong interaction; +—: weak interaction; —: no interaction.

doi:10.1371/journal.pone.0044717.t002

CENP-Q in the nucleoplasm outside kinetochores (data not shown).

These data show that, with the two exceptions CENP-O/-P and CENP-Q/-R, the pairwise CENP-O class protein interactions detected by F3H do not result in a homo- or hetero-dimerisation of these proteins stable enough for FCCS detection. Since these proteins do not pre-aggregate, they must enter the nucleoplasm as single proteins. CENP-O, -P, -Q and -R are small enough (molecular weights <34 kDa) for not needing a nuclear localisation domain (NLS) for entering the nucleus. Only CENP-U is larger (47.5 kDa) and indeed contains two NLS [57,58].

### PORQU loads onto kinetochores in S-phase and form a stable subcomplex

We next asked when during the cell cycle the CENP-PORQU complex assembles. By applying SNAP-tag technology, we determined at which cell cycle phase CENP-O is loaded to the kinetochore. The SNAP protein tag can catalyze the formation of a covalent bond to a benzyl-guanine moiety coupled to different fluorescent or non-fluorescent membrane-permeable reagents [59]. This tag allows pulse-chase experiments at a single protein level. Consistent with previous data [60], we detected TMR-star fluorescence on SNAP-CENP-A only in G1 cells, confirming that CENP-A is specifically loaded in G1, while we observed a time window of mid G1 to G2 for CENP-N binding and loading to kinetochores [44]. Here we transfected a SNAP-CENP-O construct. After double-thymidine and aphidicolin block release and applying the same protocol, we found SNAP-CENP-O present at kinetochores of G2 cells (Fig. 5A), indicating that CENP-O is loaded onto kinetochores in or before G2. To extend our temporal analysis to further phases of the cell cycle, we repeated these experiments in U2OS cells since these cells have a longer cell cycle: 12 hrs after release and following the same experimental procedure, U2OS cells can be analysed in late-S-phase. Here, TMR-star fluorescence for SNAP-CENP-O was already detected in late S-phase as judged by PCNA-GFP fluorescence (Fig. 5B). Thus, CENP-O assembles at kinetochores already in late S-phase or earlier. Finally, to measure the earliest time point at which CENP-O can assemble into kinetochores, SNAP-CENP-O transfected HeLa cells were arrested in mitosis for 12 hrs by a nocodazole block and quenched with BTP for 30 min. 4 hrs after quenching, the cells were released from nocodazole arrest. Further 5 hrs later, SNAP-tagged CENP-O was

fluorescently labelled with TMR-star for 30 min and fixed for examination. No TMR-star fluorescence was detected indicating that SNAP-CENP-O is not loaded in G1 (Fig. 5C). Overall these experiments suggest a time window of S-phase to G2 for CENP-O loading to kinetochores. Also for CENP-T and -W [61], CENP-N [44] and CENP-U [62] loading to kinetochores in S-phase was observed.

Our recent work showed that CENP-T and -W [61] as well as CENP-N [44] are loaded to human kinetochores by slow loading dynamics, mainly during the second half of S-phase. This is in contrast to CENP-A which is loaded at the end of mitosis and G1 [55,60]. We speculated that the CENP-O class proteins might also be loaded slowly, mainly in S-phase. We thus studied the dynamic binding of these EGFP-tagged CENPs by Fluorescence Recovery After Photobleaching (FRAP) in living human U2OS cells. For none of the five CENP-O class proteins, at any cell cycle phase, we could detect fluorescence recovery within 150 sec after bleaching, indicating rather stable kinetochore binding of all five proteins, consistent with observations of Minoshima et al. [38] for CENP-U. We then studied fluorescence recovery of these five proteins during the cell cycle in a longer time frame, now over 4 hours. Different cell cycle phases were identified by staining with CENP-F and by co-expressing mRFP-PCNA for identifying S-phase and its sub-phases [63,64], as recently described [44,55,65]. In G1, all five CENP-O class proteins show complete recovery; four proteins have an exchange rate ( $t_{1/2}$ ) of about one hour while only CENP-R exchanges slower with  $t_{1/2} = 2$  hrs. In S-phase and G2, CENP-O, -P and -Q show partial recovery values of 40 to 80% with a slower exchange rate compared to G1 of about 2 hrs (see Table 3 and Fig. 6; in some cases for CENP-O and -P, the recovery only allows to estimate the final recovery level (values in brackets)). These recovery amplitudes are in the same range of values as for those of CENP-T and -W ( $70 \pm 8\%$ ) [61] and CENP-N ( $45 \pm 6\%$ , see Table 3) [44]. The slow recovery times during the second half of S-phase coincide with the slow recovery times of CENP-T and -W ( $t_{1/2} = 70 \pm 10$  min) [61], but are slower than the exchange of CENP-N ( $t_{1/2} = 38 \pm 7$  min) [44]. In G2, CENP-P and -Q seem to show slightly faster recovery times compared to S-phase. The FRAP dynamics of CENP-U and -R are distinct from that of CENP-O, -Q and -P. CENP-U shows 100% recovery throughout the cell cycle with the exception of late S-phase when most of CENP-U ( $71 \pm 2\%$ ) is immobile (the remaining 29% of CENP-U exchange with  $t_{1/2} = 50 \pm 8$  min). Our FRET data indicate that CENP-U di- or multimerises in late S-phase. This CENP-U self-

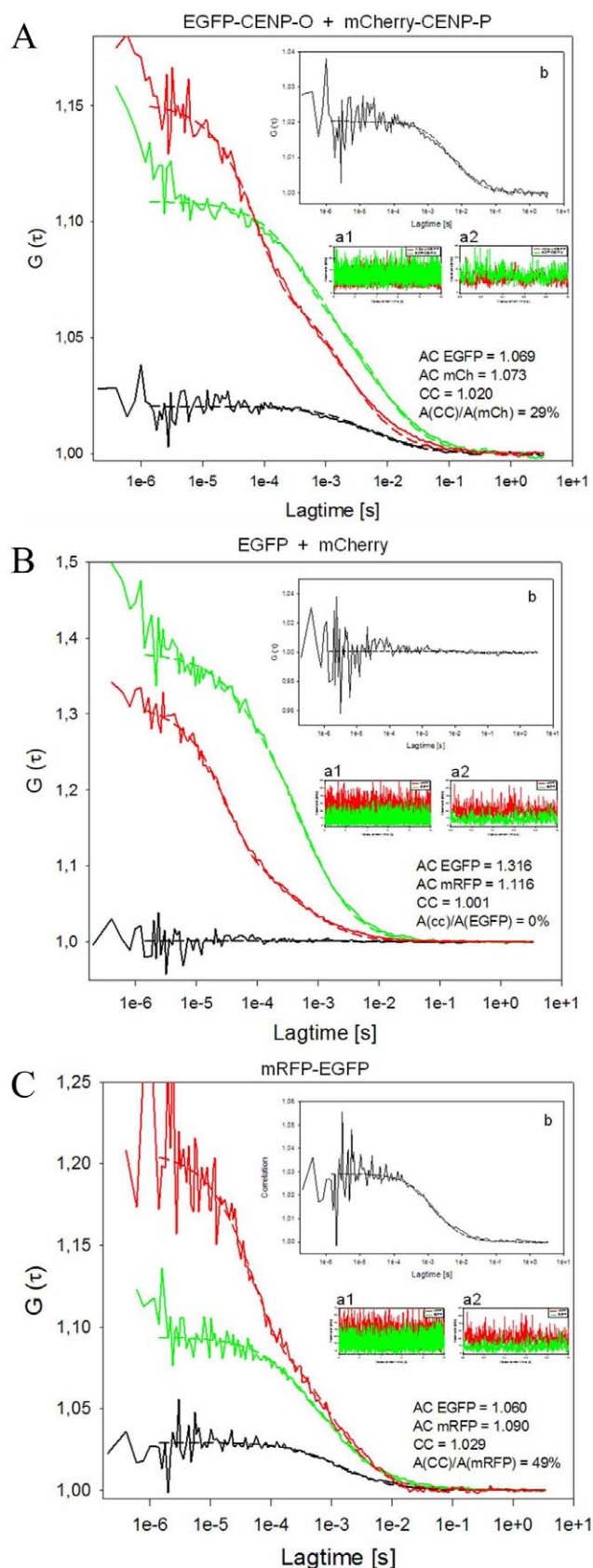


**Figure 4. FCCS measurements displaying  $G$  versus lag time.** Red: mCherry (A, B) or mRFP (C), green: EGFP, black: auto-correlation. Count rates are displayed over 10 sec (inserts a1) indicating the

absence of photobleaching, and 1 sec (inserts a2) indicating the absence of larger protein aggregates. The cross-correlation analyses are amplified in inserts b. (A) EGFP-CENP-O and mCherry-CENP-P indicate complex formation in the nucleoplasm (amplitude of cross-correlation/amplitude of mCherry signal: 29%). The amplitude of the cross-correlation curve  $A(CC)$ , relative to the diffusion-related amplitude of one of the autocorrelation curves  $A(AC)$  of EGFP or mCherry, is a measure of binding or dynamic colocalization [49,50]. According to this ratio of amplitudes  $A(CC)/A(AC)$ , up to 20–30% of nucleoplasmic CENP-O and -P are hetero-dimers. Count rates were recorded simultaneously for both fluorophores. The count rate detected in a 10 sec measurement (insert a1) demonstrates the absence of photobleaching, while the count rate in a 1 sec resolution time scale (insert a2) indicates the absence of larger protein aggregates. The autocorrelations yielded 1.069 and 1.073 for EGFP-CENP-O and mCherry-CENP-P, respectively. The cross-correlation analysis (with a magnified scale of  $G(\tau)$ ; insert b) resulted in a correlation of 1.02 indicating that 29% of the molecules are co-migrating in the nucleoplasm. (B) EGFP and mCherry expressed as single non-fused proteins (negative control) do not show any cross-correlation ( $A(CC)/A(EGFP) = 0\%$ ). The count rates (inserts a1 and a2) indicate the absence of photobleaching and larger proteins. The autocorrelations yielded 1.316 and 1.116 for EGFP and mRFP, respectively. The cross-correlation curve (with a magnified scale of  $G(\tau)$ , insert b) resulted in a value of 1.001 indicating the absence of any complexation between EGFP and mRFP. (C) mRFP-EGFP fusion protein (positive control) shows cross-correlation ( $A(CC)/A(mRFP) = 49\%$ ). The count rates indicate that photobleaching and the presence of larger protein aggregates can be excluded (inserts a1, a2) and that the autocorrelations of EGFP (1.06) and mRFP (1.09) were comparable to the values obtained for EGFP-CENP-O and mCherry-CENP-P. Cross-correlating the two channels against each other, we obtained a value of 1.029 indicating that about 50% of the molecules are detected as a complex (with a magnified scale of  $G(\tau)$  in insert b). doi:10.1371/journal.pone.0044717.g004

assembly could reduce CENP-U exchange at the kinetochore in late S-phase, explaining the high immobile fraction detected by FRAP. This CENP-U/-U interaction seems not be mediated by Plk1 since Plk1 binding to kinetochores occurs during late G2 [41]. Our data indicate that CENP-Q and CENP-U form di- or oligomers after kinetochore binding before the onset of mitosis, potentially denoting a conformational change.

Different from the behaviour of the other four proteins, for all cell cycle phases CENP-R shows recovery values of 100% with slow loading times of 2 to 3 hrs (Table 3). Thus, CENP-R recovery is considerably slower than that of the other four CENP-O class proteins. The observed distinct dynamical behaviour of the CENP-O class proteins indicates that the complex does not bind to the kinetochore as a pre-formed complex in the nucleoplasm and that these proteins retain distinct dynamic behaviour also when bound to the kinetochore.

### Cell-cycle dependent protein abundance

The CCAN protein CENP-N shows varying abundance in the cell with a maximal protein level at kinetochores in late S-phase [8,44]. Furthermore, the presence of CENP-U at HeLa kinetochores increases during late G1 and early S-phase, remains high through late S and G2 and decreases strongly during M-phase [40]. For human CENP-O, a decrease in kinetochore presence down to about 60% from interphase to mitosis was detected by immuno-fluorescence [33]. Here we extended these CENP-O data and measured the cell cycle dependent amount of CENP-O relative to tubulin in HEp-2 cells by Western blot 2, 4, 6 (S-phase), 8 (G2), and 10 hours (M-phase) after release from a double thymidine block (Fig. 7A). The cellular amount of CENP-O remains rather stable from G1/S over the entire S-phase, is reduced already in G2 and reduces further in M-phase, consistent with findings of McAinsh et al. [33]. A corresponding Western blot



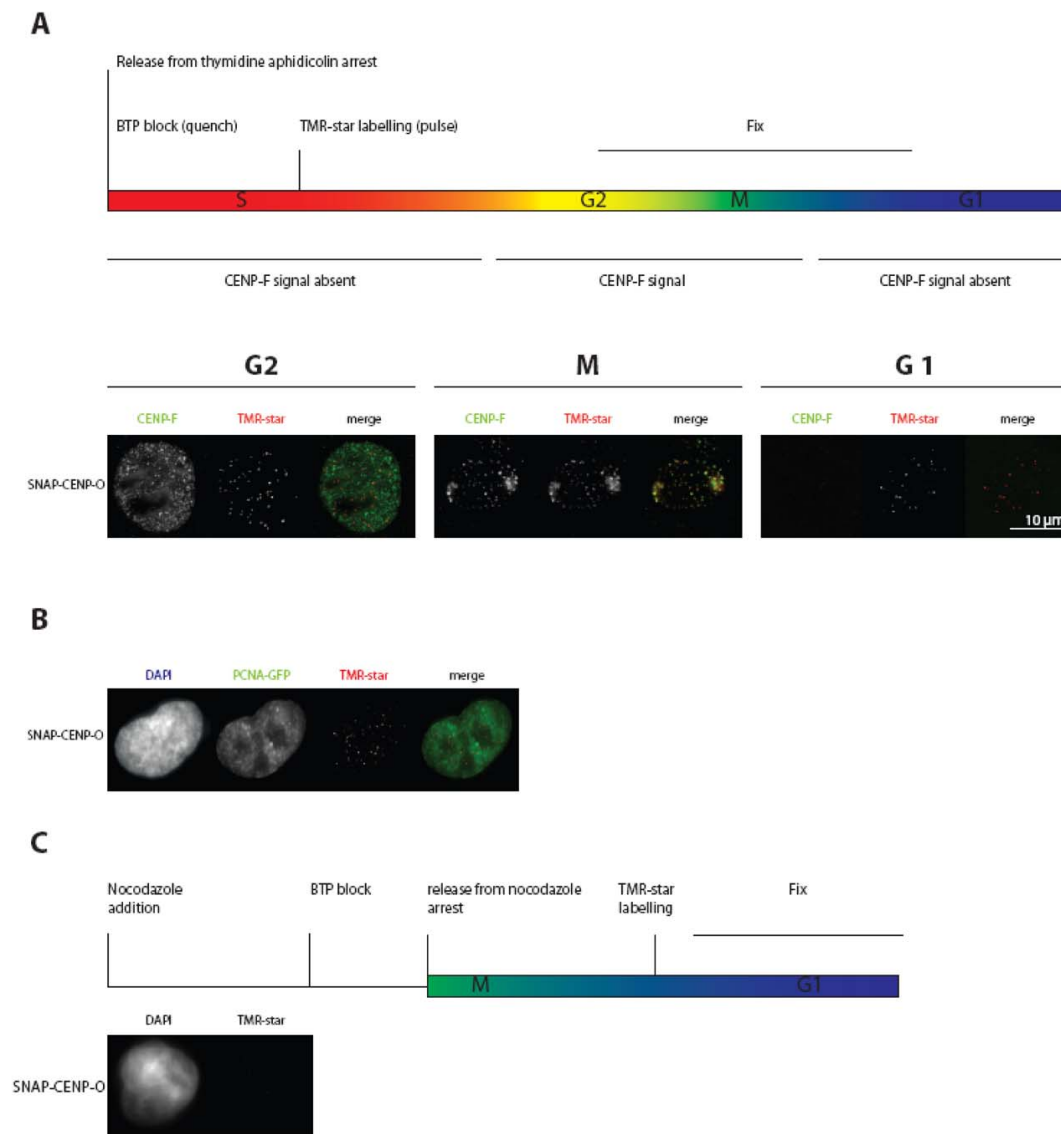


**Figure 5. CENP-O loading to kinetochores measured by the SNAP-tag technology.** (A) Top: schematic representation of the performed experiment. Below: representative images of cells showing TMR-star fluorescence for SNAP-CENP-O in G2, M-phase and the following G1. Cell cycle phases G2 (CENP-F staining of the whole nucleus) and mitosis (specific kinetochore binding of CENP-F) are clearly identified. (B) The same experiment as in (A) was performed with U2OS cells stably expressing PCNA-GFP. SNAP-CENP-O fluorescence appears at kinetochores in late S-phase as judged from cellular PCNA distributions. (C) Top: schematic representation of the performed experiment. Below: representative images of cells expressing SNAP-CENP-O showing no fluorescence at kinetochores during G1. CENP-O is thus loaded to kinetochores in S-phase.

doi:10.1371/journal.pone.0044717.g005

analysis was conducted for CENP-P and CENP-Q: The level of CENP-P decreases from late S-phase through G2 to M-phase (Fig. 7B, D), whereas CENP-Q displayed stable protein levels from G1/S into mitosis (Fig. 7C, D). In contrast to the constant level of CENP-Q levels in the cell, immune-fluorescence detected an increase of the amounts of CENP-Q at kinetochores during S-phase, reaching a maximum in late S-phase and strongly decreasing in G2 (Fig. 7E, F).

## Discussion

The centromeric histone H3 variant CENP-A is the central marker of centromere location and inherits this location to daughter cells [55]. The kinetochore recognizes this epigenetic mark, in part, through the CCAN network of proteins. The

CENP-N subunit directly binds the CENP-A CATD region of the CENP-A containing nucleosome while the CENP-C subunit binds the C-terminal tail of CENP-A [14–16]. In addition to these CENP-A binding mechanisms, CENP-T/W/S/X form a unique centromeric chromatin structure next to histone H3 containing nucleosomes that supercoils DNA [9,12,61]. If we are to fully understand the pathways and mechanisms that allow a mature kinetochore to assemble, it will be crucial to define how these chromatin-interacting complexes recruit the other 11 CCAN subunits. Of these subunits the CENP-PORQU were reported to form a stable complex when being expressed in *E. coli* [10], whereas the CENP-H, -I, -K, -L and -M (CENP-H class) are not known to associate into any stable sub-complexes [8]. Dependency experiments show that CENP-PORQU requires the CENP-H class for kinetochore binding but not *vice versa* [5,6,8,14,52]. The

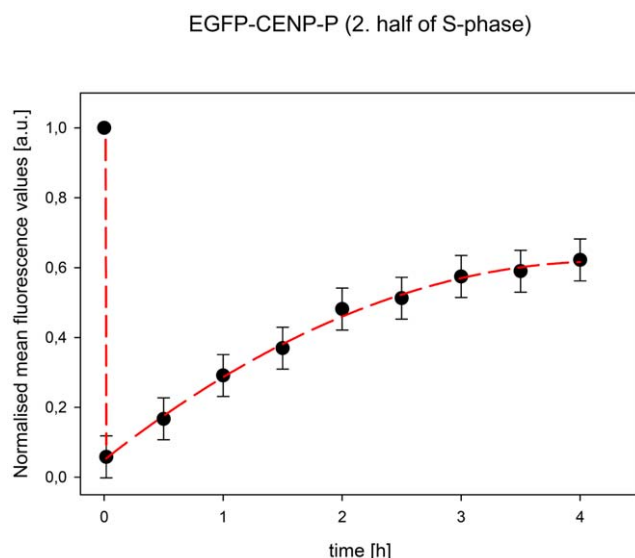


**Figure 6. Fluorescence recovery after photobleaching of EGFP-CENP-P in mid S-phase.** Normalised mean fluorescence values of 55 kinetochores taken in time steps of 30 min over 4 hours. Recovery levels off, indicative of an about 40% immobile fraction. doi:10.1371/journal.pone.0044717.g006

working model thus involves the stepwise recruitment of CENP-N/CENP-TWSX»CENP-HIKLM»CENP-PORQU [2]. In line with this, CENP-L can bind directly to CENP-N *in vitro* [14] and may be involved in stabilising CENP-N binding to the CENP-A nucleosome [44]. We now show by F3H that CENP-N, CENP-K and CENP-L are all, to some extent, capable of recruiting CENP-O, -U and -R to an ectopic chromosomal site, whereas CENP-C is not directly involved in CENP-PORQU binding. The next step will be to identify the physical interactions that mediate this assembly reaction.

The CENP-PORQU proteins assemble at kinetochores during S-phase. For example, newly synthesized CENP-O is incorporated in S-phase and remains at the kinetochore during mitosis (although levels decrease, consistent with previous findings [33]) into the following G1 where they can exchange slowly and to near completion (however, without exchange with newly synthesized CENP-O). During the cell cycle, the CENP-PORQU proteins show different protein abundance in the cell: while CENP-Q protein levels do not change from G1/S to M-phase, the levels of CENP-O and -P decrease, CENP-P levels already during S-phase but those of CENP-O only after S-phase. The protein amount at

kinetochores is maximal in late S-phase for CENP-Q, as shown here, and at late S-phase and G2 for CENP-U [40]. This variance of protein abundance in the cell and at kinetochores supports our conclusion that the CENP-PORQU complex assembles from proteins with individual behavior, and might indicate a varying stoichiometry of the CENP-PORQU proteins in the complex.

The reported stable interaction of CENP-PORQU in *E. coli* lysates [10] suggests that these proteins may form a pre-assembled complex in the nucleoplasm before loading onto kinetochores in S-phase. We show here, however, by FCCS that the CENP-PORQU subunits do not exist as a single preformed complex prior to kinetochore-binding. Instead, in the nucleoplasm, we can only detect a CENP-O/P (to an amount of about 50%), and, to a very minor extent, a CENP-Q/R heterodimer. However, by F3H we could show that each CENP-PORQU subunit can recruit two or three other proteins of this group to an ectopic chromosomal site. This confirms that these proteins specifically interact with each other in mammalian cells. One caveat of this experiment is that CCAN proteins might be specifically modified at centromere locations. These centromere specific modifications would be absent at the ectopic chromosomal site, potentially influencing protein interactions. Since pair-wise binding is weak in most cases, the strong kinetochore binding of the CENP-PORQU subunits (identified by slow FRAP recovery times) supports multi-fold CENP-PORQU interactions at the kinetochore. No single subunit of CENP-PORQU can recruit all other subunits, further supporting our finding that the complex does not pre-form in the nucleoplasm. Our FRAP experiments, consistent with previous studies [38], show that the cell cycle dependent turnover of CENP-P/O/Q is similar but distinct from the behavior of CENP-U and CENP-R. This indicates that the CENP-PORQU sub-complex does not behave as a single unit but instead is an ensemble of autonomously behaving proteins.

Our FRET measurements show that the CENP-PORQU proteins, once bound and incorporated into the inner kinetochore structure, are positioned in close proximity to one another. Previously, we reported that the amino-terminus of CENP-U was in close proximity to the amino-terminus of CENP-B and CENP-I, but not to the amino-terminus of CENP-A and CENP-C [43]. This indicates that, to some extent, CENP-PORQU is imbedded within the CCAN complex. Moreover, not all FRET connectivities should be thought of as occurring necessarily within a single CCAN inner kinetochore complex (intra-CCAN FRET). It is possible that some observed FRET proximities may reflect protein neighborhoods between two different adjacent CCAN complexes (inter-CCAN FRET). Such inter-CCAN interactions are likely, given super-resolution experiments that support models in which kinetochores are formed from multiple adjacent microtubule

**Table 3. Long term FRAP results for the CENP-PORQU proteins.**

Cell cycle	CENP-O		CENP-P		CENP-Q		CENP-U		CENP-R	
	rec/%	t <sub>1/2</sub> /min	rec/%	t <sub>1/2</sub> /min	rec/%	t <sub>1/2</sub> /min	rec/%	t <sub>1/2</sub> /min	rec/%	t <sub>1/2</sub> /min
G1	100	71±15	100	77±15	90±10	57±10	100	72±15	100	125±15
early S	(45)	-	(70)	-	59±6	118±15	100	163±40	100	147±20
mid S	(40)	-	62±6	81±5	65±6	125±30	100	93±15	100	160±15
late S	75±15	131±30	49±10	103±10	75±8	136±15	29±2	50±8	100	180±20
G2	(80)	-	56±8	78±5	64±6	90±14	100	76±8	100	137±20

rec: fluorescence recovery relative to the initial fluorescence value before bleaching, t<sub>1/2</sub>: time for half height recovery (in min). Recovery values in brackets: estimated recovery value; for these data, a t<sub>1/2</sub> value could not be determined.

doi:10.1371/journal.pone.0044717.t003

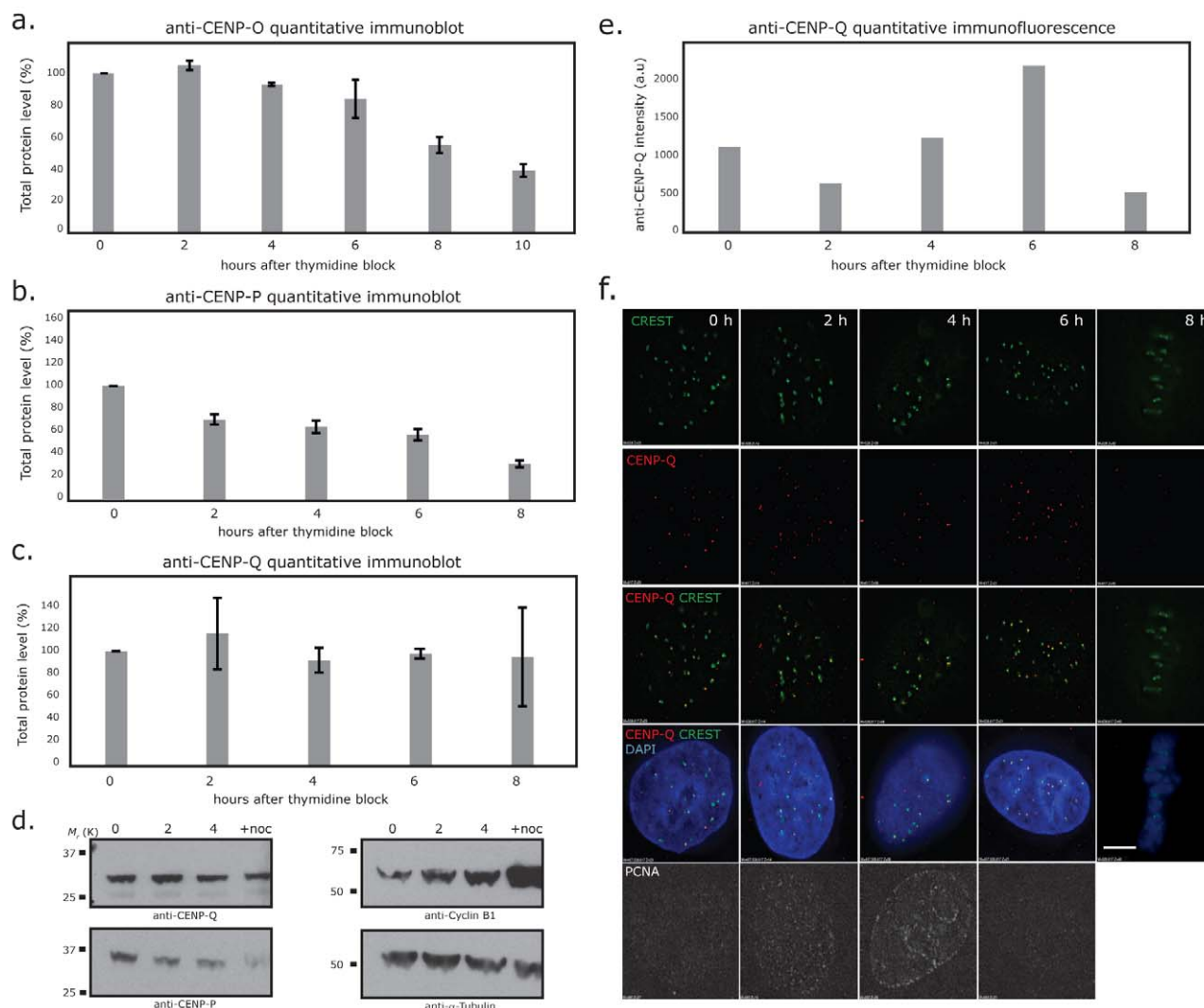


**Figure 7. Levels of CENP-O/P/Q total protein during the cell cycle.** (A) Quantitative immunoblot of CENP-O relative to  $\alpha$ -Tubulin. Protein amounts are measured at G1/S (0 h), 2, 4, 6, 8 and 10 hrs after release from the double thymidine block in synchronised human HEP-2 cells. CENP-F and PCNA staining identify the time points 2, 4, and 6 hrs as S-phase, time point 8 hrs as G2 and 10 hrs as M-phase. The cellular amount of CENP-O reduces in G2 and further in M-phase. (B, C) Quantitative immuno-blots of CENP-P and CENP-Q protein levels relative to  $\alpha$ -Tubulin at 0 (G1/S), 2 (early S), 4 (middle S), 6 (late S-phase), 8 (G2) hrs after release from double thymidine block in synchronized HeLa cells. Cycle stages were attributed from FACS analysis, PCNA staining and phase contrast microscopy (data not shown). (D) Representative immunoblots showing CENP-P, CENP-Q, Cyclin-B1 and  $\alpha$ -Tubulin at the 0 (G1/S), 2 (early S), 4 (middle S) hrs time points and cells arrested in mitosis with nocodazole (16 hrs). (E) Quantitative four-colour immuno-fluorescence using anti-CENP-Q (red), CREST (green), DAPI (blue) and anti-PCNA (far red) antibodies in the same cells used in panel B. Pixel intensities of CENP-Q (signal – background) at kinetochores ( $n = 50$  from 5 cells) are shown for each time point after release from double thymidine block (E) and representative images (F). CENP-Q loads onto kinetochores during S-phase reaching maximal binding in late S-phase (6 h). Scale bar = 5  $\mu$ m.

doi:10.1371/journal.pone.0044717.g007

binding sites [66–68]. We expect that three-dimensional inner kinetochore model building will allow us to evaluate and explore these ideas.

The multifold interactions of the CENP-PORQU proteins result in stable binding of these proteins to kinetochores, suggesting a self-assembly mechanism [69]. In this regard, CENP-U and CENP-R are able to homo-dimerise at an ectopic chromosomal site (see Table 2), although we could not detect homo-dimerisation from our FCCS measurements. Nevertheless, upon kinetochore binding and before mitosis, these proteins are proximal to themselves, as detected by FRET between CENP-U/-U. Human CENP-Q, when expressed in *E. coli*, oligomerises into octameric complexes [36]. In late S-phase, after kinetochore

binding and before mitosis, we detected FRET between the CENP-Q carboxy- as well as amino-terminal regions, indicating homo-di- or oligomerisation. We could not detect such homo-dimerisation at an ectopic chromosomal site, and found by FCCS that CENP-Q migrates as a monomer in the nucleoplasm, showing that the oligomerization event occurs at kinetochores. This self-association of CENP-U and -Q might hint towards the presence of more than one of these proteins (CENP-U, -Q) in one CCAN complex, indicating a varying stoichiometry in the complex. Alternatively, these proteins might make inter-CCAN interactions with themselves. Such an interaction between different CCAN complexes might induce or stabilize centromere specific chromatin structures and/or microtubule binding sites

[70]. The latter hypothesis is attractive given that both CENP-Q and CENP-U bind directly to microtubules *in vitro* [36,39]. We speculate that this self-association of CENP-Q and -U after kinetochore binding is a pre-mitotic maturation process that might switch kinetochores into the correct conformation for microtubule attachment.

## Acknowledgments

We thank N. Klöcker, D. Foltz, J. Langowski and I. Cheeseman for the kind gift of plasmids and S. Pfeifer and S. Ohndorf for expert technical support.

## References

- Perpelescu M, Fukagawa T (2011) The ABCs of CENPs. *Chromosoma* 120: 425–446.
- Takeuchi K, Fukagawa T (2012) Molecular architecture of vertebrate kinetochores. *Exp Cell Res* 318: 1367–1374.
- Cheeseman IM, Desai A (2008) Molecular architecture of the kinetochore-microtubule interface. *Nat Rev Mol Cell Biol* 9: 33–46.
- Przewlaka M, Glover DM (2009) The kinetochore and the centromere: a working long distance relationship. *Annu Rev Genet* 43: 439–465.
- Foltz DR, Jansen LET, Black BE, Bailey AO, Yates III JR, et al. (2006) The human CENP-A centromeric complex. *Nat Cell Biol* 8: 458–469.
- Okada M, Cheeseman IM, Hori T, Okawa K, McLeod IX, et al. (2006) The CENP-H-I complex is required for the efficient incorporation of newly synthesized CENP-A into centromeres. *Nature Cell Biol* 8: 446–457.
- Meraldi P, McAinsh AD, Rheinbay E, Sorger PK (2006) Phylogenetic and structural analysis of centromeric DNA and kinetochore proteins. *Genome Biol* 7: R23.
- McClelland SE, Borusu S, Amaro AC, Winter JR, Belwal M, et al. (2007) The CENP-A NAC/CAD kinetochore complex controls chromosome congression and spindle bipolarity. *EMBO J* 26: 5033–5047.
- Hori T, Amano M, Suzuki A, Backer CB, Welburn JP, et al. (2008) CCAN makes multiple contacts with centromeric DNA to provide distinct pathways to the outer kinetochore. *Cell* 135: 1039–1052.
- Hori T, Okada M, Maenaka K, Fukagawa T (2008) CENP-O class proteins form a stable complex and are required for proper kinetochore function. *Mol Biol Cell* 19: 843–854.
- Amano M, Suzuki A, Hori T, Backer C, Okawa K, et al. (2009) The CENP-S complex is essential for the stable assembly of outer kinetochore structure. *J Cell Biol* 186: 173–182.
- Nishino T, Takeuchi K, Gascoigne KE, Suzuki A, Hori T, et al. (2012) CENP-T-W-S-X forms a unique centromeric chromatin structure with a histone-like fold. *Cell* 148: 487–501.
- Santaguida S, Musacchio A (2009) The life and miracles of kinetochores. *EMBO J* 28: 2511–2531.
- Carroll CW, Silva MCC, Godek KM, Jansen LET, Straight AF (2009) Centromere assembly requires the direct recognition of CENP-A nucleosomes by CENP-N. *Nat Cell Biol* 11: 896–902.
- Carroll CW, Milks KJ, Straight AF (2010) Dual recognition of CENP-A nucleosomes is required for centromere assembly. *J Cell Biol* 189: 1143–1155.
- Guse A, Carroll CW, Moree B, Fuller CJ, Straight AF (2011) In vitro centromere and kinetochore assembly on defined chromatin templates. *Nature* 477: 354–358.
- Tachiwana H, Kagawa W, Shiga T, Osakabe A, Miya Y, et al. (2011) Crystal structure of the human centromeric nucleosome containing CENP-A. *Nature* 476: 232–235.
- Bui M, Dimitriadis EK, Hoischen C, An E, Quenet D, et al. (2012) Cell cycle-dependent structural transitions in the human CENP-A nucleosome in vivo. *Cell* 150: 317–326.
- De Wulf P, McAinsh AD, Sorger PK (2003) Hierarchical assembly of the budding yeast kinetochore from multiple subcomplexes. *Genes Dev* 17: 2902–2921.
- Cheeseman IM, Niessen S, Anderson S, Hyndman F, Yates JR 3rd, et al. (2004) A conserved protein network controls assembly of the outer kinetochore and its ability to sustain tension. *Genes Dev* 18: 2255–2268.
- Cheeseman IM, Chappie JS, Wilson-Kubalek EM, Desai A (2006) The conserved KMN network constitutes the core microtubule-binding site of the kinetochore. *Cell* 127: 983–997.
- Obuse C, Yang H, Nozaki N, Goto S, Okazaki T, et al. (2004) Proteomics analysis of the centromere complex from HeLa interphase cells: UV-damaged DNA binding protein 1 (DDB-1) is a component of the CEN-complex, while BML-1 is transiently co-localised with the centromeric region in interphase. *Genes to Cells* 9: 105–120.
- Liu X, McLeod I, Anderson S, Yates JR 3rd, He X (2005) Molecular analysis of kinetochore architecture in fission yeast. *EMBO J* 24: 2919–2930.
- Petrovic A, Pasqualato S, Dube P, Krenn V, Santaguida S, et al. (2010) The Mis12 complex is a protein interaction hub for outer kinetochore assembly. *J Cell Biol* 190: 835–852.
- Kiyomitsu T, Iwasaki O, Obuse C, Yanagida M (2010) Inner centromere formation requires hMis14, a trident kinetochore protein that specifically recruits HP1 to human chromosomes. *J Cell Biol* 188: 791–807.
- Liu D, Vleugel M, Backer CB, Hori T, Fukagawa T, et al. (2010) Regulated targeting of protein phosphatase 1 to the outer kinetochore by KNL1 opposes Aurora B kinase. *J Cell Biol* 188: 809–820.
- Przewlaka MR, Venkei Z, Bolanos-Garcia VM, Debski J, et al. (2011) CENP-C is a structural platform for kinetochore assembly. *Curr Biol* 21: 399–405.
- Tanaka TU, Desai A (2008) Kinetochore-microtubule interactions: the means to the end. *Curr Opin Cell Biol* 20: 53–63.
- Wan X, O'Quinn RP, Pierce HL, Joglekar AP, Gall WE, et al. (2009) Protein architecture of the human kinetochore microtubule attachment site. *Cell* 137: 672–684.
- Moree B, Meyer CB, Fuller CJ, Straight AF (2011) CENP-C recruits M18BP1 to centromeres to promote CENP-A chromatin assembly. *J Cell Biol* 194: 855–871.
- Barnhart MC, Kuich HJL, Stellfox ME, Ward JA, Bassett EA, et al. (2011) HJURP is a CENP-A chromatin assembly factor sufficient to form a functional de novo kinetochore. *J Cell Biol* 194: 229–243.
- Fukagawa T, Mikami Y, Nishihashi A, Regnier V, Haraguchi T, et al. (2001) CENP-H, a constitutive centromere component, is required for centromere targeting of CENP-C in vertebrate cells. *EMBO J* 20: 4603–4617.
- McAinsh AD, Meraldi P, Draviam VM, Toso A, Sorger PK (2006) The human kinetochore proteins Nnf1R and Mcm21R are required for accurate chromosome segregation. *EMBO J* 25: 4033–4049.
- Toso A, Winter JR, Garrod AJ, Amaro AC, Meraldi P, et al. (2009) Kinetochore-generated pushing forces separate centrosomes during bipolar spindle assembly. *J Cell Biol* 184: 365–372.
- Gascoigne KE, Takeuchi K, Suzuki A, Hori T, Fukagawa T, et al. (2011) Induced ectopic kinetochore assembly bypasses the requirement for CENP-A nucleosomes. *Cell* 145: 410–422.
- Amaro AC, Samora CP, Holtackers R, Wang E, Kingston JJ, et al. (2010) Molecular control of kinetochore-microtubule dynamics and chromosome oscillations. *Nature Cell Biol* 12: 319–329.
- Izuta H, Ikeno M, Suzuki N, Tomonaga T, Nozaki N, et al. (2006) Comprehensive analysis of the ICEN (Interphase Centromere Complex) components enriched in the CENP-A chromatin of human cells. *Genes Cells* 11: 673–684.
- Minoshima Y, Hori T, Okada M, Kimura H, Haraguchi T, et al. (2005) The constitutive centromere component CENP-50 is required for recovery from spindle damage. *Mol Cell Biol* 25: 10315–10328.
- Hua S, Wang Z, Jiang K, Huang Y, Ward T, et al. (2011) CENP-U cooperates with Hec1 to orchestrate kinetochore-microtubule attachment. *J Biol Chem* 286: 1627–1638.
- Kang YH, Park JE, Yu LR, Soung NK, Yun SM, et al. (2006) Self-regulated Plk1 recruitment to kinetochores by the Plk1-PBIP1 interaction is critical for proper chromosome segregation. *Mol Cell* 24: 409–422.
- Kang YH, Park C-H, Kim T-S, Soung N-K, Bang JK, et al. (2011) Mammalian Polo-like kinase 1-dependent regulation of the PBIP1-CENP-Q complex at kinetochores. *J Biol Chem* 286: 19744–19757.
- Schmitzberger F, Harrison SC (2012) RWD domain: a recurring module in kinetochore architecture shown by Ctf19-Mcm21 complex structure. *EMBO Rep* 13: 216–222.
- Hellwig D, Hoischen C, Ulbricht T, Diekmann S (2009) Acceptor-photobleaching FRET analysis of core kinetochore and NAC proteins in living human cells. *Eur Biophys J* 38: 781–791.
- Hellwig D, Emmerth S, Ulbricht T, Doering V, Hoischen C, et al. (2011) Dynamics of CENP-N kinetochore binding during the cell cycle. *J Cell Sci* 124: 3871–3883.
- Tsakamoto T, Hashiguchi N, Janicki SM, Tumbur T, Belmont AS, et al. (2000) Visualization of gene activity in living cells. *Nat Cell Biol* 2: 871–878.
- Rothbauer U, Zolghadr K, Tillib S, Nowak D, Schermelleh L, et al. (2006) Targeting and tracing antigens in live cells with fluorescent nanobodies. *Nat Methods* 3: 887–889.
- Zolghadr K, Mortusewicz O, Rothbauer U, Kleinhans R, Gochler H, et al. (2008) A fluorescent two-hybrid assay for direct visualization of protein interactions in living cells. *Mol Cell Proteomics* 7: 2279–2287.

## Author Contributions

Conceived and designed the experiments: AE WD SR SE DH TU VD JMB ADM PM CH HL SD. Performed the experiments: AE WD AH SR SE DH TU VD JMB MCC CH HL. Analyzed the data: AE WD AH SR SE DH TU VD JMB ADM PM CH HL SD. Contributed reagents/materials/analysis tools: WD JMB MCC. Wrote the paper: DH ADM HL CH SD.

48. Orthaus S, Biskup C, Hoffmann B, Hoischen C, Ohndorf S, et al. (2008) Assembly of the inner kinetochore proteins CENP-A and CENP-B in living human cells. *Chem Bio Chem* 9: 77–92.
49. Bacia K, Schwill P (2003) A dynamic view of cellular processes by *in vivo* fluorescence auto- and cross-correlation spectroscopy. *Methods* 29: 74–85.
50. Bacia K, Schwill P (2007) Practical guidelines for dual-color fluorescence cross-correlation spectroscopy. *Nature Protocols* 2: 2842–2856.
51. Orthaus S, Klement K, Happel N, Hoischen C, Diekmann S (2009) Linker Histone H1 is present in centromeric chromatin of living human cells next to inner kinetochore proteins. *Nucl Acids Res* 37: 3391–3406.
52. Milks KJ, Moree B, Straight AF (2009) Dissection of CENP-C directed centromere and kinetochore assembly. *Mol Biol Cell* 20: 4246–4255.
53. Qui SL, Wang JN, Yu C, He DC (2009) CENP-K and CENP-H may form coiled-coils in the kinetochores. *Sci China Ser C-Life Sci* 52: 352–359.
54. Digman MA, Brown CM, Sengupta P, Wiseman PW, Horwitz AR, et al. (2005) Measuring fast dynamics in solutions and cells with a laser scanning microscope. *Biophys J* 89: 1317–1327.
55. Hemmerich P, Weidtkamp-Peters S, Hoischen C, Schmiedeberg L, Erliandri I, et al. (2008) Dynamics of inner kinetochore assembly and maintenance in living cells. *J Cell Biol* 180: 1101–1114.
56. Kohl T, Hausteil E, Schwill P (2005) Determining protease activity *in vivo* by fluorescence cross-correlation analysis. *Biophys J* 89: 2770–2782.
57. Hanissian SH, Akbar U, Teng B, Janjetovic Z, Hoffmann A, et al. (2004) cDNA cloning and characterization of a novel gene encoding the MLF1-interacting protein MLF1IP. *Oncogene* 23: 3700–3707.
58. Suzuki H, Arakawa Y, Ito M, Saito S, Takeda N, et al. (2007) MLF1-interacting protein is mainly localized in nucleolus through N-terminal bipartite nuclear localization signal. *Anticancer Res* 27: 1423–1430.
59. Keppler A, Gendreizig S, Gronemeyer T, Pick H, Vogel H, et al. (2003) A general method for the covalent labelling of fusion proteins with small molecules *in vivo*. *Nat Biotechnol* 21: 86–89.
60. Jansen LET, Black BE, Foltz DR, Cleveland DW (2007) Propagation of centromeric chromatin requires exit from mitosis. *J Cell Biol* 176: 795–805.
61. Prendergast L, van Vuuren C, Kaczmarczyk A, Döring V, Hellwig D, et al. (2011) Premitotic assembly of human CENPs -T and -W switches centromeric chromatin to a mitotic state. *PLoS Biol* 9: e1001082.
62. Lee KS, Oh DY, Kang YH, Park JE (2008) Self-regulated mechanism of Plk1 localisation to kinetochores: lessons from the Plk1-PBIP1 interaction. *Cell Div* 3: 4.
63. Leonhardt H, Rahn HP, Weinzierl P, Sporbert A, Cremer T, et al. (2000) Dynamics of DNA replication factories in living cells. *J Cell Biol* 149: 271–280.
64. Sporbert A, Domaing P, Leonhardt H, Cardoso MC (2005) PCNA acts as a stationary loading platform for transiently interacting Okazaki fragment maturation proteins. *Nucleic Acids Res* 33: 3521–3528.
65. Schmiedeberg L, Weissart K, Diekmann S, Meyer zu Hoerste G, Hemmerich P (2004) High- and low-mobility populations of HP1 in heterochromatin of mammalian cells. *Mol Biol Cell* 15: 2819–2833.
66. Ribeiro SA, Vagnarelli P, Dong Y, Hori T, McEwen BF, et al. (2010) A super-resolution map of the vertebrate kinetochore. *Proc Natl Acad Sci USA* 107: 10484–10489.
67. Johnston K, Joglekar A, Hori T, Suzuki A, Fukagawa T, Salmon ED (2010) Vertebrate kinetochore protein architecture: protein copy number. *J Cell Biol* 189: 937–943.
68. Lawrimore J, Bloom KS, Salmon ED (2011) Point centromeres contain more than a single centromere-specific Cse4 (CENP-A) nucleosome. *J Cell Biol* 195: 573–582.
69. Hemmerich P, Schmiedeberg L, Diekmann S (2011) Dynamic as well as stable protein interactions contribute to genome function and maintenance. *Chromosome Res* 19: 131–151.
70. Dong Y, VandenBeldt KJ, Meng X, Khodjakov A, McEwen BF (2010) The outer plate in vertebrate kinetochores is a flexible network with multiple microtubule interactions. *Nat Cell Biol* 9: 516–522.



2.4 Binding of the Heterogeneous Ribonucleoprotein K (hnRNP K)  
to the Epstein-Barr Virus Nuclear Antigen 2 (EBNA2)  
Enhances Viral LMP2A Expression

---





# Binding of the Heterogeneous Ribonucleoprotein K (hnRNP K) to the Epstein-Barr Virus Nuclear Antigen 2 (EBNA2) Enhances Viral LMP2A Expression

Henrik Gross<sup>1</sup>, Christine Hennard<sup>2</sup>, Ilias Masouris<sup>2</sup>, Christian Cassel<sup>1</sup>, Stephanie Barth<sup>1</sup>, Ute Stober-Grässer<sup>1</sup>, Alfredo Mamiani<sup>1</sup>, Bodo Moritz<sup>3</sup>, Dirk Ostareck<sup>4</sup>, Antje Ostareck-Lederer<sup>4</sup>, Nils Neuenkirchen<sup>5</sup>, Utz Fischer<sup>5</sup>, Wen Deng<sup>6</sup>, Heinrich Leonhardt<sup>6</sup>, Elfriede Noessner<sup>2</sup>, Elisabeth Kremmer<sup>2</sup>, Friedrich A. Grässer<sup>1\*</sup>

**1** Institute of Virology, Saarland University Medical School, Homburg/Saar, Germany, **2** Institute of Molecular Immunology, Helmholtz Zentrum München, German Research Center for Environmental Health, Munich, Germany, **3** Institute of Biochemistry and Biotechnology, Martin-Luther-University Halle-Wittenberg, Halle (Saale), Germany, **4** Experimental Research Unit, Department of Intensive Care and Intermediate Care, University Hospital Aachen, RWTH Aachen University, Aachen, Germany, **5** Department of Biochemistry, Biocenter of the University of Würzburg, Würzburg, Germany, **6** Department of Biology, Center for Integrated Protein Science Munich, Ludwig Maximilians University Munich, Planegg-Martinsried, Germany

## Abstract

The Epstein-Barr Virus (EBV) -encoded EBNA2 protein, which is essential for the *in vitro* transformation of B-lymphocytes, interferes with cellular processes by binding to proteins via conserved sequence motifs. Its Arginine-Glycine (RG) repeat element contains either symmetrically or asymmetrically di-methylated arginine residues (SDMA and ADMA, respectively). EBNA2 binds via its SDMA-modified RG-repeat to the survival motor neurons protein (SMN) and via the ADMA-RG-repeat to the NP9 protein of the human endogenous retrovirus K (HERV-K (HML-2) Type 1). The hypothesis of this work was that the methylated RG-repeat mimics an epitope shared with cellular proteins that is used for interaction with target structures. With monoclonal antibodies against the modified RG-repeat, we indeed identified cellular homologues that apparently have the same surface structure as methylated EBNA2. With the SDMA-specific antibodies, we precipitated the Sm protein D3 (SmD3) which, like EBNA2, binds via its SDMA-modified RG-repeat to SMN. With the ADMA-specific antibodies, we precipitated the heterogeneous ribonucleoprotein K (hnRNP K). Specific binding of the ADMA- antibody to hnRNP K was demonstrated using *E. coli* expressed/ADMA-methylated hnRNP K. In addition, we show that EBNA2 and hnRNP K form a complex in EBV- infected B-cells. Finally, hnRNP K, when co-expressed with EBNA2, strongly enhances viral latent membrane protein 2A (LMP2A) expression by an unknown mechanism as we did not detect a direct association of hnRNP K with DNA-bound EBNA2 in gel shift experiments. Our data support the notion that the methylated surface of EBNA2 mimics the surface structure of cellular proteins to interfere with or co-opt their functional properties.

**Citation:** Gross H, Hennard C, Masouris I, Cassel C, Barth S, et al. (2012) Binding of the Heterogeneous Ribonucleoprotein K (hnRNP K) to the Epstein-Barr Virus Nuclear Antigen 2 (EBNA2) Enhances Viral LMP2A Expression. PLoS ONE 7(8): e42106. doi:10.1371/journal.pone.0042106

**Editor:** Dong-Yan Jin, University of Hong Kong, Hong Kong

**Received:** March 15, 2012; **Accepted:** July 2, 2012; **Published:** August 3, 2012

**Copyright:** © 2012 Gross et al. This is an open-access article distributed under the terms of the Creative Commons Attribution License, which permits unrestricted use, distribution, and reproduction in any medium, provided the original author and source are credited.

**Funding:** This work was supported by Deutsche Forschungsgemeinschaft through grant KR2218/2-1 to EK, OS290/3-2 to AO-L and DHO and GR950/12-1 to FG and the Biomedicine Network Munich to HL. WD was supported by the Chinese Scholarship Council. The funders had no role in study design, data collection and analysis, decision to publish, or preparation of the manuscript.

**Competing Interests:** The authors have declared that no competing interests exist.

\* E-mail: graesser@uks.eu

## Introduction

The Epstein-Barr virus (EBV) is associated with various human malignancies [1] and growth-transforms primary human B-lymphocytes which are the *in vitro* correlate of EBV-associated post-transplant lymphoproliferative disease (PTLD) (for review, see [2]). In EBV-transformed lymphocytes, 11 so-called latent genes are expressed. Of these, only the nuclear antigens EBNA1, -2, -3a, -3c and the latent membrane protein LMP1 are necessary for transformation (reviewed in [3]).

EBNA2 is a multifunctional transcriptional activator that does not bind directly to DNA but is tethered to promoter elements by interacting with DNA-bound transcription factors. For example, it associates through a Trp-Trp-Pro ("WWP<sub>325</sub>") motif at position 323–325 (see Figure 1) with the DNA-bound repressor RBPjκ

[4,5,6]. EBNA2 is the viral functional homologue to the cellular transmembrane receptor Notch which also activates gene expression via RBPjκ (reviewed in [7]). Binding of EBNA2 or Notch converts the repressor RBPjκ to the transcriptionally active form. Figure 1 shows a schematic representation of EBNA2. A virus encoding an EBNA2 protein with a mutation in the WWP-motif is unable to immortalise B-lymphocytes and does not activate the viral oncogene LMP1 [8]. In addition to RBPjκ, EBNA2 binds to a variety of basal transcription factors [2] and forms complexes with proteins involved in RNA metabolism like the DEAD-box protein DDX20 (DP103/Gemin3) [9] or the survival of motor neurons (SMN) protein [10,11]. The binding of EBNA2 to a variety of other host proteins is reflected by its presence in high molecular weight complexes of different composition [12,13,14]. Adjacent to the WWP-motif, EBNA2 contains an Arginine-

Glycine (RG-) repeat element at aa 339–354 with methylated arginine residues [10,15]. The deletion of the RG-repeat results in a five-fold higher ability of EBNA2 to stimulate LMP1 expression, but a recombinant virus featuring this deletion in EBNA2 has a reduced transforming activity and needs an extended time span to induce outgrowth of transformed cell clones [16]. The EBNA2A protein from type A isolates was originally shown to confer a higher transforming capacity than EBNA2B derived from type B isolates of EBV [17]. Recently, it was demonstrated that the RG- repeat, among other C-terminal sequences, is important to confer the higher transforming activity of EBNA2A vs. EBNA2B [18].

Methylation is a post-translational modification that affects protein-protein interactions [19]. Methylation at arginine residues [20] may lead to three known forms in higher eukaryotes:  $\omega$ -N<sup>G</sup> MonoMethyl-arginine (MMA),  $\omega$ -N<sup>G</sup>,N<sup>G</sup>-Asymmetric DiMethyl-arginine (ADMA) and  $\omega$ -N<sup>G</sup>,N<sup>G</sup>-Symmetric DiMethyl-arginine (SDMA). The methylation is carried out by two types of Protein-Arginine-Methyl-Transferases (PRMTs): Type I enzymes (PRMT1, 2, 3, 4, 6 and -8) catalyse the formation of ADMA whereas type II enzymes (PRMT5, -7 and -9) account for the formation of SDMA ([21,22,23]).

hnRNP K was originally detected as a polycytidylic acid binding protein purified from heterogeneous nuclear ribonucleoprotein particles [24]. Later on, it was found that hnRNP K is involved in various cellular processes such as chromatin reorganisation, mRNA translation, transcriptional regulation, splicing, RNA shuttling and cell survival (for review, see [25,26]). Recently, it was proposed that hnRNP K activates the VEGF-A promoter by binding to unwound superhelical single stranded C-rich sequences upstream of the transcription start site and to support association of transcription initiation factors [27]. hnRNP K is composed of modular regions that confer binding both to RNA or DNA as well as protein-protein interaction domains [28]. It binds to tyrosine kinases like c-Src and Lck as well as transcription factors such as C/EBP. The interaction with c-Src and its activation by hnRNP K is modulated by asymmetric dimethylation of five arginine residues catalysed by PRMT1 [29]. Reduced PRMT1 expression in induced erythroid maturation of human K562 cells leads to a decreased methylation of newly synthesised hnRNP K. This correlates with hnRNP K tyrosine phosphorylation and activation of the human reticulocyte 15-lipoxygenase (r15-LOX) mRNA translation, which is inhibited by hnRNP K in early erythroid maturation [30,31].

We have previously developed monoclonal antibodies against the methylated RG-repeat of EBNA2 and found that it contains either SDMA or ADMA residues but does not exist in non-methylated (NMA) form [15]. SDMA-modified EBNA2 (SDMA-EBNA) forms a complex with the SMN protein [10], while ADMA-modified EBNA2 (ADMA-EBNA2) preferentially binds to the NP9 protein encoded by the human endogenous retrovirus HERV-K (HML-2) Type 1 [32]. It is known that SMN binds only to SDMA-modified proteins [33;34], for example to the SDMA-modified Smd3 protein which in turn is part of the SMN complex [35]. We therefore reasoned that the methylated surface of EBNA2 at the RG-repeat resembles cellular proteins engaging in similar interactions and that the antibodies should recognize these conserved epitopes. These cellular proteins in turn should be able to interact with proteins bound to EBNA2. Here we show that the immunoprecipitation of cellular proteins using the SDMA-specific antibodies indeed yields Smd3. Likewise, the ADMA-antibodies precipitated, among other proteins, hnRNP K. Further analysis demonstrated that EBNA2 does not only share a conserved surface epitope with hnRNP K but that it also forms a complex with hnRNP K. Most importantly, hnRNP K, when co-expressed with EBNA2, strongly increases the ability of EBNA2 to activate the viral LMP2A promoter.

## Results

### Monoclonal Antibodies Against SDMA- and ADMA-EBNA2 Precipitate Cellular Proteins with Methylated Arginine Residues

We employed previously developed monoclonal antibodies directed against ADMA- or SDMA-modified EBNA2 [15] for the precipitation of cellular and/or viral proteins from EBV-infected cells. The precipitated proteins were analysed by mass spectrometry as previously described [36] and are listed in Table 1. Also indicated in Table 1 is the methylation status where known. Among the proteins precipitated by the SDMA-antibody, we identified Smd3 known to be a core component of spliceosomal U snRNPs and a major component of the SMN complex (see, for instance, [37,38]). Smd3 was precipitated both from EBV-infected and non-infected cells as Smd3 has an RG-containing repeat structure comparable to that of EBNA2 which attaches to the SMN protein [35]. The SMN protein was not found, presumably because the binding to the SDMA-modified protein(s) precluded the reaction with the SDMA-

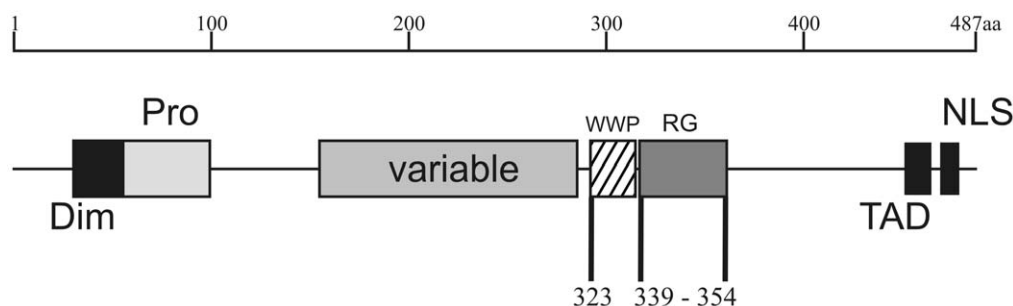
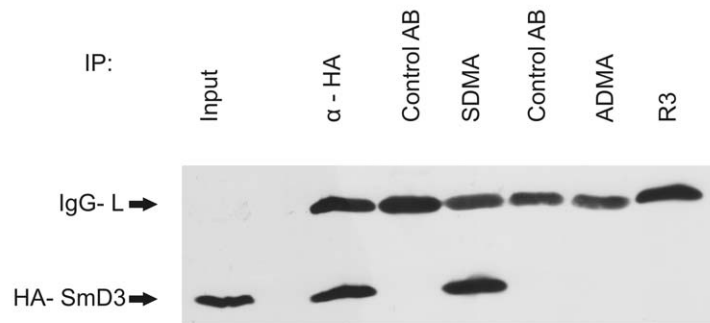


**Figure 1. Schematic representation of the Epstein-Barr virus nuclear antigen 2 (EBNA2).** EBNA2 of the standard B95.8 strain (accession number: AJ507799) of EBV consists of 487 amino acids (aa) present in an A-type virus. The N-terminal dimerization domain ("Dim") is located next to a poly-Proline stretch ("Pro"). The variable region ("variable") differs between the A-type viruses and B-type viruses. B-type viruses have a reduced *in vitro* transformation potential. The binding site for RBPjk ("WWP") is located around a Trp-Trp-Pro motif at aa 323–325. The adjacent Arginine-Glycine repeat ("RG") between aa 339–354 confers binding to the survival of motor neurons (SMN) protein and represents the second nuclear localization signal ("NLS") in addition to the canonical NLS found at the extreme C-terminus between aa 468–487. The C-terminal acidic transactivation domain ("TAD") between aa 424–468 interacts with various basal transcription factors. doi:10.1371/journal.pone.0042106.g001

A



B

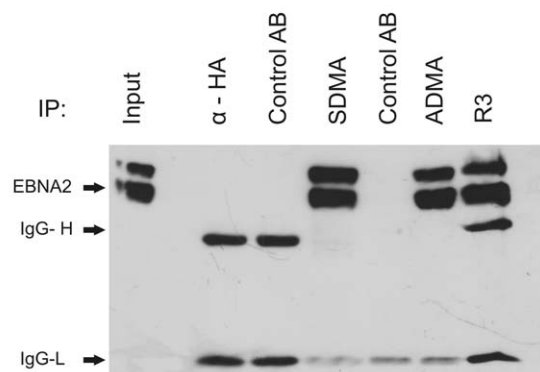


**Figure 2. SmD3 is precipitated by the SDMA- EBNA2 specific antibody.** (A) Monoclonal antibodies (mAbs) directed against the SDMA- and ADMA- containing Arginine-Glycine (RG)-repeat of EBNA2 were tested by precipitation using extracts of HEK 293-T cells expressing EBNA2-wt and HA- SmD3. For each antibody, an appropriate isotype control was tested in parallel to exclude unspecific binding to the protein G Sepharose used for precipitation. Precipitated HA- SmD3 protein was visualised using the HA -specific mAb 3F10. The position of HA- SmD3 is indicated by an arrow. (B) Immunoprecipitation of EBNA2 from transiently transfected cells. HEK 293-T cells expressing EBNA2-wt and HA- SmD3 were precipitated with monoclonal antibodies directed against the SDMA- and ADMA- containing Arginine-Glycine (RG)-repeat of EBNA2 using appropriate isotype control antibodies. Precipitated EBNA2 protein was visualised using the EBNA2 mAb R3. The position of EBNA2 is indicated by an arrow.

doi:10.1371/journal.pone.0042106.g002

**Table 1. Proteins precipitated by the EBNA2- SDMA antibody.**

Protein	Size	Accession number	Methylationstatus
Pre-mRNA processing splicing factor 8	~200 kDa	Q6P2Q9	unknown
U5 small nuclear ribonucleoprotein 200 kDa helicase	~200 kDa	O75643	unknown
Gem-associated protein 5 (gemin 5)	~150 kDa	Q8TEQ6	unknown
U1 snRNP 70 K	~55 kDa	P08621	sDMA
SmD3	~14 kDa	P62318	sDMA

**Proteins precipitated by the EBNA2- ADMA antibody**

Protein	Size	Accession number	Methylationstatus
ATP dependent RNA helicase	~140 kDa	Q08211	aDMA
Caprin-1	~80 kDa	Q14444	unknown
Ras-GTPase-activating protein (SH3-domain-binding protein variant)	~55 kDa	Q53HH4	unknown
hnRNP K	~55 kDa	Q5T6W5	aDMA

doi:10.1371/journal.pone.0042106.t001

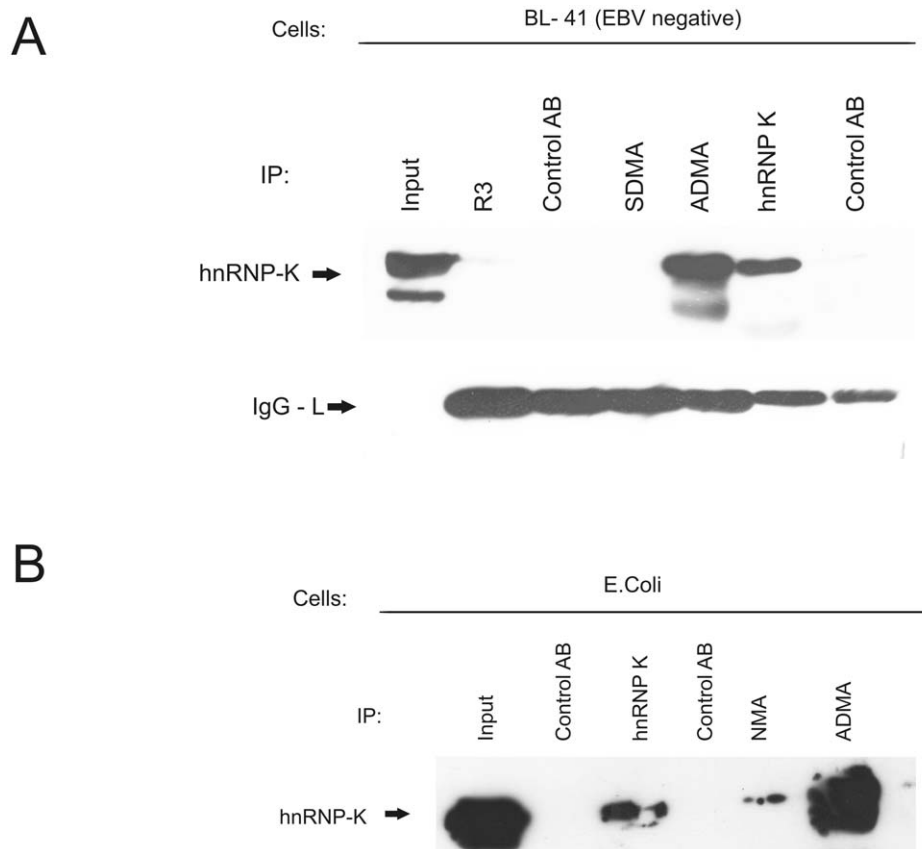


**Figure 3. hnRNP K is precipitated by the ADMA- specific antibody.** (A) Immunoprecipitation of hnRNP K from BL-41 cells. EBV negative BL-41 cells were precipitated with monoclonal antibodies directed against the SDMA- and ADMA- containing Arginine-Glycine (RG)-repeat of EBNA2 and an hnRNP K specific antibody using appropriate isotype control antibodies. The EBNA2 specific mAb R3 served as a negative control. The position of hnRNP K is indicated by an arrow. (B) ADMA- modified hnRNP K is precipitated by the ADMA- specific antibody. Soluble extract containing ADMA- hnRNP K methylated in *E. coli* with the type I methyltransferase PRMT1 was subjected to immunoprecipitation using either a hnRNP K- specific mAb, the ADMA- specific mAb and the NMA- specific mAb. Precipitated hnRNP K was visualised using the hnRNP K mAb.  
doi:10.1371/journal.pone.0042106.g003

specific antibody. To confirm this result, we generated an expression vector for HA-tagged SmD3. In cell extract containing HA-SmD3, we could precipitate SmD3 with the SDMA- but not the ADMA-specific antibody or the EBNA2- specific R3 antibody. The staining of the precipitated SmD3 with the HA-specific antibody is shown in Figure 2A. In the control experiment depicted in Figure 2B, EBNA2 was precipitated with both methylation-specific antibodies and R3 but not with the isotype control antibodies. Note that due to the use of rat and mouse monoclonal antibodies, not all the heavy chains ("IgG-H") were stained by the secondary antibodies; however, the light chains ("IgG-L") were clearly present. These data show that the antibodies specific for the methylated surface of EBNA2 react with epitopes on cellular proteins that interact with the same interaction partners, in this case the SMN protein. We were mainly interested in the analysis of proteins identified with the ADMA-specific antibody because our previous analysis had shown that ADMA-EBNA2 is predominantly present at EBNA2-regulated viral promoters [15]. The proteins reactive with the SDMA-antibody were thus not pursued further.

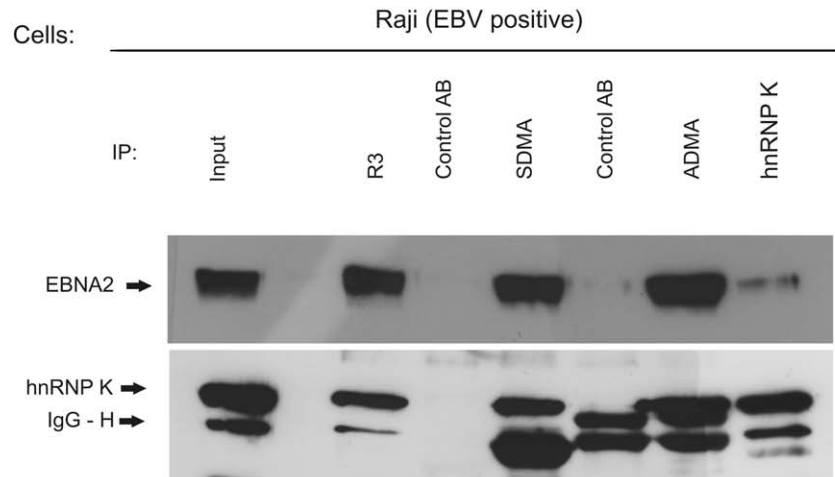
#### EBNA2 Forms a Complex with hnRNP K in EBV-infected Cells

We used the ADMA-specific monoclonal antibodies for the precipitation of methylated proteins from non-infected BL41 and

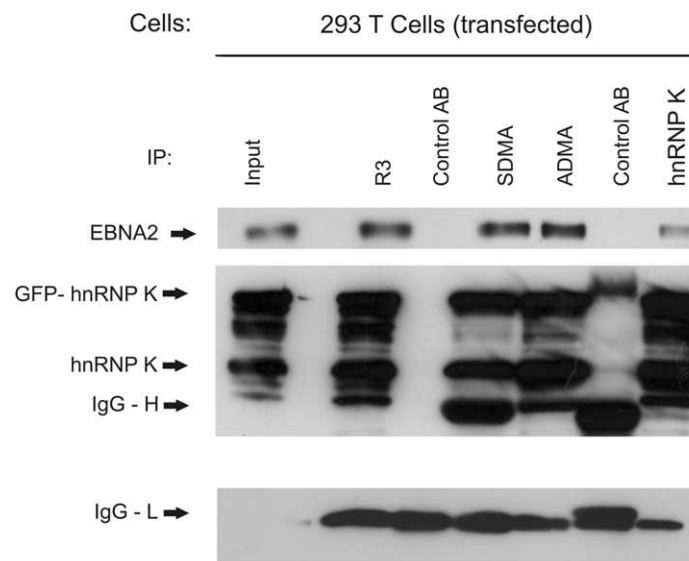
EBV-infected EBNA2-containing Raji Burkitt's lymphoma cells. Among the proteins identified by the mass spectrometric analysis, we found hnRNP K in both EBNA2-positive and EBNA2-negative cell extracts. To confirm this result, we first subjected extract of non-infected BL41 cells to precipitation using the EBNA2-specific monoclonal antibody R3 which binds at the C-terminus outside of the methylation region [39], the SDMA- and ADMA-antibodies and the hnRNP K specific monoclonal antibody D6. As can be seen in Figure 3A, only the ADMA- or the hnRNP K-specific antibody D6, but not the SDMA-specific antibody precipitated hnRNP K. As expected, R3 did not yield a signal, and the absence of EBNA2 in the BL41 extract was confirmed by western blot (data not shown).

We decided to confirm the reactivity of the ADMA-antibody using hnRNP K synthesised and asymmetrically dimethylated in *E. coli* by coexpressed PRMT1. Soluble *E. coli* extract containing ADMA- methylated hnRNP K was subjected to immunoprecipitation with either an hnRNP K-specific monoclonal antibody, the ADMA-specific antibody or the previously described monoclonal antibody against the non-methylated RG-repeat of EBNA2 (NMA) [15]. As shown in Figure 3B, the hnRNP K-specific as well as the ADMA-specific antibody clearly precipitated hnRNP K from the *E. coli* extract confirming the reactivity of the ADMA-specific antibody with hnRNP K in the absence of other eukaryotic proteins. Furthermore, we excluded binding to

A



B



C

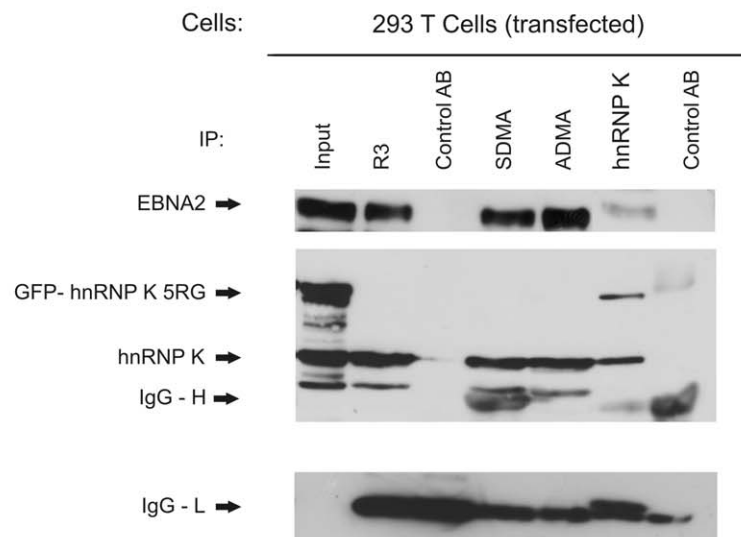


**Figure 4. EBNA2 is co-precipitated with wild- type hnRNP K but not with the methylation deficient hnRNP K 5RG mutant.** (A) Co-immunoprecipitation of EBNA2 and hnRNP K from EBV positive Raji cells. Raji cells expressing EBNA2 were precipitated with monoclonal antibodies directed against the SDMA- and ADMA- containing Arginine-Glycine (RG)-repeat of EBNA2, an EBNA2 specific mAb (R3) and an hnRNP K specific mAb (D6). The positions of EBNA2 and hnRNP K are indicated by arrows. (B) Co-immunoprecipitation of EBNA2 and GFP - hnRNP K from transfected 293T cells. The cells were precipitated with monoclonal antibodies directed against the SDMA- and ADMA- containing Arginine-Glycine (RG)-repeat of EBNA2, an EBNA2 specific mAb (R3) and an hnRNP K specific mAb (D6). The positions of EBNA2 and hnRNP K are indicated by arrows. (C) No co-immunoprecipitation of EBNA2 and GFP - hnRNP K 5RG is observed from transfected 293T cells. The cells were precipitated with monoclonal antibodies directed against the SDMA- and ADMA- containing Arginine-Glycine (RG)-repeat of EBNA2, an EBNA2 specific mAb (R3) and an hnRNP K specific mAb (D6). The positions of EBNA2 and hnRNP K are indicated by arrows.  
doi:10.1371/journal.pone.0042106.g004

PRMT1 which is complexed to hnRNP K [29,40] (data not shown). We also observed binding of a small fraction of hnRNP K by the NMA-antibody. Our previous experiments had shown that this antibody only reacted with (non-methylated) EBNA2 when the EBV-infected cell was treated with the methylation inhibitor Adox [15]. The binding of this antibody to hnRNP K again indicated that non-methylated hnRNP K apparently has a surface at its methylation site similar to the one of EBNA2.

We next subjected Raji cells to precipitation either with the ADMA-, SDMA- or the methylation-independent EBNA2-specific monoclonal antibody R3, and the hnRNP K specific monoclonal antibody D6. As can be seen in Figure 4A, upper panel, the methylation-specific antibodies and R3 precipitated EBNA2, while the control antibody did not. When the same extracts were probed with the hnRNP K specific antibody D6, hnRNP K was found co-precipitated by R3, the SDMA- and ADMA as well as the hnRNP K antibody (Figure 4A, lower panel). Conversely, the hnRNP K-specific antibody D6 co-precipitated EBNA2. The fact that R3 and also the SDMA-antibody precipitated hnRNP K from the EBNA2-containing extract indicated that both proteins are in a complex with each other, because only EBNA2 but not hnRNP K contains SDMA residues [29].

### The EBNA2-hnRNP K-interaction is Dependent of Methylation of hnRNP K

To further investigate if the binding of the two proteins is dependent of the methylation status of hnRNP K, we carried out co-immunoprecipitations from 293T cells either transfected with wild-type GFP- hnRNP K and EBNA2 or the methylation deficient mutant GFP- hnRNP K 5RG and EBNA2. As can be seen in Figure 4B, the binding of EBNA2 to hnRNP K is unaffected by the GFP- tag of hnRNP K and EBNA2 is co-precipitated by the hnRNP K specific antibody and *vice versa*. These findings confirm the results from EBV positive Raji cells (Figure 4A). In contrast, the methylation deficient 5RG mutant of hnRNP K is unable to bind to EBNA2 whereas the binding of EBNA2 to endogenous hnRNP K is unaffected. Furthermore the ADMA- specific antibody is not able to precipitate GFP - hnRNP K 5RG, which further highlights its specificity (Figure 4C).

To corroborate the above results, GST-pull-down assays were carried out. For this purpose, we generated a GST-EBNA2 fusion protein containing aa 300–400 of EBNA2 including the methylation site at 339–354. This fusion protein was then treated either with *E. coli*-expressed His- tagged PRMT1 to generate ADMA-EBNA2 or *Baculovirus* expressed PRMT5/WD45 to generate SDMA-EBNA2. The reaction products were then precipitated with the antibodies to see whether the correct products were formed as the SDMA-specific antibody does not react in a western blot [15]. Treatment with PRMT1 yielded a GST-EBNA2 fusion protein that reacted with the NMA and the ADMA but not the SDMA antibody as shown in Figure S2. The detection of *E. coli*-expressed PRMT1 with the novel PRMT1-specific antibody 7D2 (see Materials and Methods) is shown in Figure S1. This antibody was raised against a peptide encompassing amino acids 250–264 of

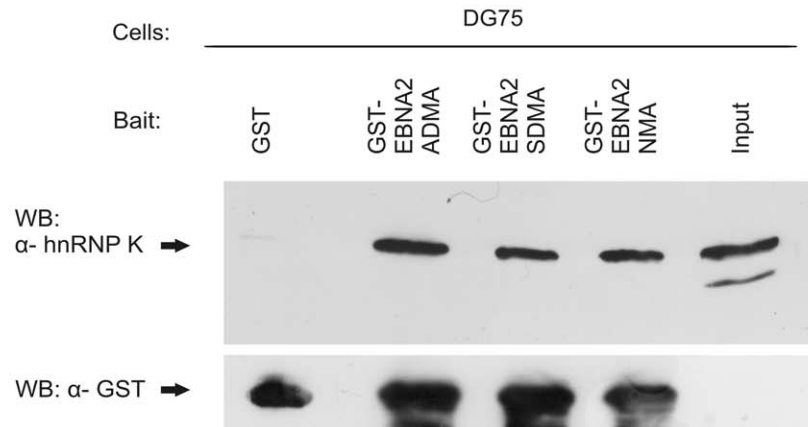
the human PRMT1 which are divergent from all other known PRMTs. The clone 7D2 (Rat IgG2a) reacted only with a single band in a western blot using DG75 cell extract and migrated to the same position as *E. coli*-expressed PRMT1 (Figure S1). Methylation with the PRMT5/WD45 complex expressed in *Baculovirus*-infected cells, however, yielded a protein that reacted with the three antibodies indicating that the PRMT5 preparation contained a contamination with a type I PRMT that catalysed the generation of ADMA residues. The precipitation from the untreated extract yielded, in addition to a strong band of non-methylated fusion protein, a faint band reactive with ADMA antibody (Figure S2). We then employed the bacterial fusion proteins for a pull-down of hnRNP K protein from extract of non-infected DG75 lymphoma cells. The extract from these cells was treated with AdOx after lysis to prevent additional and unspecific methylation of the GST-fusion proteins. As shown in Figure 5A, we observed binding of hnRNP K to non-methylated as well as methylated GST-EBNA2 fusion protein. In the control experiment using GST-protein alone, no binding was observed. The observation that non-methylated EBNA2 also binds hnRNP K indicated that residues adjacent to the RG-repeat of EBNA2 might also be involved in binding to hnRNP K. As outlined above, the SDMA-specific antibody co-precipitated hnRNP K from EBNA2-containing cell extract but not from non-infected cells showing that hnRNP K interacted both with SDMA- and ADMA-EBNA2 *in vivo*. The same results (Figure 5B) were obtained with a GST-EBNA2 (aa 300–400) mutant lacking the RG repeat ( $\Delta$ RG). This indicated also that residues adjacent to the RG-repeat are also involved in the interaction with hnRNP K.

To further characterise the binding of EBNA2 to hnRNP K, a GST- tagged EBNA2 fragment containing the C-terminal amino acids 400–487 were created. As can be seen in Figure 5C, the fragment containing the aa 400–487 is not able to bind hnRNP K in contrast to the EBNA2 fragment consisting of aa 300–400 encompassing the RG-repeat. These results suggest that hnRNP K interacts with EBNA2 via its amino acids 300–400 regardless of the presence of the methylated RG- repeat. A similar observation was previously made for the interaction of the SMN protein with the SDMA-modified RG-repeat of EBNA2, where the main but not exclusive binding region for SMN on EBNA2 was located at and around the RG-repeat [10]. In contrast, the methylation of hnRNP K appears to be necessary for binding to EBNA2 (see also below).

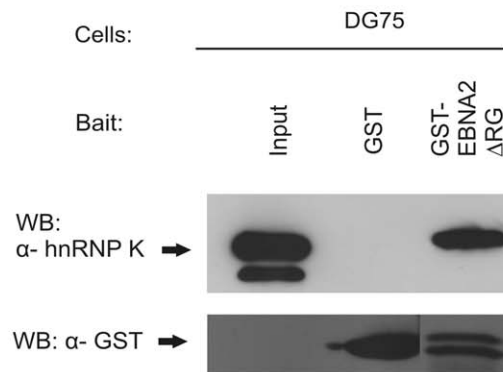
### EBNA2 and hnRNP K Co-localise

To show that EBNA2 also forms a complex with hnRNP K in intact cells, we carried out a co-localisation study using confocal laser scanning microscopy as described previously [32]. For this purpose, EGFP-EBNA2 [32] was expressed in HeLa cells. hnRNP K was visualised using the D6 antibody and secondary Alexa 647 -labelled goat anti-mouse IgG. Co-localisation of EBNA2 with hnRNP K was observed in 35.7% of the cells that expressed both proteins (a representative image is shown in Figure 6). hnRNP K and EBNA2 showed clear co-localisation at numerous spots along the inner

A



B



C

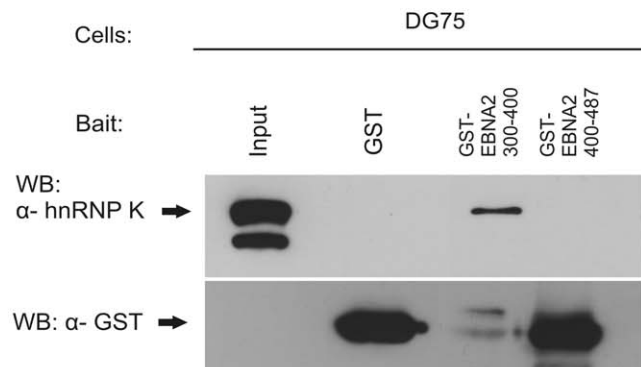
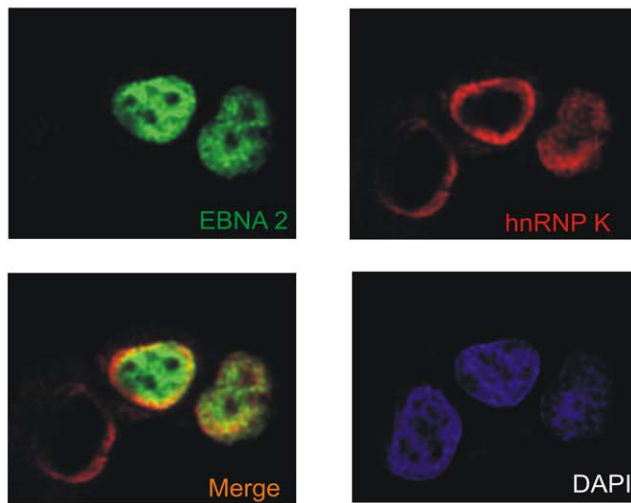


**Figure 5. hnRNP K binds to the amino acids 300 – 400 of EBNA2 regardless of the methylation or presence of the RG- repeat.** (A) *In vitro* methylated (SDMA and ADMA) and unmethylated (NMA) GST- EBNA2 fusion protein containing amino acids 300–400 of EBNA2 and GST alone were coupled to glutathione sepharose and were incubated with DG75 cell extract treated with methylation inhibitor AdOX. Precipitated hnRNP K was visualised using the hnRNP K mAb D-6. (B) GST- EBNA2ΔRG fusion protein containing amino acids 300–400 without the RG- Repeat of EBNA2 and GST alone were coupled to glutathione sepharose and were incubated with DG75 cell extract. Precipitated hnRNP K was visualised using the hnRNP K mAb D-6. (C) GST- EBNA2 aa400–487 fusion protein containing amino acids 400- 487 of EBNA2, GST- EBNA2 aa300–400 and GST alone were coupled to glutathione sepharose and were incubated with DG75 cell extract. Precipitated hnRNP K was visualised using the hnRNP K mAb D-6.

doi:10.1371/journal.pone.0042106.g005

A



B

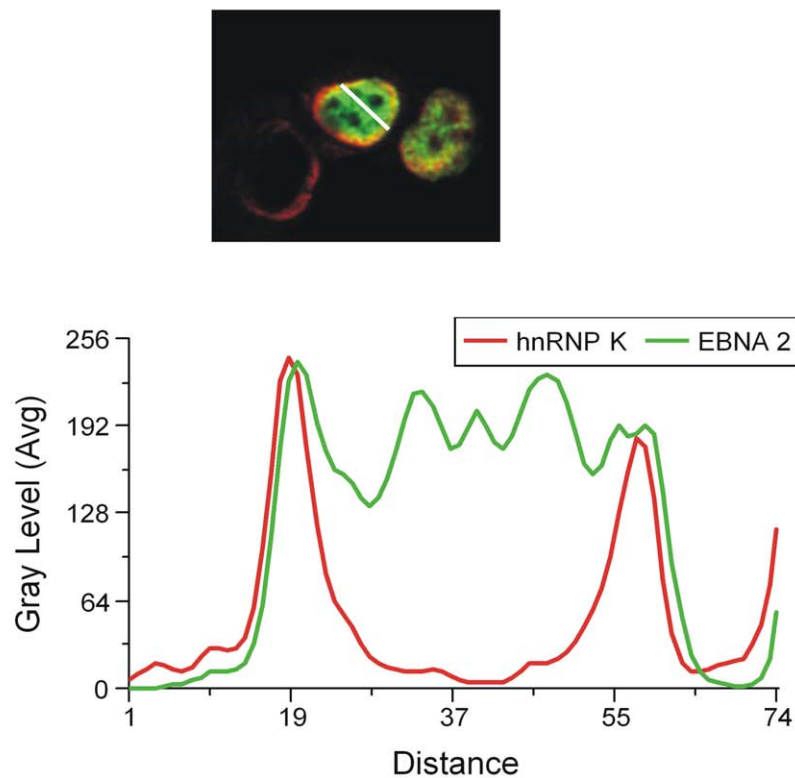
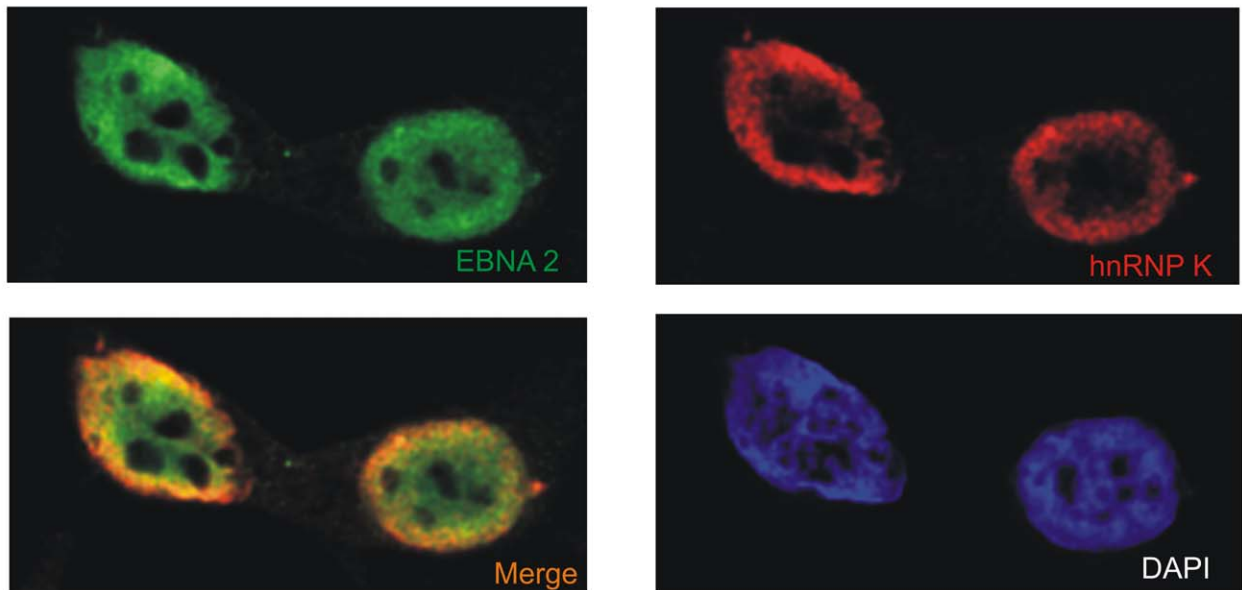


**Figure 6. hnRNP K and EBNA2 co-localize in transiently transfected cells.** (A) HeLa cells transfected with EGFP- EBNA2 were analysed by confocal laser scanning microscopy. Endogenous hnRNP K was detected using the monoclonal D-6 antibody and an Alexa 647 coupled anti mouse antibody. The signals for hnRNP K (red) or EBNA2 (green) are shown. The merged signals show co-localisation of hnRNP K and EBNA2, resulting in a yellow color. Also shown is the DAPI staining of DNA. The fluorescence profiles of hnRNP K and EBNA2 (B) at a co-localisation hotspot (indicated by the line, left picture - lower lane) were analysed with the Leica MMAF software. The signals for hnRNP K and EBNA2 show the same progression of intensity at the inner nuclear membrane.  
doi:10.1371/journal.pone.0042106.g006



A



B

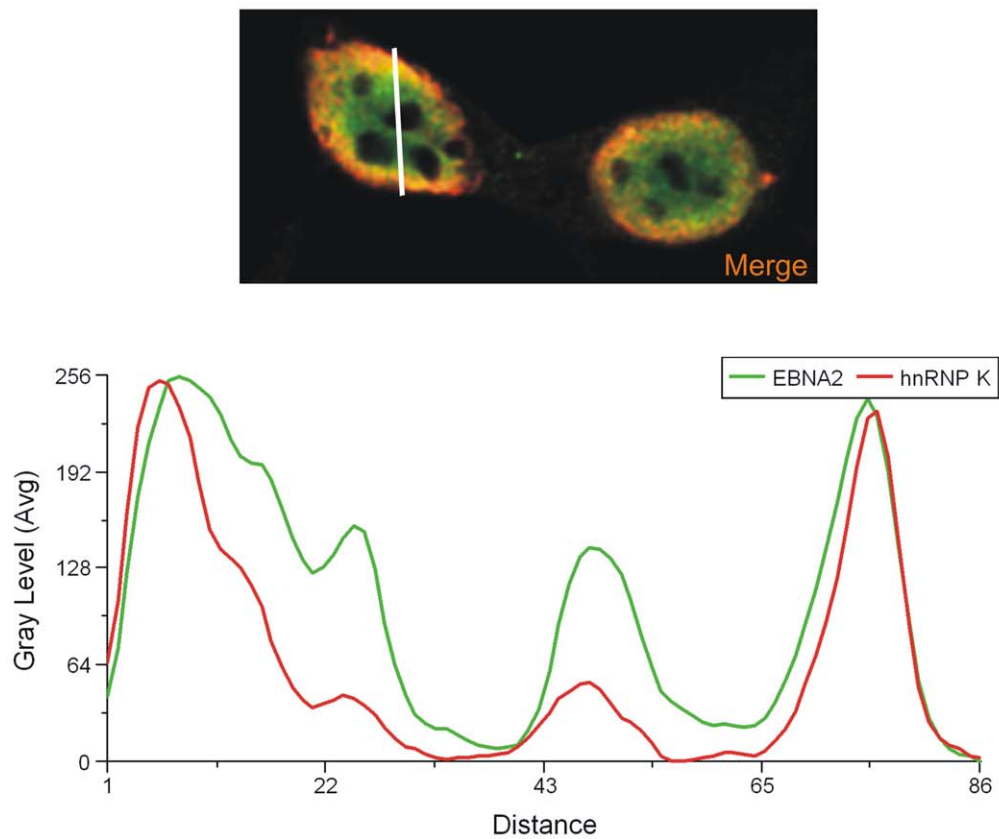


**Figure 7. hnRNP K and EBNA2 co-localize in EBV positive cells.** (A) 293-EBV cells were analysed by confocal laser scanning microscopy. Endogenous hnRNP K was detected using the monoclonal D-6 antibody and an Alexa 647 coupled anti mouse antibody. Endogenous EBNA2 expressed from the viral episome was detected using the monoclonal R3 antibody and an TRITC coupled anti rat antibody. The signals for hnRNP K (red) or EBNA2 (green) are shown. The merged signals show co-localisation of hnRNP K and EBNA2, resulting in a yellow color. Also shown is the DAPI staining of DNA. The fluorescence profiles of hnRNP K and EBNA2 (B) at a co-localization hotspot (indicated by the line, left picture - lower lane) were analysed with the Leica MMAF software. The signals for hnRNP K and EBNA2 show the same progression of intensity at the inner nuclear membrane. doi:10.1371/journal.pone.0042106.g007

nuclear membrane. A representative image of the distribution of fluorescence intensity across a line through the nucleus (“linescan”) is pictured in Figure 6B. The linescan shows that the intensities for the EBNA2 and hnRNP K signals overlap and further supports the notion that the two proteins interact.

The same results were obtained for endogenous proteins using the 293 EBV cell line. The endogenous (i.e. non-transfected) EBNA2 was visualised by the EBNA2- specific R3 antibody and goat- anti- rat TRITC -labelled antibody. hnRNP K was visualised using the D6 antibody and secondary Alexa 647 -labelled goat anti-mouse IgG. A representative cell is pictured in Figure 7A, a linescan showing the same intensity in fluorescence is shown in Figure 7B. These results, in

conjunction with the GST-pull-down study and the co-immunoprecipitation experiments (see above), strongly suggest that ADMA- and SDMA-modified EBNA2 and ADMA-methylated hnRNP K form (a) functional unit(s) in EBV-infected cells.

#### hnRNP K Interacts with EBNA2 in vivo in a Subset of Cells

To further investigate this interaction we used a cell based protein interaction assay. We immunocaptured the GFP-EBNA2 fusion protein (bait) with the GBP-lacI at the chromosomal lacO array, that becomes visible as distinct nuclear spot (Figure 8A). In about one third of all transfected cells we observed a clear co-localisation of the CFP-hnRNP K fusion protein (prey) at the lacO spot which is indicative of

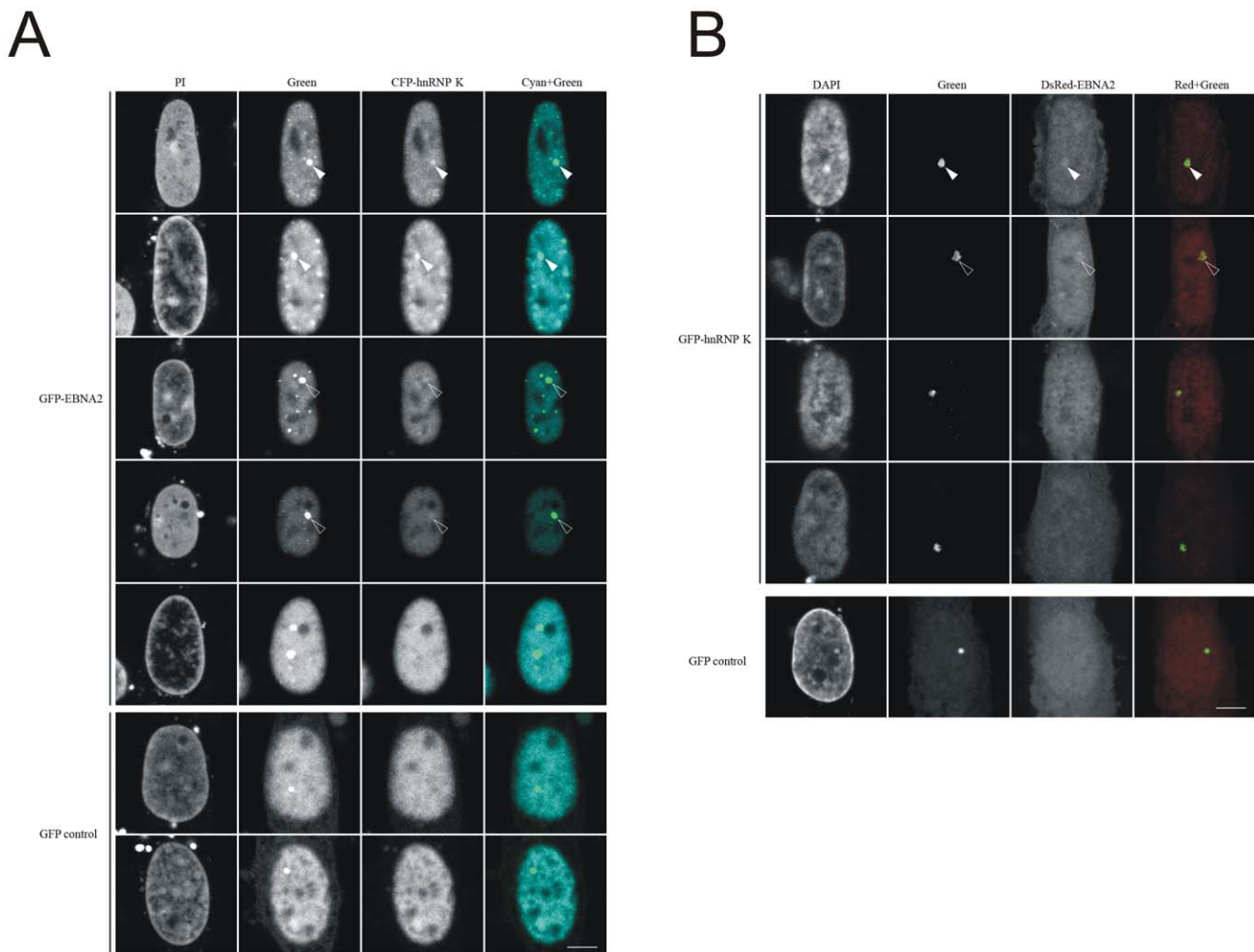
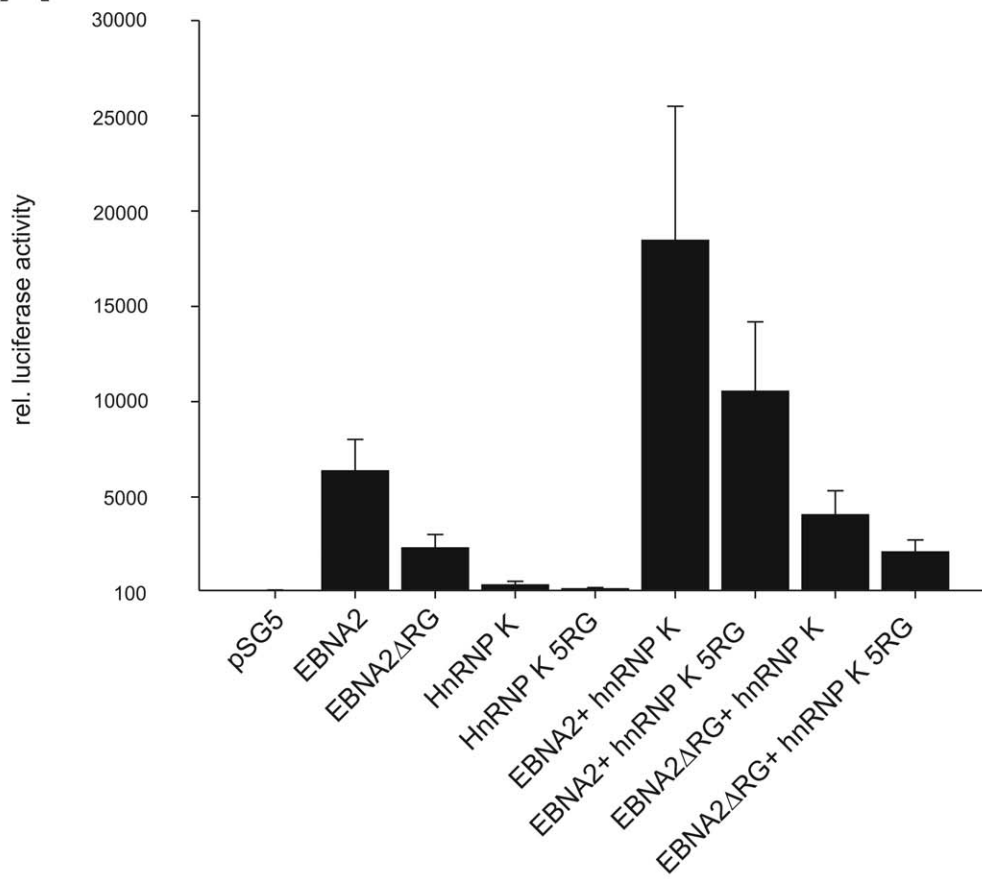


**Figure 8. hnRNP K interacts with EBNA2 in a cell based interaction system.** Cells containing a *lac* operator (*lacO*) array inserted in the genome were transfected with expression vectors for a *lac* repressor fused with a GFP binding protein (GBP) and the indicated fluorescent fusion proteins as indicated. For comparison and orientation the nucleus was stained with PI or DAPI. The GFP fusion proteins are captured at the *lac* operator array by the LacI-GBP and the co-localization of cyan or red fusion proteins visualized. Clear and weak interactions at *lacO* array spots are marked with filled and open arrow tips, respectively. The displayed cells represent the different patterns observed in several independent experiments. GFP expression vectors were used as negative control. Scale bar is 5  $\mu$ m. doi:10.1371/journal.pone.0042106.g008

**A**



**B**

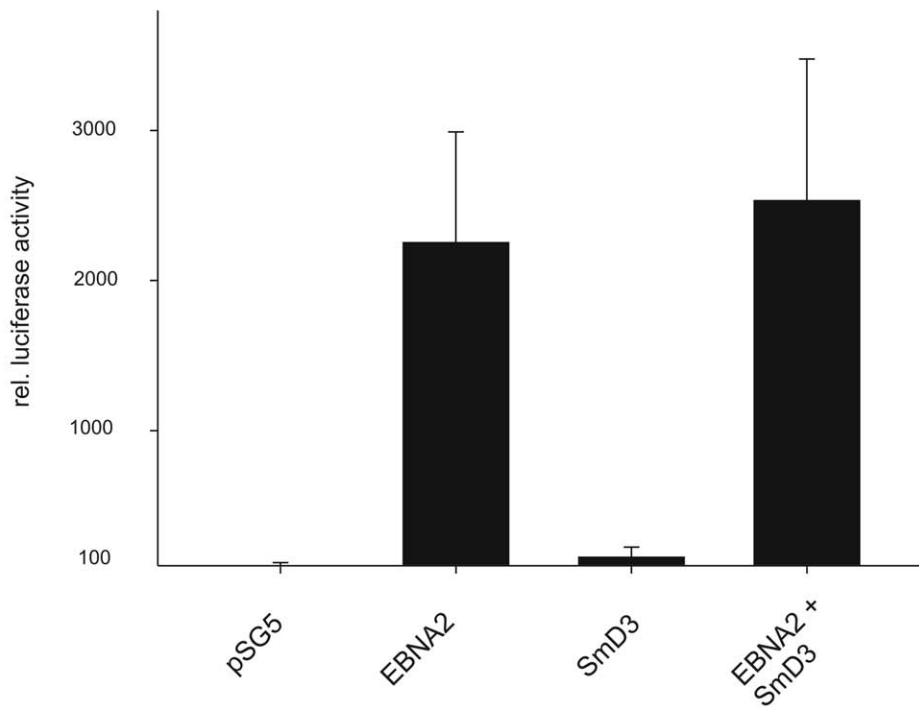


**Figure 9. hnRNP K but not SmD3 enhances the EBNA2-mediated promoter activation at the viral LMP2a promoter.** (A) A LMP2a promoter luciferase construct was co-transfected into DG75 cells with EBNA2, EBNA2- $\Delta$ RG, hnRNP K, and hnRNP K-5RG expression constructs in the indicated combinations. The luciferase value (RLU) obtained with empty pSG5 and the reporter construct was set to 100%. The graph represents the values obtained from 5 independent experiments carried out in duplicate. (B) A LMP2a promoter luciferase construct was co-transfected into DG75 cells with EBNA2 and SmD3 expression constructs in the indicated combinations. The luciferase value (RLU) obtained with empty pSG5 and the reporter construct was set to 100%. The graph represents the values obtained from 4 independent experiments carried out in duplicate. doi:10.1371/journal.pone.0042106.g009

a direct or indirect protein interaction. Another third showed a weak interaction and the remaining cells did not show any clearly detectable interaction and were indistinguishable from GFP control cells. We also performed the reciprocal experiments by switching fluorescent proteins and immobilizing GFP-hnRNP K at the lacO array spot (Figure 8B). In this combination we also observed co-localisation of the DsRed-EBNA2 at the lacO spot although with generally weaker signals. These cell based interaction assay results provide further evidence for an interaction of hnRNP K with EBNA2 *in vivo*. The displayed cells give a representative overview of the observed variability and indicate that this interaction does not occur in all cells or at least not to an equal extent. These results suggest that the hnRNP K interaction with EBNA2 is not constitutive but likely subjected to some additional regulation.

### hnRNP K Enhances EBNA2-mediated Activation of the Viral LMP2A Promoter

hnRNP K has repeatedly been shown to directly activate [41,42,43,44] or inactivate [45,46] transcription. To test whether the interaction of EBNA2 and hnRNP K changed the transactivation of a viral promoter by EBNA2, we co-expressed EBNA2-wt, hnRNP K-wt, the methylation-deficient mutants EBNA2- $\Delta$ RG [16] and hnRNP K-5RG [31] in all possible combinations together with a luciferase reporter driven by the promoter of the viral LMP2A [32]. As shown in Figure 9A, EBNA2-wt activated the promoter by about 500-fold ( $p = 0.0000000016$ ), while the activation by EBNA2- $\Delta$ RG was lower but still highly significant ( $p = 0.000009975$ ). hnRNP K-wt or the 5RG-mutant alone exerted a small but significant activation on the promoter construct ( $p = 0.000173$  and  $p = 0.00529$ , respectively), while co-expression of hnRNP K-wt enhanced the EBNA2-wt-mediated activation by up to three-fold ( $p = 0.001675$ ). The hnRNP K-5RG mutant co-activated EBNA2-wt to a smaller degree than hnRNP K-wt ( $p = 0.00833$ ). The activity of EBNA2- $\Delta$ RG was only slightly increased by hnRNP K-wt ( $p = 0.00261$ ), and no co-activation was observed for the combination of both mutants ( $p = 0.875$ ). We determined the relative levels of EBNA2 in the presence or absence of hnRNP K expression. The co-expression of hnRNP K did not change the EBNA2 level excluding a trivial explanation for the observed effect (Figure S3). This result and the results from interaction analysis using the hnRNP K-5RG mutant (Figure 4C) strongly support the notion that the interaction between EBNA2 and hnRNP K is mainly (but not exclusively) mediated by the methylation of the two proteins. The expression levels of transfected EBNA2-wt, EBNA2- $\Delta$ RG, hnRNP K-wt and hnRNP K-5RG are shown in Figure S4. We used the co-expression of SmD3 which was precipitated by the SDMA antibody (Table 1) as an additional negative control. SmD3 which does not bind to EBNA2 was not able to co-activate EBNA2 in this assay as shown in Figure 9B.

### hnRNP K is not Present in EBNA2-DNA Binding Complexes

To see whether hnRNP K is present in EBNA2-DNA complexes, we carried out a gel-shift experiment employing cell extract from EBV/EBNA2-positive Raji cells. As indicated in Figure 10, we added either HA-hnRNP K or HA-RBPjk to the Raji cell extract. EBNA2 binds DNA via the repressor RBPjk [47],

and this interaction can be inhibited by the antibody 6C8 directed against the WWP-repeat of EBNA2 [48] that is used for its interaction with RBPjk (reviewed in [49]). We have previously shown that the ADMA-form of EBNA2 is preferentially present at EBNA2-regulated promoters [15]. We thus tested whether the hnRNP K- antibody D6 which co-precipitates EBNA2 (see Figure 4A) would induce a super-shift as observed for the EBNA2-specific antibody R3 with a DNA-fragment derived from the viral LMP2A promoter. To exclude a possible unsuitability of the D6 antibody for EMSA we also tested the HA antibody in the samples which included HA-tagged hnRNP K or RBPjk, the latter serving as internal positive control. As shown in Figure 10, the EBNA2/RBPjk-containing complex designated “IV” was super-shifted by R3, while the antibody D6 against hnRNP K and the HA- antibody did not. In contrast, the HA- antibody was able to bind to and super-shift the HA-RBPjk bound to DNA (“Supershift\*”). As internal control we used the antibody 6C8 which interferes in the EBNA2-RBPjk interaction [48]. As can be seen, this antibody diminished the signal from complex IV. The absence of hnRNP K in the EBNA2/DNA-complex indicates that the observed co-activation by hnRNP K is not mediated by direct promoter binding of hnRNP K. The interaction of the two subforms of EBNA2 (SDMA and ADMA) which differ in their presence in EBNA2-DNA-binding complexes [15] to hnRNP K hints at the possibility that EBNA2 and hnRNP K co-operate in other activities, for instance in post-transcriptional processing of mRNA. The latter possibility will have to be addressed in a different set of experiments beyond the scope of this communication.

### Discussion

The hypothesis underlying our analysis was that EBNA2, as demonstrated for its interaction with RBPjk *via* its “WWP”-motif, uses the methylated RG-repeat to attach to cellular factors to use or interfere with their functions. For instance, EBNA2 binds with its SDMA-modified RG-repeat to the SMN protein and with the ADMA-modified RG-repeat to the HERV-K (HML-2) NP9 protein [10,32]. We therefore employed recently developed monoclonal antibodies against the SDMA and ADMA-repeat of EBNA2 for the identification of cellular proteins with a similar surface structure. Of the proteins precipitated by the SDMA-EBNA2-specific antibodies, we notably detected SmD3 known to be SDMA-modified by PRMT5 [33,34] and PRMT7 [50]. The precipitation of SmD3 strengthened our hypothesis that the antibody recognised not only the methylated arginine residues of EBNA2 but also the tertiary structure of the RG-motif. The RG-motif confers binding of both the SDMA-SmD3 and the SDMA-EBNA2 to SMN [10,35]. Importantly, the ADMA-EBNA2-antibody, in contrast to the SDMA-antibody, did not bind SmD3 as it does not contain ADMA residues [51]. Because SmD3 is a common component of spliceosomal U snRNP it was not surprising that the SDMA-specific antibody also precipitated components of the spliceosome, namely the U1 snRNP-specific 70K protein as well as the U5 snRNP component PRPF8 [52]. Since it was likely that these proteins co-precipitated with SmD3

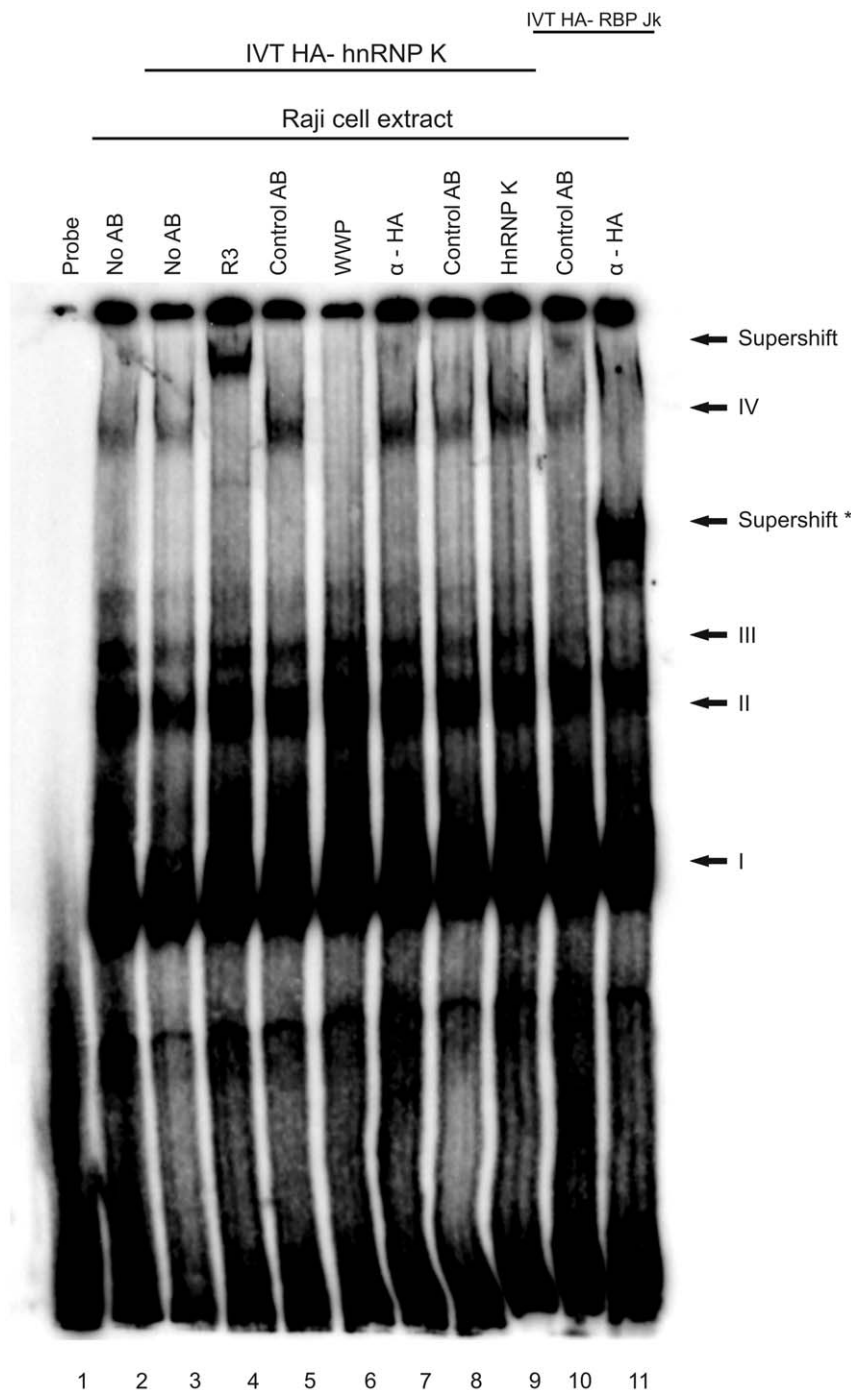


**Figure 10. hnRNP K is not present in EBNA2-containing DNA complexes.** EBNA2-containing Raji cell extract was incubated with *in vitro* translated hnRNP K and RBP- Jk and antibodies as indicated above and then assayed in a gel shift assay. R3 recognizes EBNA2 regardless of its methylation status and induces a “super- shift” indicated by the upper arrow, the mAb 6C8 directed against the “WWP”-repeat of EBNA2 destroys the EBNA2/RBPj $\kappa$ -complex IV. Control antibodies corresponded to the respective IgG-subtype of each antibody. To efficiently separate the high molecular weight complexes, the electrophoresis was carried out for an extended time. Therefore, uncomplexed  $^{32}$ P-labelled probe ran out of the gel. The position of the RBPj $\kappa$ -containing complexes I-IV as described in the text are indicated; the arrow (“Supershift”) points at the EBNA2-containing complex IV that is supershifted by R3 but not by the hnRNP K specific D6 antibody or the HA- specific antibody. The arrow (“Supershift \*”) indicates the RBP- Jk containing complex which is supershifted by the HA- specific antibody and served as an internal control.  
doi:10.1371/journal.pone.0042106.g010

due to being part of the same RNP complexes we did not pursue the SDMA-precipitated proteins further.

Of the proteins identified by the ADMA-specific antibodies, nothing is known about the Ras-GTPase-activating protein SH3-

domain-binding protein variant (gi: 62896771) identified in our study. Its splice variant, G3BP1, was shown to be associated with SMN and with Caprin-1 which was formerly known as GPI-anchored membrane protein 1 or cell cycle associated protein

[53,54]. Caprin-1 was also detected in our analysis. The role of Caprin-1 and the G3BP1 variant in EBV transcription or replication is unknown, however, a role of Caprin-1 in *Vaccinia* virus replication was previously demonstrated [55]. The G3BP1 variant contains several RGG and RG motifs at its C-terminus and might thus also be arginine-methylated. The ATP-dependent RNA helicase A (DHX9) contains ADMA and its arginine methylation is a prerequisite for nuclear localisation [56]. Like hnRNP K, DHX9 was previously found to be associated with the EBV-encoded nuclear antigen 5 (EBNA5 or EBNA-LP) [57]. As EBNA2 binds to the RNA helicase DDX20 (DP103/Gemin3) [9], it is possible that DHX9 and EBNA2 also form a complex. This is presently being investigated.

hnRNP K is highly conserved in eukaryotic cells and plays a role in various cellular processes like chromatin remodelling, transcriptional regulation, splicing, translation or signal transduction (see, for example, [30,44,58,59,60,61]). hnRNP K interacts directly or indirectly with a large number of cellular proteins [62], most notably with proteins involved in RNA metabolism. Because hnRNP K also plays a role in transcriptional activation and since the ADMA-form of EBNA2 is predominantly bound to EBNA2-responsive promoters [15], we decided to analyse the precipitation of hnRNP K by the ADMA-specific antibody in greater detail. As a precedent, the cross-reactivity between an epitope on hnRNP K and the PTB-associated splicing factor was demonstrated recently [63]. Through the use of bacterial expressed hnRNP K, which contained exclusively ADMA-methylated arginine residues we could clearly show that the ADMA-specific antibody binds to methylated hnRNP K. Interestingly, an antibody directed against non-methylated EBNA2 also detected hnRNP K indicating that both proteins share a common surface structure that is most likely used for the interaction with cellular partner proteins. Most importantly, hnRNP K and EBNA2 bind to each other, presumably *via* the methylated regions as protein arginine methylation is used either for protein-RNA or protein-protein interactions [21]. However, the GST-pull-down analysis showed that the non-methylated EBNA2 and the  $\Delta$ RG mutant also bind to hnRNP K indicating that the region surrounding the RG-repeat is also involved in binding. This is in line with the previously described association of EBNA2 with SMN, where the binding to SMN is mainly but not exclusively mediated via the RG-repeat of EBNA2 [10]. In the living cell, the EBNA2-hnRNP K-interaction might be regulated *via* methylation or another secondary modification, as we observed an interaction in the lacO-based assay system only in about 60% of the cells that expressed the GFP-labelled proteins (Figure 6). While EBNA2 does not exist in non-methylated form [15], it is possible that newly synthesized hnRNP K might undergo cell cycle-dependent differences in methylation. The functional significance of the EBNA2-hnRNP K-interaction was emphasised by the observation that hnRNP K enhanced the EBNA2-mediated activation of the viral LMP2A promoter by more than 3-fold. Interestingly, the activation of the viral C promoter by the hnRNP protein AUF1 was described by Ling and co-workers; however, the interaction domains between EBNA2 and AUF1 were not mapped [64].

A previous report showed that hnRNP K is present in transcriptionally active sites in EBV-transformed cells and that hnRNP K was highly enriched at loci with high EBV viral RNA content [65]. This is reflected by the fact that hnRNP K strongly co-activated EBNA2. The observation that the splicing machinery was distributed randomly *vis-à-vis* the viral DNA but was enriched at the transcript site [65] indicated that there is a recruitment of splicing factors to nascent viral transcripts. The role of EBNA2 in

this process remains unclear. However, we assume that the interaction between EBNA2 and hnRNP K indicates a co-operation during transcription and that the binding of EBNA2 to proteins of the splicing machinery reflects the close link between transcription and splicing [66,67]. However, the lack of hnRNP K at EBNA2-containing DNA complexes indicates that the enhancement of LMP2A expression might take place at a post-transcriptional level. Further studies will be needed to address the question whether the binding of EBNA2 influences other activities of hnRNP K, *i.e.* the known interaction with c-Src or its activity in mRNA translation, *i.e.* the *c-myc* gene, which is a target for both hnRNP K and EBNA2 [43,68,69,70].

## Materials and Methods

### Cell Lines and Tissue Culture

HEK 293-T, 293-EBV and HeLa cells were cultured in DMEM medium (GIBCO), supplemented with 10% FCS and antibiotics, non-adherent cell lines were grown in RPMI 1640 medium (GIBCO), supplemented with 10% FCS, Na-Pyruvate and antibiotics. The EBV-infected cell lines Raji and 293-EBV, the EBV-negative cell lines DG75 [71] and BL-41 as well as 293-T and HeLa cells were previously described [32,72].

### Transfection/Electroporation/Luciferase Assay

For transient expression of the various proteins,  $5 \times 10^6$  293-T cells were transfected with 8  $\mu$ g/10 cm dish of the expression vectors and combinations thereof using Nanofectin® (PAA, Cölbe, Germany). Western blotting by the ECL®-method (GE Healthcare, Munich, Germany) was carried out as described. Electroporation and luciferase analysis was carried out as described [32]. DG75 cells were electroporated using a Bio-Rad Gene Pulser at 250 V and 950  $\mu$ F. Briefly,  $10^7$  cells were washed once and resuspended in 0.25 ml of ice-cold RPMI 1640 without supplements and placed on ice. Then, 4  $\mu$ g of reporter plasmid, 10  $\mu$ g of each respective effector plasmid, and 2  $\mu$ g of pGFP-C1 (Clontech, Palo Alto, CA, USA) were added. Parental pSG5 vector (Agilent Technologies, Waldbronn, Germany) was used to adjust DNA amounts. After electroporation, cells were kept on ice for 10 min, suspended in 10 ml of RPMI with 20% fetal calf serum, and grown for 48 h. To determine the transfection efficiency, 100  $\mu$ l of the cells were fixed and analysed in a Becton Dickinson FACScan analyser for eGFP-positive cells, gated on the living population. The remainder of cells were washed in PBS and lysed in 100  $\mu$ l  $1 \times$  CCLR-buffer (Promega, Mannheim, Germany). The luciferase activity of the supernatants was determined in a Lumat LB9501 (Berthold, Bad Wildbad, Germany) by using the Promega luciferase assay system® (Promega) as recommended by the manufacturer.

### Plasmids

To express quantitatively asymmetrically methylated hnRNP K in *E. coli* the plasmid pET28-PRMT1, a kind gift of X. Cheng, Emory University, Atlanta, GA, [73] was completed with a second Shine-Dalgarno- and PRMT1 coding sequence (PCR primers 5' AAACTCGA GAACCTTTAAGAAGGAGATATACCATG 3'; 5' TTTCTCGAG TTCAGCGCATCCGGTA GTCGG 3') inserted into *Xho* I and a Shine-Dalgarno- (His<sub>6</sub>)-hnRNP K sequence [74] (PCR primers 5' TTTGTGACAAAC TTTAAGAAGGAGATATACCATG 3'; 5' TTTGTGACCCG GATCATCAGTGGTG 3') in the *Sal* I site. pGFP-EBNA2 was described previously [11]. pSG5-HA-hnRNP K and pSG5-HA-hnRNP K 5RG were constructed using the pGFP-hnRNP K and pGFP-hnRNP K 5RG plasmids [29]. dsRed-EBNA2 was constructed using the pGFP-

EBNA2 plasmid [11] and the dsRed Monomer C1 vector (Clontech). peCFP- hnRNP K was constructed using the peGFP- hnRNP K plasmid [29] and the peCFP- C1 vector (Clontech). GST- EBNA2 fragment fusion proteins were constructed using the pGEX- 4T1 Vector (Amersham). The complete coding sequence of PRMT1 was amplified by PCR from a HeLa-cDNA library with primers 5'PRMT1-TACAGGATCCATGGAGGTGTCCTG TGGCCAGGCG G-3' and 3'PRMT1 5'-GACGGGATCCGAATTCAGCGCATCCGGTAGTCGGTGGAGCAG -3' and cloned into the BamHI-digested eukaryotic expression vectors pSG5 or the BamHI-digested pGEX-4T1 vector for expression of a GST-PRMT1 fusion protein in *E.coli*.

### Preparation of Native Whole Cell Extract

Raji or DG75 cells were lysed for 30 min on ice in PBS supplemented with 0.5% IGEPAL (Sigma) and 0.15 M NaCl and protease inhibitors (Complete mini®, Roche). The lysate was centrifuged at 15,000×g for 15 min, and the supernatant was used for further analysis.

### Antibodies

The rat mAb 8C3 (IgG2b) reacts with NMA-EBNA2, the mouse mAb 13B10 (IgG2c) recognises SDMA-EBNA2, the mouse mAb 6F12 (IgG2b) binds to ADMA-EBNA2 [15], and the rat mAb R3 (IgG2a) binds to a C-terminal epitope outside the methylation region of EBNA2 [39]. Monoclonal anti-hnRNP K antibody (D-6) was from Santa Cruz (Heidelberg, Germany), goat-anti- mouse Alexa 647 was from Life Technologies (Invitrogen, Darmstadt, Germany), peroxidase-coupled anti-rat or anti-rabbit IgG were from Sigma (Munich, Germany). The monoclonal antibody 3F10 (Roche, Penzberg, Germany) binds to the HA-tag. For production of anti-PRMT1 monoclonal antibodies, a peptide encompassing amino acids G<sub>250</sub>MRPNAKNNRDL<sub>264</sub> of human PRMT1 coupled to BSA was used to immunize Lou/C rats according to a standard protocol [75]. A clone designated 7D2 (Rat IgG2a) that reacted with GST-PRMT1 but not an irrelevant GST-fusion protein in a western blot was stably subcloned and used for further analysis. The reactivity of this antibody with *E.coli*-expressed non-fused PRMT1 and GST-PRMT1 as well as endogenous cellular PRMT1 from the human cell line DG75 [71] is shown in Figure S2.

### Confocal Immunofluorescence Microscopy

HeLa cells were seeded on microscopy cover slips. Cells were transfected with a plasmid encoding EGFP-EBNA2 [32] and endogenous hnRNP K was visualized with the D6 antibody and secondary Alexa 647-labeled goat anti-mouse IgG2a (Invitrogen, Molecular Probes). Nuclei were stained with DAPI. Slides were mounted using Vectashield (Vector Laboratories). Fluorescence images (Figure 6) were captured with a laser scanning microscope, Leica TCS SP2 (Leica Microsystems, Heidelberg, Germany) equipped with an HCX PL APO 63×1.40 NA oil immersion objective lens using scan settings of pinhole 1.0 Airy units, 512×512 pixel image format, four frame averages, and a TD488/543/633 dichromatic beam splitter. Fluorescence spill-over was excluded by using sequential image recording and tightly controlled excitation power and detection channel settings (EGFP-EBNA2 excitation: 44% of 488-nm laser; Alexa 647 excitation: 81% of 633-nm laser, DAPI excitation: 49% of 405-nm laser). The co-localisation of endogenous (i.e. non-transfected) EBNA2 and hnRNP K was carried out in 293-EBV cells [76]. EBNA2 expressed from the viral episome was detected using the monoclonal R3 antibody and a TRITC-coupled anti-rat antibody. Endogenous hnRNP K was visualized with the D6 antibody and

secondary Alexa 647-labeled goat anti-mouse IgG2a. Secondary antibodies were highly cross-adsorbed and showed not cross-recognition. Images were captured using the TCS SP5 II/AOBS Leica confocal system (Figure 7). Fluorescence images were acquired in a sequential scan mode with HyD detectors with tightly controlled laser powers and acquisition windows to prevent spill-over (scan 1:4% 405-nm with 3% 561-nm; scan 2:6% 488-nm with 16% 633-nm). All images were recorded as stacked series of confocal single z-planes (step size: 488 nm using magnification with 4× frame average of 630× with zoom factor of at least 2.5. Editing of contrast and brightness was applied to the whole image using Leica LAS AF software. For EBNA2-hnRNP K co-localisation, 56 double-positive cells expressing both fusion proteins were evaluated. Co-localisation was analysed using the Leica Lite software profile tool. Co-localisation hotspots were defined as regions with coinciding high fluorescence intensity of hnRNP K and EBNA2 in the same optical z-plane. The percentage of cells showing co-localisation was calculated among the cells expressing both proteins. Additional de-convolution was performed using the Autoquant plug-in of the Leica MMAF Software (Leica Microsystems, Heidelberg, Germany).

### Cell Based Protein Interaction Assay

Fluorescent two-hybrid assays [77] were performed with a few modifications to visualize and test protein interactions. BHK cells containing a *lac* operator repeat array inserted in the genome [78] were seeded on coverslips and cultured in DMEM medium with 10% FCS. After attachment cells were co-transfected with expression vectors for the indicated fluorescent fusion proteins and a GBP- LacI fusion [79] using polyethylenimine (Sigma). After about 16 h cells were fixed with 3.7% formaldehyde in PBS for 10 min, washed with PBST (PBS with 0.02% Tween), stained with DAPI or PI and mounted in Vectashield medium (Vector Laboratories) (Figure 8). For PI staining RNA was eliminated by RNase treatment after fixation.

### Immunoprecipitation

The rat monoclonal antibody (mAb) R3 (rat IgG2a) recognises a C-terminal epitope of EBNA2 while the clone 6C8 (rat IgG2a) binds to the Trp-Trp-Pro motif of EBNA2 and interferes with binding to RBPjκ [48]. For immunoprecipitation appropriate mouse or rat IgG isotype controls were used. For precipitation, 400 µl of mAb supernatant were coupled to 100 µl of settled protein-G-sepharose (PGS, GE Healthcare, München, Germany) for 1 h at 4°C under agitation, sedimented at 5,000 rpm and washed once with 1 ml of lysis buffer 1. For precipitation experiments either 400 µg protein of native whole cell extract or 100 µg protein of native nuclear extract was added and incubated for 2 h at 4°C under agitation, washed three times with lysis buffer 2 (PBS with 0.5% IGEPAL and 0.5 M NaCl) and once with lysis buffer 1. The pellet was resuspended in 2× SDS sample-buffer and incubated for 10 min at RT or heated at 98°C.

### Co-immunoprecipitation Analysis

Raji cells were lysed for 30 min on ice in PBS supplemented with 0.5% IGEPAL (Sigma) and 0.15 M NaCl containing protease inhibitors (Complete mini®, Roche, Penzberg, Germany). After incubation, the solution was sonicated with a 10 s pulse and centrifuged at 13,000×g for 15 min, and the supernatant was used for further incubation with antibody immobilised on 30 µl of settled protein G Sepharose® (GE Healthcare). The cells were washed twice with ice-cold PBS and lysed for 30 min on ice in buffer 1 (PBS supplemented with 0.5% IGEPAL (Sigma) and 0.15 M NaCl) containing protease inhibitors (Complete mini®,

Roche). After incubation, the solution was sonicated with a 10 s pulse, centrifuged at 13,000×g and 4°C and incubated for 4 h at 4°C with antibody immobilised on 30 µl of settled protein G sepharose (GE Healthcare). The beads were collected and washed repeatedly with lysis buffer. The immune complexes were dissolved in SDS-gel buffer and separated in 10% polyacrylamide gel electrophoresis and transferred to a nitrocellulose membrane. The antibody R3 binds to the C-terminus of EBNA2. The antibodies 6F12 and 13B10 which recognise the asymmetrically and symmetrically di-methylated arginine-Glycine repeat of EBNA2, respectively, and the GST-specific monoclonal antibody 6G9 have been described recently. hnRNP K was detected using monoclonal antibody D6 (sc-13133, Santa Cruz, Heidelberg, Germany).

### In vitro Methylation Assays

Competent *E. coli* BL21- bacteria were transformed with appropriate expression vectors, protein expression was induced with IPTG and soluble extracts were purified with NAP<sup>TM</sup>25 columns (GE Healthcare, Freiburg, Germany) as described previously [32]. *In vitro* methylation assays were carried out using 20 µl of His-PRMT1 extract or 5 µl of PRMT5/WD45 extract, 20 µl of GST- EBNA2 (aa300-400) fusion protein extract and 5 µl of 0.5 M SAM. The mixture was incubated for 1 h at 37°C.

*GST- pull- down assays:* For GST- EBNA2 and GST competent *E. coli* BL21- bacteria were transformed and protein expression was induced with IPTG as described previously [32]. The GST fusion proteins were adsorbed to glutathione-Sepharose beads (GE Healthcare, Freiburg, Germany) for 2 h at 4°C with rotation, and subsequently washed twice with lysis buffer containing 0.15 M NaCl. For binding of cellular proteins to the GST fusion proteins, typically 500 µl of AdOX- treated native whole cell extract (see above) was added to the mixture and incubated for 2 h at 4°C with rotation and subsequently washed 5 times with lysis buffer containing 0.5 M NaCl. The beads were suspended in SDS-gel electrophoresis buffer, boiled and separated by 10% SDS-PAGE. GST-EBNA2 and GST were detected in western-blotting using 6G9 antibody. hnRNP K was detected using the D-6 monoclonal antibody (Santa Cruz , D-6, sc-28380).

### Electrophoretic Mobility Shift Assay (EMSA)

Nuclear cell extracts were prepared essentially as described [80]. Shortly, approx. 10<sup>8</sup> cells were collected for 5 minutes at 1200 rpm and 4°C and washed twice with cold PBS. The pellet was resuspended in a 4-fold volume of buffer A (10 mM HEPES pH 7.9, 10 mM KCl, 1.5 mM MgCl<sub>2</sub>) [80] and kept on ice for at least 20 minutes. Cells were broken up by several strokes in a dounce homogenizer until the lysate contained about 50% intact nuclei by staining with Trypan blue. The lysate was centrifuged for 15 seconds at 14,000 rpm and 4°C and washed once with a 2-fold volume of buffer A. The resulting nuclear pellet was resuspended a 1-fold volume of buffer B (20 mM HEPES pH 7.9, 420 mM NaCl, 1.5 mM MgCl<sub>2</sub>, 2 mM EDTA pH 8.5) and kept on ice for 30 minutes. The lysate was centrifuged for 20 minutes at 15,000 rpm and 4°C and the supernatant was used for further experiments or stored at -80°C. Electrophoretic mobility shift assays were carried out exactly as described [4,81]. The probe used for EMSA is derived from the viral LMP2a promoter and

contains two RBPjk-binding sites. For supershift experiments, we employed the EBNA2-specific rat monoclonal antibody R3 [39] or an appropriate isotype (rat IgG2a) control. The monoclonal antibody 6C8 binds to the Trp-Trp-Pro (“WWP”) motif of EBNA2 interferes with binding to RBKJk and destroys the EBNA2-containing DNA-RBPjk-EBNA2-complex [48]. *In vitro* transcription-translation of HA-tagged hnRNP K and HA-tagged RBPjk using vector AJ247 [82] was performed using the TNT<sup>®</sup> Coupled Reticulocyte Lysate System (Promega, Mannheim, Germany) as described [10,15] following the instruction of the manufacturer. Typically, 50 µl of the transcription-translation mix were programmed with 1 µg of vector DNA using T7 RNA polymerase.

### Supporting Information

**Figure S1 Expression control of His- PRMT1 and characterization of the PRMT1 specific rat monoclonal antibody 7D2.** *E.Coli* extract containing His- tagged PRMT1, *E.Coli* extract containing GST- tagged PRMT1 and DG75 whole cell extract was analysed by western blotting. (TIF)

**Figure S2 In vitro methylation of GST-EBNA2-300-400.** The *E.coli*-expressed unmethylated GST-EBNA2-300-400 fusion protein was subjected to *in vitro* methylation by PRMT5/WD45 purified from a baculovirus expression system or PRMT1 expressed in *E.coli*. The methylated fusion proteins as well as an unmethylated control were immunoprecipitated with the EBNA2-methylation specific antibodies (NMA, SDMA and ADMA) and the appropriate isotype controls. Precipitated GST-EBNA2-300-400 fusion protein was detected in a western blot using the GST-specific 6G9 monoclonal antibody. (TIF)

**Figure S3 EBNA2 expression is not affected by hnRNP K.** DG75 cells were transfected with pSG5 – EBNA2 and pSG5-HA- hnRNP K and the cell extract was analysed by western blotting. EBNA2 was visualized using the R3 antibody, hnRNP K was visualized with the D6 antibody. (TIF)

**Figure S4 Expression control of the plasmids used in luciferase activity assays.** DG75 cells were transfected with pSG5 – EBNA2, pSG5 – EBNA2ΔRG, pSG5-HA- hnRNP K and pSG5-HA- hnRNP K 5RG and the cell extract was analysed by western blotting. EBNA2 was visualized using the R3 antibody, HA- hnRNP K and HA- hnRNP K 5RG was visualized with the HA antibody. (TIF)

### Acknowledgments

We thank Ruth Nord for expert technical assistance.

### Author Contributions

Conceived and designed the experiments: FG EK . Performed the experiments: HG CH CC AM IM US-G WD SB. Analyzed the data: HG CH HL EN EK FG. Contributed reagents/materials/analysis tools: DHO AO-L BM NN UF. Wrote the paper: HG FG.

### References

- Crawford DH (2001) Biology and disease associations of Epstein-Barr virus. *Philos Trans R Soc Lond B Biol Sci* 356: 461–473.
- Kieff E, Rickinson AE (2007) Epstein-Barr Virus and its replication. In: Knipe D, Griffin DE, Lamb RA, Strauss SE, Howley PM, et al., editors. *Fields Virology*. 5 ed. Philadelphia: Lippincott-Raven. 2603–2654.



3. Bornkamm GW, Hammerschmidt W (2001) Molecular virology of Epstein-Barr virus. *Philos Trans R Soc Lond B Biol Sci* 356: 437–459.
4. Zimmer Strobl U, Kremmer E, Grässer F, Marshall G, Laux G, et al. (1993) The Epstein-Barr virus nuclear antigen 2 interacts with an EBNA2 responsive cis-element of the terminal protein 1 gene promoter. *EMBO J* 12: 167–175.
5. Ling PD, Hayward SD (1995) Contribution of conserved amino acids in mediating the interaction between EBNA2 and CBF1/RBPJk. *J Virol* 69: 1944–1950.
6. Henkel T, Ling PD, Hayward SD, Peterson MG (1994) Mediation of Epstein-Barr virus EBNA2 transactivation by recombination signal-binding protein J kappa. *Science* 265: 92–95.
7. Zimmer Strobl U, Strobl LJ (2001) EBNA2 and Notch signalling in Epstein-Barr virus mediated immortalization of B lymphocytes. *Semin Cancer Biol* 11: 423–434.
8. Cohen JI, Wang F, Kieff E (1991) Epstein-Barr virus nuclear protein 2 mutations define essential domains for transformation and transactivation. *J Virol* 65: 2545–2554.
9. Grundhoff AT, Kremmer E, Tureci O, Glieden A, Gindorf C, et al. (1999) Characterization of DP103, a novel DEAD box protein that binds to the Epstein-Barr virus nuclear proteins EBNA2 and EBNA3C. *J Biol Chem* 274: 19136–19144.
10. Barth S, Liss M, Voss MD, Dobner T, Fischer U, et al. (2003) Epstein-Barr virus nuclear antigen 2 binds via its methylated Arginine- glycine repeat to the survival motor neuron protein. *J Virol* 77: 5008–5013.
11. Voss MD, Hille A, Barth S, Spurk A, Hennrich F, et al. (2001) Functional cooperation of Epstein-Barr virus nuclear antigen 2 and the survival motor neuron protein in transactivation of the viral LMP1 promoter. *J Virol* 75: 11781–11790.
12. Tsui S, Schubach WH (1994) Epstein-Barr virus nuclear protein 2A forms oligomers in vitro and in vivo through a region required for B-cell transformation. *J Virol* 68: 4287–4294.
13. Wu DY, Krumm A, Schubach WH (2000) Promotor-specific targeting of human SWI-SNF complex by Epstein-Barr virus nuclear protein 2. *J Virol* 74: 8893–8903.
14. Grässer FA, Haiss P, Göttel S, Mueller Lantzsch N (1991) Biochemical characterization of Epstein-Barr virus nuclear antigen 2A. *J Virol* 65: 3779–3788.
15. Gross H, Barth S, Palermo RD, Mamiani A, Hennard C, et al. (2010) Asymmetric Arginine dimethylation of Epstein-Barr virus nuclear antigen 2 promotes DNA targeting. *Virology* 397: 299–310.
16. Tong X, Yalamanchili R, Harada S, Kieff E (1994) The EBNA-2 Arginine-glycine domain is critical but not essential for B-lymphocyte growth transformation; the rest of region 3 lacks essential interactive domains. *J Virol* 68: 6188–6197.
17. Rickinson AB, Young LS, Rowe M (1987) Influence of the Epstein-Barr virus nuclear antigen EBNA 2 on the growth phenotype of virus-transformed B cells. *J Virol* 61: 1310–1317.
18. Cancian L, Bosshard R, Lucchesi W, Karstegl CE, Farrell PJ (2011) C-Terminal Region of EBNA-2 Determines the Superior Transforming Ability of Type 1 Epstein-Barr Virus by Enhanced Gene Regulation of LMP-1 and CXCR7. *PLoS Pathog* 7: e1002164.
19. Gary JD, Clarke S (1998) RNA and protein interactions modulated by protein Arginine methylation. *Prog Nucleic Acid Res Mol Biol* 61: 65–131.
20. Paik WK, Kim S (1967) Enzymatic methylation of protein fractions from calf thymus nuclei. *Biochem Biophys Res Commun* 29: 14–20.
21. Bedford MT, Richard S (2005) Arginine methylation an emerging regulator of protein function. *Mol Cell* 18: 263–272.
22. Cook JR, Lee JH, Yang ZH, Krause CD, Herth N, et al. (2006) FBXO11/PRMT9, a new protein Arginine methyltransferase, symmetrically dimethylates Arginine residues. *Biochem Biophys Res Commun* 342: 472–481.
23. Lee J, Sayegh J, Daniel J, Clarke S, Bedford MT (2005) PRMT8, a new membrane-bound tissue-specific member of the protein Arginine methyltransferase family. *J Biol Chem* 280: 32890–32896.
24. Swanson MS, Dreyfuss G (1988) Classification and purification of proteins of heterogeneous nuclear ribonucleoprotein particles by RNA-binding specificities. *Mol Cell Biol* 8: 2237–2241.
25. Bomsztyk K, Denisenko O, Ostrowski J (2004) hnRNP K: one protein multiple processes. *Bioessays* 26: 629–638.
26. Ostareck-Lederer A, Ostareck DH (2004) Control of mRNA translation and stability in haematopoietic cells: the function of hnRNPs K and E1/E2. *Biol Cell* 96: 407–411.
27. Uribe DJ, Guo K, Shin YJ, Sun D (2011) Heterogeneous nuclear ribonucleoprotein K and nucleolin as transcriptional activators of the vascular endothelial growth factor promoter through interaction with secondary DNA structures. *Biochemistry* 50: 3796–3806.
28. Ostareck-Lederer A, Ostareck DH, Hentze MW (1998) Cytoplasmic regulatory functions of the KH-domain proteins hnRNPs K and E1/E2. *Trends Biochem Sci* 23: 409–411.
29. Ostareck-Lederer A, Ostareck DH, Rucknagel KP, Schierhorn A, Moritz B, et al. (2006) Asymmetric Arginine dimethylation of heterogeneous nuclear ribonucleoprotein K by protein-Arginine methyltransferase 1 inhibits its interaction with c-Src. *J Biol Chem* 281: 11115–11125.
30. Naarmann IS, Harnisch C, Flach N, Kremmer E, Kuhn H, et al. (2008) mRNA silencing in human erythroid cell maturation: heterogeneous nuclear ribonucleoprotein K controls the expression of its regulator c-Src. *J Biol Chem* 283: 18461–18472.
31. Naarmann IS, Harnisch C, Muller-Newen G, Urlaub H, Ostareck-Lederer A, et al. (2010) DDX6 recruits translational silenced human reticulocyte 15-lipoxygenase mRNA to RNP granules. *Rna* 16: 2189–2204.
32. Gross H, Barth S, Pfuhl T, Willnecker V, Spurk A, et al. (2011) The NP9 protein encoded by the human endogenous retrovirus HERV-K(HML-2) negatively regulates gene activation of the Epstein-Barr virus nuclear antigen 2 (EBNA2). *Int J Cancer* 129: 1105–1115.
33. Meister G, Eggert C, Buhler D, Brahms H, Kambach C, et al. (2001) Methylation of Sm proteins by a complex containing PRMT5 and the putative U snRNP assembly factor pICln. *Curr Biol* 11: 1990–1994.
34. Friesen WJ, Massenet S, Paushkin S, Wyce A, Dreyfuss G (2001) SMN, the product of the spinal muscular atrophy gene, binds preferentially to dimethylarginine-containing protein targets. *Mol Cell* 7: 1111–1117.
35. Friesen WJ, Dreyfuss G (2000) Specific sequences of the Sm and Sm-like (Lsm) proteins mediate their interaction with the spinal muscular atrophy disease gene product (SMN). *J Biol Chem* 275: 26370–26375.
36. Hennard C, Pfuhl T, Buettner M, Becker KF, Knofel T, et al. (2006) The antibody 2B4 directed against the Epstein-Barr virus (EBV)-encoded nuclear antigen 1 (EBNA1) detects MAGE-4: implications for studies on the EBV association of human cancers. *J Pathol* 209: 430–435.
37. Meister G, Buhler D, Pillai R, Lottspeich F, Fischer U (2001) A multiprotein complex mediates the ATP-dependent assembly of spliceosomal U snRNPs. *Nat Cell Biol* 3: 945–949.
38. Liu Q, Fischer U, Wang F, Dreyfuss G (1997) The spinal muscular atrophy disease gene product, SMN, and its associated protein SIP1 are in a complex with spliceosomal snRNP proteins. *Cell* 90: 1013–1021.
39. Kremmer E, Kranz B, Hille A, Klein K, Eulitz M, et al. (1995) Rat monoclonal antibodies differentiating between the Epstein-Barr virus nuclear antigens 2A (EBNA2A) and 2B (EBNA2B). *Virology* 208: 336–342.
40. Chan JY, Hsieh TY, Liu ST, Chou WY, Chung MH, et al. (2009) Physical and functional interactions between hnRNP K and PRMT family proteins. *FEBS Lett* 583: 281–286.
41. Li H, Liu J (2010) Identification of heterogeneous nuclear ribonucleoprotein K as a transactivator for human low density lipoprotein receptor gene transcription. *J Biol Chem* 285: 17789–17797.
42. Ritchie SA, Pasha MK, Batten DJ, Sharma RK, Olson DJ, et al. (2003) Identification of the SRC pyrimidine-binding protein (SPY) as hnRNP K: implications in the regulation of SRC1A transcription. *Nucleic Acids Res* 31: 1502–1513.
43. Takimoto M, Tomonaga T, Matunis M, Avigan M, Krutzsch H, et al. (1993) Specific binding of heterogeneous ribonucleoprotein particle protein K to the human c-myc promoter, in vitro. *J Biol Chem* 268: 18249–18258.
44. Michelotti GA, Michelotti EF, Pullner A, Duncan RC, Eick D, et al. (1996) Multiple single-stranded cis elements are associated with activated chromatin of the human c-myc gene in vivo. *Mol Cell Biol* 16: 2656–2669.
45. Hsieh TY, Matsumoto M, Chou HC, Schneider R, Hwang SB, et al. (1998) Hepatitis C virus core protein interacts with heterogeneous nuclear ribonucleoprotein K. *J Biol Chem* 273: 17651–17659.
46. Lau JS, Baumeister P, Kim E, Roy B, Hsieh TY, et al. (2000) Heterogeneous nuclear ribonucleoproteins as regulators of gene expression through interactions with the human thymidine kinase promoter. *J Cell Biochem* 79: 395–406.
47. Zimmer Strobl U, Strobl LJ, Meitinger C, Hinrichs R, Sakai T, et al. (1994) Epstein-Barr virus nuclear antigen 2 exerts its transactivating function through interaction with recombination signal binding protein RBP-J kappa, the homologue of Drosophila Suppressor of Hairless. *EMBO J* 13: 4973–4982.
48. Sauder C, Götzinger N, Schubach WH, Horvath GC, Kremmer E, et al. (1996) Mutational analysis of the Epstein-Barr virus nuclear antigen 2 by far-Western blotting and DNA-binding studies. *J Gen Virol* 77: 991–996.
49. Zimmer-Strobl U, Strobl LJ (2001) EBNA2 and Notch signalling in Epstein-Barr virus mediated immortalization of B lymphocytes. *Semin Cancer Biol* 11: 423–434.
50. Lee JH, Cook JR, Yang ZH, Mirochnitchenko O, Gunderson S, et al. (2004) PRMT7: A new protein Arginine methyltransferase that synthesizes symmetric dimethylarginine. *J Biol Chem* 279: 19.
51. Brahms H, Raymackers J, Union A, de Keyser F, Meheus L, et al. (2000) The C-terminal RG dipeptide repeats of the spliceosomal Sm proteins D1 and D3 contain symmetrical dimethylarginines, which form a major B-cell epitope for anti-Sm autoantibodies. *J Biol Chem* 275: 17122–17129.
52. Jurica MS, Moore MJ (2003) Pre-mRNA splicing: awash in a sea of proteins. *Mol Cell* 12: 5–14.
53. Zou T, Yang X, Pan D, Huang J, Sahin M, et al. (2011) SMN deficiency reduces cellular ability to form stress granules, sensitizing cells to stress. *Cell Mol Neurobiol* 31: 541–550.
54. Hua Y, Zhou J (2004) Survival motor neuron protein facilitates assembly of stress granules. *FEBS Lett* 572: 69–74.
55. Rosales R, Sutter G, Moss B (1994) A cellular factor is required for transcription of vaccinia viral intermediate-stage genes. *Proc Natl Acad Sci U S A* 91: 3794–3798.
56. Smith WA, Schurter BT, Wong-Staal F, David M (2004) Arginine methylation of RNA helicase a determines its subcellular localization. *J Biol Chem* 279: 22795–22798.

57. Forsman A, Ruetschi U, Ekholm J, Rymo L (2008) Identification of intracellular proteins associated with the EBV-encoded nuclear antigen 5 using an efficient TAP procedure and FT-ICR mass spectrometry. *J Proteome Res* 7: 2309–2319.
58. Mikula M, Bomsztyk K (2011) Direct recruitment of ERK cascade components to inducible genes is regulated by heterogeneous nuclear ribonucleoprotein (hnRNP) K. *J Biol Chem* 286: 9763–9775.
59. Wei CC, Zhang SL, Chen YW, Guo DF, Ingelfinger JR, et al. (2006) Heterogeneous nuclear ribonucleoprotein K modulates angiotensinogen gene expression in kidney cells. *J Biol Chem* 281: 25344–25355.
60. Adolph D, Flach N, Mueller K, Ostareck DH, Ostareck-Lederer A (2007) Deciphering the cross talk between hnRNP K and c-Src: the c-Src activation domain in hnRNP K is distinct from a second interaction site. *Mol Cell Biol* 27: 1758–1770.
61. Marchand V, Santerre M, Aigueperse C, Fouillen L, Saliou JM, et al. (2011) Identification of protein partners of the human immunodeficiency virus 1 tat/rev exon 3 leads to the discovery of a new HIV-1 splicing regulator, protein hnRNP K. *RNA Biol* 8: 325–342.
62. Mikula M, Dzwonek A, Karczmarski J, Rubel T, Dadlez M, et al. (2006) Landscape of the hnRNP K protein-protein interactome. *Proteomics* 6: 2395–2406.
63. Garcia-Jurado G, Llanes D, Moreno A, Soria B, Tejedo JR (2011) Monoclonal antibody that recognizes a domain on heterogeneous nuclear ribonucleoprotein K and PTB-associated splicing factor. *Hybridoma (Larchmt)* 30: 53–59.
64. Fuentes Panana EM, Peng R, Brewer G, Tan J, Ling PD (2000) Regulation of the Epstein-Barr virus C promoter by AUF1 and the cyclic AMP/protein kinase A signaling pathway. *J Virol* 74: 8166–8175.
65. Melcak I, Cermanova S, Jirsova K, Koberna K, Malinsky J, et al. (2000) Nuclear pre-mRNA compartmentalization: trafficking of released transcripts to splicing factor reservoirs. *Mol Biol Cell* 11: 497–510.
66. Steinmetz EJ (1997) Pre-mRNA processing and the CTD of RNA polymerase II: the tail that wags the dog? *Cell* 89: 491–494.
67. Neugebauer KM, Roth MB (1997) Distribution of pre-mRNA splicing factors at sites of RNA polymerase II transcription. *Genes Dev* 11: 1148–1159.
68. Kaiser C, Laux G, Eick D, Jochner N, Bornkamm GW, et al. (1999) The proto-oncogene c-myc is a direct target gene of Epstein-Barr virus nuclear antigen 2. *J Virol* 73: 4481–4484.
69. Alfieri C, Birkenbach M, Kieff E (1991) Early events in Epstein-Barr virus infection of human B lymphocytes. *Virology* 181: 595–608.
70. Lee MH, Mori S, Raychaudhuri P (1996) trans-Activation by the hnRNP K protein involves an increase in RNA synthesis from the reporter genes. *J Biol Chem* 271: 3420–3427.
71. Ben-Bassat H, Goldblum N, Mitrani S, Goldblum T, Yoffey JM, et al. (1977) Establishment in continuous culture of a new type of lymphocyte from a “Burkitt like” malignant lymphoma (line D.G.-75). *Int J Cancer* 19: 27–33.
72. Barth S, Pfuhl T, Mamiani A, Ehlers C, Roemer K, et al. (2008) Epstein-Barr virus-encoded microRNA miR-BART2 down-regulates the viral DNA polymerase BALF5. *Nucleic Acids Res* 36: 666–675.
73. Zhang X, Cheng X (2003) Structure of the predominant protein Arginine methyltransferase PRMT1 and analysis of its binding to substrate peptides. *Structure* 11: 509–520.
74. Ostareck DH, Ostareck-Lederer A, Shatsky IN, Hentze MW (2001) Lipoxigenase mRNA silencing in erythroid differentiation: The 3'UTR regulatory complex controls 60S ribosomal subunit joining. *Cell* 104: 281–290.
75. Szczyrba J, Nolte E, Wach S, Kremmer E, Stohr R, et al. (2011) Down-regulation of Sec23A Protein by miRNA-375 in Prostate Carcinoma. *Mol Cancer Res* 9: 791–800.
76. Delecluse HJ, Hilsenrath T, Pich D, Zeidler R, Hammerschmidt W (1998) Propagation and recovery of intact, infectious Epstein-Barr virus from prokaryotic to human cells. *Proc Natl Acad Sci U S A* 95: 8245–8250.
77. Zolghadr K, Mortusewicz O, Rothbauer U, Kleinhans R, Goehler H, et al. (2008) A fluorescent two-hybrid assay for direct visualization of protein interactions in living cells. *Mol Cell Proteomics* 7: 2279–2287.
78. Tsukamoto T, Hashiguchi N, Janicki SM, Tumber T, Belmont AS, et al. (2000) Visualization of gene activity in living cells. *Nat Cell Biol* 2: 871–878.
79. Dambacher S, Deng W, Hahn M, Sadic D, Frohlich J, et al. (2012) CENP-C facilitates the recruitment of M18BP1 to centromeric chromatin. *Nucleus* 3.
80. Dignam JD, Lebovitz RM, Roeder RG (1983) Accurate transcription initiation by RNA polymerase II in a soluble extract from isolated mammalian nuclei. *Nucleic Acids Res* 11: 1475–1489.
81. Sauder C, Haiss P, Grässer FA, Zimmer Strobl U, Mueller Lantzsch N (1994) DNA-binding studies of the Epstein-Barr virus nuclear antigen 2 (EBNA-2): evidence for complex formation by latent membrane protein gene promoter-binding proteins in EBNA-2-positive cell lines. *J Gen Virol* 75: 3067–3079.
82. Maier S, Santak M, Mantik A, Grabusic K, Kremmer E, et al. (2005) A somatic knockout of CBF1 in a human B-cell line reveals that induction of CD21 and CCR7 by EBNA-2 is strictly CBF1 dependent and that downregulation of immunoglobulin M is partially CBF1 independent. *J Virol* 79: 8784–8792.



## S1

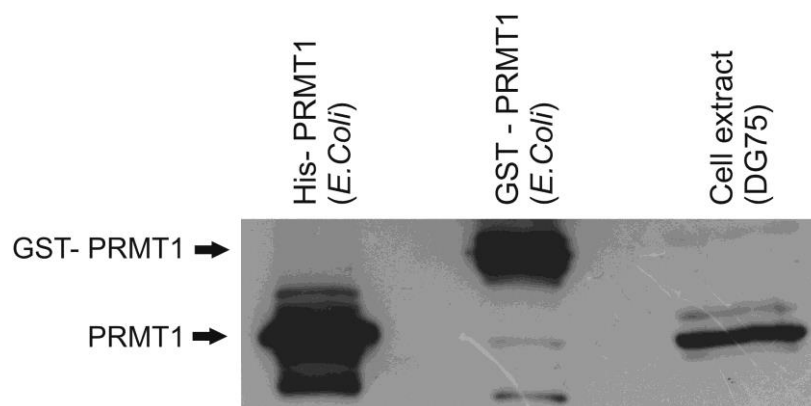


Figure S1. Expression control of His- PRMT1 and characterization of the PRMT1 specific rat monoclonal antibody 7D2. E.Coli extract containing His- tagged PRMT1, E.Coli extract containing GST- tagged PRMT1 and DG75 whole cell extract was analyzed by western blotting.

## S2

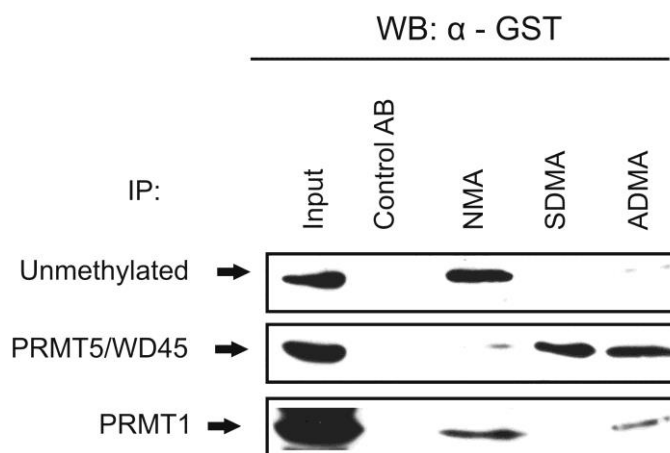


Figure S2. *In vitro* methylation of GST-EBNA2-300-400. The E.coli-expressed unmethylated GST-EBNA2-300-400 fusion protein was subjected to *in vitro* methylation by PRMT5/WD45 purified from a baculovirus expression system or PRMT1 expressed in E.coli. The methylated fusion proteins as well as an unmethylated control were immunoprecipitated with the EBNA2-methylation specific antibodies (NMA, SDMA and ADMA) and the appropriate isotype controls. Precipitated GST-EBNA2-300-400 fusion protein was detected in a western blot using the GST-specific 6G9 monoclonal antibody.

S3

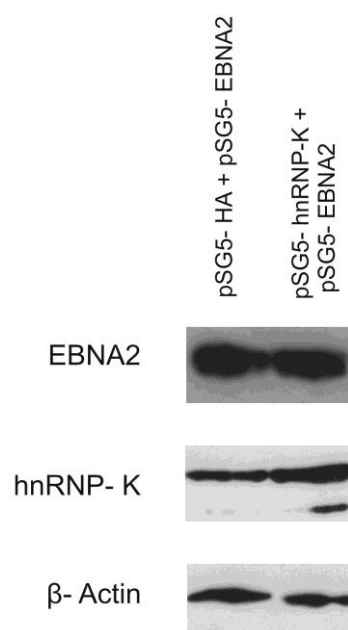


Figure S3. EBNA2 expression is not affected by hnRNP K. DG75 cells were transfected with pSG5 – EBNA2 and pSG5-HA- hnRNP K and the cell extract was analysed by western blotting. EBNA2 was visualized using the R3 antibody, hnRNP K was visualized with the D6 antibody.

S4

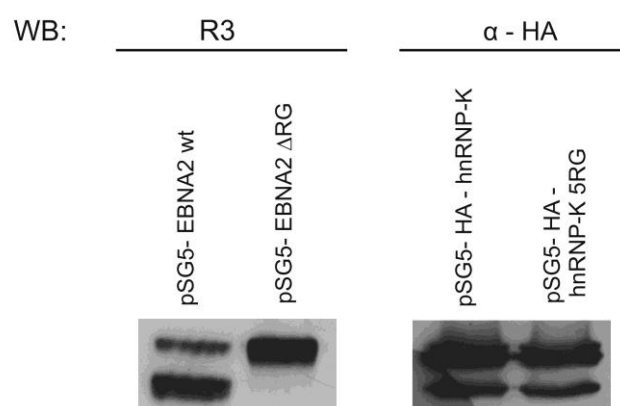


Figure S4. Expression control of the plasmids used in luciferase activity assays. DG75 cells were transfected with pSG5 – EBNA2, pSG5 – EBNA2ΔRG, pSG5-HA- hnRNP K and pSG5-HA- hnRNP K 5RG and the cell extract was analyzed by western blotting. EBNA2 was visualized using the R3 antibody, HA- hnRNP K and HA- hnRNP K 5RG was visualized with the HA

### 3. Discussion

#### 3.1 F3H – a versatile tool for protein manipulation and interaction studies

##### 3.1.1 F3H as a method to study protein-protein interactions

In the last decade, a variety of methods to study protein-protein interactions have been developed. These methods are based on different principles and all of them have their own advantages and disadvantages. As a fluorescence-based method to study protein interaction, the F3H- approach utilizes a specific GFP- binding protein to recruit GFP-tagged proteins and their RFP-tagged interaction partners to an artificial chromatin locus *in vivo*. The F3H-method combines fluorescence technology and eukaryotic expression systems to identify protein-protein interactions in a fast and simple way.

The F3H- approach is very similar to our fluorescence two-hybrid (F2H) method (Zolghadr et al., 2008). In both methods, a genetically modified cell line, in which multiple repeats of the bacterial *lac* operator (*lacO*) DNA sequence were inserted into the genome, is used. The Lac repressor specifically binds to this *lac* operator sequence, so it could be used to trace the chromatin locus on the genome. Initially, this artificial chromosomal locus was used to study chromatin organization, such as chromatin dynamics and condensation (Robinett et al., 1996), and was also used to visualize gene expression activity (Tsukamoto et al., 2000). And recently, the formation of ectopic kinetochores was studied using the *lacO*/repressor system (Gascoigne et al., 2011; Barnhart et al., 2011). Besides all these applications, our group established a method based on the *lacO*/repressor system to visualize protein-protein interactions *in vivo* (Zolghadr et al., 2008). We generated two constructs: a triple fusion of RFP-LacI-bait, and a GFP-tagged prey protein. The bait is localized to the *lacO* spot and visualized by the fused RFP. The GFP-prey protein is recruited and colocalized with the bait at the *lacO* spot, and the interaction is visualized by the fluorescent proteins. In this system, the two fluorescent constructs are co-expressed, so we called it F2H. The development of a GFP binding protein (GBP) (Rothbauer et al., 2008) gave us the possibility to bypass the need for special RFP-LacI-bait triple fusion constructs. We used a GBP-lacI fusion to recruit the GFP-bait to the *lacO* spot instead of the FP-lacI-bait triple fusion used in F2H. In the later system, three components are recruited to the *lacO* spot to give an indication of the protein interaction, so the system is called F3H. With this F3H system, any kind of GFP and RFP fused proteins could be used to detect their interactions. The independency of a special construct which is necessary in F2H gives this method much more flexibility and can thus be used more widely.

As a new method to studying protein interaction, the F3H assay has several distinguishing features. F3H assay is used in a mammalian cell system to test protein-protein interaction *in vivo*, so the natural structure and post-translational modifications

of the bait and prey proteins are kept, which makes this method especially suitable for testing of interactions between proteins from higher eukaryotic organism. Also, using fluorescence as a detection signal, this method directly visualizes two interacting proteins, intuitively giving information on PPI. In addition, the F3H assay could reveal quantitative binding affinity between two interacting proteins by means of measuring the signal ratio of the prey to the bait protein at *lacO* spot according to their fluorescent signal. Thus, the F3H method enables not only a qualitative analysis of specific interactions but also provides semi-quantitative affinity data for the interacting proteins. In comparison to conventional protein-protein interaction assays, the F3H assay has several advantages. This method is simpler and easier in comparison with other biochemical methods like Co-IP or cross-linking technology, saving both time and efforts. The enrichment of the GFP-tagged bait proteins at the *lacO* array enhances the signal-to-noise ratio; by changing the number of *lacO* repeats on the chromosomal foci, the signal intensity could be controlled to achieve a better signal-to-noise ratio, which could increase detecting sensitivity. Also, conventional co-localization assays study PPI by analyzing the localization co-efficiency of two proteins in the cell, this could give both false positive (such as co-localization not resulted from interaction) and false negative results (such as in the presence of interaction competitor proteins or unbalanced expression level). In the F3H assay, proteins of interesting are recruited to an artificial locus in the nucleus, this to some extent excludes co-localizations which do not result from direct or indirect interactions between the two proteins, thus providing more convincing results. In contrast to previous data (Frieman et al., 2007), we found that although the severe acute respiratory syndrome coronavirus (SARS-CoV) protein ORF6 co-localized with the human KPNA2 protein at the nuclear envelop, these two proteins did not interact (unpublished data).

Moreover, F3H directly visualizes protein-protein interactions in living cell in real-time; this feature gives it the unique ability to trace dynamic changes between the interacting partners, providing the possibility to identify cell cycle- or differentiation-dependent protein-protein interactions. This makes it especially suitable for studying interactions that regulate or are regulated by cell cycle or differentiation processes. In chapter 2.2, we found Mis18bp1 localized at centromere in a cell-cycle dependent way. CENP-C interacts with and facilitates the targeting of M18bp1 to the centromere. Since CENP-C constantly localizes at centromeres, our data suggest that the interaction between these two proteins may occur in a cell cycle-dependent way. Further studies using the F3H assay should be performed to analyze this interaction in different cell-cycle phases, to clarify the possible role of M18bp1 modification on the regulation of its interaction with CENP-C.

Similar to almost all other methods which study protein-protein interactions, the F3H assay can result in false positive or false negative results due to unspecific binding or fluorescence cross-talk. On the one hand, some prey proteins themselves bind to the chromosomal loci because of their intrinsic properties, such as the heterochromatin

protein HP1 $\alpha$ , which specifically binds to the H3K9me3 which exists at the *lacO* chromatin. In this case, it is difficult to differentiate whether the binding of the prey to *lacO* focus is a result of an interaction with the bait or mediated by the H3K9me3 binding property of HP1 $\alpha$ . This kind of proteins should not be used as preys but as baits by means of changing the fluorescence protein tag or use different anchor point. On the other hand, although there is little overlap between GFP and RFP emission light, occasional cross-talk between the two fluorescence proteins may still occur depending on the filters used. Experimental conditions should be optimized to eliminate bleed-through. In practice, we often exchange the bait/prey combinations and always check for possible bleed-through between GFP and RFP constructs by expressing only one of them to rule out these possible artifacts.

As mentioned above, GFP fusion proteins can be targeted to the *lacO* loci using the GBP-LacI fusion protein. The fusion protein which is recruited to the *lacO* spot may change the structure or characteristics of the *lacO* chromatin. For example, Dnmt1, which is the maintenance DNA methyltransferase in mammalian cells, can change the methylation states of the *lac* operator DNA sequences. In case of a histone acetyltransferase (HAT) anchored to the *lacO* spot, the acetylation of the histones would increase, and can lead to more open chromatin at the *lacO* chromatin. These properties create a new possibility to exploit the F3H assay. For example, by analyzing the altered *lacO* chromatin characteristics such as the chromatin accessibility or specific DNA/histone modifications, one could gain insight on the biological functions of the *lacO* targeted proteins, especially for epigenetic key factors that regulate the chromatin structure, such as chromatin remodelers or DNA/ histone modifiers. Additionally, these anchored proteins can recruit their interaction partners, leading to different biological consequences. For example, using a similar method, anchoring of HJURP (Barnhart et al., 2011) and CENP-C/CENP-T (Gascoigne et al., 2011) to *lacO* foci lead to ectopic neo-centromere formation and ectopic kinetochore assembly respectively.

To study protein interactions in a wider range and different cellular context, we developed several variants of the F3H assay. We utilize proteins of different cellular structures as anchors for the F3H assay.

Firstly, we fused the GBP to the methyl-CG binding domain (MBD) of MeCP2. This MBD domain preferentially binds to methylated CpG sites on the genome. Using the MBD-GBP fusion construct, one can artificially target proteins of interest to constitutive heterochromatin to study protein interaction. Alternatively one can investigate the function of these proteins on heterochromatin regulation by measuring the change after their targeting as mentioned above.

In another approach, we fused the GBP with Lamin B1 to target the bait to the nuclear envelope. The GBP-LaminB1 can recruit the GFP-bait fusion and its interaction partners to the nuclear membrane, leading to co-localization of the two tagged fluorescent proteins at the nuclear envelope. By anchoring the proteins to the nuclear membrane, we successfully avoided the false positive resulting from prey proteins binding to

heterochromatin. Moreover, when using the nuclear envelope as a targeting platform, it does not need any specific genomic modification (as the insertion of *lacO* arrays) of the cell line, and can be performed in nearly all kinds of cell lines, making the F3H assay even more flexible and broadly applicable.

In comparison with *lacO* mediated F3H, this nuclear envelop recruiting system has a modest signal-to-noise ratio because of the wide distribution of the bait and prey over the whole nuclear envelope. Thus a higher bait/prey expression level might be required to get a better signal-to-noise ratio. Another disadvantage is that the GBP-lamin fusion proteins would interfere with endogenous lamin protein, leading to an abnormal nuclear envelope structure when the GBP-lamin expression level is extremely high, which may lead to negative selection and cell death in long term culturing.

In the assay mentioned above, either at a chromosomal site (*lacO*/repressor) or at the nuclear membrane (lamin), the interactions of the bait and prey proteins are detected in the nucleus. However, under native biological conditions, many interactions occur in the cytoplasm. In our previous study, we showed that, although the detection of the protein-protein interaction took place in the nucleus, the F2H assay can also detect interaction natively occurring in the cytoplasm. Even interactions of mitochondrial proteins were successfully detected with the F2H assay in the nucleus (Zolghadr et al., 2008).

In the *lacO*- or Lamin-mediated F3H assay, proteins interact at the *lacO* focus or nuclear membrane, which means the bait and prey protein must translocate into the nucleus after translation. Proteins smaller than about 40 kD can pass through the nuclear pore by free diffusion, but proteins with a larger size could only be translocated into the nucleus by active transport. The protein active import depends on transferring proteins called importins, which strongly bind to proteins containing a nuclear localization signal (NLS) peptide. To improve the nuclear translocation efficiency of the GFP-baits fusion, we inserted the NLS of the SV40 large T antigen (Kalderon et al., 1984) at the N-terminus of GFP. With this NLS, the nuclear localization of some GFP-bait fusion proteins could effectively be increased and thus a better detection signal be obtained.

Although with the added NLS sequences, concentrations of some large proteins in the nucleus may be still low due to their low transport efficiency or the presence of a nuclear export sequence (NES) in the protein, which would direct the export of the protein from the nucleus into the cytoplasm. In any case, for detecting interactions of cytoplasmic proteins, it seems reasonable to use an anchor site in the cytoplasm rather than in the nucleus. So we further developed cytoplasmic anchor sites to improve the F3H assay.

Centrosomes locate in the cytoplasm and serve as microtubule organizing center (MTOC), which is important for cell-cycle progression in most cells (vertebrate muscle cells and mature oocytes lack centrosomes). In mammalian somatic cells, the centrosome is composed of two centrioles plus the pericentriolar material (PCM) around the two centrioles. Each of the two centrioles is based on 9 triplet microtubules which



arrange in a wheel-like pattern and form a cylindrical structure. The two centrioles are orthogonally arranged and surrounded by the PCM. Centrin, which is essential for centriole formation, localizes in the lumen of the centriole and also in the PCM (Fig. 15). Since centrin localizes at the centriole, we also tried to use centrin as a cytoplasmic anchor site for the F3H assay by fusing GBP to centrin. Using this GBP-centrin fusion, the bait and prey proteins were successfully recruited to the centrosomal site, demonstrating that this cytoplasmic anchor point can be used for protein-protein interaction assays. For example, the interaction between p53 and HDM2 was detected in this system (Chapter 2.1).

Although centrin-mediated F3H can detect protein interactions in the cytoplasm, in practice, we found that this centrosomal anchor system has some disadvantages for PPI assay. On the one hand, the size of the centrosome is quite small, resulting in a weak bait and prey signal in comparison with the conventional F3H assay, limiting its detecting sensitivity. On the other hand, centrin localizes not only at the centrosome but also in the cytoplasm, which increases the background noise. And also, owing to the small size of centriole lumen, larger bait and prey proteins cannot enter the lumen thus could not be effectively targeted to centrosome. Due to these reasons, this centrosomal anchored F3H assay is suitable for strong cytoplasmic interactions between small proteins but less suited for other cases.

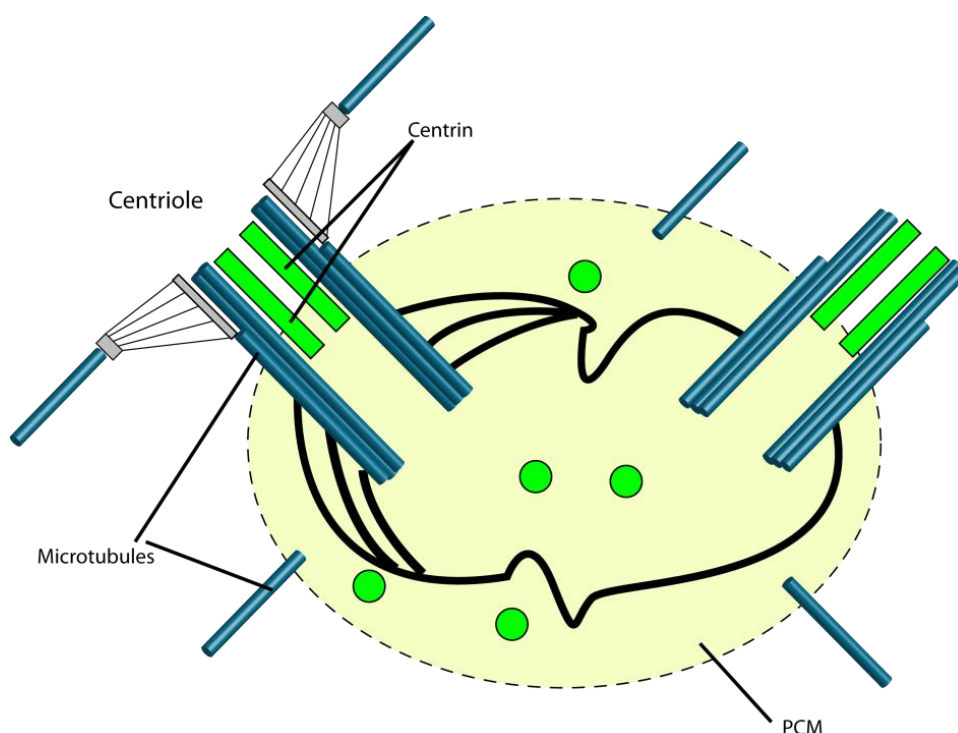


Fig. 15 The localization of centrin at the centrosome. Two orthogonally arranged centrioles are connected by the so-called pericentriolar material (PCM, shown as yellow dashed circle). The centriole is composed of 9 triplet microtubules arranged wheel-like, forming a cylindrical structure. Centrin (shown green) locates in the inner space of the centriole formed by the triplet microtubules. Besides the centrosome-bound centrin, there is also free centrin distributed in the PCM and the cytoplasm.

Because of the limitations of centrin-mediated F3H, we also tried to develop a second anchor sites in the cell cytoplasm. Microtubules are part of the cell skeleton, forming a fiber-like structure in the cytoplasm and can be easily detected by staining. We fused the GBP with tubulin  $\alpha$  to recruit the bait protein onto microtubules, expecting a fiber-like localization of GFP in the cytoplasm. However, we did not see a nice fiber-like localization of the GFP signal but an equal distribution of the GFP signal in the cytoplasm. This may be because the GBP in the GBP-tubulin fusion blocks the tubulin heterodimer formation, so the GBP-tubulin fusions can not incorporate into the microtubules, leading to an equal distributed GFP signal in the cytoplasm. To pursue this, a GBP-tubulin fusion protein that does not interfere with oligomerization, e.g. by using a flexible linker peptide or a C-terminal fusion, should be constructed and tested.

As another component of the cell skeleton, actin filament is necessary for cell survival since it is involved in many basic biological processes, such as cell mechanical support, cell movements and material transport. Actin filaments form unique cellular structures and could easily be detected in the cytoplasm, so it could be an ideal cytoplasmic protein anchoring site for the F3H assay.

A GBP- $\beta$ -actin construct was made to target GFP-bait proteins onto the actin filaments in the cytosol. When co-transfected with GFP-p53 (NLS free) and mCh-HDM2 into HeLa cells, mCh-HDM2 and GFP-p53 nicely colocalized at actin filaments in the cytoplasm, giving a convincing result of interaction between p53 and HDM2 (unpublished data). Of course, additional cytoplasmic protein interactions should be tested in the future to assess the applicability of this actin-mediated F3H assay.

In summary, we developed a variety of anchor sites both in nucleus and cytoplasm in mammalian cells for the F3H assay. Using these different sites as protein anchor points, protein interactions occurring either in the nucleus or in the cytoplasm can be studied easily and reliably (Fig. 16).

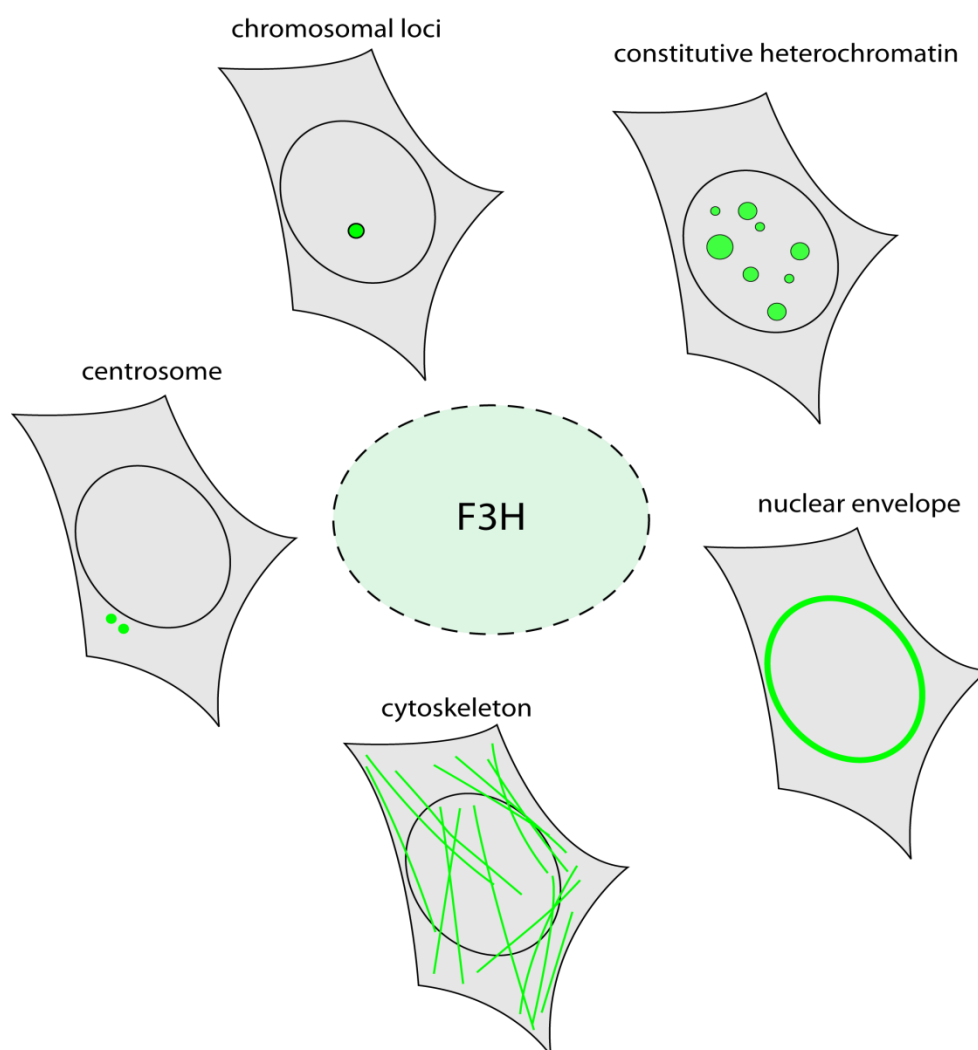


Fig. 16 Overview of F3H assays using different anchor points. In the nucleus, artificial chromosomal *lacO* sites and constitutive heterochromatin binding sites are used, in combination with GBP-lacI and GBP-MBD, respectively. In addition, GBP-lamin is used to target interaction partners to the nuclear envelope. In the cytoplasm, centrin and tubulin can be used to target proteins to the centrosome and cytoskeleton.

### 3.1.2 Application of the F3H assay for high-throughput screens

To expand the F3H assay to a high-throughput assay, I established a protocol for F3H assay in 96-well plate. Cells are seeded in a 96-well plate, transfected, fixed and stained. To efficiently acquiring images and evaluate the data, an Operetta imaging platform is used, which is an automatic multi-channel fluorescence microscope. With this imaging system, signals for nucleus, bait and prey (DAPI, GFP and RFP) are acquired and stored as images. These images are then further automatically analyzed with a multiple step protocol I developed with the InCell Analyzer image analysis software (Fig. 17).

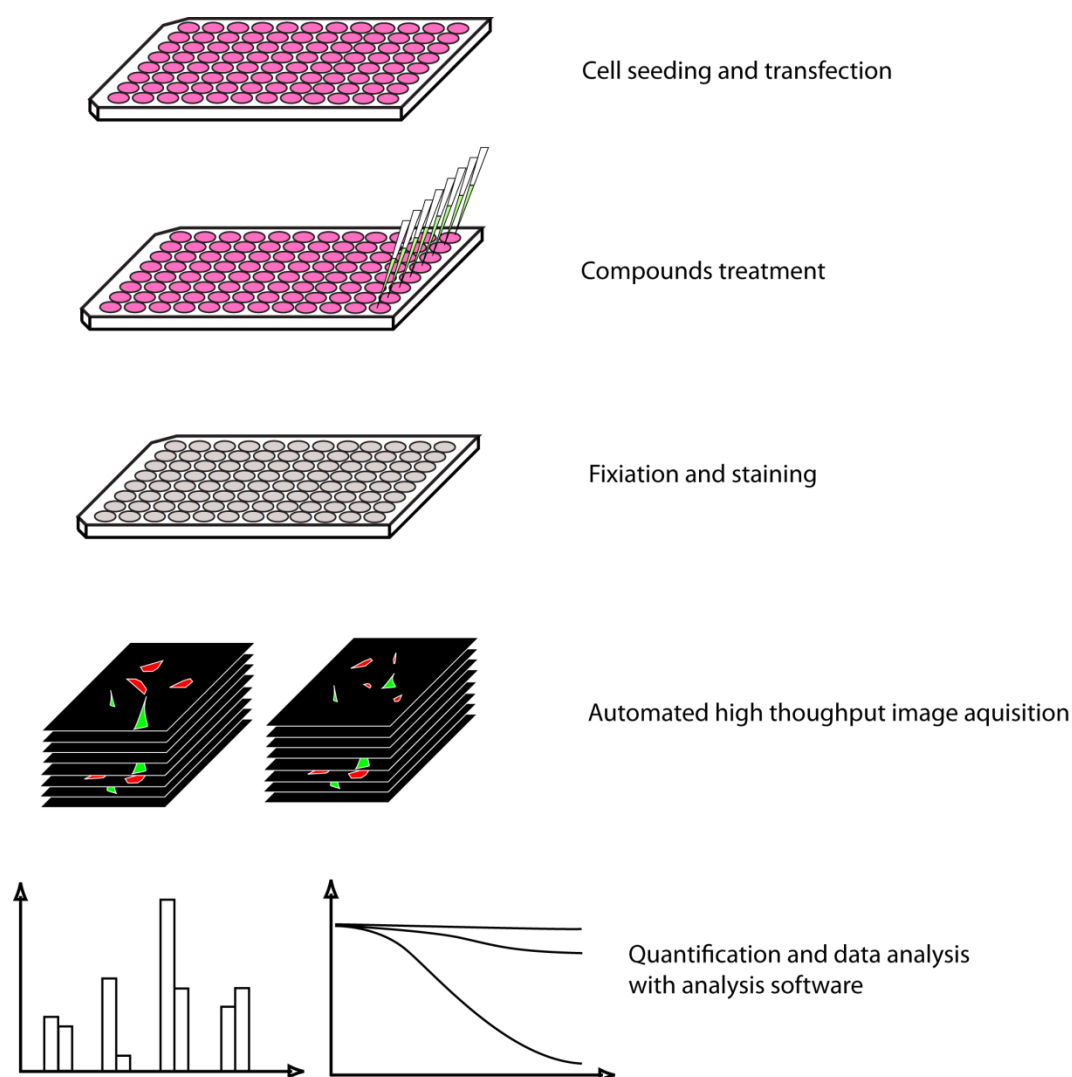


Fig. 17 Schematic representation of the F3H assay in 96-well plates. Cells are seeded, transfected, fixed and stained in a 96-well plate. Images of the DAPI, GFP and RFP channels were acquired with an InCell Analyzer. The data are then further analyzed by a project-specific software package to obtain information about the ratio of cells showing interaction and relative affinities of the interacting proteins.

To analyze the F3H images automatically, I developed an image analysis protocol. Firstly, images from DAPI channel were segmented depending on the size and intensities of signal to distinguish between the nuclear region and the background. Cells in apoptosis or mitosis can be filtered out by specific characteristics such as too high intensities, too small sizes or not enough roundness of the object area in comparison to normal cells. After this segmentation step, nuclear masks were generated, which contained the areas of every single nucleus. Secondly, we defined the GFP signal resulted from the *lacO*-anchored bait proteins. Within the nuclear mask regions, the GFP signal area having a higher intensity than the average whole nuclear GFP signal was selected, and was considered to be a region of *lacO*-anchored baits if the area had a suitable size as the known *lacO* spot. By adjusting the segmentation sensitivity, which is the intensity difference threshold to differentiate the object from the whole nucleus background, one

can distinguish most of the spot regions. For the next step of analysis, we proceeded with cells with one or two spots, which is the possible number of *lacO* spots per single cell, to exclude the GFP-bait negative cells without spots and cells with more than two spots derived from other nuclear structures. Finally, we measured the signal intensities of GFP and RFP in the nuclear and the spot area to calculate the intensity ratio at the *lacO* spot of RFP-prey and GFP-bait (Fig. 18).

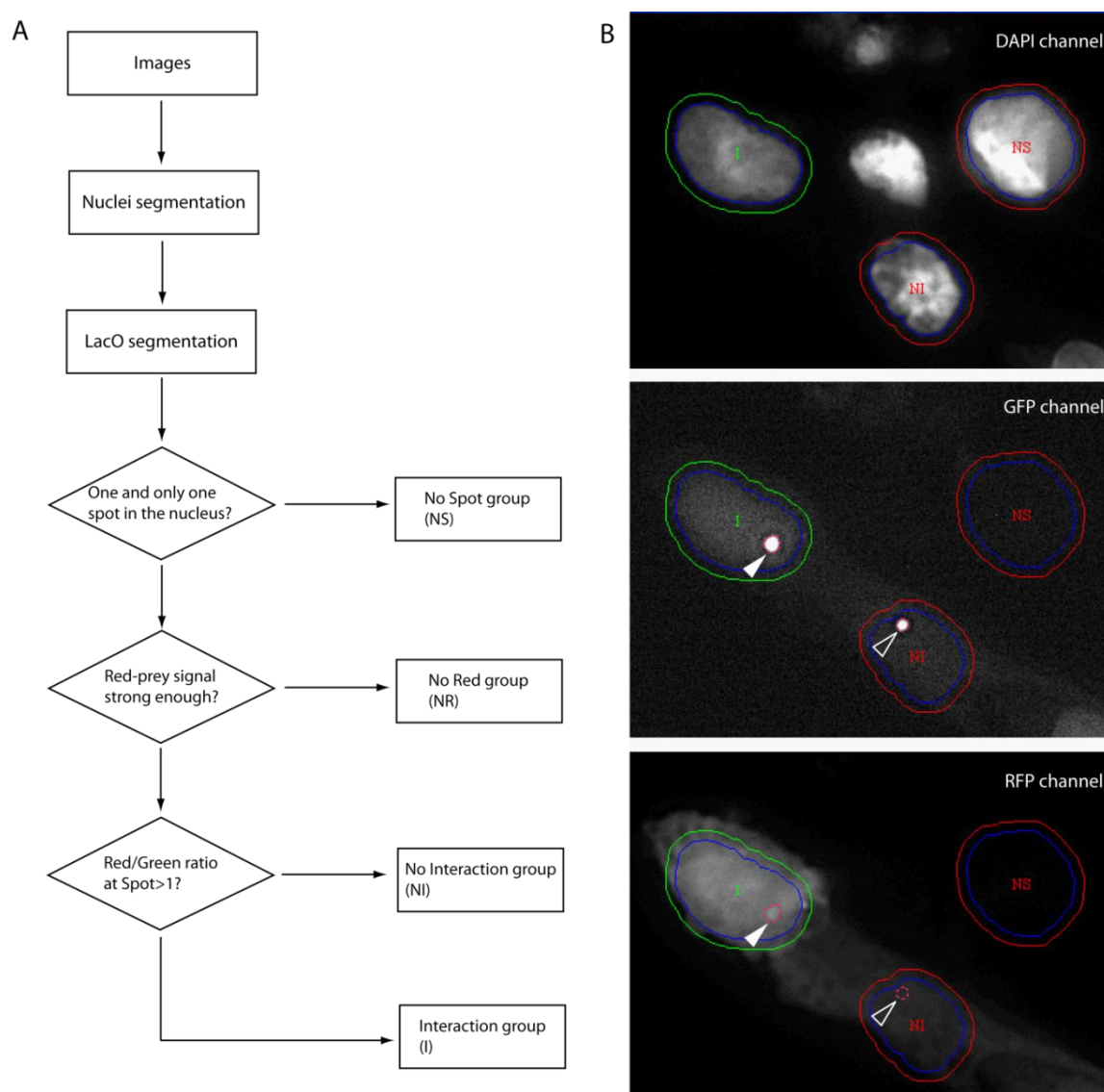


Fig. 18 High-throughput data analysis. (A) Workflow of data analysis and the decision-tree to subgroup the cells. Firstly, nuclear regions were identified using the intensities of the DAPI signal. Next, the *lacO* spot regions were segmented by the intensities of the GFP channel. The cells were divided into two groups depending on the number of recognized *lacO* spots. Cells with one spot are further analyzed by measuring the RFP intensity. Cells without detectable RFP signal are put into the 'No Red group'. Cells with RFP signal are grouped into 'non-interaction' (NI) group and 'interaction' (I) according to the RFP/GFP intensity ratio at the spot. (B) Image representing the automated image analysis. The nuclei were identified as indicated in blue lines. Red or green lines represent the cell area as an expansion of the nuclei. The *lacO* spots are shown in pink dashed lines. Cells without *lacO* spot are grouped into the 'No Spot' (NS) group. Cells with one spot are divided into 'Interaction' (I) or 'No Interaction' (NI) group, depending on their *lacO*/nucleus intensity ratio. Arrow heads point to the identified spots.

### 3.1.3 Developing a method for protein interaction inhibitor studies

The feature of the F3H assay to identify protein-protein interactions in living cell enables a broad variety of applications. One of the most innovative usages is to visualize protein interaction dynamics after inhibitor treatment, which makes this assay suitable for high-throughput compound testing in living cells.

The interaction between p53 and Mdm2 is of therapeutic interest because of its role in tumorigenesis. The specific inhibition of the interaction between p53 and Mdm2 is the most promising strategy to activate the p53-mediated apoptosis pathway in tumor cells. So far, several chemical compounds and peptide inhibitors were developed.

We used the F3H assay to visualize the interaction between GFP-p53 and RFP-hdm2 in living cells and to test different inhibitors such as nutlin-3 and Mi-63, which are known to inhibit this interaction (Vassilev et al., 2004; Canner et al., 2009). Consistent with previous studies, we could observe the inhibitory effects of these compounds with the F3H assay, demonstrating that this assay can be used to study PPI inhibitors. Although several other biochemical or biophysical methods for protein interaction inhibitor study - such as ELISA, fluorescent polarization (FP) and NMR - were developed (Graham et al., 2007; Choi et al., 2012; Shimaoka, 2012), the F3H assay has its unique advantages. First, the effect of the inhibitor (either compound or peptide) could be directly visualized in real time, thus giving an intuitive and direct output of the drug effect. Second, unlike *in vitro* assays such as NMR, the F3H assay studies the effect of inhibitors in living cells, thus the assay are performed under *in vivo* condition and provides information on cell permeability or cellular uptake and bio-availability. Third, the F3H assay is practically simple and does not need special equipment or complicate experimental procedure, which saves both labor and cost in large-scale screening.

In chapter 2.1 we monitored the dynamics of the p53/HDM2 interaction after inhibitor treatment using a spinning disc microscope. Interestingly, we found that after the drug (nutlin-3) being added into the cell, it only takes less than 3 minutes to completely show its effect. This means the diffusion of nutlin-3 into cells is quite fast, and the cellular membrane penetration of nutlin-3 is really effective. Besides the data shown in chapter 2.1, we also tested another compound, which showed an inhibitory effect in NMR study, but did not show any disruptive effect in our *in vivo* assay (unpublished data). The different inhibitory effects of these two compounds in this cell based assay may be due to low cell permeability of the drug. With the F3H assay, I also tested several peptide inhibitors which worked well in NMR, but none of these peptides can disrupt p53/HDM2 in F3H assay due to their bad permeability. These data showed the cellular uptake is one of the most important key factors for the drug to function. On the one hand, our method could directly identify the compounds with good cell permeability. On the other hand, this F3H assay could also miss those inhibitors which are not naturally permeable but can be made well permeable by further chemical modifications.

Even at low inhibitory nutlin-3 concentration, we could detect potential disruption of the p53/HDM2 interaction, indicating the high sensitivity of the F3H assay (Chapter 2.1 supplementary figure S4). At a concentration of 0.5  $\mu$ M, we could already see the effect of nutlin-3, and the half disruption concentration is between 1  $\mu$ M and 2  $\mu$ M, which are quite similar with other cell-based methods (Dudgeon et al., 2010; Li et al., 2011). Since there were no available data on nutlin-3 affinity to HDM2 in cells, our data for the first time give the information about nutlin-3 affinity in living cells. This affinity is approximately the same (Pazgier et al., 2009; Lawrence et al., 2009; 2011; Mochizuki et al., 2012) or slightly lower (Vassilev et al., 2004) than *in vitro*. This also showed that nutlin-3 is really efficient to penetrate into the cell.

In our studies in chapter 2.1, we studied the fast kinetics of the drug effect. Since the assay is based on living cell, this method can analyze drug characteristics that can not be assessed with traditional biochemical methods. Firstly, drug metabolism could be studied over a long time. After drug treatment, due to cellular drug metabolism and an effective drop of inhibitor concentration, the disrupted interaction protein pairs could re-interact so the drug pharmacokinetics (PK) profile could also be studied. Secondly, toxicity of the drug could also be assessed in our cell based studies. After drug treatment, the percentage surviving cells can be analyzed, which could be an indication of drug toxicity, or the effect of drug on cell cycle progression could be analyzed (Easwaran et al., 2005). Thirdly, drugs which may be functional only after being modified in cells could also be studied with this assay. This is very important to screen PPI inhibitor *de novo*, since some drugs work in such a way.

As a PPI and PPI inhibitor study method, it is necessary to perform the assay in a high through-put way for large scale PPI inhibitor analysis. We established the inhibitor assay in 96-well plates, tested with several inhibitors at different concentrations. With this medium through-put assay, we successfully observed the inhibitory effect of the drugs at different concentration and got inhibitory curves of different drugs. Consistent with previous studies (Canner et al., 2009), we found that both Mi-63 and nutlin-3 inhibit the interaction between p53 and HDM2 in living cells, and the inhibition effect of Mi-63 is about 10-times stronger than nutlin-3 at the same concentration. We could not observe any effect of another compound, RITA, which supports a previous study that showed RITA did not block the interaction between p53 and HDM2 *in vitro* by NMR (Krajewski et al., 2005). The next step would be try to establish a high throughput assay (e.g. 384-well plate assay) and use it to screen a compound library at large scale to identify new p53-HDM2 inhibitors, and also to expand this assay to other PPI inhibitor screening.

Peptide inhibitors were also tested in our study. In comparison with compound inhibitors which typically have a molecular weight around several hundred Dalton, peptides have much larger size and can not pass through cell membranes by free diffusion. To resolve this permeability problem, peptides could be either delivered by other vehicles such as liposome (Liu et al., 2010) or cell penetrating peptides (Schwarze et al., 1999; Derossi et al., 1994). In our study, we used the TAT cell-penetrating peptide

(derived from HIV Tat protein) to mediate cellular uptake of the inhibitory peptide. Since the TAT peptide has a similar size as the functional peptide, it may interfere and reduce the inhibitory efficiency of the functional peptide after entering into the cytoplasm. Therefore, we coupled the functional peptide D8A with cell-penetrating peptide TAT via a disulfide bond. Once the D8A peptide is transferred into cytosol together with TAT, the disulfide bridge will be cleaved releasing the D8A peptide from the TAT peptide. This eliminates the interference of the TAT peptide with D8A function. After cleavage, the peptide inhibitor is free to diffuse into the nucleus and the cytosol to bind to HDM2, while the TAT peptide would locate to the nucleolus (Lättig-Tünnemann et al., 2011). By this strategy, we can deliver the peptide inhibitors with a high efficiency and without reduce its inhibitory effects. Further studies on the stability and PK profile of the peptide should be performed in the future.

#### 3.1.4 Application of the GFP binding protein and nanobodies

By fusing the GFP binding protein to other proteins, we could target GFP fusion proteins to specific sites in living cells to study protein interactions. Another possible application is to use the GFP binding protein to study protein functions as we discussed in chapter 3.1.1, for example, targeting of Tet (Ten-eleven translocation) proteins to the *lacO* heterochromatin site could study its DNA hydroxylation activity by monitoring the 5-hmC change at the *lacO* locus (unpublished data). Besides all these application mentioned above, GBP could be used to target and manipulate GFP fusion proteins in special biological pathways.

Caussinus *et al* developed a method to degrade proteins in living cell using a GFP antibody fragment. They first generated a *sqh* gene knockout fly and rescued the fly with *sqh-gfp* fusion. Then the researchers used the anti-GFP VHH domain to substitute the substrate-recognition domain of the F-box protein, which is an adaptor protein mediating the proteasomal degradation of its substrate proteins. This F-Box-GBP protein binds to SQH-GFP fusion proteins *in vivo*, and targets it onto E3 ligase. The SQH-GFP fusion proteins are thus poly-ubiquitinated by the E3 ligase and degraded by ubiquitin-mediated proteasomal degradation. Using the GFP binding protein, they successfully generated the loss-of-function phenotypes of SQH in *drosophila* embryo (Caussinus et al., 2012). In their study, they targeted GFP fusion protein into ubiquitin mediated protein degradation pathways *in vivo* using a transgene fly. The targeting process is indirect and quite complicate. To make it simpler and without traditional genetic modification, we are trying to directly target endogenous cellular protein for destruction using nanobodies in living cell. And also we are trying to target and manipulate endogenous proteins in different pathways such as signal transduction pathways, cellular apoptotic pathways in living cells This could be a powerful and simple method to manipulate and study the function of proteins *in vivo*.



## 3.2 Cell cycle coupled control of CENP-A incorporation

During S phase, nucleosomes have to be destabilized to release free DNA prior to DNA replication. After replication, DNA together with histones re-organize into nucleosomes and form chromatin. After this process, not only the genetical information, but also the epigenetical information, such as DNA methylation, histone modifications and also histone variants in the nucleosomes, have to be replicated and stably transmitted to daughter cells. CENP-A, a histone H3 variant, specifically incorporates into centromeric chromatin and is the essential factor of centromere formation in metazoans. It was shown that the genetic ablation of CENP-A lead to severe defects in genome stability. How the CENP-A level is maintained at centromeres to keep the stability of the centromere after cell division is a basic question and it is also the key to understand the mechanism how the centromeres are determined in higher eukaryotes.

### 3.2.1 Recruitment of Mis18bp1 to the centromere

To understand the mechanism how CENP-A is maintained during cell-cycle, It is crucial to identify at which stage of the cell cycle, the newly synthesized CENP-A incorporates into the centromere. The synthesis of CENP-A protein peaks in S phase, but its incorporation is uncoupled with its synthesis (Shelby et al., 2000; Jansen et al., 2007). In contrast to the replication-coupled assembly of canonical histones during S phase, the incorporation of newly synthesized CENP-A occurs from late telophase to the G1 phase of the cell cycle in human cells (Jansen et al., 2007). This time period of CENP-A incorporation is surprising. On the one hand, CENP-A is most abundant in S phase. On the other hand, in S phase after DNA replication the nucleosome is reassembled and most histone variants are incorporate into chromatin at this time. There is evidence that after DNA replication in S phase, H3.3 first incorporated into the histone gaps resulted from replication, and then H3.3 was substituted by CENP-A in the next G1 phase (Dunleavy et al., 2011). This incorporation pattern reflects the special character and function of CENP-A nucleosome. As one of the key factors required for CENP-A deposition, M18bp1 localizes to the centromere in a cell cycle-dependent way. To study the role of mouse M18bp1 in CENP-A deposition, the localization of M18bp1 during the cell cycle in mouse cells were analyzed. A GFP knock-in mouse embryonic stem (mES) cell line was generated to observe the localization of endogenous M18bp1. It was shown that M18bp1 associates with centromeric chromatin from anaphase to G1 phase in mES (Chapter 2.2). These data are consistent with a previous study which showed that human M18BP1 associates at centromeres from late telophase to G1 phase (Fujita et al., 2007). The similar centromere localization of M18bp1 in mouse and human cells suggests that the role of M18bp1 in CENP-A loading is conserved in mammals.

Since the time window of M18bp1 at centromere is clear, we asked the question what is the role of CCAN proteins in M18bp1 mediated CENP-A incorporation. Using our F3H method, we screened the interactions between CCAN members and M18bp1 to identify

CENPs that play a role in M18bp1 recruitment. We found CENP-C was the only CCAN member which interacts with and recruits M18bp1 to centromeres. CENP-C is believed to be a platform for the assembly of the kinetochore (Przewloka et al., 2011). It recognizes the CENP-A nucleosome and connects the centromeric chromatin with the outer kinetochore by interacting with the Mis12 complex (Carroll et al., 2010; Screpanti et al., 2011). Our findings revealed a new function of CENP-C in CENP-A deposition, i.e. facilitating M18bp1 recruitment to the centromere.

To further test the role of CENP-C in M18bp1 mediated CENP-A incorporation, siRNA-mediated knock-down experiments of CENP-C were performed and showed that the localization of M18bp1 and CENP-A at centromeres was reduced. These results are consistent with a similar study, which showed that CENP-C interacts with M18bp1 in human and *Xenopus* cells, and that the depletion of CENP-C results in disruption of CENP-A incorporation in G1 phase (Moree et al., 2011). The level of M18bp1 at centromeres decreased but not totally disappeared when CENP-C was knocked-down in our experiments (Chapter 2.2). This could either result from the remaining CENP-C, which could still recruit M18bp1 to centromeres or from CENP-C being partially responsible for the M18bp1 centromeric localization, possibly pointing to alternative mechanisms for the centromeric recruitment of M18bp1.

### 3.2.2 Mis18 complex regulates the epigenetic state of centromeric chromatin

M18bp1 together with Mis18 $\alpha$  and Mis18 $\beta$  forms the so-called Mis18 complex. This complex was shown to be essential for incorporation of newly synthesized CENP-A into the centromere. Interestingly, none of these three proteins shows a direct interaction with Cenp-A (Fujita et al, 2007). Also, the centromeric localization of this complex occurs from anaphase to mid G1, just prior to CENP-A incorporation. These data suggest that the complex is involved indirectly in CENP-A assembly. In the current model of CENP-A assembly, the role of Mis18 complex is believed to be a license factor to regulate the start of CENP-A incorporation.

Fujita *et al* found that Trichostatin A (TSA), which is a histone deacetylase inhibitor, could suppress the phenotype which resulted from Mis18 complex defects (Fujita et al, 2007). This suggests that the Mis18 complex regulates chromatin modifications such as acetylation. Recently Kim *et al* did not find a rescue effect of TSA in cells with Mis18 $\alpha$  defect, but they found that the Mis18 complex modulates DNA methylation and histone modifications at centromeric chromatin (Kim et al., 2012). These results support the idea that the Mis18 complex regulates CENP-A loading by changing the epigenetic state of the centromeric chromatin.

The epigenetic state of centromeric chromatin is not fully understood yet. Centromeric chromatin was considered as heterochromatin in early studies. But later studies correct this idea. It was reported that centromeric H3 was marked by transcriptional active markers such as mono- and di-methylation of H3K4 and di- and trimethylation of H3K36 (Sullivan and Karpen, 2004; Gopalakrishnan et al., 2009; Bergmann et al., 2011, 2012).

Some centromeric transcripts were also found in a variety of species (Chen et al., 2008; Ferri et al., 2009, Pezer and Ugarkovic, 2008, Chan et al., 2012). These data showed that centrochromatin contains both euchromatin and heterochromatin. A recent study showed a role of H3K9 acetylation/methylation balance in the incorporation of CENP-A (Ohzeki et al., 2012). They found that the *de novo* formation of ectopic centromere can be facilitated by histone acetyltransferases (HATs) and be blocked by histone H3K9 methyltransferase Suv39h1, and that M18bp1 is not required for HATs induced *de novo* assembly of ectopic centromere, suggesting that it works in the early step of the CENP-A incorporation.

Altogether, these data suggest that the Mis18 complex indeed is an epigenetic regulator recruiting HATs to increase the acetylation level at centromeric chromatin to facilitate the assembly of nucleosomes and thus regulates the incorporation of CENP-A.

### 3.2.3 Cell cycle-dependent regulation of the Mis18 complex and CENP-A incorporation

As discussed above, CENP-A expression and assembly occurs independently in a short time window during the cell cycle. When CENP-A was constitutively expressed, the assembly still only happened in G1 phase (Jansen et al., 2007). This suggests that the incorporation of CENP-A is cell cycle-dependent controlled by a mechanism independent of the CENP-A expression.

While CENP-C is a CCAN member which localizes at the centromeres during the whole cell cycle, our study showed that its interacting partner M18bp1 is present at centromeres only from anaphase to G1 phase. This indicates that the interaction between CENP-C and M18bp1 is cell cycle-dependent. As shown in chapter 2.2, we found that in the GFP knock-in K1B2 mES cells, some cells with high CENP-C localization but without M18bp1 enrichment at centromeres were observed. This observation also supports the idea that M18bp1/CENP-C interaction is cell cycle-dependent. However, a cell cycle-dependent interaction between these two proteins was not observed in the F3H assay, this could be due to the over-expression of CENP-C and M18bp1, so that the regulatory machinery may not be able to control the interaction correctly.

So it is really interesting to understand the regulation mechanism behind this cell cycle-dependent interaction. Silva *et al* found that the Cdk1 (cyclin-dependent kinase 1) and Cdk2 control CENP-A assembly during the cell cycle (Silva et al., 2012).

Cdk1 and Cdk2 are mainly active during S, G2 and the M phase of the cell cycle. Cdk1 and Cdk2 associate with cyclin B and cyclin A, respectively, and regulate CENP-A incorporation by phosphorylating M18bp1. In S, G2 and M phase, M18bp1 is phosphorylated which prevents its binding to centromeres in HeLa cells, and in the other cell cycle phases (later telophase and G1) unphosphorylated M18bp1 localizes and plays its role at the centromere (Silva et al., 2012). These data are consistent with our observation (Chapter 2.2 Fig. 1). However, it remains elusive whether this phosphorylation mediates the inhibition of the interaction between CENP-C and

M18bp1 and whether this phosphorylation of M18bp1 regulates its centromeric localization. Our current data show that the middle part of M18bp1 (from aa 441 to aa 800), which contains the SANT domain, is responsible for its interaction with CENP-C. Future studies with the possible phosphorylation site mutants are necessary to test whether the phosphorylation of this SANT domain is the regulatory mechanism of the cell cycle-dependent interaction between CENP-C and M18bp1.

In summary, our data are consistent with and contribute to a model for the regulation of Mis18 complex in CENP-A incorporation (Silva et al., 2012). From anaphase to G1 phase, the Mis18 complex localizes at the centromere by interacting with CENP-C which stays at centromeric chromatin during all cell cycle phases. The Mis18 complex then recruits HATs, which acetylate histones in the centromeric chromatin. The acetylated centromeric chromatin then is opened by chromatin remodelers to assemble newly synthesized CENP-A into centromeric chromatin by its chaperon HJURP. During S, G2 and M phase, HJURP, M18bp1 and other related proteins are phosphorylated, and the phosphorylation of M18bp1 prevents its centromeric localization. Cdk1 and Cdk2 phosphorylate a variety of proteins S, G2 and M phase of the cell cycle, thus inhibit CENP-A incorporation (Fig. 19).

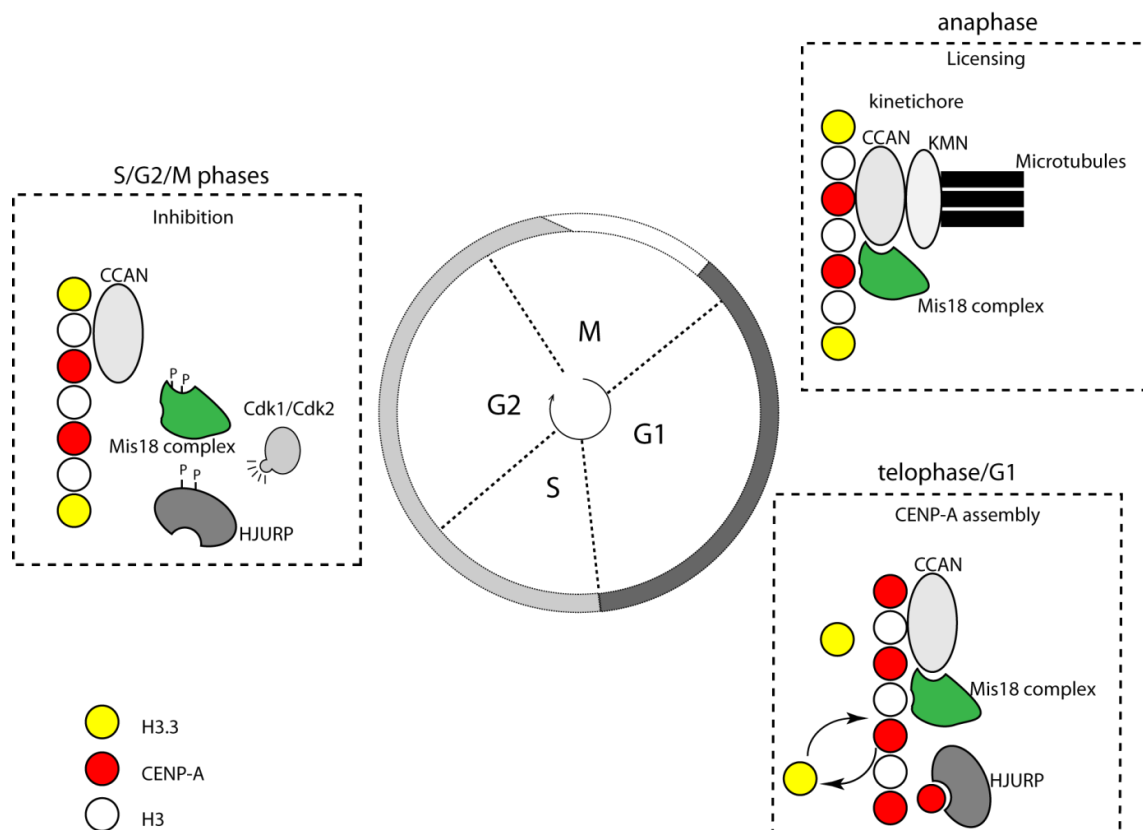


Fig. 19 Model of CENP-A incorporation control during the cell cycle. From anaphase to G1 phase, the Mis18 complex is recruited by CENP-C to the centromere and recruits HATs to acetylate the histones at the centromere. The acetylated nucleosomes lead to more open chromatin to allow the CENP-A incorporation mediated by its chaperon HJURP. During the S, G2 and M phase, both HJURP and M18bp1 are phosphorylated by Cdk1 and Cdk2. These phosphorylated proteins can not bind to centromeric chromatin, and the incorporation of CENP-A is inhibited in these cell cycle phases. (Figure modified from Valenta et al., 2012)

Although this model could give an overview of the CENP-A incorporation regulation in different cell cycles, there are still some open questions. How does the Mis18 complex regulate the epigenetic states of centromeric chromatin? What is the difference between CENP-A chromatin and canonical H3 chromatin? And also why is the CENP-A incorporation not associated with DNA replication? Further studies are necessary to answer these questions and complete the model in more details.

### 3.3 Assembly of CENP-O class protein

#### 3.3.1 Dependency of CCAN protein assembly

The kinetochore is composed of multiple proteins. Of these multiple proteins, the CCAN members localize at centromeres during the whole cell cycle, and the other proteins only localize to centromeres in mitosis when forming the entire functional kinetochore. The CCAN proteins coordinate and form the core of the kinetochore, bridging the gap between outer kinetochore (KMN) and the centromeric chromatin. However, how these CCAN proteins are organized is still not clear.

Among these 16 CCAN proteins, CENP-A is a histone H3 variant which forms centromeric nucleosomes. Centromeric chromatin, including CENP-A nucleosomes and its adjacent H3 nucleosomes, must be recognized by other members of the CCANs so that the CCAN could assemble at the chromatin site. CENP-C and CENP-N are important proteins to connect CCANs with centromeric chromatin, since they were shown to bind to CENP-A nucleosome (Carroll et al., 2009, 2010; Guse et al., 2011). And also, recent studies showed that the CENP-T/W/S/X together form a special centromeric chromatin to supercoil the DNA at centromeres. These data show that CENP-A and CENP-T/W/S/X act at the most basic level of forming centromeric chromatin. It is essential to investigate how the other CCAN members recognize the basic level structure and gradually assemble to a kinetochore.

CCAN proteins are grouped into different classes depending on their assembly similarity. The CENP-P/O/R/Q/U was reported to form a complex when expressed in *E. coli*, and the phenotypes are similar when each of the members is knocked-out in chicken DT40 cell (Hori et al., 2008). Knock-out of single member of CENP-P/O/R/Q/U family proteins did not show mitotic defects (Hori et al., 2008). The centromeric localization of CENP-P/O/R/Q/U depends on the CENP-H class proteins. However, the CENP-P/O/R/Q/U group of proteins does not affect the localization of CENP-H class proteins (Hori et al., 2008). According to previous studies, the CENP-P/O/R/Q/U is at the last step of the CCAN complex stepwise assembly in the current model (Takeuchi and Fukagawa, 2012). In chapter 2.3, we found that CENP-N, -H and -L can recruit three CENP-P/O/R/Q/U members - CENP-O, -U and -R. But another centromeric protein, CENP-C, which is a platform of kinetochore assembly, is not responsible for recruiting of CENP-P/O/R/Q/U proteins to the kinetochore. Our data are consistent with the previous model and clarified the CENP-P/O/R/Q/U recruiting mechanism.

#### 3.3.2 The CENP-P/O/R/Q/U is not a pre-assembled complex

Studies in *E.coli* suggested that CENP-P/O/R/Q/U form a pre-assembled stable sub-complex and then the sub-complex is assembled as a whole unit into the kinetochore (Hori et al., 2008). To understand whether this is true in mammalian cells, interactions between the members of this class were tested. We observed interactions between most members of the CENP-P/O/R/Q/U by F3H *in vivo*, and found that most members of

this group can recruit some of the others but not all members to the ectopic *lacO* chromosomal site. However, the FCCS data showed that only part of the free CENP-O/P and a little CENP-Q/R in the nucleus can form heterodimers before their assembly into the kinetochore (Chapter 2.3 Figure 4A).

While the F3H data showed that most members of the CENP-P/O/R/Q/U family can recruit some of the other members, the FCCS data suggest that the suspected pre-assembled complex does not exist. One possible explanation for these data is that the assembly of these CENPs to kinetochores needs certain post-translational modifications on the CENPs. Once the protein is marked with this modification, it will be assembled with the other members onto the kinetochore. These modified and assembled CENPs could be detected as the interactions at the ectopic chromosomal site in F3H assay. At the same time, the free nucleoplasmic CENP-P/O/R/Q/U class proteins which lack this modification could not assemble onto the kinetochore and do not show a dimerization in FCCS assay. A recent study supports this hypothesis. It was shown that localization of the CENP-U/Q complex at kinetochores was controlled by Plk1 (polo-like kinase 1)-mediated phosphorylation (Kang et al., 2011). Indeed, the fact that none of the five members of this group can recruit all the other members in the F3H assay also suggests the pre-assembled complex does not exist in cells.

Furthermore, in chapter 2.3 Table 3 the FRAP data of the CENP- P/O/R/Q/U members showed that CENP-P, -O and -R had a similar turnover pattern at centromeres during the cell cycle, but CENP-U and CENP-R showed a different behavior as CENP- P/O/R.

Altogether, our data indicate that the CENP-P/O/R/Q/U family proteins are not pre-assembled as a sub-complex before their kinetochore assembly, and the CENP-P/O/R/Q/U proteins do not always act as one single unit but as a cluster of individual proteins with their own features.

### 3.3.3 Self-assembly of the CENP-P/O/R/Q/U at kinetochores

In chapter 2.3, we observed multiple interactions between the CENP-P/O/R/Q/U members. While the pre-assembly model for the CENP-P/O/R/Q/U sub-complex is excluded, the interactions between the CENP-P/O/R/Q/U members are likely to contribute to their assembly into a stable CENP-P/O/R/Q/U sub-complex at kinetochore. Consistent with a previous study (Hemmerich et al., 2011), our data support a stepwise assembly model, of which the CENP-O/P heterodimer and the CENP-P, -O, -R, -Q and -U single unit are recruited and assembled into the kinetochore depending on their interactions.

Among these five members, the F3H assay shows CENP-U and CENP-R form a homodimer. The FRET data also showed that CENP-U and CENP-U molecules are close to each other at kinetochores, but FCCS showed the free CENP-U in the nucleoplasm is not dimerized. These data suggest that, the free nucleoplasmic CENP-U exists as monomer, and when it is recruited to the kinetochore, it dimerizes and this dimerization contributes to the assembly of CENP-U. Likewise, CENP-Q is shown oligomerizing into

octamers when expressed in *E.coli* (Amaro et al., 2010). The FRET assay also detected the close proximity between the CENP-Q molecules in late S phase, when a fully functional kinetochore is formed. However, both FCCS and F3H did not show this homo-dimerization/-oligomerization. These data suggest that this dimerization or oligomerization only occurs when CENP-U and CENP-Q is assembled at kinetochores and may contribute to the assembly of CENP-U and -Q.

This dimerization of CENP-U and CENP-Q indicates that there is more than one copy of these two proteins in one CCAN complex if the dimerization happens in one CCAN (intraCCAN); if the dimerization happens between two CCANs, this would indicate that this dimerization of proteins connects the adjacent CCANs and increases the stability of kinetochores structure. Since CENP-Q and CENP-U are involved in microtubule attachment, this intra/inter CCAN dimerization offers more anchor points for the microtubules and contributes to spindle formation (Amaro et al., 2010; Hua et al., 2011). The FRET data showed that the members of CENP-P/O/R/Q/U are close to each other when they are assembled at the kinetochore. CENP-U is shown close to CENP-B and CENP-I but not close to the CENPs which directly bind centromeric chromatin such as CENP-A or CENP-C in the kinetochore (Hellwig et al., 2009). However, the details of how CENP-P/O/R/Q/U are organized within the CCAN complex and how two adjacent CCAN complexes are connected to each other is still largely unknown. To clarify these questions, systematic studies of the interactions between all the CCAN members have to be performed. We already investigated the interactions between the CCAN members by F3H assay, but further studies are necessary to understand the structure and the assembly mechanism of the CCAN complex.



## 4. Annex

### 4.1 References

- Amano, M., Suzuki, A., Hori, T., Backer, C., Okawa, K., Cheeseman, I. M. and Fukagawa, T. (2009) The CENP-S complex is essential for the stable assembly of outer kinetochore structure. *The Journal of Cell Biology*, 186, 173-182.
- Amaro, A. C., Samora, C. P., Holtackers, R., Wang, E., Kingston, I. J., Alonso, M., Lampson, M., McAinsh, A. D. and Meraldi, P. (2010) Molecular control of kinetochore-microtubule dynamics and chromosome oscillations. *Nature Cell Biology*, 12, 319-329.
- Ando, S., Yang, H., Nozaki, N., Okazaki, T. and Yoda, K. (2002) CENP-A, -B, and -C chromatin complex that contains the I-type  $\alpha$ -satellite array constitutes the prekinetochore in HeLa cells. *Molecular and Cellular Biology*, 22, 2229-2241.
- Baker, S. J., Fearon, E. R., Nigro, J. M., Hamilton, Preisinger, A. C., Jessup, J. M., vanTuinen, P., Ledbetter, D. H., Barker, D. F., Nakamura, Y., White, R. and Vogelstein, B. (1989) Chromosome 17 deletions and p53 gene mutations in colorectal carcinomas. *Science*, 244, 217-221.
- Barak, Y., Juven, T., Haffner, R. and Oren, M. (1993) Mdm2 expression is induced by wild type p53 activity. *EMBO J*, 12, 461-468.
- Barnhart, M. C., Kuich, P. H. J. L., Stellfox, M. E., Ward, J. A., Bassett, E. A., Black, B. E. and Foltz, D. R. (2011) HJURP is a CENP-A chromatin assembly factor sufficient to form a functional de novo kinetochore. *The Journal of Cell Biology*, 194, 229-243.
- Bassett, E., DeNizio, J., Barnhart-Dailey, M., Panchenko, T., Sekulic, N., Rogers, D., Foltz, D. and Black, B. (2012) HJURP uses distinct CENP-A surfaces to recognize and to stabilize CENP-A/histone H4 for centromere assembly. *Developmental Cell*, 22, 749-762.
- Baudendistel, N., Müller, G., Waldeck, W., Angel, P. and Langowski, J. (2005) Two-hybrid fluorescence cross-correlation spectroscopy detects protein-protein interactions in vivo. *ChemPhysChem*, 6, 984-990.
- Bergmann, J. H., Jakubsche, J. N., Martins, N. M., Kagansky, A., Nakano, M., Kimura, H., Kelly, D. A., Turner, B. M., Masumoto, H., Larionov, V. and Earnshaw, W. C. (2012) Epigenetic engineering: histone H3K9 acetylation is compatible with kinetochore structure and function. *Journal of Cell Science*, 125, 411-421.
- Bergmann, J. H., Rodriguez, M. G., Martins, N. M. C., Kimura, H., Kelly, D. A., Masumoto, H., Larionov, V., Jansen, L. E. T. and Earnshaw, W. C. (2011) Epigenetic engineering shows H3K4me2 is required for HJURP targeting and CENP-A assembly on a synthetic human kinetochore. *EMBO J*, 30, 328-340.
- Bernstein, D. S., Buter, N., Stumpf, C. and Wickens, M. (2002) Analyzing mRNA-protein complexes using a yeast three-hybrid system. *Methods*, 26, 123-141.
- Black, B. E., Foltz, D. R., Chakravarthy, S., Luger, K., Woods, V. L. and Cleveland, D. W. (2004) Structural determinants for generating centromeric chromatin. *Nature*, 430, 578-582.
- Black, B. E., Jansen, L. E. T., Maddox, P. S., Foltz, D. R., Desai, A. B., Shah, J. V. and Cleveland, D. W. (2007) Centromere identity maintained by nucleosomes assembled with histone H3 containing the CENP-A targeting domain. *Molecular Cell*, 25, 309-322.
- Bottger, V., Bottger, A., Howard, S. F., Picksley, S. M., Chene, P., Garcia-Echeverria, C., Hochkeppel, H. K. and Lane, D. P. (1996) Identification of novel mdm2 binding peptides by phage display. *Oncogene*, 13, 2141-2147.

- Brown, M. T., Goetsch, L. and Hartwell, L. H. (1993) MIF2 is required for mitotic spindle integrity during anaphase spindle elongation in *Saccharomyces cerevisiae*. *The Journal of Cell Biology*, 123, 387-403.
- Bush, S. M., Folta, S. and Lannigan, D. A. (1996) Use of the yeast one-hybrid system to screen for mutations in the ligand-binding domain of the estrogen receptor. *Steroids*, 61, 102-109.
- Camahort, R., Li, B., Florens, L., Swanson, S. K., Washburn, M. P. and Gerton, J. L. (2007) Scm3 is essential to recruit the histone H3 variant cse4 to centromeres and to maintain a functional kinetochore. *Molecular Cell*, 26, 853-865.
- Carroll, C. W., Silva, M. C. C., Godek, K. M., Jansen, L. E. T. and Straight, A. F. (2009) Centromere assembly requires the direct recognition of CENP-A nucleosomes by CENP-N. *Nature Cell Biology*, 11, 896-902.
- Caussinus, E., Kanca, O. and Affolter, M. (2012) Fluorescent fusion protein knockout mediated by anti-GFP nanobody. *Nature Structure Molecular Biology*, 19, 117-121.
- Chan, F. L., Marshall, O. J., Saffery, R., Won Kim, B., Earle, E., Choo, K. H. A. and Wong, L. H. (2012) Active transcription and essential role of RNA polymerase II at the centromere during mitosis. *Proceedings of the National Academy of Sciences*, 109, 1979-1984.
- Chang, C., Simmons, D. T., Martin, M. A. and Mora, P. T. (1979) Identification and partial characterization of new antigens from simian virus 40-transformed mouse cells. *Journal of Virology*, 31, 463-471.
- Cheeseman, I. M., Chappie, J. S., Wilson-Kubalek, E. M. and Desai, A. (2006) The conserved KMN network constitutes the core microtubule-binding site of the kinetochore. *Cell*, 127, 983-997.
- Cheeseman, I. M. and Desai, A. (2008) Molecular architecture of the kinetochore-microtubule interface. *Nat Rev Mol Cell Biol*, 9, 33-46.
- Chen, E. S., Zhang, K., Nicolas, E., Cam, H. P., Zofall, M. and Grewal, S. I. S. (2008) Cell cycle control of centromeric repeat transcription and heterochromatin assembly. *Nature*, 451, 734-737.
- Chen, L., Yin, H., Farooqi, B., Sebt, S., Hamilton, A. D. and Chen, J. (2005) p53 alpha-Helix mimetics antagonize p53/MDM2 interaction and activate p53. *Molecular Cancer Therapeutics*, 4, 1019-1025.
- Chikashige, Y., Kinoshita, N., Nakaseko, Y., Matsumoto, T., Murakami, S., Niwa, O. and Yanagida, M. (1989) Composite motifs and repeat symmetry in *S. pombe* centromeres: Direct analysis by integration of NotI restriction sites. *Cell*, 57, 739-751.
- Choi, J. W., Kang, D. K., Park, H., deMello, A. J. and Chang, S. I. (2012) High-throughput analysis of protein-protein interactions in picoliter-volume droplets using fluorescence polarization. *Analytical Chemistry*, 84, 3849-3854.
- Chun, Y., Park, B., Koh, W., Lee, S., Cheon, Y., Kim, R., Che, L. and Lee, S. (2011) New centromeric component CENP-W is a RNA-associated nuclear matrix protein that interacts with nucleophosmin (B23). *J. Biol. Chem*, 286, 42758-42769.
- Clarke, L. and Baum, M. P. (1990) Functional analysis of a centromere from fission yeast: a role for centromere-specific repeated DNA sequences. *Molecular and Cellular Biology*, 10, 1863-1872.
- Clarke, L. and Carbon, J. (1980) Isolation of a yeast centromere and construction of functional small circular chromosomes. *Nature*, 287, 504-509.
- Clegg, H. V., Itahana, K. and Zhang, Y. (2008) Unlocking the mdm2-p53 loop: ubiquitin is the key. *Cell Cycle*, 7, 287-292.

- Coffman, V. C., Wu, P., Parthun, M. R. and Wu, J.-Q. (2011) CENP-A exceeds microtubule attachment sites in centromere clusters of both budding and fission yeast. *The Journal of Cell Biology*, 195, 563-572.
- Conde e Silva, N., Black, B. E., Sivolob, A., Filipski, J., Cleveland, D. W. and Prunell, A. (2007) CENP-A-containing nucleosomes: easier disassembly versus exclusive centromeric localization. *Journal of Molecular Biology*, 370, 555-573.
- DeLeo, A. B., Jay, G., Appella, E., Dubois, G. C., Law, L. W. and Old, L. J. (1979) Detection of a transformation-related antigen in chemically induced sarcomas and other transformed cells of the mouse. *Proceedings of the National Academy of Sciences*, 76, 2420-2424.
- Derossi, D., Joliot, A. H., Chassaing, G. and Prochiantz, A. (1994) The third helix of the Antennapedia homeodomain translocates through biological membranes. *Journal of Biological Chemistry*, 269, 10444-10450.
- Ding, K., Lu, Y., Nikolovska-Coleska, Z., Wang, G., Qiu, S., Shangary, S., Gao, W., Qin, D., Stuckey, J., Krajewski, K., Roller, P. P. and Wang, S. (2006) Structure-based design of spiro-oxindoles as potent, specific small-molecule inhibitors of the MDM2-p53 interaction. *Journal of Medicinal Chemistry*, 49, 3432-3435.
- Dippold, W. G., Jay, G., DeLeo, A. B., Khoury, G. and Old, L. J. (1981) p53 transformation-related protein: Detection by monoclonal antibody in mouse and human cells. *Proceedings of the National Academy of Sciences*, 78, 1695-1699.
- Dudgeon, DD., Shinde, SN., Shun, TY., Lazo, JS., Strock, CJ., Giuliano, KA., Taylor, DL., Johnston, PA. and Johnston, PA. (2010) Characterization and optimization of a novel protein-protein interaction biosensor high-content screening assay to identify disruptors of the interactions between p53 and hDM2. *Assay Drug Dev Technol*, 8, 437-458.
- Duli, V., Kaufmann, W. K., Wilson, S. J., Tlsty, T. D., Lees, E., Harper, J. W., Elledge, S. J. and Reed, S. I. (1994) p53-dependent inhibition of cyclin-dependent kinase activities in human fibroblasts during radiation-induced G1 arrest. *Cell*, 76, 1013-1023.
- Dunleavy, E. M., Pidoux, A. L., Monet, M., Bonilla, C., Richardson, W., Hamilton, G. L., Ekwall, K., McLaughlin, P. J. and Allshire, R. C. (2007) A NASP (N1/N2)-related protein, sim3, binds CENP-A and is required for its deposition at fission yeast centromeres. *Molecular Cell*, 28, 1029-1044.
- Dunleavy, E. M., Roche, D., Tagami, H., Lacoste, N., Ray-Gallet, D., Nakamura, Y., Daigo, Y., Nakatani, Y. and Almouzni-Pettinotti, G. (2009) HJURP is a cell-cycle-dependent maintenance and deposition factor of CENP-A at centromeres. *Cell*, 137, 485-497.
- Dunleavy, E.M., Almouzni, G. and Karpen, G.H. (2011) H3.3 is deposited at centromeres in S phase as a placeholder for newly assembled CENP-A in G1 phase. *Nucleus*, 2, 146-157.
- Easwaran, HP., Leonhardt, H., and Cardoso, MC. (2005) Cell cycle markers for live cell analyses. *Cell Cycle*, 4, 453-455
- Earnshaw, W. C. and Rothfield, N. (1985) Identification of a family of human centromere proteins using autoimmune sera from patients with scleroderma. *Chromosoma*, 91, 313-321.
- El-Deiry, W. S., Kern, S. E., Pietenpol, J. A., Kinzler, K. W. and Vogelstein, B. (1992) Definition of a consensus binding site for p53. *Nature Genetics*, 1, 45-49.
- El-Deiry, W. S., Tokino, T., Velculescu, V. E., Levy, D. B., Parsons, R., Trent, J. M., Lin, D., Mercer, W. E., Kinzler, K. W. and Vogelstein, B. (1993) WAF1, a potential mediator of p53 tumor suppression. *Cell*, 75, 817-825.
- Elson, E. L. and Magde, D. (1974) Fluorescence correlation spectroscopy. I. Conceptual basis and theory. *Biopolymers*, 13, 1-27.

- Fabbro, M. and Henderson, B. R. (2003) Regulation of tumor suppressors by nuclear-cytoplasmic shuttling. *Experimental Cell Research*, 282, 59-69.
- Fan, J. Y., Cui, Z. Q., Wei, H. P., Zhang, Z. P., Zhou, Y. F., Wang, Y. P. and Zhang, X. E. (2008) Split mCherry as a new red bimolecular fluorescence complementation system for visualizing protein-protein interactions in living cells. *Biochemical and Biophysical Research Communications*, 367, 47-53.
- Fang, S., Jensen, J. P., Ludwig, R. L., Vousden, K. H. and Weissman, A. M. (2000) Mdm2 is a RING finger-dependent ubiquitin protein ligase for itself and p53. *Journal of Biological Chemistry*, 275, 8945-8951.
- Fernandez-Suarez, M., Chen, T. S. and Ting, A. Y. (2008) Protein-protein interaction detection in vitro and in cells by proximity biotinylation. *J Am Chem Soc*, 130, 9251-9253.
- Ferri, F., Bouzinba-Segard, H., Velasco, G., Hube, F. and Francastel, C. (2009) Non-coding murine centromeric transcripts associate with and potentiate Aurora B kinase. *Nucleic Acids Res*, 37, 5071-5080.
- Fields, S. and Song, O.-k. (1989) A novel genetic system to detect protein-protein interactions. *Nature*, 340, 245-246.
- Finlay, C. A., Hinds, P. W. and Levine, A. J. (1989) The p53 proto-oncogene can act as a suppressor of transformation. *Cell*, 57, 1083-1093.
- Fitzgerald-Hayes, M., Clarke, L. and Carbon, J. (1982) Nucleotide sequence comparisons and functional analysis of yeast centromere DNAs. *Cell*, 29, 235-244.
- Foltz, D. R., Jansen, L. E. T., Bailey, A. O., Yates, J. R., Bassett, E. A., Wood, S., Black, B. E. and Cleveland, D. W. (2009) Centromere-Specific Assembly of CENP-A Nucleosomes Is Mediated by HJURP. *Cell*, 137, 472-484.
- Foltz, D. R., Jansen, L. E. T., Black, B. E., Bailey, A. O., Yates, J. R. and Cleveland, D. W. (2006) The human CENP-A centromeric nucleosome-associated complex. *Nat Cell Biol*, 8, 458-469.
- Fowler, K. J., Hudson, D. F., Salamonsen, L. A., Edmondson, S. R., Earle, E., Sibson, M. C. and Choo, K. H. A. (2000) Uterine dysfunction and genetic modifiers in centromere protein B-deficient mice. *Genome Research*, 10, 30-41.
- Fukagawa, T. and Brown, W. R. A. (1997) Efficient conditional mutation of the vertebrate CENP-C gene. *Human Molecular Genetics*, 6, 2301-2308.
- Fukagawa, T., Mikami, Y., Nishihashi, A., Regnier, V., Haraguchi, T., Hiraoka, Y., Sugata, N., Todokoro, K., Brown, W. and Ikemura, T. (2001) CENP-H, a constitutive centromere component, is required for centromere targeting of CENP-C in vertebrate cells. *EMBO J*, 20, 4603-4617.
- Fukagawa, T., Pendon, C., Morris, J. and Brown, W. (1999) CENP-C is necessary but not sufficient to induce formation of a functional centromere. *EMBO J*, 18, 4196-4209.
- Furuyama, S. and Biggins, S. (2007) Centromere identity is specified by a single centromeric nucleosome in budding yeast. *Proceedings of the National Academy of Sciences*, 104, 14706-14711.
- Galatin, P. S. and Abraham, D. J. (2004) A nonpeptidic sulfonamide inhibits the p53-mdm2 interaction and activates p53-dependent transcription in mdm2-overexpressing cells. *J Med Chem*, 47, 4163-4165.
- Garcia-Echeverria, C., Chene, P., Blommers, M. J. and Furet, P. (2000) Discovery of potent antagonists of the interaction between human double minute 2 and tumor suppressor p53. *J Med Chem*, 43, 3205-3208.

- Gascoigne, K., Takeuchi, K., Suzuki, A., Hori, T., Fukagawa, T. and Cheeseman, I. (2011) Induced Ectopic Kinetochores Bypasses the Requirement for CENP-A Nucleosomes. *Cell*, 145, 410-422.
- Ghosh, I., Hamilton, A. D. and Regan, L. (2000) Antiparallel leucine zipper-directed protein reassembly: application to the green fluorescent protein. *Journal of the American Chemical Society*, 122, 5658-5659.
- Gopalakrishnan, S., Sullivan, B. A., Trazzi, S., Della Valle, G. and Robertson, K. D. (2009) DNMT3B interacts with constitutive centromere protein CENP-C to modulate DNA methylation and the histone code at centromeric regions. *Human Molecular Genetics*, 18, 3178-3193.
- Graham, N. A., Pope, M. D., Rimchala, T., Huang, B. K. and Asthagiri, A. R. (2007) A microtiter assay for quantifying protein-protein interactions associated with cell-cell adhesion. *Journal of Biomolecular Screening*, 12, 683-693.
- Grasberger, B. L., Lu, T., Schubert, C., Parks, D. J., Carver, T. E., Koblisch, H. K., Cummings, M. D., LaFrance, L. V., Milkiewicz, K. L., Calvo, R. R., Maguire, D., Lattanze, J., Franks, C. F., Zhao, S., Ramachandren, K., Bylebyl, G. R., Zhang, M., Manthey, C. L., Petrella, E. C., Pantoliano, M. W., Deckman, I. C., Spurlino, J. C., Maroney, A. C., Tomczuk, B. E., Molloy, C. J. and Bone, R. F. (2005) Discovery and cocrystal structure of benzodiazepinedione HDM2 antagonists that activate p53 in cells. *Journal of Medicinal Chemistry*, 48, 909-912.
- Greaves, I. K., Rangasamy, D., Ridgway, P. and Tremethick, D. J. (2007) H2A.Z contributes to the unique 3D structure of the centromere. *Proceedings of the National Academy of Sciences*, 104, 525-530.
- Grunstein, M. (1997) Histone acetylation in chromatin structure and transcription. *Nature*, 389, 349-352.
- Guse, A., Carroll, C. W., Moree, B., Fuller, C. J. and Straight, A. F. (2011) In vitro centromere and kinetochore assembly on defined chromatin templates. *Nature*, 477, 354-358.
- Hahnenberger, K. M., Baum, M. P., Polizzi, C. M., Carbon, J. and Clarke, L. (1989) Construction of functional artificial minichromosomes in the fission yeast *Schizosaccharomyces pombe*. *Proceedings of the National Academy of Sciences*, 86, 577-581.
- Hahnenberger, K. M., Carbon, J. and Clarke, L. (1991) Identification of DNA regions required for mitotic and meiotic functions within the centromere of *Schizosaccharomyces pombe* chromosome I. *Molecular and Cellular Biology*, 11, 2206-2215.
- Hansen, R. S., Wijmenga, C., Luo, P., Stanek, A. M., Canfield, T. K., Weemaes, C. M. R. and Gartler, S. M. (1999) The DNMT3B DNA methyltransferase gene is mutated in the ICF immunodeficiency syndrome. *Proceedings of the National Academy of Sciences*, 96, 14412-14417.
- Harms, K. L. and Chen, X. (2006) The functional domains in p53 family proteins exhibit both common and distinct properties. *Cell Death Differ*, 13, 890-897.
- Haupt, Y., Maya, R., Kazanietz, A. and Oren, M. (1997) Mdm2 promotes the rapid degradation of p53. *Nature*, 387, 296-299.
- Hellwig, D., Hoischen, C., Ulbricht, T. and Diekmann, S. (2009) Acceptor-photobleaching FRET analysis of core kinetochore and NAC proteins in living human cells. *European Biophysics Journal*, 38, 781-791.
- Hemmerich, P., Schmiedeberg, L. and Diekmann, S. (2011) Dynamic as well as stable protein interactions contribute to genome function and maintenance. *Chromosome Res*, 19, 131-151.

- Hemmerich, P., Weidtkamp-Peters, S., Hoischen, C., Schmiedeberg, L., Erliandri, I. and Diekmann, S. (2008) Dynamics of inner kinetochore assembly and maintenance in living cells. *The Journal of Cell Biology*, 180, 1101-1114.
- Henikoff, S. and Henikoff, J. G. (2012) 'Point' centromeres of *Saccharomyces* harbor single centromere-specific nucleosomes. *Genetics*, 190, 1575-1577.
- Hieter, P., Pridmore, D., Hegemann, J. H., Thomas, M., Davis, R. W. and Philippsen, P. (1985) Functional selection and analysis of yeast centromeric DNA. *Cell*, 42, 913-921.
- Hollstein, M., Shomer, B., Greenblatt, M., Soussi, T., Hovig, E., Montesano, R. and Harris, C. C. (1996) Somatic point mutations in the p53 gene of human tumors and cell Lines: updated compilation. *Nucleic Acids Research*, 24, 141-146.
- Hollstein, M., Sidransky, D., Vogelstein, B. and Harris, C. C. (1991) p53 mutations in human cancers. *Science*, 253, 49-53.
- Honda, R., Tanaka, H. and Yasuda, H. (1997) Oncoprotein MDM2 is a ubiquitin ligase E3 for tumor suppressor p53. *FEBS letters*, 420, 25-27.
- Hori, T., Amano, M., Suzuki, A., Backer, C. B., Welburn, J. P., Dong, Y., McEwen, B. F., Shang, W.-H., Suzuki, E., Okawa, K., Cheeseman, I. M. and Fukagawa, T. (2008a) CCAN makes multiple contacts with centromeric DNA to provide distinct pathways to the outer kinetochore. *Cell*, 135, 1039-1052.
- Hori, T., Okada, M., Maenaka, K. and Fukagawa, T. (2008b) CENP-O class proteins form a stable complex and are required for proper kinetochore function. *Molecular Biology of the Cell*, 19, 843-854.
- Hu, C. D., Chinenov, Y. and Kerppola, T. K. (2002) Visualization of interactions among bZIP and Rel family proteins in living cells using bimolecular fluorescence complementation. *Molecular Cell*, 9, 789-798.
- Hu, C. D. and Kerppola, T. K. (2003) Simultaneous visualization of multiple protein interactions in living cells using multicolor fluorescence complementation analysis. *Nat Biotech*, 21, 539-545.
- Hua, S., Wang, Z., Jiang, K., Huang, Y., Ward, T., Zhao, L., Dou, Z. and Yao, X. (2011) CENP-U cooperates with Hec1 to orchestrate kinetochore-microtubule attachment. *Journal of Biological Chemistry*, 286, 1627-1638.
- Huang, H., Jedynek, B. M. and Bader, J. S. (2007) Where have all the interactions gone? estimating the coverage of two-hybrid protein interaction maps. *PLoS Comput Biol*, 3, e214.
- Hudson, D. F., Fowler, K. J., Earle, E., Saffery, R., Kalitsis, P., Trowell, H., Hill, J., Wreford, N. G., de Kretser, D. M., Cancilla, M. R., Howman, E., Hii, L., Cutts, S. M., Irvine, D. V. and Choo, K. H. A. (1998) Centromere protein B null mice are mitotically and meiotically normal but have lower body and testis weights. *The Journal of Cell Biology*, 141, 309-319.
- Itahana, K., Mao, H., Jin, A., Itahana, Y., Clegg, H. V., Lindström, M. S., Bhat, K., Godfrey, V. L., Evan, G. I. and Zhang, Y. (2007) Targeted inactivation of mdm2 RING finger E3 ubiquitin ligase activity in the mouse reveals mechanistic insights into p53 regulation. *Cancer Cell*, 12, 355-366.
- Ito, T., Chiba, T., Ozawa, R., Yoshida, M., Hattori, M. and Sakaki, Y. (2001) A comprehensive two-hybrid analysis to explore the yeast protein interactome. *Proceedings of the National Academy of Sciences*, 98, 4569-4574.
- Izuta, H., Ikeno, M., Suzuki, N., Tomonaga, T., Nozaki, N., Obuse, C., Kisu, Y., Goshima, N., Nomura, F., Nomura, N. and Yoda, K. (2006) Comprehensive analysis of the ICEN

- (Interphase Centromere Complex) components enriched in the CENP-A chromatin of human cells. *Genes to Cells*, 11, 673-684.
- Jach, G., Pesch, M., Richter, K., Frings, S. and Uhrig, J. F. (2006) An improved mRFP1 adds red to bimolecular fluorescence complementation. *Nat Meth*, 3, 597-600.
- Jaco, I., Canela, A., Vera, E. and Blasco, M. A. (2008) Centromere mitotic recombination in mammalian cells. *The Journal of Cell Biology*, 181, 885-892.
- James, P., Halladay, J. and Craig, E. A. (1996) Genomic libraries and a host strain designed for highly efficient two-hybrid selection in yeast. *Genetics*, 144, 1425-1436.
- Jansen, L. E. T., Black, B. E., Foltz, D. R. and Cleveland, D. W. (2007) Propagation of centromeric chromatin requires exit from mitosis. *The Journal of Cell Biology*, 176, 795-805.
- Jeanpierre, M., Turleau, C., Aurias, A., Prieur, M., Ledest, F., Fischer, A. and Viegas-Pequignot, E. (1993) An embryonic-like methylation pattern of classical satellite DNA is observed in ICF syndrome. *Human Molecular Genetics*, 2, 731-735.
- Johnsson, N. and Varshavsky, A. (1994) Split ubiquitin as a sensor of protein interactions in vivo. *Proceedings of the National Academy of Sciences*, 91, 10340-10344.
- Kang, Y. H., Park, C. H., Kim, T. S., Soung, N. K., Bang, J. K., Kim, B. Y., Park, J. E. and Lee, K. S. (2011) Mammalian polo-like kinase 1-dependent regulation of the PBIP1-CENP-Q complex at kinetochores. *J Biol Chem*, 286, 19744-19757.
- Kawai, H., Wiederschain, D., Kitao, H., Stuart, J., Tsai, K. K. C. and Yuan, Z.-M. (2003) DNA damage-induced MDMX degradation is mediated by MDM2. *Journal of Biological Chemistry*, 278, 45946-45953.
- Kerppola, T. K. (2006) Visualization of molecular interactions by fluorescence complementation. *Nat Rev Mol Cell Biol*, 7, 449-456.
- Kim, I. S., Lee, M., Park, K. C., Jeon, Y., Park, J. H., Hwang, E. J., Jeon, T. I., Ko, S., Lee, H., Baek, S. H. and Kim, K. I. (2012) Roles of Mis18alpha in epigenetic regulation of centromeric chromatin and CENP-A loading. *Mol Cell*, 46, 260-273.
- Koblish, H. K., Zhao, S., Franks, C. F., Donatelli, R. R., Tominovich, R. M., LaFrance, L. V., Leonard, K. A., Gushue, J. M., Parks, D. J., Calvo, R. R., Milkiewicz, K. L., Marugan, J. J., Raboisson, P., Cummings, M. D., Grasberger, B. L., Johnson, D. L., Lu, T., Molloy, C. J. and Maroney, A. C. (2006) Benzodiazepinedione inhibitors of the Hdm2:p53 complex suppress human tumor cell proliferation in vitro and sensitize tumors to doxorubicin in vivo. *Mol Cancer Ther*, 5, 160-169.
- Koo, D. H., Han, F., Birchler, J. A. and Jiang, J. (2011) Distinct DNA methylation patterns associated with active and inactive centromeres of the maize B chromosome. *Genome Research*, 21, 908-914.
- Krajewski, M., Ozdowj, P., D'Silva, L., Rothweiler, U. and Holak, T. A. (2005) NMR indicates that the small molecule RITA does not block p53-MDM2 binding in vitro. *Nat Med*, 11, 1135-1136; author reply 1136-1137.
- Krassovsky, K., Henikoff, J. G. and Henikoff, S. (2011) Tripartite organization of centromeric chromatin in budding yeast. *Proceedings of the National Academy of Sciences*, 109, 243-248.
- Kubbutat, M. H. G., Jones, S. N. and Vousden, K. H. (1997) Regulation of p53 stability by Mdm2. *Nature*, 387, 299-303.
- Kuhn, R. M., Clarke, L. and Carbon, J. (1991) Clustered tRNA genes in *Schizosaccharomyces pombe* centromeric DNA sequence repeats. *Proceedings of the National Academy of Sciences*, 88, 1306-1310.

- Kulyyassov, A., Shoaib, M., Pichugin, A., Kannouche, P., Ramanculov, E., Lipinski, M. and Ogryzko, V. (2011) PUB-MS: A mass spectrometry-based method to monitor protein-protein proximity in vivo. *Journal of Proteome Research*, 10, 4416-4427.
- Kunitoku, N., Sasayama, T., Marumoto, T., Zhang, D., Honda, S., Kobayashi, O., Hatakeyama, K., Ushio, Y., Saya, H. and Hirota, T. (2003) CENP-A phosphorylation by Aurora-A in prophase is required for enrichment of Aurora-B at inner centromeres and for kinetochore function. *Developmental Cell*, 5, 853-864.
- Kuo, M. H., Brownell, J. E., Sobel, R. E., Ranalli, T. A., Cook, R. G., Edmondson, D. G., Roth, S. Y. and Allis, C. D. (1996) Transcription-linked acetylation by Gcn5p of histones H3 and H4 at specific lysines. *Nature*, 383, 269-272.
- Kussie, P. H., Gorina, S., Marechal, V., Elenbaas, B., Moreau, J., Levine, A. J. and Pavletich, N. P. (1996) Structure of the MDM2 oncoprotein bound to the p53 tumor suppressor transactivation domain. *Science*, 274, 948-953.
- Kwon, M. S., Hori, T., Okada, M. and Fukagawa, T. (2007) CENP-C is involved in chromosome segregation, mitotic checkpoint function, and kinetochore assembly. *Molecular Biology of the Cell*, 18, 2155-2168.
- Lagana, A., Dorn, J. F., De Rop, V., Ladouceur, A.-M., Maddox, A. S. and Maddox, P. S. (2010) A small GTPase molecular switch regulates epigenetic centromere maintenance by stabilizing newly incorporated CENP-A. *Nat Cell Biol*, 12, 1186-1193.
- Lahav, G., Rosenfeld, N., Sigal, A., Geva-Zatorsky, N., Levine, A. J., Elowitz, M. B. and Alon, U. (2004) Dynamics of the p53-Mdm2 feedback loop in individual cells. *Nat Genet*, 36, 147-150.
- Lawrimore, J., Bloom, K. S. and Salmon, E. D. (2011) Point centromeres contain more than a single centromere-specific Cse4 (CENP-A) nucleosome. *The Journal of Cell Biology*, 195, 573-582.
- Lättig-Tünnemann, G., Prinz, M., Hoffmann, D., Behlke, J., Palm-Apergi, C., Morano, I., Herce, HD. and Cardoso, MC., (2011) Backbone rigidity and static presentation of guanidinium groups increases cellular uptake of arginine-rich cell-penetrating peptides. *Nat Commun*, 2, 453. doi:10.1038/ncomms1459.
- Li, J., Zhang, S., Gao, L., Chen, Y. and Xie, X. (2011) A cell-based high-throughput assay for the screening of small-molecule inhibitors of p53-MDM2 interaction. *Journal of Biomolecular Screening*, 16, 450-456.
- Licitra, E. and Liu, J. (1996) A three-hybrid system for detecting small ligand-protein receptor interactions. *Proceedings of the National Academy of Sciences*, 93, 12817-12821.
- Linares, L. K., Hengstermann, A., Ciechanover, A., Mueller, S. and Scheffner, M. (2003) HdmX stimulates Hdm2-mediated ubiquitination and degradation of p53. *Proceedings of the National Academy of Sciences*, 100, 12009-12014.
- Linzer, D. I. H. and Levine, A. J. (1979) Characterization of a 54K Dalton cellular SV40 tumor antigen present in SV40-transformed cells and uninfected embryonal carcinoma cells. *Cell*, 17, 43-52.
- Liu, M., Li, C., Pazgier, M., Li, C., Mao, Y., Lv, Y., Gu, B., Wei, G., Yuan, W., Zhan, C., Lu, W.-Y. and Lu, W. (2010b) D-peptide inhibitors of the p53-MDM2 interaction for targeted molecular therapy of malignant neoplasms. *Proceedings of the National Academy of Sciences*, 107, 14321-14326.
- Liu, M., Pazgier, M., Li, C., Yuan, W., Li, C. and Lu, W. (2010a) A left-handed solution to peptide inhibition of the p53-MDM2 interaction. *Angewandte Chemie International Edition*, 49, 3649-3652.



- Liu, S. T., Hittle, J. C., Jablonski, S. A., Campbell, M. S., Yoda, K. and Yen, T. J. (2003) Human CENP-I specifies localization of CENP-F, MAD1 and MAD2 to kinetochores and is essential for mitosis. *Nat Cell Biol*, 5, 341-345.
- Liu, S. T., Rattner, J. B., Jablonski, S. A. and Yen, T. J. (2006) Mapping the assembly pathways that specify formation of the trilaminar kinetochore plates in human cells. *The Journal of Cell Biology*, 175, 41-53.
- Llères, D., Swift, S. and Lamond, A. I. (2007) Detecting protein-protein interactions in vivo with FRET using multiphoton fluorescence lifetime imaging microscopy (FLIM). *Current Protocols in Cytometry*. Chapter 12, unit 12.10.
- Lorincz, M. C., Dickerson, D. R., Schmitt, M. and Groudine, M. (2004) Intragenic DNA methylation alters chromatin structure and elongation efficiency in mammalian cells. *Nat Struct Mol Biol*, 11, 1068-1075.
- Lu, Y., Nikolovska-Coleska, Z., Fang, X., Gao, W., Shangary, S., Qiu, S., Qin, D. and Wang, S. (2006) Discovery of a nanomolar inhibitor of the human murine double minute 2 (MDM2)-p53 interaction through an integrated, virtual database screening strategy. *Journal of Medicinal Chemistry*, 49, 3759-3762.
- Luo, S. and Preuss, D. (2003) Strand-biased DNA methylation associated with centromeric regions in Arabidopsis. *Proceedings of the National Academy of Sciences*, 100, 11133-11138.
- Maddox, P. S., Corbett, K. D. and Desai, A. (2012) Structure, assembly and reading of centromeric chromatin. *Current Opinion in Genetics & Development*, 22, 139-147.
- Magde, D., Elson, E. L. and Webb, W. W. (1974) Fluorescence correlation spectroscopy. II. An experimental realization. *Biopolymers*, 13, 29-61.
- Mahadevan, L. C., Willis, A. C. and Barratt, M. J. (1991) Rapid histone H3 phosphorylation in response to growth factors, phorbol esters, okadaic acid, and protein synthesis inhibitors. *Cell*, 65, 775-783.
- Matson, D. R., Demirel, P. B., Stukenberg, P. T. and Burke, D. J. (2012) A conserved role for COMA/CENP-H/I/N kinetochore proteins in the spindle checkpoint. *Genes & Development*, 26, 542-547.
- Matsuda, E., Sugioka-Sugiyama, R., Mizuguchi, T., Mehta, S., Cui, B. and Grewal, S. I. S. (2011) A homolog of male sex-determining factor SRY cooperates with a transposon-derived CENP-B protein to control sex-specific directed recombination. *Proceedings of the National Academy of Sciences*, 108, 18754-18759.
- McClelland, S. E., Borusu, S., Amaro, A. C., Winter, J. R., Belwal, M., McAinsh, A. D. and Meraldi, P. (2007) The CENP-A NAC/CAD kinetochore complex controls chromosome congression and spindle bipolarity. *EMBO J*, 26, 5033-5047.
- McGrew, J., Diehl, B. and Fitzgerald-Hayes, M. (1986) Single base-pair mutations in centromere element III cause aberrant chromosome segregation in *Saccharomyces cerevisiae*. *Molecular and Cellular Biology*, 6, 530-538.
- Milks, K. J., Moree, B. and Straight, A. F. (2009) Dissection of CENP-C directed Centromere and Kinetochore Assembly. *Molecular Biology of the Cell*, 20, 4246-4255.
- Mizuguchi, G., Xiao, H., Wisniewski, J., Smith, M. M. and Wu, C. (2007) Nonhistone scm3 and histones cenH3-H4 assemble the core of centromere-specific nucleosomes. *Cell*, 129, 1153-1164.
- Momand, J., Zambetti, G. P., Olson, D. C., George, D. and Levine, A. J. (1992) The mdm-2 oncogene product forms a complex with the p53 protein and inhibits p53-mediated transactivation. *Cell*, 69, 1237-1245.

- Moree, B., Meyer, C. B., Fuller, C. J. and Straight, A. F. (2011) CENP-C recruits M18BP1 to centromeres to promote CENP-A chromatin assembly. *J Cell Biol*, 194, 855-871.
- Murakami, S., Matsumoto, T., Niwa, O. and Yanagida, M. (1991) Structure of the fission yeast centromere cen3: direct analysis of the reiterated inverted region. *Chromosoma*, 101, 214-221.
- Shimaoka, M., Nishida, N. and Shimada, I. An NMR method to study protein - protein Interactions in integrin and cell adhesion molecules, *Methods in Molecular Biology*, 757, 129-137.
- Nishihashi, A., Haraguchi, T., Hiraoka, Y., Ikemura, T., Regnier, V., Dodson, H., Earnshaw, W. C. and Fukagawa, T. (2002) CENP-I is essential for centromere function in vertebrate cells. *Developmental Cell*, 2, 463-476.
- Nishino, T., Takeuchi, K., Gascoigne, K., Suzuki, A., Hori, T., Oyama, T., Morikawa, K., Cheeseman, I. and Fukagawa, T. (2012) CENP-T-W-S-X forms a unique centromeric chromatin structure with a histone-like fold. *Cell*, 148, 487-501.
- Obuse, C., Yang, H., Nozaki, N., Goto, S., Okazaki, T. and Yoda, K. (2004) Proteomics analysis of the centromere complex from HeLa interphase cells: UV-damaged DNA binding protein 1 (DDB-1) is a component of the CEN-complex, while BMI-1 is transiently co-localized with the centromeric region in interphase. *Genes to Cells*, 9, 105-120.
- Ohzeki, J.-i., Bergmann, J. H., Kouprina, N., Noskov, V. N., Nakano, M., Kimura, H., Earnshaw, W. C., Larionov, V. and Masumoto, H. (2012) Breaking the HAC Barrier: Histone H3K9 acetyl/methyl balance regulates CENP-A assembly. *Embo J*, 31, 2391-2402.
- Okada, M., Cheeseman, I. M., Hori, T., Okawa, K., McLeod, I. X., Yates, J. R., Desai, A. and Fukagawa, T. (2006) The CENP-H-I complex is required for the efficient incorporation of newly synthesized CENP-A into centromeres. *Nat Cell Biol*, 8, 446-457.
- Oliner, J. D., Pietenpol, J. A., Thiagalingam, S., Gyuris, J., Kinzler, K. W. and Vogelstein, B. (1993) Oncoprotein MDM2 conceals the activation domain of tumour suppressor p53. *Nature*, 362, 857-860.
- Olivier, M., Eeles, R., Hollstein, M., Khan, M. A., Harris, C. C. and Hainaut, P. (2002) The IARC TP53 database: new online mutation analysis and recommendations to users. *Hum Mutat*, 19, 607-614.
- Palmer, D. K., O'Day, K., Trong, H. L., Charbonneau, H. and Margolis, R. L. (1991) Purification of the centromere-specific protein CENP-A and demonstration that it is a distinctive histone. *Proceedings of the National Academy of Sciences*, 88, 3734-3738.
- Palmer, D. K., O'Day, K., Wener, M. H., Andrews, B. S. and Margolis, R. L. (1987) A 17-kD centromere protein (CENP-A) copurifies with nucleosome core particles and with histones. *The Journal of Cell Biology*, 104, 805-815.
- Panchenko, T., Sorensen, T. C., Woodcock, C. L., Kan, Z.-y., Wood, S., Resch, M. G., Luger, K., Englander, S. W., Hansen, J. C. and Black, B. E. (2011) Replacement of histone H3 with CENP-A directs global nucleosome array condensation and loosening of nucleosome superhelical termini. *Proceedings of the National Academy of Sciences*, 108, 16588-16593.
- Parant, J., Chavez-Reyes, A., Little, N. A., Yan, W., Reinke, V., Jochemsen, A. G. and Lozano, G. (2001) Rescue of embryonic lethality in Mdm4-null mice by loss of Trp53 suggests a nonoverlapping pathway with MDM2 to regulate p53. *Nature genetics*, 29, 92-95.
- Park, Y. J., Dyer, P. N., Tremethick, D. J. and Luger, K. (2004) A new fluorescence resonance energy transfer approach demonstrates that the histone variant H2AZ stabilizes the

- histone octamer within the nucleosome. *Journal of Biological Chemistry*, 279, 24274-24282.
- Paulmurugan, R. and Gambhir, S. S. (2005) Firefly luciferase enzyme fragment complementation for imaging in cells and living animals. *Analytical Chemistry*, 77, 1295-1302.
- Paulmurugan, R., Umezawa, Y. and Gambhir, S. S. (2002) Noninvasive imaging of protein-protein interactions in living subjects by using reporter protein complementation and reconstitution strategies. *Proceedings of the National Academy of Sciences*, 99, 15608-15613.
- Pearson, C. G., Yeh, E., Gardner, M., Odde, D., Salmon, E. D. and Bloom, K. (2004) Stable kinetochore-microtubule attachment constrains centromere positioning in metaphase. *Current Biology*, 14, 1962-1967.
- Pelletier, J. N., Campbell-Valois, F. X. and Michnick, S. W. (1998) Oligomerization domain-directed reassembly of active dihydrofolate reductase from rationally designed fragments. *Proceedings of the National Academy of Sciences*, 95, 12141-12146.
- Perez-Castro, A. V., Shamanski, F. L., Meneses, J. J., Lovato, T. L., Vogel, K. G., Moyzis, R. K. and Pedersen, R. (1998) Centromeric protein B null mice are viable with no apparent abnormalities. *Developmental biology*, 201, 135-143.
- Perpelescu, M., Nozaki, N., Obuse, C., Yang, H. and Yoda, K. (2009) Active establishment of centromeric CENP-A chromatin by RSF complex. *The Journal of Cell Biology*, 185, 397-407.
- Pezer, Z. and Ugarkovic, D. (2008) RNA Pol II promotes transcription of centromeric satellite DNA in beetles. *PLoS ONE*, 3, e1594.
- Pietenpol, J. A., Tokino, T., Thiagalingam, S., el-Deiry, W. S., Kinzler, K. W. and Vogelstein, B. (1994) Sequence-specific transcriptional activation is essential for growth suppression by p53. *Proceedings of the National Academy of Sciences*, 91, 1998-2002.
- Polizzi, C. and Clarke, L. (1991) The chromatin structure of centromeres from fission yeast: differentiation of the central core that correlates with function. *The Journal of Cell Biology*, 112, 191-201.
- Prendergast, L., van Vuuren, C., Kaczmarczyk, A., Doering, V., Hellwig, D., Quinn, N., Hoischen, C., Diekmann, S. and Sullivan, K. F. (2011) Premitotic assembly of human CENPs -T and -W switches centromeric chromatin to a mitotic state. *PLoS Biol*, 9, e1001082.
- Przewloka, M. R., Venkei, Z., Bolanos-Garcia, V. M., Debski, J., Dadlez, M. and Glover, D. M. (2011) CENP-C is a structural platform for kinetochore assembly. *Current biology*, 21, 399-405.
- Puig, O., Caspary, F., Rigaut, G., Rutz, B., Bouveret, E., Bragado-Nilsson, E., Wilm, M. and Seraphin, B. (2001) The Tandem Affinity Purification (TAP) Method: a general procedure of protein complex purification. *Methods*, 24, 218-229.
- Remy, I. and Michnick, S. W. (2006) A highly sensitive protein-protein interaction assay based on Gaussia luciferase. *Nat Meth*, 3, 977-979.
- Rizwana, R. and Hahn, P. J. (1999) CpG methylation reduces genomic instability. *Journal of Cell Science*, 112, 4513-4519.
- Robida, A. M. and Kerppola, T. K. (2009) Bimolecular fluorescence complementation analysis of inducible protein interactions: effects of factors affecting protein folding on fluorescent protein fragment association. *Journal of Molecular Biology*, 394, 391-409.
- Robinett, C. C., Straight, A., Li, G., Willhelm, C., Sudlow, G., Murray, A. and Belmont, A. S. (1996) In vivo localization of DNA sequences and visualization of large-scale chromatin organization using lac operator/repressor recognition. *The Journal of Cell Biology*, 135, 1685-1700.

- Rothbauer, U., Zolghadr, K., Muyldermans, S., Schepers, A., Cardoso, M. C. and Leonhardt, H. (2008) A versatile nanotrap for biochemical and functional studies with fluorescent fusion proteins. *Mol Cell Proteomics*, 7, 282-289.
- Roux, K. J., Kim, D. I., Raida, M. and Burke, B. (2012) A promiscuous biotin ligase fusion protein identifies proximal and interacting proteins in mammalian cells. *The Journal of Cell Biology*, 196, 801-810.
- Rutkowska, A., Haering, C. H. and Schultz, C. (2011) A FIAsh-Based cross-linker to study protein interactions in living cells. *Angewandte Chemie International Edition*, 50, 12655-12658.
- Saitoh, H., Tomkiel, J., Cooke, C. A., Ratrie Iii, H., Maurer, M., Rothfield, N. F. and Earnshaw, W. C. (1992) CENP-C, an autoantigen in scleroderma, is a component of the human inner kinetochore plate. *Cell*, 70, 115-125.
- Sakurai, K., Schubert, C. and Kahne, D. (2006) Crystallographic analysis of an 8-mer p53 peptide analogue complexed with MDM2. *Journal of the American Chemical Society*, 128, 11000-11001.
- Samel, A., Cuomo, A., Bonaldi, T. and Ehrenhofer-Murray, A. E. (2012) Methylation of CenH3 arginine 37 regulates kinetochore integrity and chromosome segregation. *Proceedings of the National Academy of Sciences*, 109, 9024-9034.
- Schleiffer, A., Maier, M., Litos, G., Lampert, F., Hornung, P., Mechtler, K. and Westermann, S. (2012) CENP-T proteins are conserved centromere receptors of the Ndc80 complex. *Nat Cell Biol*, 14,604-613.
- Schneider, K., Fuchs, C., Dobay, A., Rottach, A., Qin, W., Wolf, P., Álvarez-Castro, J., Nalaskowski, M., Kremmer, E., Schmid, V., Leonhardt, H. and Schermelleh, L. (2013). Dissection of cell cycle-dependent dynamics of Dnmt1 by FRAP and diffusion-coupled modeling. *Nucleic Acids Res.*, 41, 4860-4876.
- Schwille, P., Meyer-Almes, F. J. and Rigler, R. (1997) Dual-color fluorescence cross-correlation spectroscopy for multicomponent diffusional analysis in solution. *Biophysical Journal*, 72, 1878-1886.
- Schwarze, SR., Ho, A., Vocero-Akbani, A., Dowdy, SF. (1999) In vivo protein transduction: delivery of a biologically active protein into the mouse. *Science*. 285, 1569–1572.
- Scoumanne, A., Harms, K. L. and Chen, X. (2005) Structural basis for gene activation by p53 family members. *Cancer Biology & Therapy*, 4, 1178-1185.
- Screpanti, E., De Antoni, A., Alushin, G. M., Petrovic, A., Melis, T., Nogales, E. and Musacchio, A. (2011) Direct binding of Cenp-C to the Mis12 complex joins the inner and outer kinetochore. *Current Biology*, 21, 391-398.
- Shaner, N. C., Campbell, R. E., Steinbach, P. A., Giepmans, B. N. G., Palmer, A. E. and Tsien, R. Y. (2004) Improved monomeric red, orange and yellow fluorescent proteins derived from *Discosoma* sp. red fluorescent protein. *Nat Biotech*, 22, 1567-1572.
- Shangary, S., Qin, D., McEachern, D., Liu, M., Miller, R. S., Qiu, S., Nikolovska-Coleska, Z., Ding, K., Wang, G., Chen, J., Bernard, D., Zhang, J., Lu, Y., Gu, Q., Shah, R. B., Pienta, K. J., Ling, X., Kang, S., Guo, M., Sun, Y., Yang, D. and Wang, S. (2008) Temporal activation of p53 by a specific MDM2 inhibitor is selectively toxic to tumors and leads to complete tumor growth inhibition. *Proc Natl Acad Sci U S A*, 105, 3933-3938.
- Sharp, D. A., Kratowicz, S. A., Sank, M. J. and George, D. L. (1999) Stabilization of the MDM2 oncoprotein by interaction with the structurally related MDMX protein. *Journal of Biological Chemistry*, 274, 38189-38196.
- Shelby, R. D., Monier, K. and Sullivan, K. F. (2000) Chromatin assembly at kinetochores is uncoupled from DNA replication. *The Journal of Cell Biology*, 151, 1113-1118.

- Shelby, R. D., Vafa, O. and Sullivan, K. F. (1997) Assembly of CENP-A into centromeric chromatin requires a cooperative array of nucleosomal DNA contact sites. *The Journal of Cell Biology*, 136, 501-513.
- Shuaib, M., Ouararhni, K., Dimitrov, S. and Hamiche, A. (2010) HJURP binds CENP-A via a highly conserved N-terminal domain and mediates its deposition at centromeres. *Proceedings of the National Academy of Sciences*, 107, 1349-1354.
- Shvarts, A., Steegenga, W. T., Riteco, N., vanLaar, T., Dekker, P., Bazuine, M., vanHam, R. C. A., vanOordt, W. V., Hateboer, G., vanderEb, A. J. and Jochemsen, A. G. (1996) MDMX: A novel p53-binding protein with some functional properties of MDM2. *EMBO J.*, 15, 5349-5357.
- Shyu, Y. J., Suarez, C. D. and Hu, C.-D. (2008) Visualization of AP-1-NF- $\kappa$ B ternary complexes in living cells by using a BiFC-based FRET. *Proceedings of the National Academy of Sciences*, 105, 151-156.
- Silva, M. C., Bodor, D. L., Stellfox, M. E., Martins, N. M., Hocheegger, H., Foltz, D. R. and Jansen, L. E. (2012) Cdk activity couples epigenetic centromere inheritance to cell cycle progression. *Dev Cell*, 22, 52-63.
- Slattery, S. D., Moore, R. V., Brinkley, B. R. and Hall, R. M. (2008) Aurora-C and Aurora-B share phosphorylation and regulation of cenp-A and borealin during mitosis. *Cell Cycle*, 7, 787-795.
- Slaughter, B. D., Schwartz, J. W. and Li, R. (2007) Mapping dynamic protein interactions in MAP kinase signaling using live-cell fluorescence fluctuation spectroscopy and imaging. *Proceedings of the National Academy of Sciences*, 104, 20320-20325.
- Slavoff, S. A., Liu, D. S., Cohen, J. D. and Ting, A. Y. (2011) Imaging protein-protein interactions inside living cells via interaction-dependent fluorophore ligation. *Journal of the American Chemical Society*, 133, 19769-19776.
- Soderberg, O., Gullberg, M., Jarvius, M., Ridderstrale, K., Leuchowius, K.-J., Jarvius, J., Wester, K., Hydbring, P., Bahram, F., Larsson, L.-G. and Landegren, U. (2006) Direct observation of individual endogenous protein complexes in situ by proximity ligation. *Nat Meth*, 3, 995-1000.
- Stoler, S., Rogers, K., Weitze, S., Morey, L., Fitzgerald-Hayes, M. and Baker, R. E. (2007) Scm3, an essential *Saccharomyces cerevisiae* centromere protein required for G2/M progression and Cse4 localization. *Proceedings of the National Academy of Sciences*, 104, 10571-10576.
- Stoll, R., Renner, C., Hansen, S., Palme, S., Klein, C., Belling, A., Zeslawski, W., Kamionka, M., Rehm, T., Mühlhahn, P., Schumacher, R., Hesse, F., Kaluza, B., Voelter, W., Engh, R. A. and Holak, T. A. (2000) Chalcone derivatives antagonize interactions between the human oncoprotein MDM2 and p53? *Biochemistry*, 40, 336-344.
- Suganuma, T. and Workman, J. L. (2011) Signals and combinatorial functions of histone modifications. *Annual Review of Biochemistry*, 80, 473-499.
- Sugata, N., Li, S., Earnshaw, W. C., Yen, T. J., Yoda, K., Masumoto, H., Munekata, E., Warburton, P. E. and Todokoro, K. (2000) Human CENP-H multimers colocalize with CENP-A and CENP-C at active centromere-kinetochore complexes. *Human Molecular Genetics*, 9, 2919-2926.
- Sugata, N., Munekata, E. and Todokoro, K. (1999) Characterization of a novel kinetochore protein, CENP-H. *Journal of Biological Chemistry*, 274, 27343-27346.

- Sullivan, B. A. and Karpen, G. H. (2004) Centromeric chromatin exhibits a histone modification pattern that is distinct from both euchromatin and heterochromatin. *Nat Struct Mol Biol*, 11, 1076-1083.
- Sullivan, K. F., Hechenberger, M. and Masri, K. (1994) Human CENP-A contains a histone H3 related histone fold domain that is required for targeting to the centromere. *The Journal of Cell Biology*, 127, 581-592.
- Suto, R. K., Clarkson, M. J., Tremethick, D. J. and Luger, K. (2000) Crystal structure of a nucleosome core particle containing the variant histone H2A.Z. *Nat Struct Mol Biol*, 7, 1121-1124.
- Suzuki, A., Hori, T., Nishino, T., Usukura, J., Miyagi, A., Morikawa, K. and Fukagawa, T. (2011) Spindle microtubules generate tension-dependent changes in the distribution of inner kinetochore proteins. *The Journal of Cell Biology*, 193, 125-140.
- Tachiwana, H., Kagawa, W., Shiga, T., Osakabe, A., Miya, Y., Saito, K., Hayashi-Takanaka, Y., Oda, T., Sato, M., Park, S.-Y., Kimura, H. and Kurumizaka, H. (2011) Crystal structure of the human centromeric nucleosome containing CENP-A. *Nature*, 476, 232-235.
- Takayama, Y., Sato, H., Saitoh, S., Ogiyama, Y., Masuda, F. and Takahashi, K. (2008) Biphasic Incorporation of Centromeric Histone CENP-A in Fission Yeast. *Molecular Biology of the Cell*, 19, 682-690.
- Takeuchi, K. and Wagner, G. (2006) NMR studies of protein interactions. *Current Opinion in Structural Biology*, 16, 109-117.
- Tanimura, S., Ohtsuka, S., Mitsui, K., Shirouzu, K., Yoshimura, A. and Ohtsubo, M. (1999) MDM2 interacts with MDMX through their RING finger domains. *FEBS letters*, 447, 5-9.
- Thomson, J. P., Skene, P. J., Selfridge, J., Clouaire, T., Guy, J., Webb, S., Kerr, A. R. W., Deaton, A., Andrews, R., James, K. D., Turner, D. J., Illingworth, R. and Bird, A. (2010) CpG islands influence chromatin structure via the CpG-binding protein Cfp1. *Nature*, 464, 1082-1086.
- Thyagarajan, A. and Ting, A. Y. (2010) Imaging Activity-Dependent Regulation of Neurexin-Neurologin Interactions Using trans-Synaptic Enzymatic Biotinylation. *Cell*, 143, 456-469.
- Tomkiel, J., Cooke, C. A., Saitoh, H., Bernat, R. L. and Earnshaw, W. C. (1994) CENP-C is required for maintaining proper kinetochore size and for a timely transition to anaphase. *The Journal of Cell Biology*, 125, 531-545.
- Tsukamoto, T., Hashiguchi, N., Janicki, S. M., Tumber, T., Belmont, A. S. and Spector, D. L. (2000) Visualization of gene activity in living cells. *Nat Cell Biol*, 2, 871-878.
- Tuck-Muller, C. M., Narayan, A., Tsien, F., Smeets, D. F., Sawyer, J., Fiala, E. S., Sohn, O. S. and Ehrlich, M. (2000) DNA hypomethylation and unusual chromosome instability in cell lines from ICF syndrome patients. *Cytogenet Cell Genet*, 89, 121-128.
- Valdivia, M. M. and Brinkley, B. R. (1985) Fractionation and initial characterization of the kinetochore from mammalian metaphase chromosomes. *The Journal of Cell Biology*, 101, 1124-1134.
- Vassilev, L. T., Vu, B. T., Graves, B., Carvajal, D., Podlaski, F., Filipovic, Z., Kong, N., Kammlott, U., Lukacs, C., Klein, C., Fotouhi, N. and Liu, E. A. (2004) In vivo activation of the p53 pathway by small-molecule antagonists of MDM2. *Science*, 303, 844-848.
- Verdaasdonk, J. S. and Bloom, K. (2011) Centromeres: unique chromatin structures that drive chromosome segregation. *Nat Rev Mol Cell Biol*, 12, 320-332.
- Walfridsson, J., Bjerling, P., Thalen, M., Yoo, E.-J., Park, S. D. and Ekwall, K. (2005) The CHD remodeling factor Hrp1 stimulates CENP-A loading to centromeres. *Nucleic Acids Research*, 33, 2868-2879.

- Wallrabe, H. and Periasamy, A. (2005) Imaging protein molecules using FRET and FLIM microscopy. *Current Opinion in Biotechnology*, 16, 19-27.
- Walter, M., Chaban, C., Schütze, K., Batistic, O., Weckermann, K., Näke, C., Blazevic, D., Grefen, C., Schumacher, K., Oecking, C., Harter, K. and Kudla, J. (2004) Visualization of protein interactions in living plant cells using bimolecular fluorescence complementation. *The Plant Journal*, 40, 428-438.
- Wang, F., Dai, J., Daum, J. R., Niedzialkowska, E., Banerjee, B., Stukenberg, P. T., Gorbsky, G. J. and Higgins, J. M. G. (2010) Histone H3 Thr-3 phosphorylation by Haspin positions Aurora B at centromeres in mitosis. *Science*, 330, 231-235.
- Wendt, M. D., Wang, S., Zhao, Y., Bernard, D., Aguilar, A. and Kumar, S. (2012) Targeting the MDM2-p53 protein-protein interaction for new cancer therapeutics. In *Protein-Protein Interactions*, Vol. 8 Springer Berlin Heidelberg, pp. 57-79.
- Wennmalm, S., Thyberg, P., Xu, L. and Widengren, J. (2009) Inverse-fluorescence correlation spectroscopy. *Analytical Chemistry*, 81, 9209-9215.
- Wennmalm, S. and Widengren, J. (2010) Inverse-fluorescence cross-correlation spectroscopy. *Analytical Chemistry*, 82, 5646-5651.
- Westermann, S., Cheeseman, I. M., Anderson, S., Yates, J. R., Drubin, D. G. and Barnes, G. (2003) Architecture of the budding yeast kinetochore reveals a conserved molecular core. *The Journal of Cell Biology*, 163, 215-222.
- Winey, M., Mamay, C. L., O'Toole, E. T., Mastronarde, D. N., Giddings, T. H., McDonald, K. L. and McIntosh, J. R. (1995) Three-dimensional ultrastructural analysis of the *Saccharomyces cerevisiae* mitotic spindle. *The Journal of Cell Biology*, 129, 1601-1615.
- Wong, A. K. C. and Rattner, J. B. (1988) Sequence organization and cytological localization of the minor satellite of mouse. *Nucleic Acids Research*, 16, 11645-11661.
- Wu, X., Bayle, J. H., Olson, D. and Levine, A. J. (1993) The p53-mdm-2 autoregulatory feedback loop. *Genes & Development*, 7, 1126-1132.
- Xiao, H., Mizuguchi, G., Wisniewski, J., Huang, Y., Wei, D. and Wu, C. (2011) Nonhistone Scm3 binds to AT-Rich DNA to organize atypical centromeric nucleosome of budding yeast. *Molecular Cell*, 43, 369-380.
- Xu, G.-L., Bestor, T. H., Bourc'his, D., Hsieh, C.-L., Tommerup, N., Bugge, M., Hulten, M., Qu, X., Russo, J. J. and Viegas-Pequignot, E. (1999a) Chromosome instability and immunodeficiency syndrome caused by mutations in a DNA methyltransferase gene. *Nature*, 402, 187-191.
- Xu, Y., Piston, D. W. and Johnson, C. H. (1999b) A bioluminescence resonance energy transfer (BRET) system: Application to interacting circadian clock proteins. *Proceedings of the National Academy of Sciences*, 96, 151-156.
- Yamagishi, Y., Honda, T., Tanno, Y. and Watanabe, Y. (2010) Two histone marks establish the inner centromere and chromosome bi-orientation. *Science*, 330, 239-243.
- Yin, H., Lee, G. I., Sedey, K. A., Kutzki, O., Park, H. S., Orner, B. P., Ernst, J. T., Wang, H. G., Sebt, S. M. and Hamilton, A. D. (2005) Terphenyl-based bak BH3 alpha-helical proteomimetics as low-molecular-weight antagonists of Bcl-xL. *J Am Chem Soc*, 127, 10191-10196.
- Zaal, K. J. M., Smith, C. L., Polishchuk, R. S., Altan, N., Cole, N. B., Ellenberg, J., Hirschberg, K., Presley, J. F., Roberts, T. H., Siggia, E., Phair, R. D. and Lippincott-Schwartz, J. (1999) Golgi membranes are absorbed into and reemerge from the ER during mitosis. *Cell*, 99, 589-601.

- Zamyatnin, A. A., Solov'yev, A. G., Bozhkov, P. V., Valkonen, J. P. T., Morozov, S. Y. and Savenkov, E. I. (2006) Assessment of the integral membrane protein topology in living cells. *The Plant Journal*, 46, 145-154.
- Zaratiegui, M., Vaughn, M. W., Irvine, D. V., Goto, D., Watt, S., Bahler, J., Arcangioli, B. and Martienssen, R. A. (2011) CENP-B preserves genome integrity at replication forks paused by retrotransposon LTR. *Nature*, 469, 112-115.
- Zeitlin, S. G., Barber, C. M., Allis, C. D. and Sullivan, K. (2001a) Differential regulation of CENP-A and histone H3 phosphorylation in G2/M. *Journal of Cell Science*, 114, 653-661.
- Zeitlin, S. G., Shelby, R. D. and Sullivan, K. F. (2001b) CENP-A is phosphorylated by Aurora B kinase and plays an unexpected role in completion of cytokinesis. *The Journal of Cell Biology*, 155, 1147-1158.
- Zhang, W., Lee, H.-R., Koo, D.-H. and Jiang, J. (2008) Epigenetic modification of centromeric chromatin: hypomethylation of DNA sequences in the CENH3-associated chromatin in *Arabidopsis thaliana* and Maize. *The Plant Cell Online*, 20, 25-34.
- Zolghadr, K., Mortusewicz, O., Rothbauer, U., Kleinhans, R., Goehler, H., Wanker, E. E., Cardoso, M. C. and Leonhardt, H. (2008) A fluorescent two-hybrid assay for direct visualization of protein interactions in living cells. *Molecular & Cellular Proteomics*, 7, 2279-2287.



## 4.2 Abbreviations

aa: amino acids  
AD: activating domain  
*ADE2*: gene encoding phosphoribosylamino-imidazole-carboxylase  
AP: acceptor peptide  
ATP: Adenosine-5'-triphosphate  
BAT: biotin acceptor tag  
BFP: blue fluorescent protein  
BiFC: bimolecular fluorescence complementation  
BirA: biotin ligase  
bp: base pair(s)  
BRET: bioluminescence resonance energy transfer  
C: cytosine  
CAF1: chromatin assembly factor 1  
CATD: CENP-A centromere-targeting domain  
CBP: calmodulin binding peptide  
CCAN: constitutive centromere-associated network  
CDE: centromere DNA element  
cdk: cyclin dependent kinase  
CENP: centromere protein  
CFP: cyan fluorescent protein  
ChIP: chromatin IP  
cnt: central core sequence  
co-IP: co-immunoprecipitation  
CPC: chromosomal passenger complex  
CREST: calcinosis, Raynaud phenomenon, esophageal dysmotility, sclerodactyly, and telangiectasia syndrome  
DB: DNA binding domain  
DNA: deoxyribonucleic acid  
Dnmt: DNA methyltransferase  
EBV: Epstein-Barr virus  
eGFP: enhanced GFP  
Em: emission light  
Ex: excitation light  
F2H: fluorescent two-hybrid  
F3H: fluorescent three-hybrid  
FACT: facilitates chromatin transcription  
FCCS: fluorescence cross-correlation spectroscopy  
FCS: fluorescence correlation spectroscopy  
FISH: fluorescence *in situ* hybridization  
FLIM: fluorescence-lifetime imaging microscopy  
FLIP: fluorescence loss in photobleaching  
FP: fluorescent protein or fluorescence polarization  
FRAP: fluorescence recovery after photobleaching

FRET: Förster resonance energy transfer or fluorescence resonance energy transfer  
GBP: GFP binding protein  
GFP: green fluorescent protein  
GST: Glutathione-S-transferase  
HAT: Histone acetylase  
HDAC: Histone deacetylase  
Hdm2: human homolog of mouse *mdm2* gene  
HFD: histone fold domain  
HIRA: HIR histone cell cycle regulation defective homolog A  
HIS3: yeast gene encoding Imidazoleglycerol-phosphate dehydratase  
HJURP: Holliday junction recognition protein  
IC50: half maximal inhibitory concentration  
ICEN: interphase centromere complex  
ICF: Immunodeficiency, Centromeric region instability, Facial anomalies syndrome  
ID-PRIME: Interaction-Dependent PProbe Incorporation Mediated by Enzymes  
iFCCS: inverse FCCS  
iFCS: inverse FCS  
iFRAP: inverse FRAP  
imrL: inverted repeats left  
imrR: inverted repeats right  
IP: immunoprecipitation  
ITC: isothermal titration calorimetry  
KMN: KNL1, Mis12 complex, Ndc80 complex network  
KNL2: knockout null 2, *C. elegans* homolog of m18bp1  
LPNA2: karyopherin alpha 2  
lacI: lac repressor  
*lacO*: lactose operator  
LacZ: bacterial enzyme  $\beta$ -galactosidase  
LAP1: LplA acceptor peptide  
LplA: lipoic acid ligase A  
M18bp1: mis18 binding protein 1  
mdm2: murine double minute 2  
me: methylation  
mES: mouse embryonic stem cell  
Mi: MDM2 inhibitor  
mRFP: monomeric red fluorescent protein  
MS: mass spectrometry  
MTOC: microtubule-organizing center  
NAC: CENP-A nucleosome associated  
NADH: Nicotinamid-Adenin-Dinucleotid-Hydrogen  
NES: nuclear export signals  
NLS: nuclear localization signal  
NMR: nuclear magnetic resonance  
otr: outer repeats  
ph: phosphorylation

PMI: peptide MDM2 inhibitor  
PK: pharmacokinetics  
PR: pro rich domain of p53  
PTM: post-translational modification  
RacGAP1: Rac GTPase-activating protein 1  
RCA: rolling-circle amplification  
RFP: red fluorescent protein  
RING: really interesting new gene  
RNA: Ribonucleic acid  
ROI: regions of interest  
RSF: remodeling and spacing factor  
SANT: A domain first found and named from the SWI-SNF and ADA complexes, the transcriptional co-repressor N-CoR and TFIIB  
S: Serine amino acid  
SILAC: stable isotope labeling with amino acids in cell culture  
siRNA: small interfering RNA  
SPR: surface plasmon resonance  
T: thymidine or threonine amino acid  
TAP: tandem affinity purification  
Tet:ten-eleven translocation protein  
TEV protease: tobacco etch virus protease  
TSA: Trichostatin A  
xCrAsH: 5(6)-Carboxy-FlAsH  
X-gal: 5-bromo-4-chloro-indolyl- $\beta$ -D-galactopyranoside  
Y2H: yeast two-hybrid  
YFP: yellow fluorescent protein

### 4.3 Contributions

*Declaration of contributions to “Visualization and targeted disruption of protein interactions in living cells”*

I and Prof. Heinrich Leonhardt conceived the project. I cloned the p53 and Hdm2 fluorescence constructs and tested their interactions in the F3H assay. Also I performed all the compound inhibitors testing, and developed the high throughput assay together with the analysis protocol. I organized and contributed to all other figures and supplementary figures except fig 4, fig. S7, S8, S9 (done by Herce HD) and S5, S6 (done by Helma J). Moreover, I wrote corresponding part of the manuscript.

*Declaration of contributions to “CENP-C facilitates the recruitment of M18BP1 to centromeric chromatin”*

I conceived this project together with Schotta group, and I performed the screening and mapping of the interaction between M18bp1 and CCANs/CENP-C by F3H assay. And also I analyzed the interaction of M18bp1 fragments with CENP-C by InCell analyzer. Besides, I prepared figures 2 and 3.

*Declaration of contributions to “Step-Wise Assembly, Maturation and Dynamic Behavior of the Human CENP-P/O/R/Q/U Kinetochore Sub-Complex”*

I performed the *in vivo* protein interaction assays and made Figure 3 and Table 2. Also I wrote the corresponding figure legends as well as the corresponding material and methods section with the help of Prof. Heinrich Leonhardt.

*Declaration of contributions to “Binding of the Heterogeneous Ribonucleoprotein K (hnRNP K) to the Epstein-Barr Virus Nuclear Antigen 2 (EBNA2) Enhances Viral LMP2A Expression”*

I performed the *in vivo* interaction assays between hnRNP K and EBNA2. I made figure 8, wrote the *in vivo* interaction part of the manuscript and also the figure legend with the help of Prof. Heinrich Leonhardt.

## 4.4 Declaration

### Eidesstattliche Erklärung

Ich versichere hiermit an Eides statt, dass die vorgelegte Dissertation von mir selbständig und ohne unerlaubte Hilfe angefertigt ist.

München, den .....

(unterschrift)

### Erklärung

Hiermit erkläre ich, \*

- ☐ dass die Dissertation nicht ganz oder in wesentlichen Teilen einer anderen Prüfungskommission vorgelegt worden ist
- ☐ dass ich mich anderweitig einer Doktorprüfung ohne Erfolg nicht unterzogen habe.
- ☐ dass ich mich mit Erfolg der Doktorprüfung im Hauptfach.....  
und in den Nebenfächern .....  
bei der Fakultät für ..... der .....  
(Hochschule/ Universität)  
unterzogen habe
- ☐ dass ich ohne Erfolg versucht habe, eine Dissertation einzureichen oder mich der Doktorprüfung zu unterziehen.

München, den .....

(unterschrift)

\*) Nichtzutreffendes streichen

## 4.5 Acknowledgements

First of all, I would like to thank my supervisor Prof. Dr. Heinrich Leonhardt. I am really grateful to have the opportunity to finish my PhD work in his lab. His patient supervising and instructive discussion helped me so much in my research, and his wise opinion enlightened me a lot on the life beside scientific research. Especially, I would like to thank him for encouraging me when I was frustrated. His support gave me the possibility to finish my PhD work.

I am very grateful to all my collaborators in Prof. Cristina Cardoso's, Prof. Gunnar Schotta's, Prof. Stephen Diekmann's and Prof. Friedrich Graesser's Lab. With the pleasant and successful cooperation, I expanded my horizon and got fruitful publications, thanks to you all.

Of course, I would also like to thank the CSC for the scholarship, which is very important for me to finish my studies.

I also would like to thank Dr. Kourosh Zolghadr and Dr. Weihua Qin for their kind help with my experiments. Thanks to Anja and Susanne for their warm help and support.

Furthermore, I want to thank all the former and present lab members: Garwin, Sebastian, Jonas, Nan, Irina, Boris, Mengxi, Karin, Andrea, Fabio, Daniela, Katrin, Patricia, Christine, Andreas, Katharina, Congdi, Cindy, Kamila, Tobi, Udo, Christina, Christopher, Martha, Jürgen and Yolanda. They helped me a lot and gave me a nice and active work atmosphere, thank you.

Thanks to all my friends and colleagues in Munich. Because of them, days in Munich become colorful and worth to remember. And the special girl, who shared her days in Munich with me, helped me to think independently, and let me realize some of the most beautiful things in the world – love, kindness and justice - I would like to say thank you. Life is going on, memories belong to Munich will be kept in Munich, but I am not the same person anymore. Thank you.

Last but not least, I would like to thank my family. Their love and endless support accompany me in every single step of my life, giving me the courage to face the unknown future in this imperfect world. 感谢你们，爸爸妈妈！我爱你们！

## Curriculum Vitae

Wen Deng

Telephone: +49 89 2180 74227

Email: deng@bio.lmu.de

### Personal information

Date of Birth	10.04.1984
Place of birth	Shaanxi, China
Nationality	Chinese
Current work address	Ludwig Maximilians University (LMU), Munich Department of Biology II, Biocenter Großhaderner Str. 2, 82152, Planegg-Martinsried, Germany

### Education

10/2008 – Present	PhD student in Biology, Ludwig Maximilians University, Munich, Germany Supervisor: Prof. Dr. Heinrich Leonhardt
09/2005 – 07/2008	Master of Science in Agriculture (Preventive veterinary medicine) Northwest A&F University, Yangling, China
09/2002 – 07/2006	Bachelor of Science, majored in Biology Northwest A&F University, Yangling, China

**Publications**

Eskat A\*, **Deng W\***, Hofmeister A., Rudolphi S., Emmerth S., Hellwig D., Ulbricht T., Döring V., Bancroft JM., McAinsh AD., Cardoso MC., Meraldi P., Hoischen C., Leonhardt H., Diekmann S. (2012) Step-wise assembly, maturation and dynamic behavior of the human CENP-P/O/R/Q/U kinetochore sub-complex. PLoS ONE 7(9): e44717.

\* Joint first authors

Dambacher, S\*, **Deng W\***, Hahn M\*, Sadic D., Fröhlich J, Nuber A., Hoischen C., Diekmann S., Leonhardt H., Schotta G. (2012).CENP-C facilitates the recruitment of M18BP1 to centromeric chromatin. Nucleus 3(1): 101-110

\* Joint first authors

Gross H., Hennard C., Masouris I., Cassel C., Barth S., Stober-Grässer U., Mamiani A., Moritz B., Ostareck D., Ostareck-Lederer A., Neuenkirchen N., Fischer U., **Deng W.**, Leonhardt H., Noessner E., Kremmer E., Grässer FA. (2012) Binding of the heterogeneous ribonucleoprotein K (hnRNP K) to the Epstein-Barr virus nuclear antigen 2 (EBNA2) enhances viral LMP2A expression. PLoS ONE 7(8): e42106.

Liu N., Wang M., **Deng W.**, Schmidt CS., Qin W., Leonhardt H., Spada F. (2013) Connections between Tet dioxygenases and CXXC zinc finger modules. PLoS ONE 8(5): e62755.

Herce HD\*, **Deng W\***, Helma J., Leonhardt H., Cardoso MC. Visualization and targeted disruption of protein interactions in living cells. Nature Communication. 4: 2660.

\* Joint first authors